DEVELOPMENT AND APPLICATION OF A 3-D PERFUSION BIOREACTOR CELL CULTURE SYSTEM FOR BONE TISSUE ENGINEERING

A Dissertation
Presented to
The Academic Faculty

by

Blaise Damian Porter

In Partial Fulfilment
of the Requirements for the Degree
Doctor of Philosophy in Mechanical Engineering
George W. Woodruff School of Mechanical Engineering

Georgia Institute of Technology
December 2005

Copyright 2005 © Blaise Damian Porter

DEVELOPMENT AND APPLICATION OF A 3-D PERFUSION BIOREACTOR CELL CULTURE SYSTEM FOR BONE TISSUE ENGINEERING

Approved by:

Dr. Robert E. Guldberg, Advisor
Woodruff School of Mechanical Engineering
Georgia Institute of Technology

Dr. David Fyhrie
Department of Orthopaedic Surgery
University of California Davis

Dr. Andrés J. García
Woodruff School of Mechanical Engineering
Georgia Institute of Technology

Dr. G. Paul Neitzel
Woodruff School of Mechanical Engineering
Georgia Institute of Technology

Dr. Timothy Wick
School of Chemical and Biomolecular Engineering
Georgia Institute of Technology

Date Approved: November 14, 2005

If everything worked right the first time, it would be called Search…

to my Parents, and

the One who is perfect for me…

ACKNOWLEDGEMENTS

In no particular order, since that would be elitist and I don't really have a good way to rank everyone anyway, I offer my sincere gratitude and thanks to the following individuals:

Wait, I misspoke, I have to place two people first, outside the realm of family, friends and colleagues. Dr. Bob Groover and Dr. Pat Kelly, my neurologist and surgeon, who are largely responsible for me being any sort of a productive member of society. If not for Dr. Groover's patient, dogged persistence and willingness to exhaust all reasonable tests, my brain tumor might never have been detected until it was a serious problem. Dr. Kelly's work with experimental surgery made my procedure an event which I had virtually no concern and my feelings were absolutely correct. Thanks to both of you.

Dr. Bryan Marshall, my current roommate and sage friend, who taught me what it meant to be All Conference. Thrashers games, Argonaut t-shirts, late nights at the Central City and Northside Taverns, random Monday nights when we catalogued labels, and hammers caught in the back corner of the end zone are just a smattering of the ways Bryan helped keep me sane these past few years. I had always aspired to follow the Marshall Plan, but it turns out that I needed even more time because Bryan taught me how to have fun along the way. Dr. Joe Berglund and Dr. Stacy Imler complete the team that terrorized Phillips Arena and gave me an appreciation for drinks with lids. Joe's ability to keep me on my toes with the latest news/completely untrue rumor was surpassed only by his knack for finding the most obscure news releases and websites of anyone I know. Stacy shared her passion for all things sports (except baseball) with me

through Tech football, Hawks playoff games in the Dome, running hundreds of miles throughout the country, a little road trip to San Antonio, and as co-champions now and forever of the AFDC Whopper Mile.

Dr. Robert E. Guldberg took a chance on a physics major with no formal engineering training from a tiny liberal arts college in the middle of a cow pasture and for that I am forever grateful. My only constraint for experimental design or assay was my own imagination and I know and am thankful for how spoiled I was. We may have different organizational styles, but Bob's willingness to let me grow at my own pace has made all the difference. I guess I'm thanking him for introducing me to the Groover Road Run (the worst 2.7 miles ever); which I'm certain will become even more infamous over the years. Hopefully Bob will tell later students that I ran it in 15:04, not 17:04. In those early years (after I realized she wasn't our new undergrad student worker), Dr. Sarah Cartmell was a tremendous help in developing the perfusion cell culture techniques as well as giving me an appreciation for different cell culture techniques and the British culture. Dr. Andrés J. García offered a contrasting style to my advisor and I deeply appreciated his concern over my progress. Some of my favorite times in the lab occurred when Andrés would hold court, regaling us with stories of his past. He tells us every year during March Madness that he was there when Duke beat Kentucky and I guess I believe him. I thank Drs. Tim Wick and Paul Neitzel for impressing upon me the importance of experimental design and for their relaxed demeanor during my proposal and defense. Dr. David Fyhrie was the initial driving force behind the CFD modeling and gave me the idea to look at the distribution of collagen within the scaffold using the Picro Sirius Red stain. I thank Dr. Bill Wepfer for being such an amazing recruiter for the mechanical

engineering department. You are the reason that I ended up at Tech. I have deep gratitude towards Dr. Bob Nerem, who lent a word of support during my quals and much financial support for me to attend several conferences. It's fun to walk with the giants in my field.

Jason Stammen and John Koontz came in with me in 1998 and I finally realized how they got out of here so quickly. It was all a function of finding the right woman, if only I had caught on sooner. Jason, besides bringing a whole new meaning to the movie "Roger and Me," thanks for teaching me what it's like to live on my own and go to the "grocery." John, thanks (I think) for introducing me to the world of all things fantasy sports as well as my first foray into Indian cuisine. My third model for a long distance relationship took the form of my longtime roommate Dr. Ben Byers. An absolute standup individual, even when I didn't make things easy for him, I am forever grateful for his maturity. And yes, you're right Ben, we'll always have Kelly Campbell on the end around and the monster dunks of Is'mail Mohammed. I am thankful for my friendship with Dr. Matt Tate, certainly one of the very bright lights and most dominant trivia players I've had the pleasure to interact with. If you would only learn how to do math and realize that one drink at the Atlanta Beer Garden is not $20. Dr. Ben Keselowsky, thank you for your sense of style and proclivity for variegated facial hair. Dr. Janna Kay, these seven years could have been a lifetime (in your case maybe several). Thank you for challenging me in my faith so that it became stronger and for teaching me to be tolerant and patient, because I like where we ended up. Kristin Michael, thanks for being so open and honest about who you are as a person. I am thankful to know such a giving, thoughtful individual who made sure that my stuff got turned in when I could no

longer function properly. Jenn Phillips, it's good to know a white girl can bring it on the dance floor and the court, lay off the carbs though. Tim Petrie, thanks for our late night discussions on point spreads and perfusion.

The support staff at IBB has been superb during my time here. I thank the administrative wing for working with me whether it was reserving a room for my defense, or watching the World Cup at 5am in the morning. I thank Vivian Johnson for her energy and attitude; anyone who can bust out what was on BET uncut on Friday at 3am during lab lunch is A-OK in my book. Thank you to Tracy Couse, histologist extraordinaire, with a great sense of humor and personality to boot, even if she is Canadian. Additionally, I would like to acknowledge my funding sources: the ERC Shared Facility supported by the National Science Foundation under Award Number EEC-9731643 as well as the Whitaker Foundation.

I thank Mamta Patel for her ebullient state of being. Thank you for showing boundless appreciation for the small things that are done for you. I suppose that's why people are so happy to interact with you. Thank you for being the first person I could share my joy with regarding Jenny. Heather Sharpe, thank you for letting me know it is right to expect more. Kate Shropshire, than you for raising my social consciousness and your indomitable spirit in fighting for what is right and good. Thank you to all of the Good Times team for welcoming me into your summer league family, you filled my Ultimate fix. Eric Vanderploeg has been a voice of reason over the last 6 years, with a little bit of mischievousness thrown in for good measure. I never would have eaten "all the appetizers" without your cerebral egging on. Thanks for teaming up with me to make an interesting roommate combination at those inaugural conferences. Catherine Reyes,

thanks for sharing your love of books (and whatever maven like expertise I was needing at whatever time). Charlie Gersbach, thanks for introducing me to the world of Texas Hold 'em, I'm sure it will serve me well.

Drs. Angel Duty and Natasha Case were the heart and soul of the Guldberg lab when I got to Tech and throughout most of my tenure here. Thank you Angel for teaching me what it is like to be around a person without guile. Fortunately I was able to recognize it again when I met Jenny. Thanks for those talks late at night or in the middle of the afternoon when it seemed like things were spiraling out of control. Your steadfast Faith helped bolster mine. Oh, and I'm glad you could point out that I was a little flummoxed with my knowledge of women's intimate apparel. Obviously, Bryan needed something else to give me a hard time about. Natasha, thank you for your selflessness. I will never forget your patience the first time I did cell culture and we ended up finishing at 5am the next day. Your sense of duty and responsibility is something I aspire to. Honestly, knowing you actually makes it difficult to cheer against Duke from time to time. I thank Rhima Coleman for asking the most pointed questions of anyone at Tech. It may not be sugar coated, but it's honest as heck. Megan Oest, thanks for being a good officemate and your patience with my messiness. Chris Gemmiti, I thank you for your patience with my benchtop etiquette and your bioreactor savvy. Oh yeah, you throw a mean Superbowl party too. I thank Craig Duvall, the enforcer, for almost single handedly delivering an intramural basketball championship to me. It's a good thing he's strong to very strong, 'cuz we were all along for the ride. Yash Kolombkar and Ken Dupont, I know the lab is in good hands with those that will follow and I thank you for that. I thank Dr. Alex Peister for the huge push at the end to put me over the top. I really

appreciate the confidence you showed in me, which bolstered my own confidence. Angela Lin and Srin Nagaraja. My "world class athlete" friend, and my "brown" friend, thanks for being surrogate parents☺ I hope I've made you proud. Angela, thank you for countless hours of help with cell culture and inane questions at all hours regarding the CT. But mostly, thanks for opening my eyes to the world of the ATL after 2am, Guinness double shotguns, the prettiest breakmark backhand I ever did see, a magnanimous spirit and the fact that you're just friggin' fun to be around. King Cobra, thanks for showing me how you break other people down with honesty, bluntness, and caring. My appreciation of Will Smith, Eddie Murphy, and James Brown soared to new heights in your presence. I didn't think I could like a guy that bleeds maize and blue, but somehow you proved me wrong. Your passion for life and excitement is surpassed only by your dedication to do the right thing. Oh yeah, thanks for the ben gay balls as well.

OK, so without trying I ended up leaving the biggies for the end. I guess I just allowed things to settle to the 1s state and that's what I was left with. I'd like to thank my three younger brothers for nipping at my heels so that I was constantly trying to reset the bar after they reached it. Although we seem very dissimilar, thank you Jerome for showing me parts of me in you that I didn't know existed. There are few things in life that give me greater joy than watching you come down on the fast break and distribute. I'd like to think I taught you some of that, but I figure I probably just pissed you off enough so that you'd be able to beat me as you got older. While you may do and say certain things that befuddle me, your wisdom often belies your age. Thanks for being the one I've talked to when I was faced with seemingly untenable positions. Luke, thanks for letting me cheer for someone who follows their passion. You are gifted in arenas I only

visit to watch other people perform in. Thanks for continually making me proud to tell people what my little brother does. Justin, thanks for being an organizational and entrepreneurial inspiration. I appreciate all the help you've given me during this job search process. You have always impressed me with your selfless attitude and kind heart, however, your concern for others was most apparent for me when you kept pestering me to contact that Jenny Rachmaciej girl. For that I am eternally grateful.

Jenny, you are my muse, motivation, and match. I thank you for your unconditional love of who I am and your patience as I try to be the best person that I can be. You know what I need before I say anything and you have supported me emotionally, mentally, physically, and incessantly since I met you. Whether it was care packages with cookies and peanut butter crackers, or weekly cards of encouragement, or impromptu visits, you have been everything I could have asked for in the person I want to share my life with. Thank you for prodding me when I didn't want it, even though I needed it, thank you for loving me, warts and all, thank you for opening up to me and letting me support you when I could, thank you for being not quite perfect, but absolutely perfect for me. You made me want to leave Georgia Tech so that I could be with you. Without you this past year, I would not have finished when I did. Therefore, these final two people are also indebted to you.

My Mom and Dad are the single most responsible individuals on this planet for where I am in the world. I could not imagine a better set of people to have as parents. I didn't need a "what would Jesus do" bracelet because I already knew what Penny and Co-burn would do. They prepared me to be a member of this world the best they knew how, and I for one have no complaints with the philosophy or the execution. Honesty,

Integrity, Spirituality, and Humility are the watchwords that I gleaned directly from them. Finally, I thank the Good Lord up above, who blessed me with an abundance of talents, a spectacular family, amazing friends, and a love for life and those around me that has made these past 30 years a joyous experience. I can only imagine what He has in store for me in my next iteration. Thank you all.

TABLE OF CONTENTS

LIST OF TABLES

LIST OF FIGURES

NOMENCLATURE

AA	Ascorbic acid
AA2-P	Ascorbic acid 2-Phosphate
ALP	Alkaline phosphatase
β-GP	β-Glycerophosphate
DEX	Dexamethasone
FN	fibronectin
FT-IR	Fourier transform infrared
HA	Hydroxyapatite
LP90%	Largest particles in each construct which constitute 90% of the total mineral volume
NO	nitric oxide
PCL	polycaprolactone
PCL-C	PCL with collagen lyophilized into the pore space
PCL-FN	PCL coated with fibronectin
PGE_2	prostaglandin E_2
rMSC	rat bone marrow stromal cell
RP	Rocker Plate constructs

SUMMARY

The need for improved clinical strategies which incorporate bone grafting techniques to restore function to damaged or degenerated bone is well recognized. Tissue engineering strategies that combine porous biomaterial scaffolds with cells capable of osteogenesis or bioactive proteins have shown promise as effective bone graft substitutes. However, due to mass transport limitations, attempts to culture bone tissue-engineering constructs thicker than 1mm *in vitro* have typically resulted in a shell of viable cells and mineralized matrix surrounding a necrotic core.

The *overall goal* of this project was to enhance the amount and distribution of cell-mediated mineralization throughout 3-D structural scaffolds *in vitro* using a perfusion bioreactor system. It was hypothesized that media perfusion would increase the amount, rate, and distribution of mineral deposited throughout cell-seeded scaffolds during *in vitro* culture compared with static control conditions.

Using our initial bioreactor design that perfused cylindrical constructs transverse to their long axis, we found that the cell viability and proliferation of MC3T3-E1 osteoblast-like cells seeded on trabecular bone scaffolds were significantly affected by perfusion flow rate. Computational fluid dynamics (CFD) modeling techniques were employed to visualize the flow distribution of media and estimate local shear stresses within perfused constructs.[1] As described in Chapter 4, flow field visualization revealed that transverse fluid flow through scaffolds with randomly interconnected pore structure was highly nonuniform and shunted to a few pathways of least resistance. More significantly, CFD modeling of axial perfusion through cylindrical scaffolds with a regular microarchitecture revealed a more uniform flow field distributed throughout the

scaffolds. We therefore redesigned our bioreactor to provide axial perfusion and switched our base scaffold material to polycaprolactone (PCL), a polymer that could be fabricated via fused deposition modeling into a structure with a repeating lattice and uniform pores.

Comparing the effects of different culture conditions on mineralized matrix synthesis and distribution within perfused constructs has proved difficult without quantitative analysis tools. Micro-computed tomography (micro-CT) scanning and 3-D image analysis offers a non-destructive, quantitative technique for assessing mineral formation, distribution, density, as well as particle number and size. The global objective and central hypothesis were tested by evaluating mineralized matrix synthesis within axially perfused, PCL scaffolds, seeded with rat marrow stromal cells (rMSC). Although the PCL scaffolds improved the distribution of perfusion, initial studies indicated that poor cell adhesion to the polymer struts was a limitation, even at very low rates of perfusion. Therefore, in Chapter 5, we evaluated the effects of lyophilizing type I collagen into PCL scaffolds (PCL+C) or coating PCL with fibronectin (PCL+FN) on cell viability and mineralized matrix synthesis.

Micro-CT was used to detect and quantify mineralized matrix volume, spatial distribution, and density within both axially perfused and statically grown, cell seeded, 3 mm thick, PCL scaffolds (66% porosity) compared with static control constructs. Perfused constructs, which were shown to develop mineralized matrix, had not exceeded 1.5 mm in thickness.[2] We therefore chose to test 3 mm thick constructs to more rigorously evaluate the benefits of perfusion. Significant increases in mineralized matrix deposition were detected within PCL+C constructs compared with scaffolds coated with

fibronectin (PCL+FN) in both static and perfused culture conditions. More importantly, after 5 weeks of culture, continuous perfusion increased mineralized matrix deposition 3-fold within PCL+C constructs compared with static cultures. Additionally, mineral was distributed throughout the entire thickness of 3 mm thick PCL+C constructs. However, possibly due to stagnant flow at the periphery (visualized with CFD modeling), 90% of the mineral was localized to the central annulus of these constructs. In an attempt to improve fluid flow through a larger diameter of the scaffold, the lip on which the constructs rest in the bioreactor was reduced in size. These positive results in the 3 mm thick constructs directed our efforts towards increasing the length of the constructs.

As described in Chapter 6, we next evaluated the feasibility of creating constructs large enough for future implantation in a preclinical, critical size, rat segmental defect model. PCL+C scaffolds (3 mm thick), seeded with rMSCs, were stacked in the perfusion bioreactor to create constructs 3, 6 and 9 mm in length. After 5 weeks in culture, mineral was detected and quantified throughout the entire length of all construct sizes. We also quantified the mineral volume within two sequentially smaller cylindrical subregions (radially excluding the outer 500 and 1000 μm of the construct) within the scaffold to determine if mineralized matrix had formed at the center of the construct. As hypothesized, the number of mineral particles within each scaffold increased proportionally as the scaffold length was increased. In addition, the total detected mineral volume tripled as the construct length was increased from 3 to 9 mm. Therefore, increasing scaffold length did not affect the mineral volume fraction (MVF) within the full volume of each construct. However, when analyzing the two cylindrical subregions at the inner core of 6 mm constructs, the MVF was significantly increased compared with

3 and 9 mm constructs. Mineral particle analysis showed an increase in mineral particle size within 6 mm constructs compared with 3 and 9 mm constructs. A large number of pores on the top surface of each construct were filled with extracellullar matrix and completely occluded. This effect was also observed in previous perfusion experiments in Chapter 5 using PCL scaffolds with a porosity of 66%. In an attempt to mitigate this effect, subsequent perfusion experiments employed scaffolds with a larger pore diameter and greater porosity.

To evaluate bone construct development *in vitro*, it would be advantageous to monitor the mineral growth and distribution non-invasively during culture. Repeat scanning offers the ability to monitor mineral growth over time, but subjecting cells to multiple x-ray scans may negatively affect cell viability and mineralized matrix synthesis. Therefore, two replicate experiments, documented in Chapter 7, were performed to assess the effect of one additional x-ray scan on cell viability, distribution and matrix production. No significant differences in cell viability, mineralized matrix volume, or mineral density were detected within constructs that had been scanned during the experiment at 3 and 5 weeks, compared with those that had only been scanned at 5 weeks.

Having validated repeat scanning and shown that perfusion culture supported mineral deposition throughout 9 mm long scaffolds, additional work, explained in Chapter 7, evaluated the response of osteoblasts to time varying flow conditions. rMSCs seeded on 9 mm long, 75% porous PCL+C scaffolds were perfused at one of three flow regimes: 0.2 ml/min continuous flow (0.2), 0.8 ml/min continuous flow (0.8), or 0.2 ml/min continuous flow for 23 hours/day followed by one hour of culture with flow

elevated to 0.8 ml/min (INT). Controls included constructs in static culture, as well as constructs placed in 6 well plates on an orbital rocker plate (RP), which was rotating at 0.5 Hz. Confocal microscopy images showed qualitative improvement in cell viability within 0.2 ml/min and INT constructs compared with all other culture groups. Constructs from all perfusion groups as well as the dynamic RP controls contained significantly more mineral at both 3 and 5 weeks compared with static controls. INT constructs consistently contained greater amounts of mineralized matrix as well as elevated rates of mineral production at both timepoints compared with all other experimental groups, however these values were statistically different from only the static and 0.8 ml/min culture groups. Visual inspection of the perfusion tubing revealed biological debris downstream of the constructs. Qualitatively, tubing for the 0.8 ml/min constructs contained the most debris, followed by the INT, and then 0.2 ml/min tubing. These results suggest that, while a minimum level of perfusion improves mineral deposition compared with static culture, flow rates above a certain level may be deleterious to matrix retention. Mineral particle analysis indicated that increases in mineral volume, from 3 to 5 weeks, within the 0.2 ml/min and INT constructs were predominantly due to growth of mineral particles that were already greater than 0.1 mm^3. Increases in total mineral volume for constructs in the 0.8 ml/min group could be attributed to a large increase in the number of particles between 0.01 and 0.1 mm^3. Compared with perfused constructs, the principal mechanism for increasing total mineral volume within Static constructs was the generation of new mineral particles. RP construct mineral volume increases were caused be a significant increase in the total number of particles as well as increases in the size of particles greater than 0.1 mm^3.

Together, these studies indicate that dynamic culture conditions enhance construct development with regards to cell viability, mineralized matrix deposition, growth rate, and distribution. The application of micro-CT image analysis techniques has provided the ability to quantitatively and nondestructively monitor the formation and growth of mineralized matrix regions within 3D tissue-engineered constructs *in vitro*. Furthermore, these techniques provide a rational approach to selecting perfusion culture conditions that optimize the amount and distribution of mineralized matrix production. Finally, the established perfusion bioreactor, in combination with micro-CT analysis, provides a foundation for evaluating new scaffolds and cell types that may be useful for the development of effective bone graft substitutes.

CHAPTER 1 INTRODUCTION

There are over six million fractures sustained in the United States each year and between five and ten percent of those result in nonunion.[3] In addition to acute trauma, segmental defects, spine instability, congenital defects and bone tumor resections are common bone deficiencies that require surgical intervention. The current gold standard treatment to stimulate bone regeneration involves harvesting autologous bone chips from the iliac crest of the patient and transplanting them to the injury site. However, donor site morbidity and pain, lack of structural integrity, and limited graft material volume are significant drawbacks. As a result, the need for improved clinical strategies to restore function to damaged or degenerated bone is well recognized.[3] Tissue engineering strategies that combine porous biomaterial scaffolds with cells capable of osteogenesis or bioactive proteins have shown promise as effective bone graft substitutes. Although acellular scaffolds have shown moderate clinical success, the delivery of osteoprogenitor cells or osteoblasts has been shown to enhance bone defect repair and may provide a more efficacious and rapid healing solution.[4] Recent work has suggested that *in vivo* repair may be further enhanced by culturing cell-seeded scaffolds *in vitro* to produce mineralized constructs prior to implantation.[5] However, attempts to culture bone tissue-engineering constructs thicker than 1mm *in vitro* have typically resulted in a shell of viable cells and mineralized matrix surrounding a necrotic core due to the absence of a vascular supply.[6] This shell can restrict vascular ingrowth as well as cell migration into the graft following implantation. To improve mass transport and nutrient exchange, Glowacki and co-workers performed 3-D *in vitro* perfusion experiments in 1998 and

showed an increase in cell viability and function within perfused collagen scaffolds compared with static controls.[7] Although this early work did not incorporate a structural scaffold or evaluate mineralized matrix synthesis, it introduced the concept of using media perfusion to create premineralized bone graft substitutes that has motivated this thesis.

The *overall goal* of this project was to enhance the amount and distribution of cell-mediated mineralization throughout 3-D structural scaffolds *in vitro* using a perfusion bioreactor system. It was hypothesized that media perfusion would increase the amount, rate, and distribution of mineral deposited throughout cell-seeded scaffolds during *in vitro* culture compared with static control conditions. This global hypothesis was tested by the following specific aims:

Aim 1: Develop a perfusion bioreactor to improve mass transport throughout 3-D constructs and test the effects of flow rate on cell viability. Static culture of cell-seeded scaffolds has been shown to produce constructs with viable cells and tissue localized to the periphery of the construct.[6] A variety of bioreactor systems have been developed to mitigate this effect, including perfusion bioreactors that direct media through scaffolds at a controlled rate.[8] Expanding on these studies, an iterative process was implemented utilizing *in vitro* experimentation and computational fluid dynamics modeling to develop a robust perfusion bioreactor system that provided consistent fluid flow throughout 3-D constructs. Multiple system designs and scaffold architectures were tested and modeled to determine the distribution of flow and estimate shear stresses throughout thick porous scaffolds. In one bioreactor design, the effects of perfusion rate

on the viability and distribution of MC3T3-E1 osteoblast-like cells seeded within human trabecular bone constructs was tested. It was hypothesized that different flow rates would modulate cell viability at the interior of perfused constructs.

Aim 2: Assess the effects of continuous media perfusion on cell viability and the amount and distribution of mineralized matrix production within cell-seeded polymeric scaffolds. A variety of scaffold materials including collagen sponge, polymer woven fibers, and titanium mesh, have been used in bioreactor systems. Perfusion of these cell seeded scaffolds has been shown to enhance rat bone marrow stromal cell (rMSC) proliferation and calcium content.[9, 10] In this Aim, we tested the effects of perfusion on matrix mineralization within cell-seeded polycaprolactone (PCL) scaffolds manufactured with a controlled and regular architecture using fused deposition modeling. A commonly observed disadvantage of polymer scaffolds is poor cell attachment. Therefore, we evaluated the effects of lyophilizing type I collagen into PCL scaffolds (PCL+C) or coating PCL with fibronectin (PCL+FN) on cell viability and mineralized matrix synthesis. The distribution of viable rMSCs inside static and perfused constructs was identified using fluorescent stains combined with confocal microscopy. Additionally, we introduced microcomputed tomography (micro-CT) based measurement techniques to quantify the effects of media perfusion on the amount and distribution of mineralized matrix deposition. It was hypothesized that perfusion would enhance cell viability and mineralized matrix deposition within polymeric constructs compared with static controls.

Aim 3: Test the effects of scaffold thickness on perfusion-mediated enhancement of mineralized matrix formation. We and others have recently demonstrated that perfusion increased mineralization within thin (0.8-3.0 mm) constructs.[2, 8, 10-12] However, eventual clinical translation of this technology will require increasing the size of these constructs. Even preclinical testing in a well-established rat segmental defect model requires an implant greater than 7 mm in length.[13] Therefore, in this Aim we evaluated the effect of increasing PCL+C scaffold length from 3 to 9 mm on perfusion-mediated enhancement of mineralized matrix formation. In addition to mineralized matrix volume and distribution, a new micro-CT image analysis technique was developed to quantify the size and number of mineral particles within the constructs. It was hypothesized that increasing scaffold length would result in a proportional increase in mineralized matrix particles and volume, and would not affect the uniformity of matrix distribution or particle size.

Aim 4: Quantify the effects of time varying perfusion on the amount, distribution, and rate of mineralized matrix formation within large 3D constructs *in vitro*. Determining mineral growth rate requires multiple mineralized matrix volume measurements on the same construct. Our previous experiments have shown that repeated micro-CT scanning did not significantly decrease mineral production of rMSCs seeded on demineralized bone matrix after 8 weeks in static culture.[14] In order to ensure repeat scans would not inhibit cells from synthesizing mineralized matrix, perfused rMSCs seeded PCL+C scaffolds were scanned at 3 and 5 weeks in a Viva Micro-CT and mineral deposition was compared with constructs scanned at only 5 weeks. We then used

repeat scanning to evaluate the effects of perfusion on construct development. Pulsatile and oscillatory flow conditions applied to osteoblasts using *in vitro* parallel-plate flow chambers have been shown to increase gene expression, intracellular Ca^{2+} concentration, and the production of nitric oxide (NO) and prostaglandin E_2 (PGE_2) in comparison to static controls.[15, 16] These time-varying flow results suggest that osteoblasts may be responsive to bouts of elevated flow rates superimposed on a low constant flow rate. In order to test the response of osteoblasts to dynamic flow conditions in a 3-D perfusion environment, rMSCs were seeded on 9 mm thick PCL+C scaffolds and perfused with one of three flow regimes: 0.2 ml/min, 0.8 ml/min, or 0.2 ml/min for 23 hours/day with one hour at 0.8 ml/min. Controls included constructs in static culture, as well as constructs placed in 6 well plates on an orbital rocker plate (RP), which was rotating at 0.5 Hz. All constructs were scanned at 3 and 5 weeks to evaluate mineral growth rate effects. It was hypothesized that intermittent elevated flow would increase the rate and amount of mineralized matrix synthesis relative to the continuous flow and control groups.

This work is significant because it addresses several key challenges in developing large, load-bearing, bioactive, bone graft substitutes *in vitro* as well as introduces innovative imaging methods to quantitatively assess 3-D mineralized matrix formation within scaffolds *in vitro*. Biodegradable polymer scaffolds, up to 4 times thicker than have previously been cultured, were utilized to test the effects of various 3-D fluid flow profiles on cell-mediated mineral growth and distribution. Constructs of this size are large enough to be used in a pre-clinical, critical sized, rat defect model.[13] Novel micro-CT scanning and analysis methods were developed to examine the mechanisms of the

observed flow-mediated responses by quantifying mineral particle size, number, and distribution. For example, repeated micro-CT scanning was validated and subsequently used to monitor mineralized matrix synthesis over time and determine mineral growth rates.

There has been little success creating large, bioresorbable, structurally sound implants that can be formed into relevant anatomic shapes and are populated throughout with osteogenic cells and matrix. Combining *in vitro* cell culture with CFD techniques, we designed and developed a perfusion bioreactor system to enhance the amount and distribution of viable cells and cell-mediated mineralization throughout 3-D cell seeded scaffolds. The results indicate that dynamic culture conditions enhance the production of mineralized matrix throughout large constructs for use in bone tissue engineering applications. Finally, this work provides a foundation for future *in vitro* evaluation of bone tissue engineering approaches that combine various cell options with multiple scaffold materials, architectures and porosities.

CHAPTER 2 LITERATURE REVIEW

Bone Anatomy, Function and Composition

The human skeleton is comprised of two types of bone, cortical and trabecular. Occupying the outer tubular region of long bones as well as the outer surface of small bones and flat bones, cortical bone is comprised of parallel cylindrical units packed tightly together called osteons. Within the osteons are concentric tubes of bone called lamella. The interfaces between the lamellae are lined with voids termed lacunae, which house bone cells that respond to mechanical signals. These units are aligned in an anisotropic fashion in order to maximize the mechanical properties of the material. Trabecular, also called spongy bone, fills the ends of long bones and is much more porous than cortical bone.[17] While it is also anisotropic in response to mechanical loading, on average, it possesses an apparent stiffness and elastic modulus one order of magnitude lower than its more dense counterpart.[18] Under compression, cortical bone strength ranges between 131-224 MPa with a modulus of 17-20 GPa.[19, 20] The strength and modulus of trabecular bone is greatly influenced by the apparent density of the trabecular bone. Human trabecular bone varies between 0.1 and 1.0 g/cm^3 compared with 1.8 g/cm^3 for cortical bone. A trabecular bone density of 0.2 g/cm^3 translates into a 90% porous segment of bone. Trabecular bone strength varies as the square of the apparent density, while the modulus varies as either the square or cube of the apparent density.[21] Additionally, due to the viscoelastic nature of bone, the strength and modulus are both load rate dependent. A reasonable value for strength would be 5-10 MPa and

50-100 MPa for modulus of elasticity.[18] Despite their very different apparent mechanical properties, the underlying similarity in composition allows both types of bone to fill many roles in maintaining the human body.

Presently, bone is thought to fulfill five primary functions in the body.[17] First, bone acts as a reservoir of calcium and phosphate that regulates ion concentrations in the body by releasing those minerals directly into the extracellular fluid environment.[18] Second, the marrow surrounding trabecular bone and within the marrow cavity of long bones supplies the body with both red and white blood cells. Third, bones provide muscle insertion sites and lever arms to facilitate locomotion. Fourth, vital organs such as the brain, heart and spinal cord are protected by the skull, rib cage and vertebrae. Finally, bones make up a rigid superstructure to support the body and its associated soft tissues.[17] The stiffness in bone is due to the mineral hydroxyapatite (HA, comprised of Ca^{2+} and PO_4^{2-}), which makes up 60-75% of bone's weight. The remaining extracellular matrix is 90% type I collagen plus non-collagenous proteins such as osteopontin, osteonecting, bone sialoprotein and osteocalcin. Organization and regulation of these constituents is carried out by a variety of cell types.

Bone Cells

There are four major types of bone cells: osteoblasts, bone-lining cells, osteocytes, and osteoclasts, each fulfilling a specific function. The job of *osteoblasts* is to form bone. Osteoblasts secrete a significant number of proteins, including all of the essential structural elements of osteoid (organic bone matrix). Not all bone matrix proteins are created at the same time, fibronectin and osteonectin are expressed early in

differentiation, while ostecalcin is produced after an established matrix has been developed.[22] After synthesizing and assembling osteoid, osteoblasts aid in precipitating mineral salts (Ca^{2+} and PO_4^{2-}) from the extracellular fluid onto the matrix to impart mechanical stiffness to the structure. Osteblasts may further differentiate into *osteocytes*, which become embedded in the lacunae within bone matrix and are joined together by small hairlike processes within caniliculi to form a connected network throughout the bone. These cells primarily sense mechanical load or tissue damage and subsequently can initiate remodeling responses. It has been postulated that osteocytes initiate remodeling by detecting strains in the bone matix or by responding to flow mediated shear stresses in the fluid filled lacunae due to bone deformation during loading.[22] *Bone-lining cells*, which cover resting bone surfaces, also share mechanosensation and adaptation duties. Lining cells can differentiate into an "osteoblastic" state as well as recruit osteoprogenitor cells. Additionally, lining cells are also instrumental in bone resorption by (1) recruiting osteoclasts (bone resorption cells) to resorption sites, (2) boosting the differentiation of osteoclast precursors, and (3) preparing the bone surface for resorption.[22] *Osteoclasts* are large, multinucleated cells, that resorb bone through simultaneous mineral dissolution and enzymatic digestion of organic molecules.[22]

Bone Formation and Healing Mechanisms

Bone formation occurs during a process called osteogenesis or ossification. *Intramembranous ossification* occurs in three stages and is responsible for the formation of all flat bones[17] as well as appositional modeling of the diaphysis (the shaft portion of long bones).[18] Initially, mesenchymal cells within a fibrous matrix aggregate and

differentiate into osteoblasts, which begin synthesizing osteoid. A network of fragile trabecular bone is formed as the osteoid accumulates and fuses together. Known as woven bone due to its irregular collagen fiber organization, this structure is infiltrated with blood vessels and encased in a vascular mesenchyme, which will become the periosteum, a thin tissue which sheaths the bone. Subsequently, the trabeculae thicken until they have fused into continuous plates of bone. As the bone matures, the woven trabecular bone is replaced with lamellar bone at the periphery.[17] A second method of bone formation is *endochondral ossification* where bone is laid down on a preexisting cartilage template. As chondrocytes proliferate, the cartilage thickness increases and hypertrophic cells at the cartilage/bone interface begin to secrete matrix vesicles, which initiate calcification of the cartilage. The cells then become apoptotic and a vascular invasion brings osteoblasts which deposit osteoid onto the calcified cartilage. This osteoid extends and fuses into woven bone comprised of trabeculae that can then be remodeled into lamellar bone.[18]

Normal fracture healing follows a similar pattern to endochondral ossification during growth. After acute trauma, a hematoma forms and a fibrin clot develops. After leukocytes and macrophages appear and remove the necrotic tissue, the repair process is initiated. Osteoblasts arrive from both the periosteum and from distant sites via the bloodstream and begin to synthesize organic matrix, which is ossified into woven bone. The amalgam of osteoblasts, cartilaginous matrix and woven bone constitutes the fracture callus, the raw materials needed for remodeling the injury site.[18] In all bone formation processes, osteoblasts synthesize osteoid, which fuses into woven trabecular bone, and may then be remodeled into lamellar cortical bone. This progression may be interrupted

if there is infection, inadequate blood supply, fracture instability or lack of available material to fuse the defect.[3] These factors can result in a non-union, which may require bone-grafting procedures.

Bone Graft Substitute Overview

The need for a bone graft substitute has been documented since the 1880s.[23] With the incidence of non-unions for fractures in the United States between 5 and 10%, each year between 300,000 and 600,000 patients require a surgical procedure to aid in repair.[3] This number does not include bone maladies arising from congenital defects, tumor resections or spine instability, which further underscores the prevalence of surgical intervention. Accepted clinical bone repair procedures include the use of autogenous trabecular bone harvested from the iliac crest of the patient, or allograft bone harvested from a cadaver. Autologous grafts may deliver viable osteoprogenitors and result in an increased rate of healing compared with allograft implants, which are devoid of a cellular component.[24] Although autograft has shown success for small voids and as a bone filler to stimulate repair at non-union sites and while allograft can be used for large, load bearing applications, neither approach provides a complete solution.[24] Autograft procedures are accompanied by increased surgical time, donor site morbidity, chronic pain, lack of adequate material, and insufficient graft structural stability.[24] Allograft methods are fraught with inferior healing capabilities, infection and inflammation complications, possible HIV transmission, as well as the need for cadaver tissue.[24, 25] Tissue engineering possesses the potential to address many of the most significant drawbacks of current clinical procedures for fixing non-unions, bone voids and acute

trauma. To develop a bone graft substitute, many researchers suggest at least one, and possibly all, of the following components for a tissue-engineered bone implant: (1) an osteoconductive scaffold or matrix, which provides structural support and can also act as a vehicle for delivery of (2) cells or (3) growth factors to the defect site.[18, 25, 26]

Bone Scaffold Requirements

The ideal bone graft substitute should exhibit the following characteristics: rapid vascular invasion, desirable handling properties, *osseointegration* (bonding directly to surface of bone without fibrous encapsulation), *osteoconduction* (the ability to support bone growth), *osteoinduction* (the ability to initiate osteoblast differentiation from uncommitted cells in the surrounding area), and *osteogenesis* (the formation of new bone within the graft material).[24-26] Because bone is a load-bearing tissue, it is prudent to consider the forces that a replacement material could experience after implantation when designing a bone graft substitute.[18] Since the repair or formation of both cortical or trabecular bone progresses through a trabecular bone phase, a replacement graft should possess mechanical properties comparable to native trabecular bone in order to mimic the natural healing response and allow a level of load-bearing on the tissue during the repair process. In addition to a simple sterilization procedure, the scaffold should have an interconnected pore structure to facilitate and promote neovascularization and cell migration throughout the graft.[18, 24] Finally, the scaffold should have the ability to be remodeled by the cells that facilitate the repair process in order to optimize the mechanical properties of the newly ossified tissue.[18] Because of the limitations of auto

and allografts documented in the previous section, synthetic grafts make for an appealing tissue-engineering alternative.

Synthetic Grafts

A variety of non-biological materials including polymers, metals, bioactive glasses, and ceramics have been used as potential bone substitutes.[24] Polymers are a promising scaffold choice because they allow for great design flexibility with regard to scaffold geometry and mechanical strength.[18] Polymers such as poly-glycolic acid (PGA), PCL, and poly(L-lactide-*co*-D, L-lactide 70:30) (PLDL) have been implanted in animal defect models[27] as well as subcutaneous sites[28] and have produced mineral with varying levels of success. PCL and PLDL, which can be fabricated with an organized microstructure and external shape, possess mechanical strength on the order of trabecular bone and have been seeded with cells for *in vitro* culturing purposes.[29, 30] Polymers can be composed such that they degrade inside the body at a designated rate. Ideally, this rate would be engineered so that the implant maintains its structural function until new tissue can take its place.[18, 31-34] Unfortunately, many polymers are hydrophobic in nature, which diminishes cell attachment and infiltration. Additionally, without a cellular or biological component, the scaffolds lack osteoinductive and osteogenic qualities. Cell attachment has been improved on polymers by modifying the surface chemistry,[35, 36] surface energy,[37] incorporating HA or other mineral composites in the polymer matrix,[38-40] as well as coating the polymer surface with bioactive molecules such as fibronectin and collagen.[41, 42]

Metals have been used extensively as bone replacements in joints since the 1950's,[43] however, they provide a temporary solution. Metals cannot biodegrade, remodel, or incorporate into the surrounding tissue. Additionally, they create a mismatch in mechanical properties at the bone/metal interface, which leads to stress shielding of the bone. Stress shielding causes resorption of the bone, thus loosening the implant, which often leads to fracture at the implant/bone interface.[44]

Bioactive glasses, which consist of varying amounts of sodium oxide, calcium oxide and silicon dioxide, can be formulated such that they will be completely non-resorbable *in vivo*. However, by altering the component amounts, it is possible to engineer a specific degradation rate until the material is entirely dissolved.[24] Both osseointegrative and osteoconductive, bioactive glasses form HA from Ca^{2+} and PO_4^{2-}, biocompatible ions that are released upon the glass's exposure to physiologic saline.[24] Unfortunately, bioactive glasses do not machine well and are prone to brittle fracture, which makes them unsuitable for load bearing applications.

HA comprises the mineral content in bone and therefore osteoblasts adhere to it with a high affinity. Sintering techniques have been developed to fabricate HA scaffolds with both ordered microstructures and, with the aid of micro-CT (to determine the correct geometry), physiologically accurate and useful macroscopic geometries.[45-47] Both synthetic and coralline (from processing calcium carbonate coral) forms of HA have been used as bone graft substitutes. Coralline HA has performed better because it resorbs more readily than synthetic HA and exhibits an interconnected pore structure which allows complete ingrowth of fibrous-osseous tissue.[18, 24] While these qualities make HA very attractive for certain tissue engineering applications, it is a slow degrading, very

brittle material with low toughness, which renders it impractical for use independently in load bearing applications.[24]

None of these synthetic scaffolds alone possesses all the components necessary for the ideal bone graft replacement. Composite scaffolds that possess both elastic (polymer) and stiff (ceramic or glass) constituents may be an efficient way to mimic the mechanical properties of bone as well as some level of osteoconduction, however, osteoinduction would be limited to cell recruitment from the surrounding host tissue without a cellular or bioactive contribution within the scaffold.

Cell Sources

A variety of cell sources have been investigated for bone-tissue engineering applications. The osteoblast phenotype is most readily expressed from osteoprogenitor cells, which have been directly harvested from bone marrow, periosteum, synovium, adipose tissue and skeletal muscle with varying levels of success.[48] Osteoblast populations have been culled from bone marrow, purified MSCs, differentiated osteoblasts, or genetically modified cells which over express specific bone marker proteins.[26] Bone marrow aspirates from the iliac crest contain osteogenic precursors and have been applied directly to fracture sites to treat non-unions as well as to grow bone ectopically before implanting into a defect. While there have been successes with cells from bone marrow, the paucity of actual osteoprogenitor cells (<0.001%) within an aspirate limits the efficacy of this source in a large number of applications.[26]

By plating bone marrow aspirate cells for 7 days and removing the non-adherent cells, a higher yield of osteoprogenitors can be obtained.[49] Researchers have shown that MSCs can be isolated and expanded more than 30 population doublings *in vitro* without

differentiating or losing osteogenic potential.[50] Implanting porous HA loaded with purified MSCs has resulted in significant increases in bone formation in both rat and canine segmental defect sites compared with acellular HA scaffolds.[26]

MSCs cultured *in vitro* have been further differentiated by the addition of the supplements Dexamethasone, sodium β-glycerophosphate and ascorbic acid.[48, 49, 51] Dexamethasone is a glucocorticoid that has been shown to significantly increase mineralization in 2-D cultures. Sodium β-glycerophosphate acts as a source of phosphate for cells to incorporate and organize with calcium into physiologic HA. Ascorbic acid is essential for collagen synthesis. These mature osteoprogenitors have then been seeded on coralline HA[52, 53] as well as PGA fiber meshes[54] prior to ectopic implantation and showed significant increased bone formation compared with undifferentiated MSCs.

Genetically modified cells such as MSCs and skeletal myoblasts have been engineered to over express the transcription factor Runx2, which is essential for controlling osteoblast differentiation and bone formation.[55, 56] After modification, these cells produce multiple bone marker proteins such as osteocalcin, osteopontin, and bone sialoprotein as well as significantly increase mineralized nodule production in both monolayer and 3-D cell culture.[27, 57] Genetic modification techniques may greatly expand the pool of potential cell sources by reprogramming cells found in abundance, such as fibroblasts or skeletal myoblasts, to behave like osteoblasts.

Cell and Scaffold Combinations

Multiple researchers advocate the combination of osteoprogenitors with a scaffolding matrix to accelerate and enhance bone repair.[18, 24-26] Chondrocytes have

been seeded on HA scaffolds and significantly increased bone formation in a rabbit ulna defect compared with acellular HA contralateral controls after 12 weeks.[58] rMSCs seeded on PLGA scaffolds in a rat femoral segmental defect model have exhibited healing characteristics comparable to autologous bone graft and significantly better than acellular PLGA scaffolds.[59] In addition to seeding osteoblasts on scaffolds just prior to implantation, other groups have precultured cellular constructs for multiple days before implanting them in rat calvarial defects.[5, 27] rMSCs seeded on titanium fiber meshes and precultured for 1, 4 or 8 days under static or flow conditions prior to implantation, showed decreasing levels of mineralization as culture time increased. However, perfused scaffolds produced more mineral than static controls after 4 subsequent weeks *in vivo*.[5] Unmodified rMSCs as well as rMSCs overexpressing Runx2, which were seeded on PLGA scaffolds, resulted in a 325 and a 2400-fold increase, respectively, in mineral volume within a rat calvarial defect as preculture time was increased from 1 to 21 days.[27] While the mineral from that study was localized to the periphery of the implant, the results suggest that creating mineralized templates through extended *in vitro* 3-D cell culture prior to *in vivo* implantation may improve the bone forming potential of the implant.

3-D Cell Culture Overview

Without a vascular blood supply *in vitro*, nutrient delivery to cells throughout 3-D tissue-engineered constructs grown in static culture must occur by diffusion. As a result, thin tissues (e.g. skin) and tissues that are naturally avascular (e.g. cartilage) have been more readily grown in static culture than thick vascular tissues such as bone.[60, 61]

Attempts to grow tissues greater than 1mm in thickness usually result in a thin shell of viable tissue and cells localized at the periphery.[6, 14, 27, 57] Ishaug-Riley found mineralization isolated to the outer 240 μm of 2mm thick poly (DL-lactic-co-glycolic acid) (PLGA) scaffolds seeded with rat calvarial and stromal cells.[6] Cartmell et al. reported a 500 μm thick layer of mineralized matrix at the periphery of 6mm ∅ by 3mm thick demineralized trabecular bone constructs seeded with rat calvarial cells.[14] It has been theorized that this effect is due to sub-optimal mass transport conditions in static culture. Therefore, tissue culture systems that provide dynamic media flow around or within tissue-engineered constructs have been designed to enhance nutrient and waste exchange *in vitro*.[7, 62-64] Such tissue culture systems may be useful as bioreactors to engineer thicker, more uniform tissues for implantation or as test bed models that simulate aspects of the *in vivo* environment. Tissue culture systems that incorporate dynamic media flow conditions for developing 3-D bone and cartilage constructs include spinner flasks,[2, 65-67] rotary cell,[68-71] concentric cylinder, and perfusion bioreactors.[11, 72, 73] In general, improved cell viability and proliferation as well as enhanced extracellular and mineralized matrix production have been demonstrated in such systems relative to static controls.

Spinner Flask Bioreactors

Spinner flasks have been used for both chondrogenic and osteogenic 3-D cell culture. Collagen hemostat scaffolds (11 mm ∅, 1.5 mm thick) were seeded with human bone marrow stromal cells and cultured for 5 weeks in a spinner flask at 50 rpm. Micro-CT analysis which employed anisotropic voxels (34 x 250 μm) showed mineral scattered

around the periphery of the construct, forming an incomplete ring.[2] To enhance mixing within spinner flask bioreactors, Bueno *et al*. introduced the wavy wall (WW) spinner flask for chondrocyte suspension cell culture. At 30 rpm, cell viability was decreased in WW cultures compared with smooth wall (SW) bioreactors. However, at 50 and 80 rpm, cell viability was indistinguishable between both groups. Additionally, the number of cell aggregates as well as the rate of aggregate growth was increased in WW bioreactors compared with SW bioreactors.[67]

Rotating Wall Vessels

Short-term (7 day) rotating wall experiments utilizing rat calvarial cells seeded on PLAGA microsphere scaffolds (4 mm ∅, 2.5 mm thick) have indicated an increase in calcium deposition as well as osteocalcin and osteopontin expression.[74] However, in addition to the short culture time, the concentration of β–glycerophosphate in the cell culture media far exceeded conventional supplement levels. Both of these conditions suggest that the mineral that was deposited was not physiologic in nature. Sikavitsas et al. seeded rMSCs on 79% porous, fibronectin coated, PLGA scaffolds (12.7 mm ∅, 6mm thick) and subjected them to spinner flask, rotating wall vessel, and static culture. After 21 days, all three experimental conditions yielded a similar number of cells/scaffold. However, constructs in the spinner flask produced a 6.6-fold increase in Ca^{2+} deposition compared with static culture and a 33-fold increase in Ca^{2+} compared with rotating vessel culture. Histology showed a thick layer of cells at the construct periphery, but a sparse cell distribution at the construct interior for all experimental groups.[66]

Concentric Cylinder Bioreactors

Concentric cylinder bioreactors are an attractive bioreactor design because they provide a uniform fluid shear loading environment for several constructs, facilitate dynamic seeding of scaffolds and possess good scale-up potential.[72] Higher seeding densities of primary bovine chondrocytes seeded on PLLA scaffolds produced a 2-fold increase in proliferation compared with the lowest seeding density. Increasing the rotation rate and shear stress applied to constructs resulted in significantly more collagen, but less glycosaminoglycan per construct.[72] The three previous bioreactor technologies all apply dynamic culture conditions to cell-seeded scaffolds, but none of them efficiently facilitates mass transport throughout the entirety of a thick construct. Possibly due to this limitation, they have been unable to consistently produce constructs that are populated with viable cells at the interior. Computational fluid dynamics analysis has shown that perfusion bioreactors address this limitation by actively forcing media throughout the full thickness of a scaffold, thus enhancing mass transport by active convection.[1]

Perfusion Bioreactors

The perfusion of culture media through porous 3D cellular constructs for bone tissue engineering purposes was first reported in 1998. 90% porous type I collagen sponges seeded with rMSCs and perfused at 1.3ml/min had increased cell viability and proliferation compared with static controls, especially in the center.[7] Alkaline phosphatase (ALP) (an early marker of osteoblast differentiation) production was upregulated in osteoblasts seeded on 80% porous PLGA foams that were perfused with media at 0.03 ml/second in comparison to static controls.[8] Cartmell et *al*. reported an

increase in cell viability at the center of MC3T3-E1 cell seeded trabecular bone constructs as flow rate decreased from 1.0 to 0.01 ml/min. However, expression of Runx2, osteocalcin, and ALP increased as flow rate increased from 0.01 to 0.2 ml/min.[64] rMSCs seeded on titanium fiber mesh scaffolds exhibited a crust of mineralized matrix on the upstream side of perfused constructs that increases in thickness as flow rate was increased from 0.3 to 3.0 ml/min.[9] Calcium content within titanium constructs was upregulated as media viscosity was increased in perfusion culture, suggesting a shear stress dependence on cell mediated matrix mineralization.[11] More recently, micro-CT has been used to quantify mineralized matrix production on rMCS seeded on large PCL+C scaffolds (6.35 mm ∅, 9 mm thick).[75]

Perfusion culture systems show promise in four specific areas: First, they may be used to cultivate mineralized constructs or stimulate biological implants that may perform better *in vivo* than non-preconditioned bone substitutes. Second, they may be used as a test bed for novel tissue engineering technologies prior to testing in animal or human models. Third, perfusion bioreactors may represent an improved model system for studying cell-mediated mineralized matrix production in a well-controlled environment. The isolation of each construct within a perfusion loop allows for individual monitoring of mineral development over time. Finally, they have the capacity to deliver specific flow mediated shear stresses as a function of flow rate, media viscosity and scaffold microarchitecture.

Effects of Fluid Flow on Cells

Improving *in vitro* mass transport is a critical challenge in producing thick cellular constructs. Several groups have developed bioreactors that perfuse cell-seeded 3-D constructs and demonstrated beneficial effects of perfusion on cell function and tissue growth. In addition to enhancing mass transport, fluid flow applies shear stresses to the cells within the scaffolds. The effects of flow-mediated shear on cells have been studied in 2-D monolayer cultures. Continuous fluid flow applied to osteoblasts *in vitro* has been shown to upregulate bone–related gene and phenotype expression.[76-81] Parallel plate flow experiments have shown that bone cells cultured in monolayer are highly responsive to flow mediated shear stresses. Shear stresses in the range of 5-15 dynes/cm^2 affect osteoblast proliferation as well as production of ALP, NO and PGE_2 (the last two instrumental in bone remodeling), suggesting that shear stress is an important regulator of osteoblast function.[77, 81-85] Additionally, shear stress has been altered on rMSCs seeded on 3-D titanium mesh scaffolds via elevated flow rates and increased media viscosity. The result was an increase in the thickness of the mineralized matrix crust on the upstream side of the scaffold.[10, 11] Pulsatile and oscillatory flow conditions applied to osteoblasts using *in vitro* parallel-plate flow chambers have also been shown to increase gene expression, intracellular calcium concentration, and the production of NO and PGE_2 in comparison to static controls.[15, 16] Furthermore, cell responsiveness has been reported to vary with fluid flow rate and frequency.[86, 87] Proposed mechanisms for the stimulation of cells by fluid flow include increased mass transport, generation of streaming potentials and application of shear stresses to the cell membranes.[16, 78] Although many of these studies were performed using 2-D cell culture systems for short-

term experiments, they suggest that variable flow conditions may also have differential effects in 3-D tissue culture systems.

Summary

The obstacles in creating a viable bone substitute are numerous, but the need for an, osteoinductive, non-toxic, structurally sound, biodegradable graft material is well documented. Using tissue engineering techniques to combine a porous polymer matrix with cell mediated mineralized matrix may result in an osteoinductive, non-brittle, load bearing bone graft substitute. Previous attempts to harness the osteoinductive and load bearing synergy of osteoblast cells and polymer scaffolds have resulted in heterogeneous distributions of mineral and cells localized to the periphery of 3-D constructs. It is now recognized that dynamic culture conditions may be beneficial for growing thick cellular constructs populated throughout with cells and mineralized matrix. However, multiple bioreactor systems have been unable to consistently produce thick constructs that are populated with viable cells and mineralized matrix at the interior. Perfusion culture systems that directly increase mass transport and deliver flow-mediated shear stresses to cells through the full thickness of 3-D constructs are a promising approach to generate large mineralized constructs that may serve as effective bone graft substitutes. Presently, a method to non-destructively quantify mineral deposition and spatial distribution during the course of an experiment has not been reported. The following work involves the design of a bioreactor that optimizes flow throughout a scaffold and allows for non-invasive monitoring of mineralized matrix deposition. Methods to improve osteoblast

attachment and function on large biodegradable polymer scaffolds as well as enhance mineralized matrix deposition and distribution are also addressed in the following studies.

CHAPTER 3 DEVELOPMENT OF A PERFUSION BIOREACTOR*

Introduction

In the absence of a vascular blood supply *in vitro*, nutrient delivery to cells throughout 3-D tissue-engineered constructs grown in static culture must occur by diffusion. As a result, thin tissues (e.g. skin) and tissues that are naturally avascular (e.g. cartilage) have been more readily grown *in vitro* than thicker, vascular tissues such as bone.[60, 88] When 3-D cellular constructs are grown in static culture, cells on the outer surface of the constructs are typically viable and proliferate readily, while cells within the construct may be less active or necrotic.[6, 51, 89] Rat calvarial osteoblasts cultured statically within 6 mm diameter by 3 mm thick demineralized trabecular bone scaffolds for 56 days produced a thin (less than 500μm) layer of mineralized matrix around the construct periphery (**Figure 3-1**).[14] Tissue culture systems that provide dynamic media flow conditions around or within tissue-engineered constructs are designed to enhance nutrient exchange and cell growth *in vitro*.[7, 8, 63] Improved cell viability, proliferation and extracellular matrix production have been demonstrated in such systems relative to static controls. Such tissue culture systems may be useful as bioreactors to engineer thicker, more uniform tissues for implantation or as test bed models that simulate aspects of the *in vivo* environment. An iterative design method was employed to design a perfusion bioreactor that could improve mass transport throughout the full thickness of

---

- Modified from

Cartmell, S.H., B.D. Porter, A.J. Garcia, and R.E. Guldberg, *Effects of medium perfusion rate on cell-seeded three-dimensional bone constructs in vitro.* Tissue Eng, 2003. 9(6): p. 1197-203

Porter, B., R. Zauel, H. Stockman, R. Guldberg, and D. Fyhrie, *3-D computational modeling of media flow through scaffolds in a perfusion bioreactor.* J Biomech, 2005. 38(3): p. 543-9

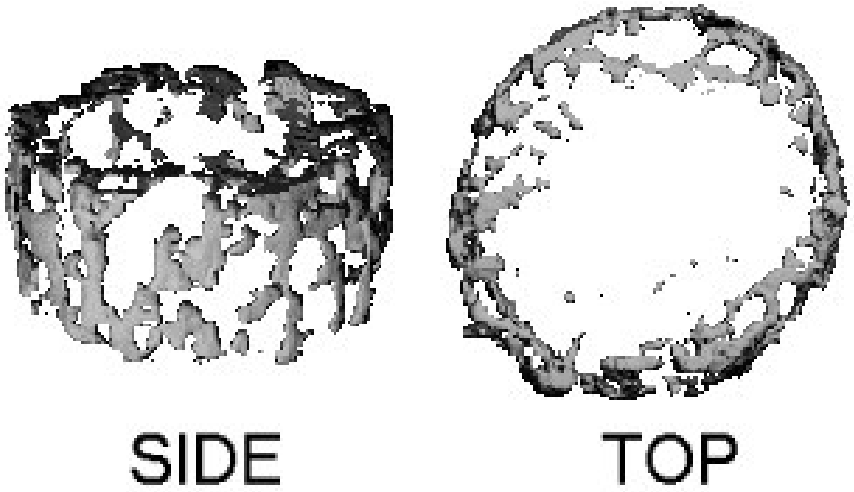

Figure 3-1. Micro-computed tomography image (16 μm voxel resolution) showing mineralization at the periphery of an 8-week stromal cell seeded demineralized trabecular bone matrix construct (6 mm ∅ x 3 mm thick).

large bone tissue engineering constructs.

In addition to enhancing mass transport, bioreactor systems may be used to deliver controlled mechanical stimuli such as flow-mediated shear stresses, matrix strains, or hydrostatic pressures to tissue constructs.[90-92] This general approach has been used to culture a variety of 3-D constructs including bone, cartilage, muscle, liver, and blood vessels.[71, 93-96] Tissue culture systems that incorporate dynamic media flow conditions for developing 3-D bone and cartilage constructs include spinner flasks,[97] rotary cell bioreactors[68-70] and perfusion systems.[2, 7-11] The shear stresses delivered by these bioreactors are a function of media viscosity and flow rate, bioreactor dimensions, and scaffold microarchitecture. However, calculating flow-mediated shear stresses within a complex 3-D porous structure is not trivial. Botchwey *et al*. used theoretical and experimental methods to estimate shear inside 3-D microcarrier scaffolds during high aspect ratio rotation. Assuming that flow through the scaffolds with an idealized pore structure of varying tortuosity obeyed Darcy's law, shear stresses were estimated within the microcarrier scaffolds.[98] While this approach provides an order of magnitude estimate of the average shear stresses, the distribution of shear stresses within complex 3-D architectures cannot be determined. Combining 2-D histology images with finite element computational fluid dynamics techniques, Raimondi et al. estimated local shear stresses on 400 x 300 micron sections of perfused mesh scaffolds seeded with chrondrocytes.[99] Although this method does estimate local shear stresses, it only includes a small 2-D slice of a much larger 3-D system.

A secondary aim of this work involved a collaboration with Dr. David Fyhrie and co-workers at Henry Ford Hospital in Detroit to model fluid perfusion through 3-D

scaffolds. The Lattice Boltzmann (LB) method with equilibrium distribution functions described by Martys and Chen was used to simulate cell culture media flowing through 3-D scaffolds with complex microarchitectures that were reconstructed using micro-CT.[100-102] Multiplying the symmetric part of the gradient from the resulting 3-D velocity field by the dynamic viscosity gave a distribution of the local internal shear stresses throughout the structure. This technique was validated by simulating flow through parallel plates and comparing the estimated shear stresses to the analytical solution shear stress values. Finally, flow fields were mapped and shear stresses were estimated within perfused 3-D biological and polymeric scaffolds in order to determine which bioreactor design and scaffold microarchitecture would result in the most uniform flow environment throughout the construct.

The goals of this study were to develop a novel 3-D tissue culture system, which delivered media throughout a cell-seeded scaffold via perfusion and investigate the influence of different continuous flow rates on constructs cultured for one week. MC3T3-E1 osteoblast-like cells seeded on cylindrical human trabecular bone scaffolds and perfused transversely showed differences in cell viability and proliferation when the media flow rate was varied. Computational fluid dynamics analysis indicated that scaffolds with heterogeneous microarchitecture produce non-uniform flow fields and highly variable local shear stresses on scaffold surfaces compared with scaffolds with uniform microarchitecture. Additionally, it was determined that an axial, rather than a transverse perfusion configuration, would produce a more uniform flow through porous constructs.

Materials and Methods

Cells

MC3T3-E1 osteoblast-like cells, derived from spontaneous immortalization of mouse calvarial cells selected by the 3T3 passaging protocol,[103] were kindly donated by Dr. Andrés García (Georgia Institute of Technology, GA) for use in this study.

Micro-Computed Tomography

Micro-CT imaging systems with associated stereology programs are widely used to non-destructively assess the 3-D morphology of radio-dense materials.[104] Two micro-CT systems (μCT-40 and VivaCT, Scanco Medical, Switzerland), consisting of a microfocus x-ray tube, a two-dimensional detector, and a fan beam reconstruction algorithm, were used for this thesis work to create three-dimensional images of various biological and polymer scaffolds with voxel sizes ranging from 16 to 34μm. Micro-CT scanning produces a data set made up of 3-D elements called voxels. Each voxel records the linear attenuation coefficient (a measure of the radiodensity of the sample) for its location in the sample that is scanned. The radiodensity is converted to a threshold scale (an integer between 0 and 1000). A threshold value is then selected for evaluation purposes to exclude voxels that are not radio-dense enough to be considered part of the sample. Image evaluation yields quantitative values for sample volume, pore size, porosity and architecture. Additionally, mineral density can be estimated using a radiodense standard that has been correlated to attenuation values acquired from calibration scans. For this study, micro-CT images were used to define the scaffold

architecture and physical boundary conditions for computational fluid dynamic simulations of 3-D fluid flow through a perfused construct.

Scaffold Preparation

Freeze-dried, gamma irradiation sterilized human trabecular bone (Georgia Tissue Bank, Atlanta, GA) was rehydrated by submersion in sterile phosphate buffered saline (PBS) for 1 hour prior to sizing. A trephine drill bit was used under sterile conditions to produce cylindrical scaffolds measuring 0.25" in diameter and length from the trabecular bone of several human femoral metaphyses. The cylinders were stored in sterile PBS at 4°C for 24 hours prior to seeding with cells. Micro-CT imaging was used to evaluate trabecular bone scaffold architecture (Figure 1B). Average porosity was 82% and average pore size was 645μm as determined by 3-D stereological analysis of micro-CT data.

Cell Seeding

Hydrated trabecular bone scaffolds were seeded in 24 well non-tissue culture treated plates with 2 million MC3T3-E1 immature osteoblast-like cells suspended in 100μl of culture medium (α-minimum essential medium) (GIBCO) containing 1% penicillin streptomycin and 10% fetal bovine serum (FBS) (Hyclone) per scaffold. MC3T3-E1 cells were selected for their ability to express proteins specific to the osteoblast phenotype and produce mineralized nodules when cultured *in vitro*. After 20 minutes, 2ml of culture medium was added to each sample. The cells were then allowed

to adhere to the constructs over a period of 24 hours prior to placement into the 3-D perfusion culture system.

Transverse Perfusion System Design

A novel 3-D tissue culture system was developed that facilitates controlled perfusion of culture media through cell-seeded constructs. For each perfusion rate experiment, eight cylindrical constructs were loaded into individual chambers of the 316L stainless steel perfusion block shown in the schematic in **Figure 3-2**. The vertical hole in the steel block, measuring 6.35 mm in diameter, defined the diameter for the cell-seeded scaffold. Media was added and removed from each reservoir using a syringe and a 19-gauge needle via a rubber sealed injection port. Side holes in the perfusion block allowed the entrance and exit of culture media to each of the independent chambers (**Figure 3-3**). Platinum cured silicone tubing connected the bioreactor to a multichannel reservoir containing 15 ml of culture medium per loop and ran to a Masterflex digital control peristaltic pump (Cole-Parmer). By compressing different sized tubing between rollers and a stationary cartridge, the pump head was capable of forcing media through the system at a rate between 0.01 and 6 ml/min. The entire system, minus the pump, was assembled on the benchtop and steam sterilized before use in the incubator.

Transverse Perfusion Culture

Constructs were inserted into the top hole of the stainless steel bioreactor and perfused transversely at continuous rates of 1.0, 0.2, 0.1 and 0.01ml/minute for 7 days. Static controls consisted of cell-seeded constructs cultured unconfined in non-tissue

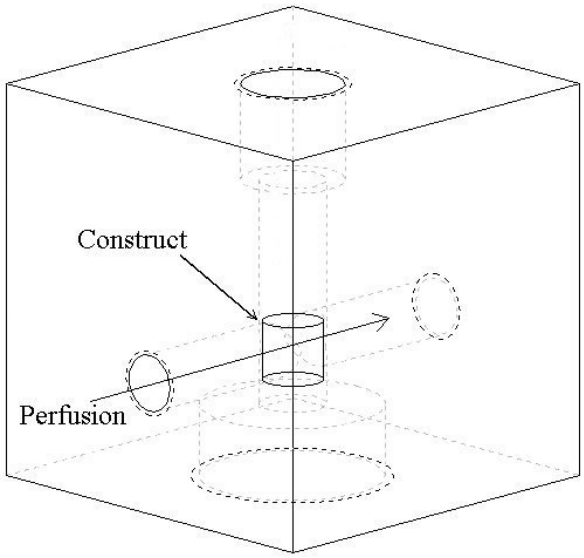

Figure 3-2. Schematic of a transverse perfusion chamber. Constructs were loaded into the bioreactor from the top. The vertical hole in the steel block, measuring 6.35 mm in diameter, defined the maximum diameter for the cell-seeded scaffold. A stainless steel cap was screwed into the top and bottom to seal the chamber.

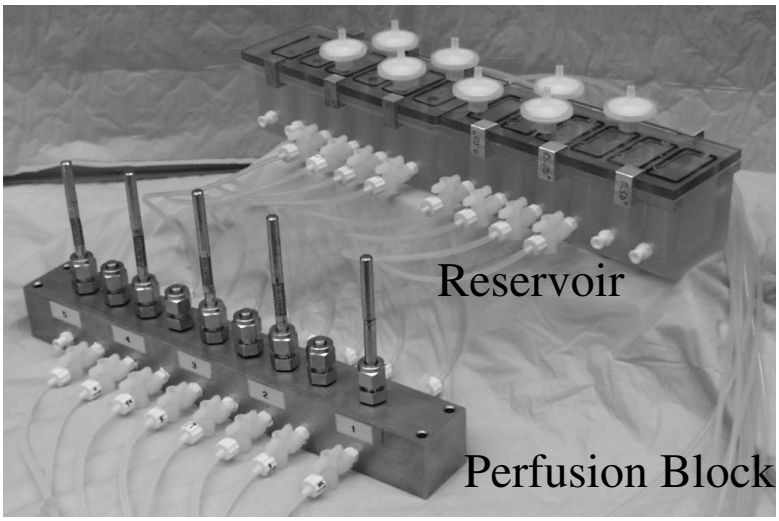

Figure 3-3. Closed loop transverse flow system. System was comprised of 316L stainless steel perfusion block with 8 individual chambers and corresponding polycarbonate block of reservoirs for culture media. Flow loop was attached to peristaltic pump (not shown) via two-stop platinum cured silicone tubing.

culture treated six well plates with 8 ml of complete culture media. Additionally, cell seeded constructs were inserted into stainless steel cubes with txo lateral ports, simulating the interior of the perfusion system. Cell culture media (α-MEM with glutamax, Invitrogen) was changed on day 2 and day 4 and contained 10% Fetal Bovine Serum (FBS), 1% penicillin-streptomycin, and standard osteogenic supplements (3mM β-Glycerophosphate, 50μg/ml ascorbic acid and 10^{-8}M dexamethasone) (Sigma). Acellular controls were also employed for each analysis group.

Cell Viability

At one and seven days, cell viability within perfused and static control constructs was assessed with a live/dead fluorescent stain (#L3224, Molecular Probes) that labels viable cells green (calcein) and dead cells red (ethidium homodimer). The cellular constructs were cut in half before staining to allow any cells in the center of the construct to be viewed. The stained cellular constructs were viewed using a laser scanning confocal microscope (Zeiss LSM 510UV).

Construct DNA Content

At one and seven days, constructs for each perfusion rate (n=6) were retrieved for total DNA content analysis in order to assess cell proliferation. Each cellular construct was placed into 1ml of PBE (phosphate buffered ethylenediaminetetraacetic acid (EDTA)) and stored at -80º C. Two freeze-thaw cycles were completed before crushing each construct using a mortar and pestle. Each sample was then sonicated to rupture cell membranes and release the cellular DNA into solution. Following centrifugation at

10,000g, 10µl of each sample was added to 200µl of working dye solution containing 10ng of Hoechst dye (Sigma) per ml of tris-EDTA-sodium buffer. A standard of calf thymus DNA (Sigma) was also prepared at 10µg/ml in PBE. The fluorescence of the samples was read on a 96 well black plate at 365nm excitation and 458nm emission.

Computational Fluid Dynamics Flow Modeling

A computational fluid dynamic modeling code based on the LB method was developed at Sandia National Laboratories [101] and adapted for this study at Henry Ford Hospital (Detroit, Michigan). The LB method breaks physical space into a large number of nodes, each comprised of a set of mass probability distributions. In each timestep, the distributions translate from node to node along any one of 18 fixed velocity vectors (**Figure 3-4**), and then undergo a collision step governed by Boltzmann theory that conserves physical properties such as momentum. We used the vector model described by Martys and Chen.[100] The end result is that the LB method approximates the Navier-Stokes equations to the second order and the model simulates a Newtonian fluid. Advantages of this method include the ability to model very complex geometries with few gridding constraints, as well as to run complicated models on modest computer hardware (e.g. ten million elements on a PC with 1.0 gigabyte of RAM). This LB code was previously validated for flow in complex geometries.[101, 102] An explanation of how the code works as well as the method for estimating shear stresses can be found in **Appendix 1**.

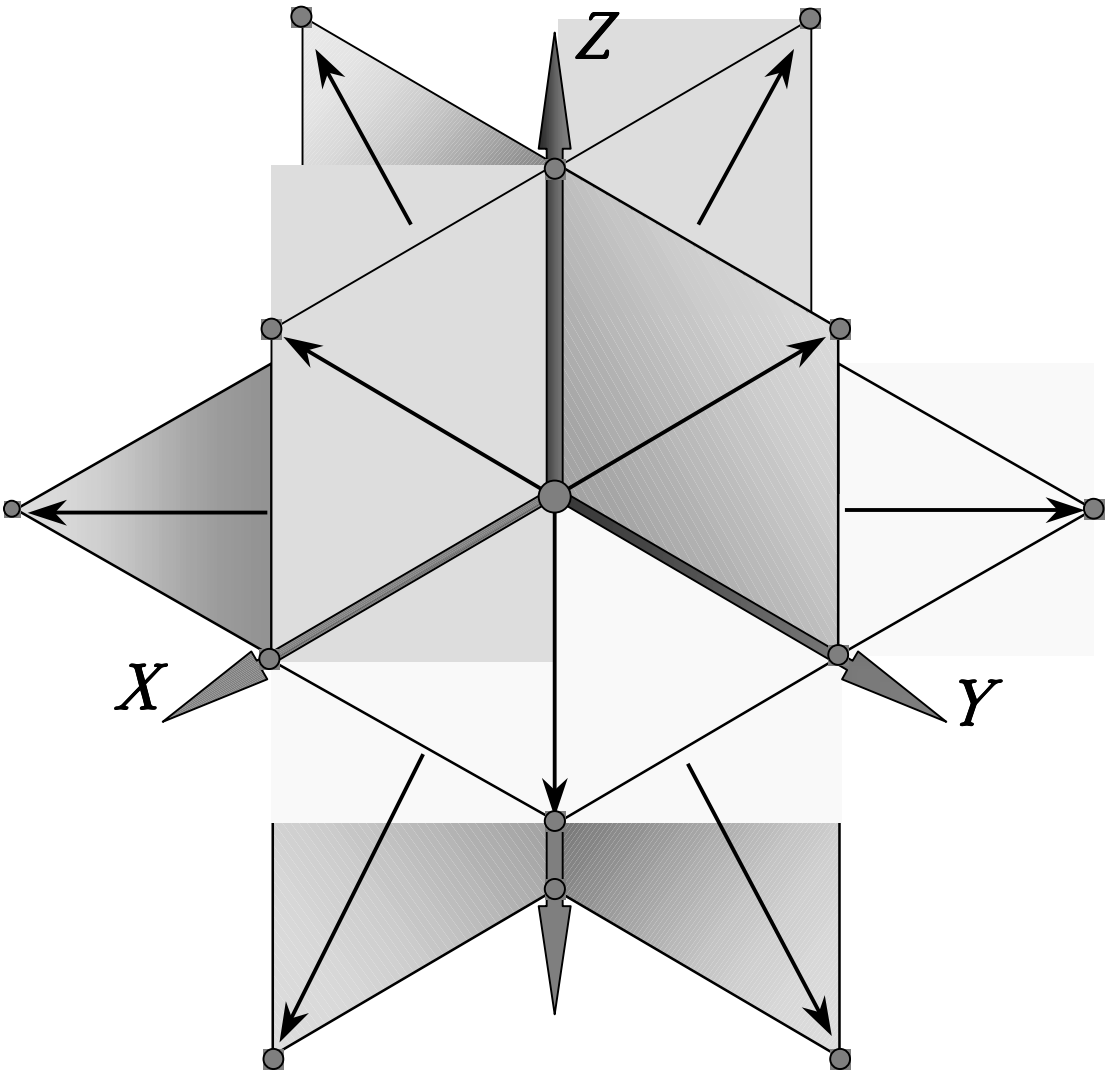

Figure 3-4. Lattice Boltzmann Vectors. Arrows represent fixed velocity vectors that mass probability distributions may travel along from node to node.

Validation of Shear Stress Estimation Technique

To validate the shear stress estimation technique, a parallel plate model was created which mimicked the flow conditions of Smalt *et al.* [105] and used to compare estimated shear stresses with the analytical solution stresses for flow between two infinite plates. The general 3-D model was comprised of two z-planes of 100x100 voxels, the upper and lower boundaries for a flow channel of user-specified gap width. Models with gap widths of 80, 160 and 400 microns between the planes were run with voxel sizes ranging from 1.6 to 26.67 microns.

The surface shear stress estimate, obtained from the derivative of the LB velocity field, was compared with the analytical solution one lattice unit (lu) away from the plane. The LB shear stress estimate was also compared with the value of shear stress directly at the wall given by the analytical solution to determine the overall computational error from the analytical surface shear stress.

Transverse Perfusion Modeling

To convert experimental space to the computer model, micro-CT scanning techniques were used to determine the microarchitecture of the trabecular bone scaffold at a resolution of 34μm (**Figure 3-5**). For the LB calculation, the geometry was coarsened so that each LB lattice unit corresponded to 68 μm, yielding approximately 2.5 million 3-D elements (220 x 112 x 100) in the total model. Of these, 1.2 million elements were fluid, 500,000 in the reactor and 700,000 in the feed pipe. The remaining 1.3 million elements were solid material, either in the scaffold or the surrounding casing. The cylindrical trabecular bone scaffolds were perfused transversely through the rounded

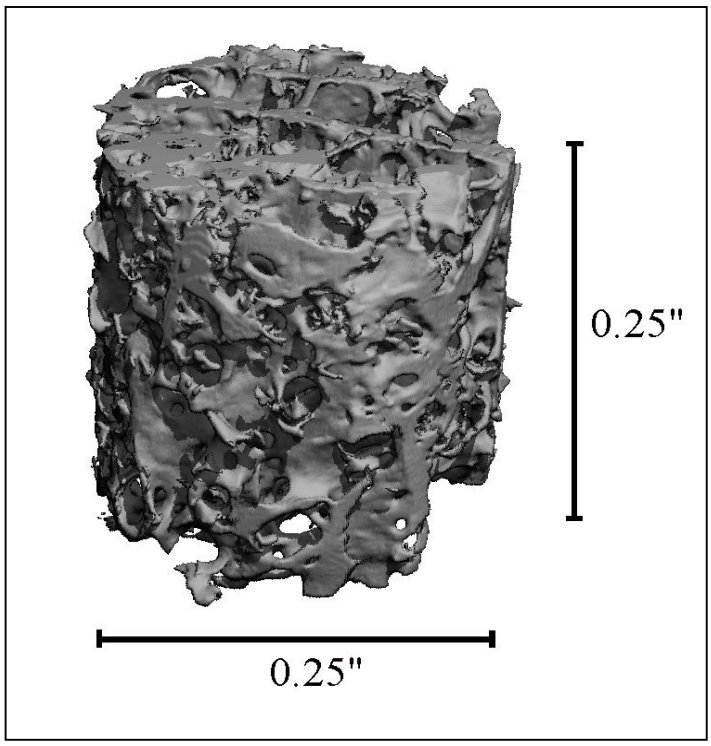

Figure 3-5. Micro-computed tomography image at 34 μm voxel resolution of typical human freeze dried trabecular bone scaffold. Bone was cleaned free of marrow and cells prior to use and sterilized by gamma irradiation.

surface at four different flow rates (0.01, 0.1, 0.2 and 1.0 ml/min), which was simulated in the computational model. The known volumetric flow was converted into an average linear velocity through the inlet cross section in μm/sec, then scaled to lu/timestep in computational space. Using a kinematic viscosity of 0.151384 mm^2/s, a gravitational body force was applied to the model until a steady-state bulk flow speed was achieved. The gradient of the flow field was calculated for the elements adjacent to the non-fluid elements and multiplied by the dynamic viscosity to estimate the local surface shear stresses.

Axial Perfusion Modeling

A second bioreactor design utilizing axial flow was built and modeled to compare fluid flow distribution with the transverse perfusion case. In this configuration, flow through two different polymer scaffolds (poly(l-lactide-*co*-dl-lactide) (PLDL) and polycaprolactone (PCL)) was modeled. PLDL scaffolds were comprised of ordered longitudinal pores combined with a random porous interconnected network which yielded a porosity between 75 and 85% and an average pore size of 300 μm **(Figure 3-6)**, while the PCL scaffolds were constructed with uniform, ordered microarchitecture throughout with an average porosity of 65% and average pore size of 500 microns **(Figure 3-7)**. Micro-CT images were used to define the scaffold architecture for the PLDL and PCL scaffolds. Flow simulations were run at 0.01, 0.1 and 0.25 ml/min for the PLDL and 0.2 ml/min for the PCL.

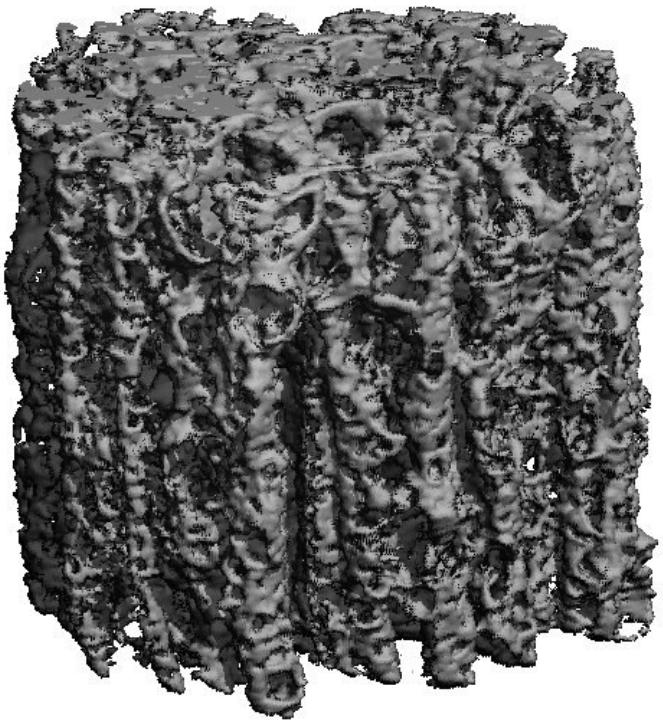

Figure 3-6. Representative micro-CT image of poly(l-lactide-co-dl-lactide) polymer scaffold with longitudinal pores between 100-200 μm combined with a random porous interconnected network. Scaffolds ranged in porosity from 75-85%.

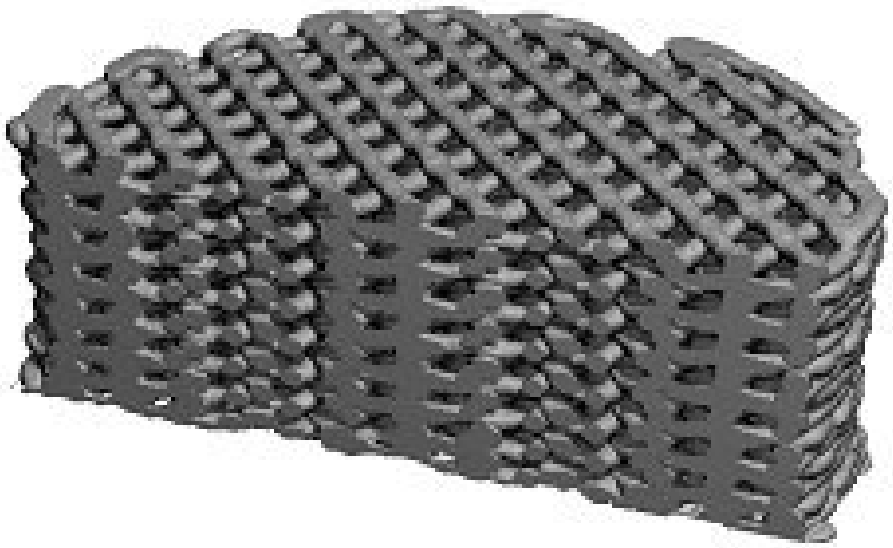

Figure 3-7. Representative polcaprolactone scaffold formed by fused deposition modeling. The architecture is ordered and uniform throughout the scaffold. Porosity can be varied between 55 and 85%.

Data Analysis

Data from sample groups were analyzed for statistical significance using a one-way ANOVA test using the Tukey least significance test for post-hoc comparisons with a significance level of $p<0.05$.

Cell Culture Results

General Observations

Initial perfusion culture attempts resulted in multiple infections. The source of these infections was traced to multiple media changes as well as the use of stopcocks, which regulated fluid flow during media changes. Non-sterile particles, which had accumulated on the stopcocks, were transferred into the tubing when the valves were rotated.

Cell Viability

Confocal microscopy revealed a clear influence of perfusion rate on cell viability (**Figure 3-8**). At day one, constructs showed adherence of MC3T3-E1 cells on the surface of the trabeculae both at the periphery and at the interior of the constructs. After one week in static culture, viable cells were nearly confluent on the periphery of the constructs, however, consistent with previous reports only a few viable cells were found at the construct center. The highest flow rate of 1ml/min resulted in nearly complete cell death throughout the construct after 7 days. Lowering the flow rate increased cell viability at both the periphery and the center of the constructs after one week of continuous perfusion. Flow rates of 0.2 and 0.1ml/min resulted in a mixture of viable and

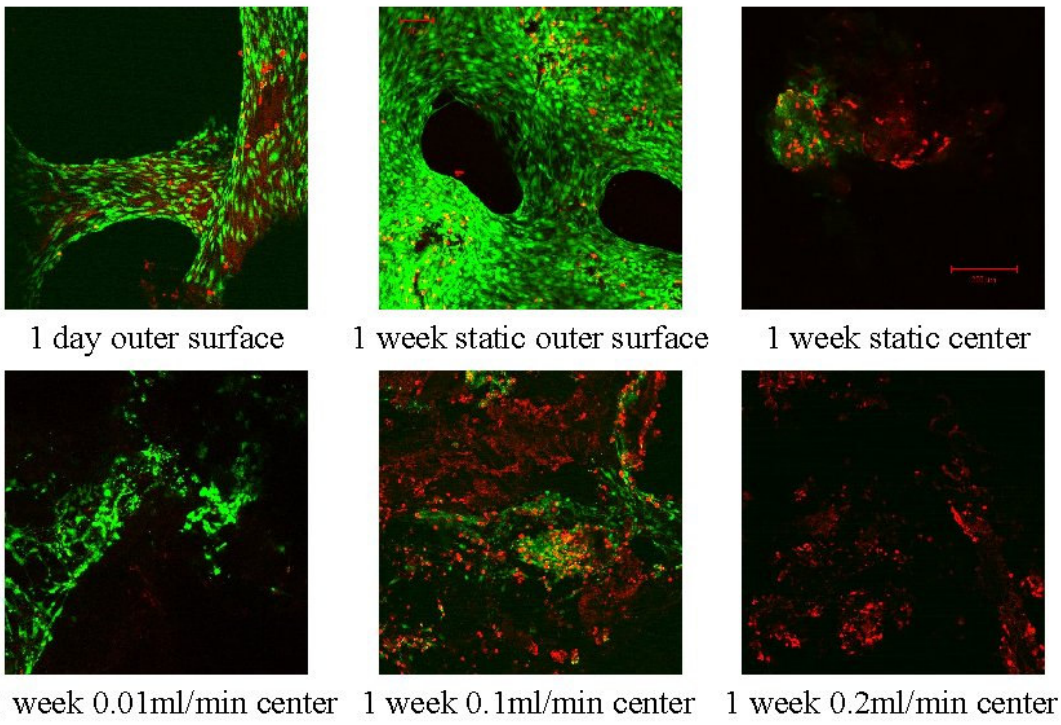

Figure 3-8. Laser scanning confocal microscopy (LSCM) images of cell viability on outer surface and in the center of trabecular bone scaffolds. Green:live, red:dead.

dead cells on the surface of the constructs with limited cell viability in the center. However, a flow rate of 0.01 ml/min resulted in a high proportion of viable cells both on the outer surface of the constructs and within the construct interior.

Cell Number

The effects of media perfusion rate on cell proliferation, as measured by total DNA content within the constructs, was consistent with the qualitative assessment of cell viability using confocal microscopy. Higher DNA levels were measured after 7 days of continuous perfusion at 0.01ml/min in comparison to both the 0.2ml/min and static control groups (**Figure 3-9**, $p<0.05$). There was also significantly greater cell proliferation in the 0.1ml/min group than in the 0.2ml/min group, however only the lowest perfusion rate of 0.01 ml/min enhanced cell number relative to static controls. As expected, negligible DNA was recovered from acellular control samples.

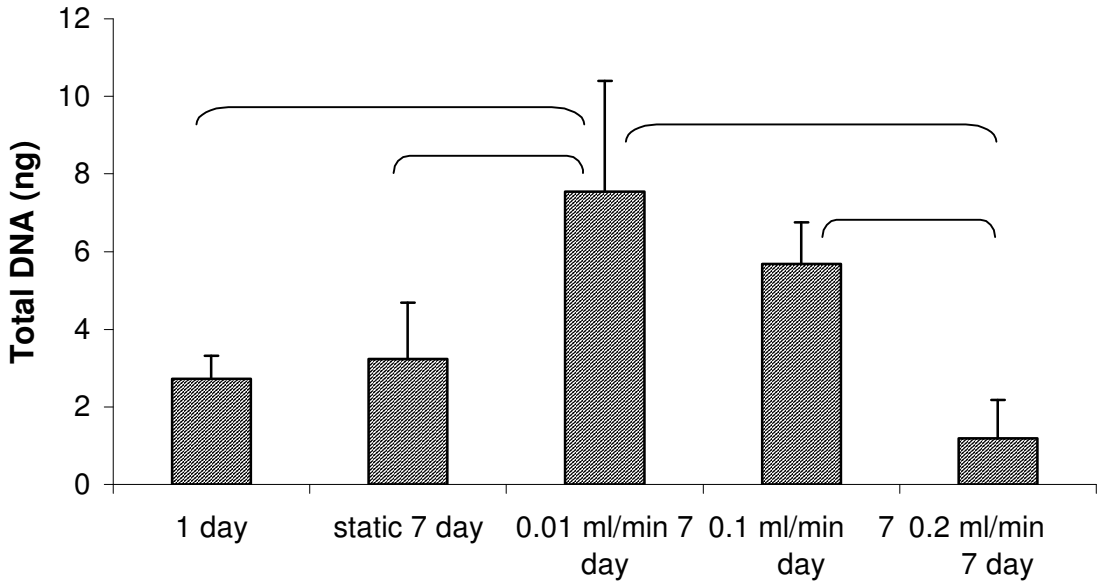

Figure 3-9. DNA assay results after 1 week of perfusion. 1 day – DNA from scaffold 1 day after it was seeded with 2 million MC3T3-E1 osteoblast-like cells, static 7 day – static sample (not perfused), 0.01, 0.1, 0.2 ml/min – flow rates for cell seeded scaffolds perfused for 1 week). $P<0.05$.

CFD Results

Accuracy of the LB Method for Shear Rates

While the LB method has been extensively validated for fluid velocities, the accuracy of the method for predicting shear rates at the solid-fluid interface is less obvious. The flow speed near solid walls is very low, and is influenced by the re-interpreted bounce-back condition. Therefore, we examined in detail the factors that influence shear rate estimation in the LB simulations.

Figure 3-10 illustrates the actual LB flow speed computations for Poiseuille flow between parallel plates (discrete diamond points), and the parabolic curve obtained from the bulk flow rate (averaged across the channel) and the equation:

$$U_{x(avg)} = -\frac{dP}{dx}\left(\frac{W^2}{12\mu}\right) \tag{4}$$

$U_{x(avg)}$ = bulk flow rate

W = width of the channel

dP/dx = pressure gradient

μ = dynamic viscosity

The points come close to the curve, even for this narrow channel, with W=3 lu. Some mismatch is expected because each point does not represent a discrete sampling of the parabolic velocities, but rather an integration of the parabola between 0.5 and 1.5 lu, 1.5 and 2.5 lu, and 2.5 and 3.5 lu on the y-axis. The shear rate at the solid-fluid interface in the model, dUx/dy (y=0.5), is desired. As indicated in **Figure 3-11**, using the difference method to determine a slope based on the first fluid node (0.5 lu out from the solid wall)

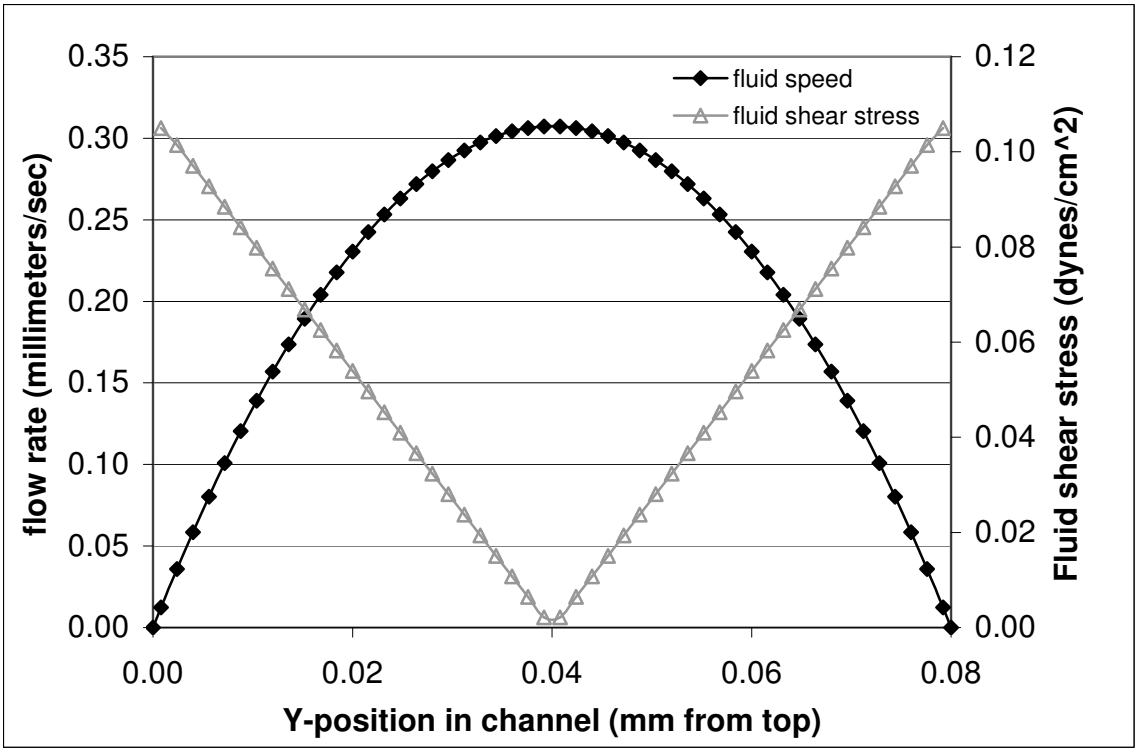

Figure 3-10. Lattice Boltzmann flow profile and shear stress estimate. Flow rate through the parallel plate model (note the parabolic flow profile) and the corresponding absolute value of shear stress for a voxel size of 1.6 microns, a plate gap width of 80 microns, and a volumetric flow of 31 µl/min.

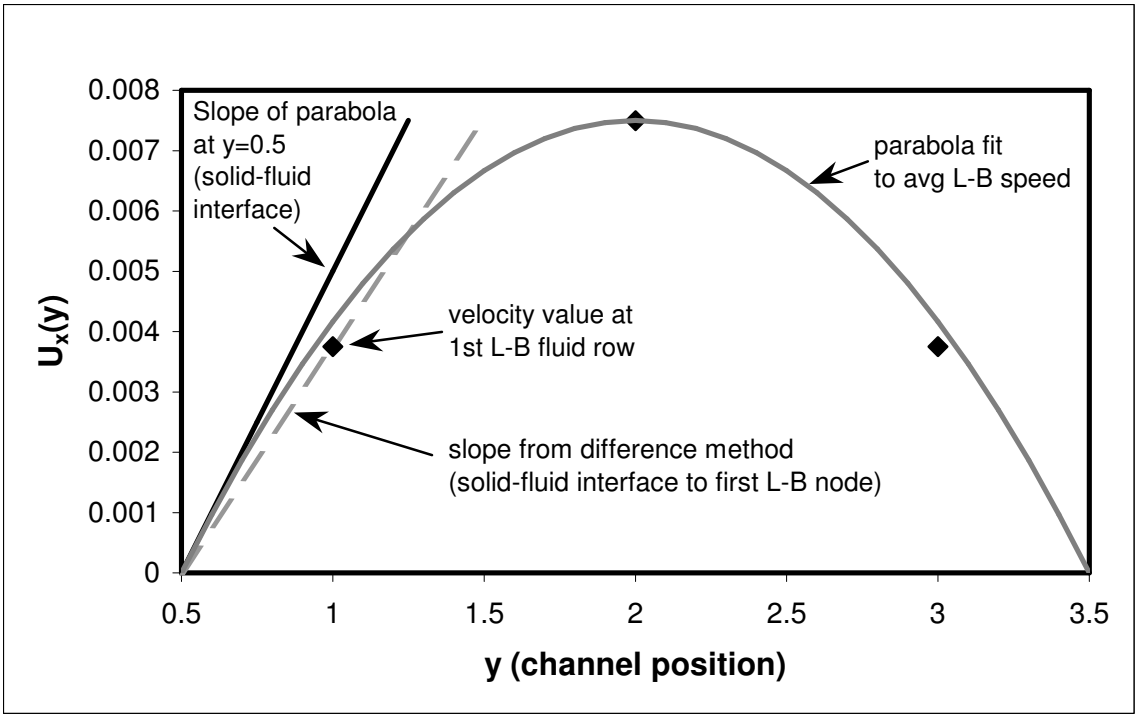

Figure 3-11. Evaluating two methods to estimate wall shear for parallel plates separated by 3 LB nodes. The dashed line shows the slope estimated from the change in velocity, U_x, at the first node in the fluid compared with the solid-fluid interface using the difference method; the solid line shows the slope of the line tangent at the solid-fluid interface to the parabola that fits the average lattice boltzmann velocity values in the channel. The placement of the wall at 0.5 and 3.5 lu is explained in Appendix 1.

would always underestimate the shear rate. In the parallel plate case, the error can be determined exactly because there is a simple analytical expression for *dUx/dy*. However, with an irregular geometry no analytical solution is known, so shear rate must be estimated from the nodes adjacent to the wall.

The parallel plane LB models exhibited well-developed parabolic flow (**Figure 3-10**), which corresponds to the result from the analytical solution. Combining the LB method and equation 3 linearly underestimated shear stresses at the wall compared with the analytical solution by the function:

$$Y = 160.59x \quad (R=0.9982) \qquad (5)$$

Y = percent error underestimation

x = lu/channel

Figure 3-12 indicates that if a pore is 10 voxels wide, the difference method will underestimate the shear stress at the pore wall by 16%. The LB method produced a more accurate estimation of the shear stress when compared with the analytical solution at specified distances away from the wall. A channel 10 lu wide resulted in underestimating the shear stress by 5.7% at 0.5 lu away from the wall. At a distance 1.5 lu away from the wall, the estimation improves such that channels only 6 lu wide are within 5% of the analytical solution.

Perfusion Flow Profiles and Shear Stresses

Flow through the scaffold microarchitecture was highly non-uniform, the highest speeds were found at the center of small orifices, while the lowest speeds occurred at scaffold surfaces and chamber walls (**Figure 3-13**). **Figure 3-13** also shows high

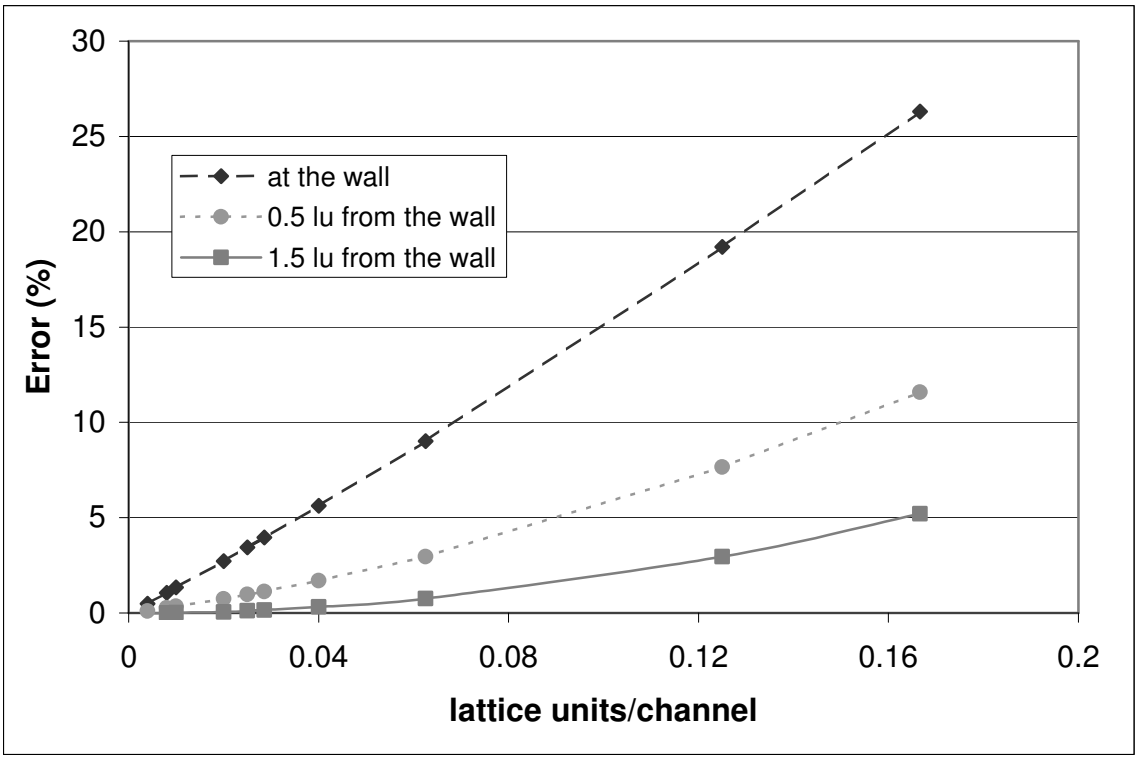

Figure 3-12. Lattice Boltzmann accuracy away from wall. The LB method underestimates shear stress compared with the analytical solution. The percent error varies as a function of the lattice units (lu) per channel and distance from the wall. The estimation improves upon moving away from the channel wall and/or by increasing the number of lu per channel. The accuracy of the LB solution is within 5 percent both at the wall with channels greater than 25 lu (lu/channel = 0.04) or at a distance 1.5 lu away from a solid-fluid interface with channels 6 lu wide.

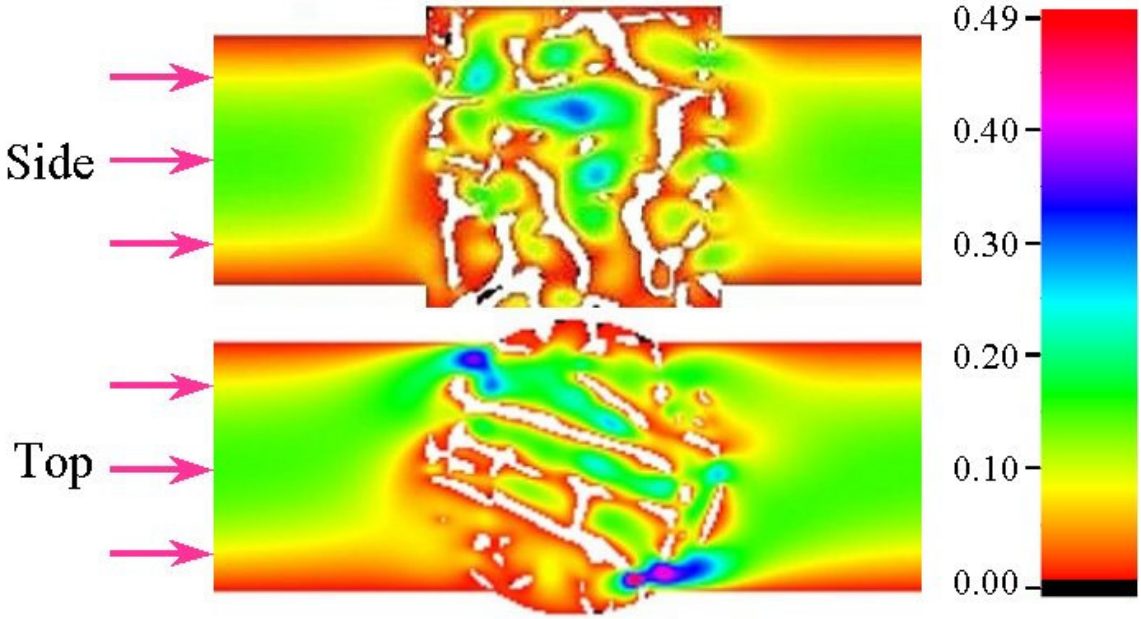

Figure 3-13. Velocity flow field (top and side views) throughout a transversely perfused cylindrical trabecular bone scaffold. Units of media flow speed are in mm/sec, trabecular bone shown in white. A no slip condition is satisfied at the boundary.

velocity flow at the rounded edges, indicating a path of least resistance at the interface between the rounded surface and the bioreactor chamber wall for the plane that was analyzed. The highest values for local shear stresses were found on the surfaces of small channels in the scaffold (**Figure 3-14**). Transversely perfused cell-seeded scaffolds with a mean surface shear stress (using the LB method with no correction factor) of 5×10^{-4} dynes/cm^2 correlated to the highest cell viability and proliferation at a flow rate of 0.01 ml/min. Flow rates above 0.2 ml/min were detrimental to cell viability with this cell and scaffold combination. Our results suggest that estimated shear stresses associated with enhanced cell number after one week of continuous transverse perfusion through 3-D constructs were considerably lower than those typically used in short-term 2-D parallel plate flow experiments.

Axial models indicated that shear stress values on the PCL and PLDL scaffold surfaces were comparable to one another for similar flow rates. However, flow through PLDL scaffolds was heterogeneous, while the flow distribution within PCL scaffolds was much more uniform **(Figure 3-15)**.

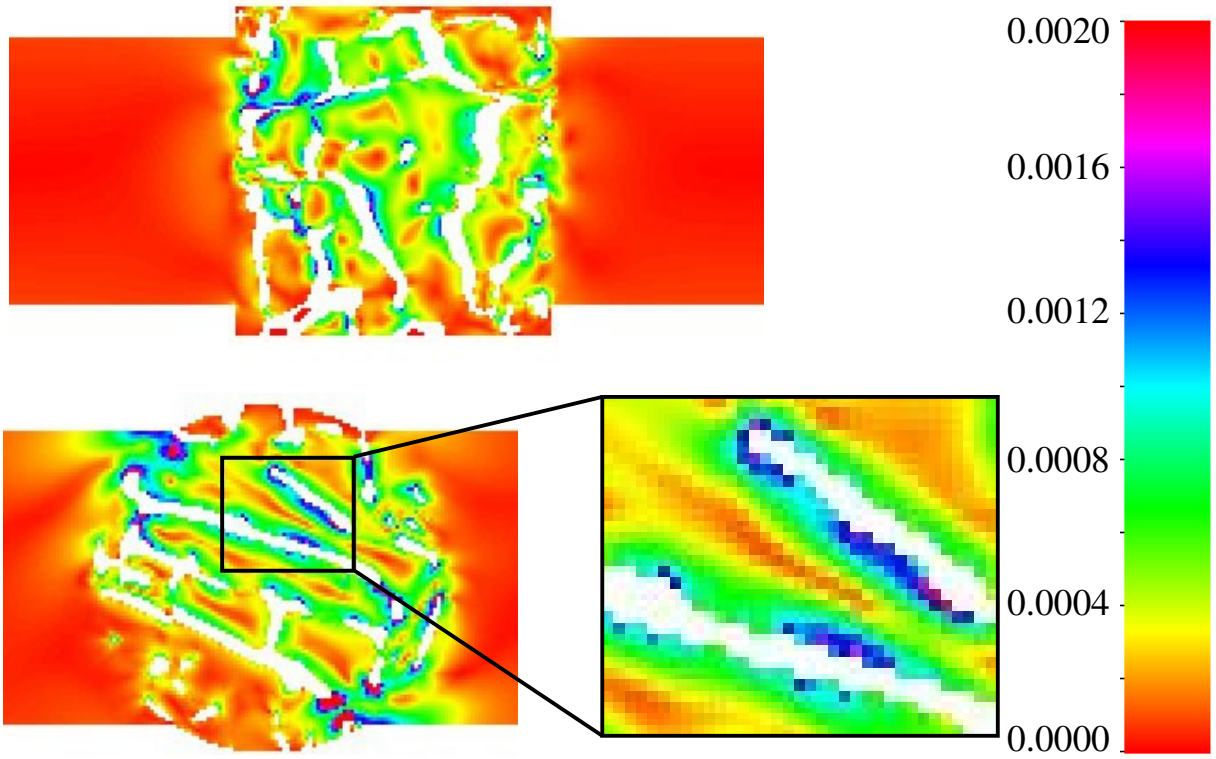

Figure 3-14. Local shear stress field. Map of shear stresses (dynes/cm^2) in media transversely perfused through a 3D trabecular bone scaffold

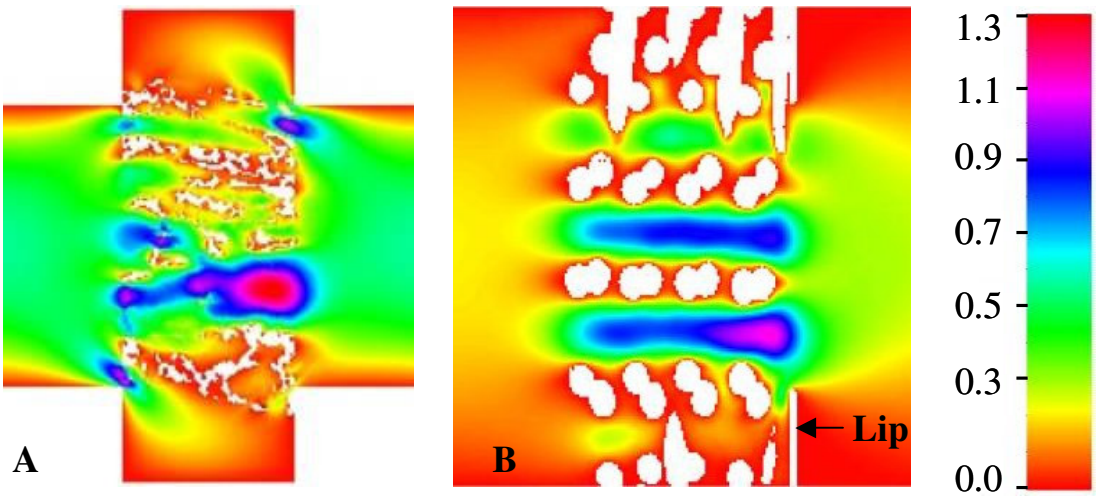

Figure 3-15. Fluid velocity map through PLDL (A) and PCL (B) scaffolds. The scaffold architecture of the PLDL results in a more heterogeneous distribution of flow throughout the scaffold. The downstream lip on the PCL case restricts flow to the periphery of the scaffold. The units of flow are mm/s.

Discussion

A critical barrier to the development of 3-D tissues *in vitro* is the limited transport of nutrients and metabolites within the construct interior. As a result, reduced cell viability or activity is typically observed at the center of tissue constructs grown in static culture. The goal of this study was to develop a perfusion tissue culture system to enhance cell viability and increased cell proliferation in 3-D cell-seeded bone constructs at low continuous perfusion rates compared with static controls.

This experimental study optimized 3-D perfusion cell culture techniques, evaluated the effect of media flow rate on cell number and viability, analyzed the effect of scaffold architecture and bioreactor orientation on fluid flow through a construct. A critical obstacle to long-term perfusion cell culture is infection. Several perfusion experiments were repeated due to infections, developed during the week. One cause of infection in the initial perfusion systems was due to the use of a sterile stopcock, which restricted fluid flow during media changes. Even though the stopcocks were cleaned with EtOH before opening and closing the valves, rotating the stopcock introduced non-sterile particles into the tubing, which subsequently contaminated the system. Handling the system (taking it in and out of the incubator) increased the possibility of infection; therefore the number of media changes per week should be reduced.

Various fluid flow conditions have been shown previously to regulate cell activity in 2D culture systems. Continuous fluid flow applied to osteoblasts *in vitro* has been shown to upregulate bone–related gene and phenotype expression.[76, 78-81] Pulsatile and oscillatory flow conditions applied to osteoblasts using *in vitro* parallel-plate flow chambers have also been shown to increase gene expression, intracellular calcium

concentration, and the production of NO and PGE_2 in comparison to static controls.[15, 16] Furthermore, cell responsiveness has been reported to vary with fluid flow rate and frequency.[86, 87] Proposed mechanisms for the stimulation of cells by fluid flow include increased mass transport, generation of streaming potentials and application of shear stresses to the cell membranes.[16, 78] Although these previous studies were performed using 2-D monolayer culture, they suggest that variable flow conditions may also have differential effects in 3-D tissue culture systems.[16]

While MC3T3-E1 cells do not produce a large amount of mineralized matrix compared with primary cells, they are known to maintain their phenotype out to 20 passages, which is advantageous for cell expansion purposes.[106] Since a large number of cells (1-2 million) were required to seed a small tissue-engineering scaffold (6mm ∅ x 3mm thick cylinder), MC3T3-E1 cells were a logical choice for use in 3-D cell culture proof of concept studies. These cells represented an economical way to attempt pilot experiments without sacrificing animals in order to harvest and use primary cells.

Cell Culture Results

Total DNA results following seven days of continuous perfusion were consistent with qualitative assessments of cell viability using confocal microscopy. **Figure 3-6** indicates that differences in the number of viable cells were most evident at the center of the constructs. In support of this qualitative observation, significantly more DNA was isolated from samples perfused at 0.01 ml/min in comparison to both static controls and samples perfused at 0.2 ml/min **(Figure 3-7)**, indicating that a very low perfusion rate was able to maintain a higher number of viable cells compared with static and other flow

groups. In addition to improved mass transport throughout the constructs, perfusing media at lower rates may also have allowed for autocrine effects to positively affect proliferation and cell adherence. Soluble proteins released by cells may have been flushed away at higher flow rates before exerting an influence on neighboring cells.

Live/dead staining and confocal microscopy showed an increasing level of cell death within the constructs associated with increasing the perfusion rate from 0.1 to 1.0 ml/min. Elevated shear stresses at the higher perfusion rates may have been responsible for the observed decrease in cell viability. The DNA present after one week of perfusion at 0.2ml/min was lower than the one-day seeded sample indicating that the original cell number had actually decreased. The loss in cell number may be due to cells being sheared off the construct due to the higher flow rates. Additionally, cells have been shown to differentiate down the osteoblastic lineage and produce mineral due to flow-mediated shear stresses in the absence of dexamethasone.[107] Therefore, the increased flow rates and associated shear stresses may have stimulated differentiation in conjunction with a decrease in cell proliferation. Although continuous perfusion at 0.1-1.0 ml/min was not beneficial to cell viability and proliferation, transient increases of flow rate superimposed on continuous slow perfusion may simultaneously enhance mass transport and accelerate osteoblast differentiation via shear stress mechanostimulation.

Much of the variability in our results may have been due to the trabecular bone scaffolds, which possess unknown levels of residual osteogenic growth factors. These bioactive factors might have masked whether proliferation and viability results were due to perfusion parameters or non-uniform local environments. During long-term culture these factors may also affect mineralized matrix deposition and may confound perfusion

effects. Therefore, polymer scaffolds with known material, mechanical and degradation properties offer an attractive alternative to trabecular bone for isolating effects cell culture conditions on mineralized matrix formation.

Computational Fluid Dynamics Modeling

A variety of perfusion systems have recently been developed in an effort to enhance the development of 3-D tissue constructs *in vitro*.[2, 7, 8, 10, 108] The effects of various media flow rates on cell behavior and matrix synthesis have typically been reported for these systems. Unfortunately, due to the dissimilar geometry of the perfusion systems and scaffolds used, the local shear stresses experienced by the cells can be vastly different even for the same input flow rate. An improved understanding of the local internal shear stresses experienced by cells under flow conditions in a 3-D scaffold as a function of flow rate and microarchitecture might aid in identifying culture conditions which would impart appropriate shear stresses as well as improve mass transport throughout constructs for enhanced cell proliferation and activity. A method to estimate shear stresses within 3-D constructs as a function of flow rate, scaffold microarchitecture, and bioreactor boundary conditions would also improve comparisons between perfusion culture systems.

Parallel plate simulations demonstrated that the accuracy of the LB shear stress estimates linearly increased as the number of lu per channel increased **(Figure 3-10)**. The accuracy of the LB technique also improved when the shear stress estimates further away from the wall were compared with the analytical solution, regardless of the relative voxel and channel sizes. Models with few nodes between plates can present special problems

for the interpretation of shear rates due to the discretization at the wall that is pronounced when using the finite differences method. Additionally, the voxel nature of the model results in an uneven surface on which to calculate shear stresses. As described in **Appendix 1**, the interface between the solid and the liquid is designated halfway between the fluid and solid nodes in order to utilize the "re-interpreted bounce back condition." Using this method, some of the LB fluid is resident in the solid nodes and must be considered in an account of the applied body force. This effect is lessened when more nodes are used to represent the same solid. As the voxel size decreases, the model performs better. One technique to improve the derivative accuracy would involve fitting a quadratic function to the nodes nearest the solid fluid interface and then differentiating the equation at the interface. A simpler method to improve the derivative accuracy would be to scan complex geometries at a smaller voxel resolution but at the cost of increasing the overall model size. The trabecular bone scaffolds had an average pore size of 645 microns and the models were comprised of 68-micron elements, a ratio of 0.105. This translates to an average underestimation of the shear stress by 16% at the wall. Since the accuracy varies depending on the ratio of voxel size to pore size, the correction factor from this plot can be used more effectively for scaffolds possessing a regular geometry with uniform pore size. Although trabecular bone scaffolds were used for this study, micro-CT imaging can provide micro architectural geometry for a wide variety of scaffold materials including porous polymers with regular microstructures.

Using the LB method and combining the 3-D modeling with the experimental data indicated that a mean surface shear stress of 5×10^{-4} dynes/cm^2 correlated to an increased number of cells seeded on transversely perfused trabecular bone scaffolds.

Peak shear stresses of 0.57 dynes/cm^2 were associated with cell death and a lower number of cells within the constructs. Although few direct comparisons exist, Raimondi et *al*. used a commercial finite element code and estimated shear stresses of 3 x 10^{-2} dynes/cm^2 within hyaluronic acid mesh scaffolds seeded with chondrocytes.[99] Therefore, the estimated shear stresses on construct surfaces from these perfusion studies were lower than those reported in 2-D flow experiments.

Shear stress magnitudes that are conducive for short-term monolayer flow studies may not be appropriate for long-term continuous 3-D perfusion studies for the following reasons. First, 2-D studies are performed on confluent monolayers, while the 3-D surfaces in our system supported subconfluent cell populations. Second, 2-D studies are generally performed over a matter of hours while the 3-D constructs were continuously perfused for a full week. Third, cell adhesion strength may be different for monolayer culture on tissue culture plastic compared with adhesion strength on various 3-D synthetic and biological materials, which could result in very different shear stress requirements for enhancement of cell growth and function. Finally, although the focus of the current study was to estimate local shear stresses, it should be noted that fluid flow also results in an increase in chemotransport, which may be very different in 2-D and 3-D culture environments. [109]

CFD model results showed that the trabecular bone scaffold architecture produced a non-uniform flow field that resulted in areas of high shear stress localized to smaller pores within the construct. Additionally, the transverse model provides a challenging set of computational boundary conditions for future CFD modeling. It is impossible to know the exact rotational orientation of the construct within the bioreactor and therefore the

architecture of the scaffold is difficult to ascertain with respect to the feed pipe. CFD modeling of longitudinal flow through the cylindrical scaffold circular cross section indicated that axial perfusion through PCL rather than PLDL scaffolds would facilitate more uniform fluid flow within the construct. Therefore, PCL polymer scaffolds that can be fabricated with a controlled and ordered microstructure using fused deposition modeling are a promising scaffold choice.

Conclusions

A low continuous flow rate enhanced the number of cells as well as cell viability at the interior of perfused trabecular bone constructs. During long-term culture, the residual bioactive factors in trabecular bone scaffolds may affect mineralized matrix deposition and also confound or mask the effect of perfusion on mineralized matrix deposition. Perfusion culture was highly susceptible to infection; therefore a simple system and cell culture method requiring a minimal number of media changes per week should be developed and implemented. CFD results indicated that shear stress values within 3-D scaffolds beneficial for cell growth and function are much lower than those used in monolayer culture. Additionally, axial perfusion through a scaffold with regular architecture resulted in a uniform flow throughout the construct. Therefore, a longitudinal perfusion system was designed and built to accommodate cylindrical, PCL polymer scaffolds measuring 6 mm in diameter and up to 10 mm in length. This bioreactor system was used to carry out all further experiments for this thesis.

CHAPTER 4 EFFECT OF PERFUSION ON CELL VIABILITY AND MINERALIZED MATRIX PRODUCTION

Introduction

Creating a biologically active, load bearing, bone graft substitute will require an appropriate scaffold material that facilitates cell attachment, retention and differentiation during culture time *in vitro*. The scaffold should be easily formed into anatomic shapes, possess structural integrity, and be comprised of a material that the body can remodel after implantation.[18, 24-26] Attempts to create osteoconductive and osteoinductive implants have taken a variety of approaches.[2, 10, 27, 66, 69, 74, 107] Cartmell and co-workers quantified mineral deposits on cell seeded 3-D polymer and demineralized bone matrix scaffolds after 4, 5, 6, 7 and 8 weeks in static culture using micro-CT at a voxel resolution of 16 μm.[14] Those culture conditions produced thin tissue growth localized to the construct periphery possibly due to mass transport limitations. Media perfusion bioreactor systems developed to overcome this limitation have been shown to enhance overall cell viability and matrix synthesis.

Perfusion culture has recently been used to increase osteogenic cell activity and matrix mineralization within a variety of scaffold materials.[2, 10, 11] Van Den Dolder, Sikavitsas and others have perfused titanium mesh scaffolds for 16 days and shown a distribution of mineral, which is localized to the top surface of the construct. That crust of mineral increases in thickness as the flow rate or shear stress is increased.[9-11, 66] Meinel *et al.* used low sensitivity micro-CT (35 x 250 μm voxel resolution) to display a heterogeneous mineral distribution within 1.5 mm thick perfused silk and collagen mesh

constructs seeded with human MSCs after 5 weeks of culture.[2] None of these approaches has resulted in a biodegradable construct possessing mechanical properties of bone, which is populated with mineralized matrix throughout the thickness of the scaffold.

Based on our findings documented in Chapter 3 regarding bioreactor flow orientation, we developed a bioreactor that can axially perfuse cylindrical scaffolds measuring 6.35 mm in diameter and up to 10 mm in length. Frequent media changes would be necessary in these experiments because the osteogenic supplement ascorbic acid, which is necessary for collagen synthesis, degrades within 48 hours. Ascorbic acid 2-phosphate (AA2-P), a more stable formulation of ascorbic acid, has been shown to maintain its activity after a week at 37° C and upregulate collagen and procollagen synthesis in human dermal fibroblasts.[110] However, the effect of substituting AA2-P for AA on mineralized matrix formation in 3-D culture has not been reported. Therefore, a study based on the work of Cartmell and co-workers[14] was completed which compared the effect of AA vs. AA2-P on matrix mineralization within 3-D constructs grown in static culture. A second experiment to evaluate the effect of media change frequency on mineral production was performed in monolayer culture. These studies are documented in **Appendix 2**.

The results from Chapter 3 also indicated that perfusion through a polymer scaffold with an ordered microstructure would produce a more uniform flow field throughout the construct compared with a scaffold with a random interconnected pore structure. Using a fused deposition modeling technique, polycaprolactone (PCL), a

biodegradable polymer, can be assembled into a lattice structure, which possesses mechanical strength and modulus on the order of those measured for trabecular bone.[111]

Experiments in our lab have shown that rMSCs do not attach well to untreated PCL scaffolds (data not shown here). Confocal microscopy revealed very few cells attached to the scaffold after one and seven days in culture. Therefore, in an attempt to improve cell adhesion and function, we evaluated the effects of lyophilizing Type I collagen into PCL scaffolds (PCL+C) or coating PCL scaffolds with fibronectin (PCL+FN) on cell viability and mineralized matrix synthesis. The end goal was to determine if perfusion would upregulate cell-mediated mineralized matrix deposition within a composite PCL seeded with rMSCs. The distributions of viable rMSCs on static and perfused constructs were identified using fluorescent stains combined with confocal microscopy. Additionally, we employed micro-CT based measurement techniques to quantify the effects of media perfusion on the amount and distribution of mineralized matrix deposition. It was hypothesized that perfusion would enhance cell viability and mineralized matrix deposition within polymeric constructs compared with static controls. It was also hypothesized that the two different scaffold treatments would modulate mineralized matrix production.

Materials and Methods

Cell Harvest

Cells were harvested after euthanizing Sasco Sprague Dawley rats via CO_2 inhalation. Under aseptic conditions, hind limbs were dissected and soft tissue was removed. The ends of the femora and tibia were clipped and the marrow was flushed out

with media (α-MEM with Pen Strep, Invitrogen) using an 18-gauge needle. Cell aggregates were broken up by trituration using a 10ml pipette and plated with media containing 10% FBS and 1% antibiotic/antimycotic at a density of 75 million cells per 100mm dish for 45 minutes to allow macrophages to adhere. The cell suspension was then collected and replated at 150 million cells per T-150 flask. After 2 days, non-adherent cells were aspirated and fresh media was added. Cells were grown for a week until confluence and then lifted off the flask with trypsin (0.25% trypsin with EDTA, Invitrogen) and frozen in 90% FBS and 10% dimethyl sulfoxide for subsequent later use.

Axial Perfusion System

A bioreactor system capable of axially perfusing constructs 6.35 mm in diameter and up to 10 mm in length was designed and built (**Figure 4-1**). Machined out of polysulfone, the three-piece bioreactor employed a collet design (**Figure 4-1A**) to prevent the tubing from twisting when the bioreactor was screwed together and sealed. Luer locks connect each bioreactor to its own media reservoir, which can hold 18 ml of media, via gas permeable tubing. Media was pumped through the system using an IP56 rated, digital modular control peristaltic pump (Masterflex, Cole-Parmer), which can impart flow rates between 0.2ml/min and 10 ml/min. The entire system, except for the pump, was steam sterilized. Detailed drawings of the bioreactor pieces and reservoir can be found in **Appendix 3**.

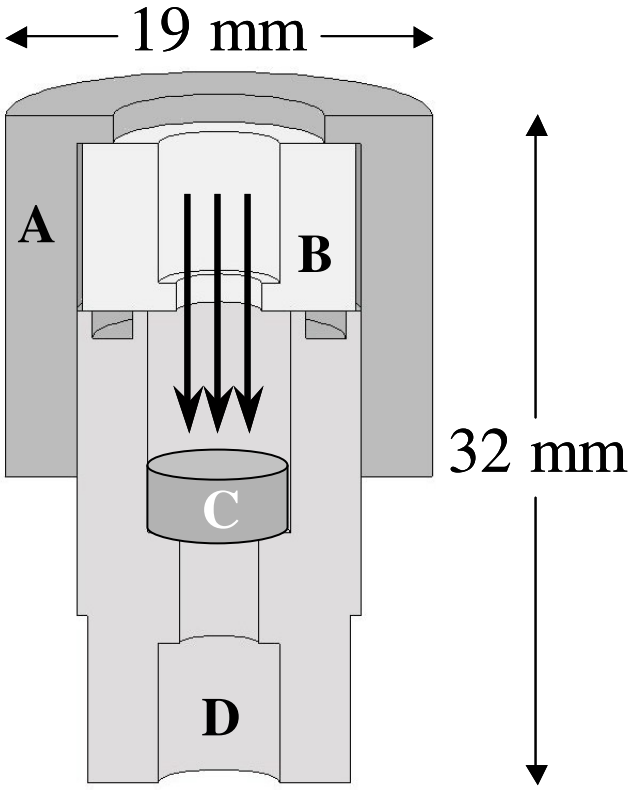

Figure 4-1. Schematic of axial perfusion bioreactor. (**A**) Collet used to screw the entire assembly together, (**B**) Spacer: luer lock connection screws into the top surface, the flat face on the bottom seals with the o-ring sitting in the groove in part (**D**) Base that holds the construct, luer lock connection screws into the bottom. D is threaded where the top overlaps with part (A). (**C**) Representative size of 3 mm thick construct.

Scaffold Preparation

Fused deposition modeling was used to fabricate 3 mm thick PCL lattice sheets comprised of 300 μm thick struts spaced 500 μm apart and layered in a 0/60/120 degree repeating pattern to produce a 66% porous structure **(Figure 4-2)**. Scaffolds were cut from the sheet using a 6mm biopsy punch (Miltex) and then incubated in 5M NaOH for 12 hours at 37°C for cleaning purposes and to partially degrade the scaffold and increase surface roughness. Scaffolds were rinsed twice in double deionized water under stir bar agitation and sterilized by 70% EtOH evaporation overnight in a cell culture flow hood. Half of the PCL scaffolds were coated with human plasma fibronectin (PCL+FN). Briefly, scaffolds were prewetted with 70% EtOH to reduce hydrophobicity and were rinsed in 2 washes of PBS before placement in FN (50 μg/ml) overnight before use. Type I rat tail collagen was lyophilized into the pore space of the remaining scaffolds, which formed a microporous mesh (PCL+COL) throughout the PCL. Briefly, 100 parts collagen (1.4mg/ml in 0.05% acetic acid) was combined with 9 parts sodium bicarbonate and subsequently 75 μl aliquots of the solution were deposited on each scaffold in order to fill the pore space. Scaffolds were transferred aseptically to 6 well plates and stood at room temperature for 30 minutes to allow the collagen to polymerize. The 6 well plates were then transferred to a –80° C freezer for 90 minutes until frozen and then placed in a lyophilizer (Labconco) overnight until dry. Lyophilized scaffolds without cells were perfused at 0.2 ml/min and imaged at 1, 3, and 7 days to monitor whether the collagen fibers remained present and intact after a week of perfusion culture conditions.

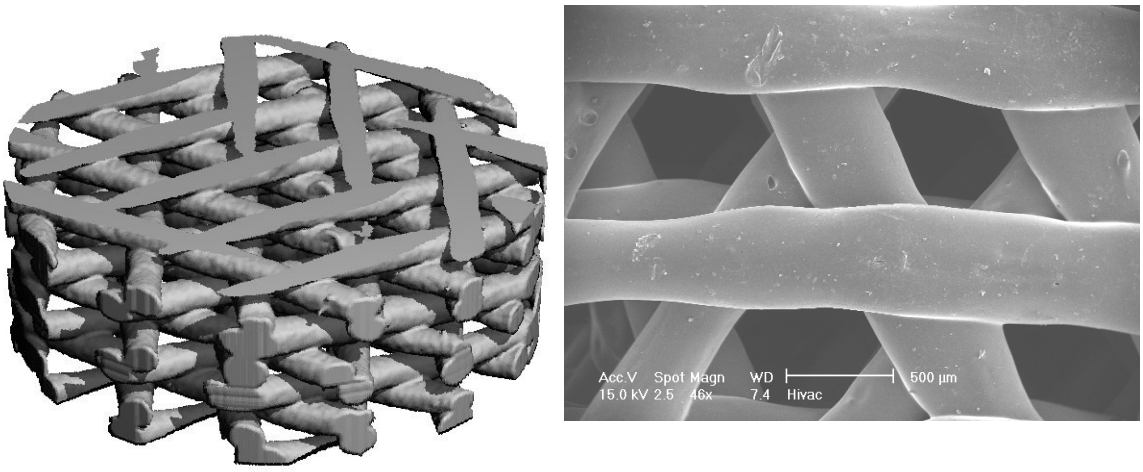

Figure 4-2. Micro-CT and scanning electron microscopy images of untreated PCL. This representative scaffold is 66% porous.

Construct Seeding and Culture

rMSC cells were thawed, placed in 150mm tissue culture dishes, expanded with one passage, trypsinized, and seeded on each scaffold. Two million cells suspended in 25 μl of media (α-MEM with 10% FBS and 1% a/a) were deposited on each scaffold and placed in the incubator. The cell suspension pooled at the bottom of the PCL+FN scaffolds, but the lyophilized collagen absorbed the cell suspension in the PCL+C scaffolds. After 1 hour, 6 ml of media was added to each well. After 1 day, seeding efficiency was determined via the PicoGreen DNA assay. Constructs were incubated for 1 week in static culture without osteogenic supplements before being placed in the bioreactor system (day 0) and perfused at 0.2ml/min (n=6), or transferred to new six well plates and cultured statically (n=6). Media with osteogenic supplements (3 mM sodium β–GP, 50 μg/ml AA2-P, 10 nM DEX) was changed once a week for 35 days.

Confocal Scanning and Electron Microscopy

PCL+C scaffolds without cells were stained with Picrosirius Red and imaged using confocal microscopy to visualize the distribution of collagen within the pore spaces. PCL+C scaffolds were also viewed under scanning electron microscopy (performed by Dr. Dietmar Hutmacher) to determine the distribution of collagen fibers throughout the scaffold. After 1 week in static culture, two PCL+FN and two PCL+C constructs were stained with calcein and ethidium homodimer, then viewed with confocal microscopy to visualize the distribution of live and dead cells prior to receiving osteogenic media and beginning perfusion culture. Constructs were also stained after 35 days in culture to examine cell distribution and viability.

Micro-CT Mineral Quantification

In vitro mineralization on perfused and static constructs was quantified using a Micro-CT 40 (Scanco) at a voxel resolution of 16 μm. Samples were evaluated at a threshold of 72, a filter width of 1.2 and filter support of 2.0. A threshold of 72 correlated to a linear attenuation of 1.15 cm^{-1} and a mineral density of 95 mg HA/cc. Mineral volume and density were measured throughout the entire construct as well as a cylindrical subregion (core) that excluded the outer 500 μm of the construct on the top and sides.

Data Analysis

Data are reported as mean ± SEM and statistical analyses using Minitab12 were carried out using a general linear model (ANOVA) and Tukey's post-hoc test for pairwise comparisons with $p<0.05$ considered significant.

Results

Seeding Efficiency, Confocal and Scanning Electron Microscopy

The PicoGreen DNA assay revealed a seeding efficiency of 37% for PCL+C constructs and 35% for PCL+FN constructs (data not shown here). Confocal microscopy **(Figure 4-3A, C)** showed collagen fibers distributed in a heterogeneous fashion within the pores of the PCL+C scaffolds. Scanning electron microscopy indicated that the collagen was regularly distributed across multiple pores **(Figure 4-3B, D).** Collagen fibers were present throughout acellular PCL+C scaffolds after 1, 3, and 7 days of

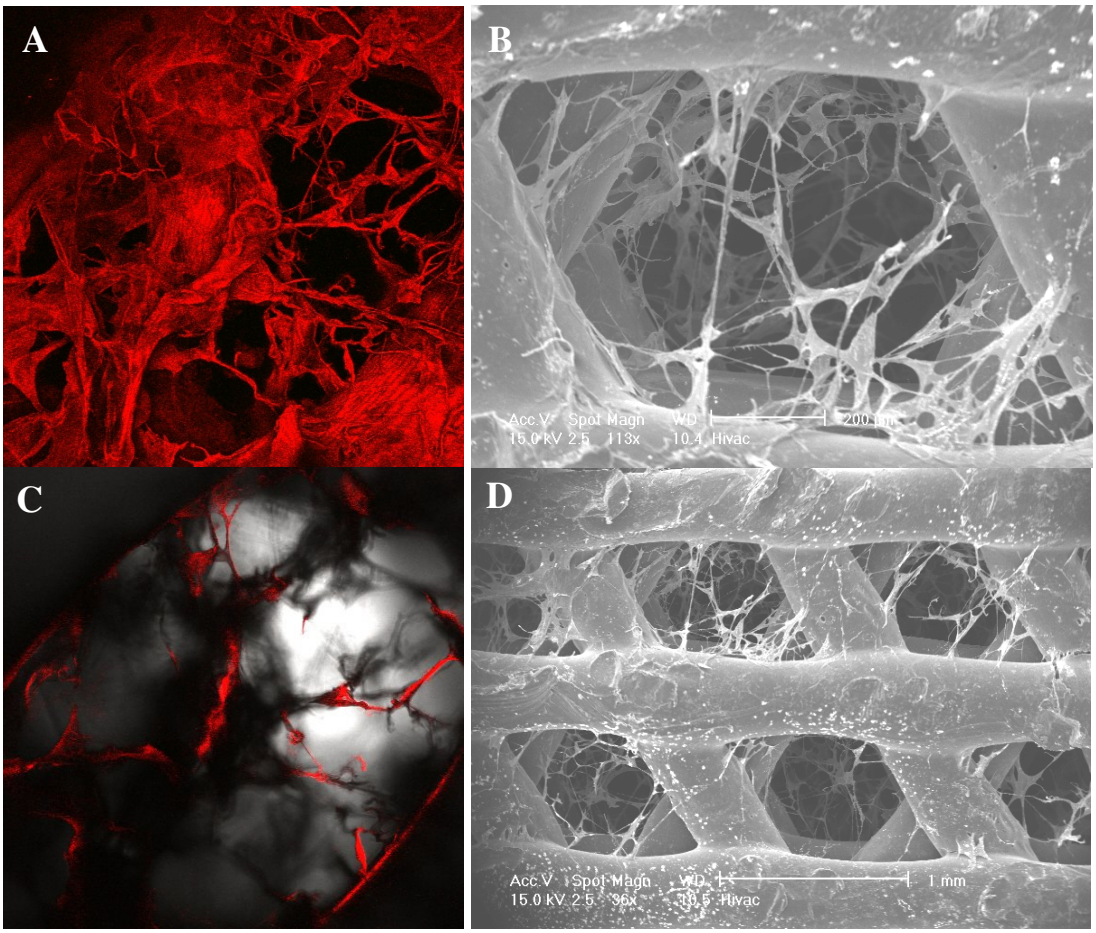

Figure 4-3. PCL+lyophilized collagen. (**A**) 10X image, collagen stained with Picrosirius Red and viewed under confocal microscopy. The collagen is spanning a 500 µm pore on the bottom of a PCL scaffold. (**B**) 10X SEM image of a similar pore. (**C**) 10X confocal image with white light to indicate pore size. (**D**) 5X SEM image to illustrate the distribution of collagen throughout the full scaffold. The collagen forms a heterogeneous mesh within each pore, but does span each of the pores.

perfusion at 0.2 ml/min. Live/dead images showed viable cells filling the pore spaces within PCL+C constructs at day 0, while cells were predominantly localized to the polymer surface of the PCL+FN constructs **(Figure 4-4)**. After 35 days, there was a confluent layer of cells on the struts of the PCL for all construct groups. Perfused PCL+C constructs still exhibited viable cells within the pore spaces, but fewer pores were populated with cells in static PCL+C constructs compared with the PCL+C constructs. Perfused PCL+FN constructs displayed thickening of the PCL strut and some partial cellular bridging of the pore space, but the cells were still primarily localized to the scaffold surface. Virtually no cells were growing in the pore spaces within the static PCL+FN constructs.

Micro-CT Images

Visual inspection of micro-CT images showed a marked difference in the mineralization results from the PCL+FN constructs compared with the PCL+COL constructs as well as differences in static vs. perfused cultures **(Figure 4-5 and 4-6)**. The PCL+C constructs were populated with substantially larger and a greater number of mineral deposits than PCL+FN constructs. Within static PCL+C constructs, the mineral particles were heterogeneous in shape and localized to the periphery of the construct. Negligible amounts of mineral were detected when the evaluation region was limited to the inner core. Conversely, PCL+C perfused scaffolds displayed a large percentage of mineral localized to the core region. Images of static PCL+FN constructs exhibited small amounts of mineral within the outer region compared with virtually no mineral present at the construct core **(Figure 4-6)**.

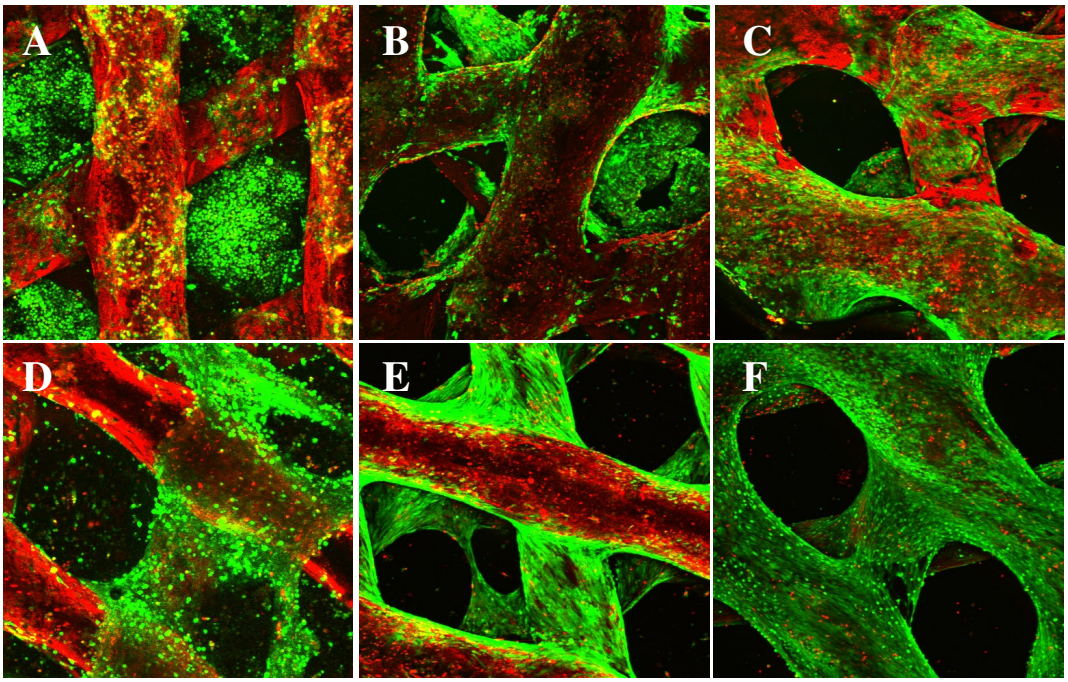

Figure 4-4. Confocal microscopy images (5X) of the top surface of cell seeded scaffolds. Green designates live cells while red designates dead cells. Diffuse red staining is due to autofluorescence of the PCL scaffold. (**A**) – Day 0 PCL+C construct. (**B**) Day 35 PCL+C perfused construct. (**C**) Day 35 PCL+C static construct. (**D**) Day 0 PCL+FN construct. (**E**) Day 35 PCL+FN perfused construct. (**F**) Day 35 PCL+FN static construct.

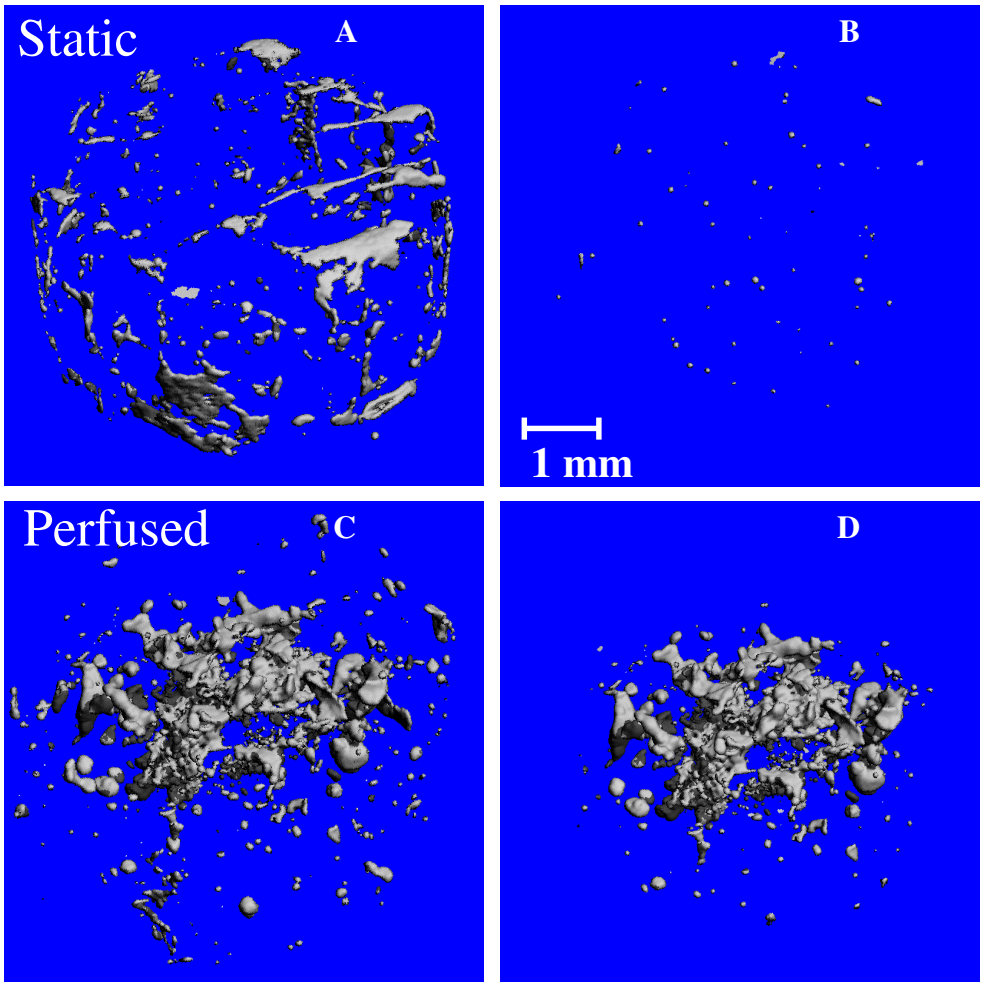

Figure 4-5. Representative micro-CT images of mineral distribution within 3 mm thick perfused and static PCL-C constructs. (**A**) Full construct in static culture. (**B**) Construct core (outer 500 μm excluded) in static culture. (**C**) Full construct in perfused culture. (**D**) Construct core (outer 500 μm excluded) in static culture.

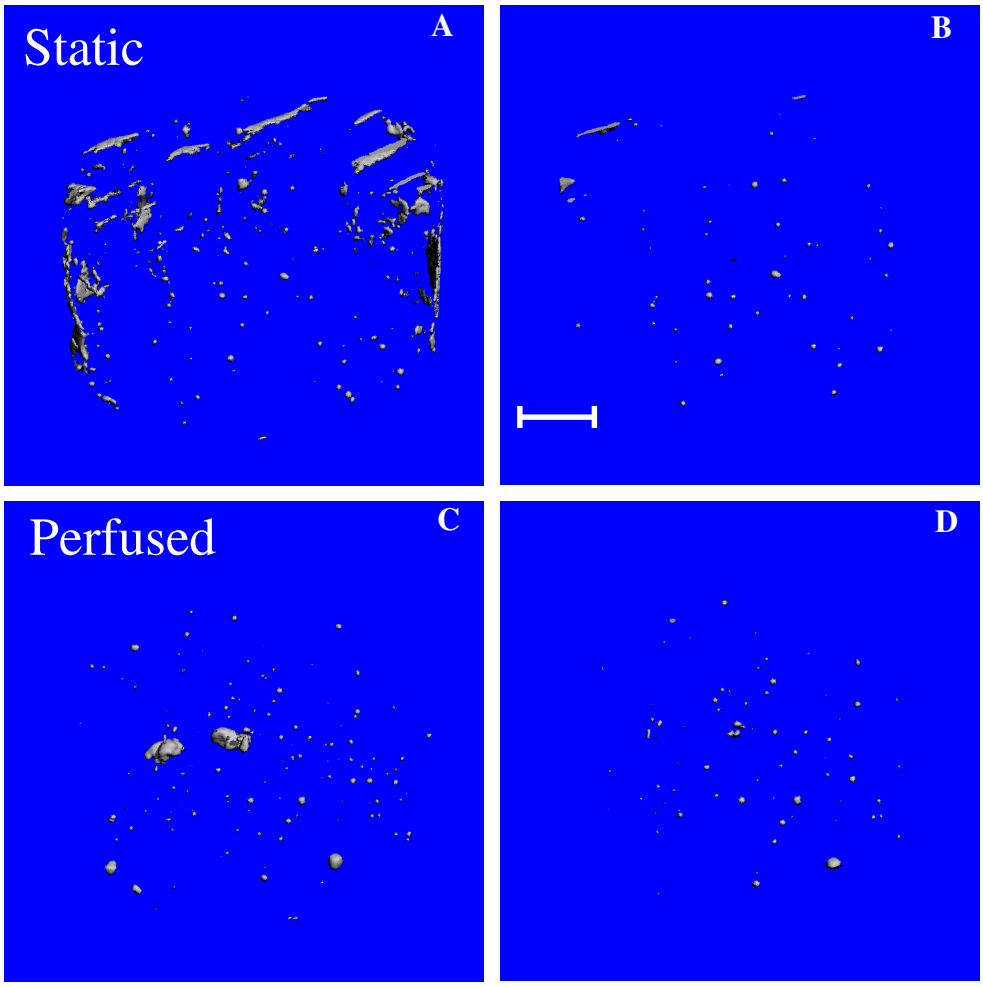

Figure 4-6. Representative micro-CT images of mineral distribution within 3 mm thick perfused and static PCL-FN constructs. (**A**) Full construct in static culture. (**B**) Construct core (outer 500 μm excluded) in static culture. (**C**) Full construct in perfused culture. (**D**) Construct core (outer 500 μm excluded) in static culture.

Quantification of Mineralized Matrix Volume

Quantitatively analyzing the mineral volume deposited throughout the entire construct demonstrated that both the static and perfused PCL+C construct groups produced significantly more mineral than either PCL+FN construct group **(Figure 4-7)**. Perfused PCL+C constructs showed a 26-fold increase in mineralized matrix compared with perfused PCL+FN constructs and a 3-fold increase compared with PCL+C static controls. Mineral deposition on PCL+C static constructs was double that of static PCL+FN constructs (0.652 to 0.307), but the difference was not statistically significant. The amount of mineral detected in the PCL+FN constructs showed no statistical differences between static and perfused groups.

Quantification of Mineralized Matrix Distribution

Comparing mineral volume at the construct core showed a significant effect of perfusion and scaffold type **(Figure 4-7)**. CFD analysis indicated that mineralized matrix deposition coincided with regions of maximal fluid flow (**Figure 4-8**). Perfusion resulted in a 134-fold increase in mineral volume within PCL+C constructs compared with static controls. There was a 65-fold increase in mineral volume for perfused PCL+C constructs compared with perfused PCL+FN constructs. However, there was no significant difference between the mean volume of mineral within the static PCL+FN and static PCL+C construct cores. Comparing the ratio of the mineral volume at the core to mineral volume throughout the entire construct yielded the results shown in **Figure 4-9**. Only 3.7 and 2.0% of the total mineral in the static PCL+FN and PCL+C constructs, respectively, resided in the core, while 41 and 90% of the total mineral in the perfused PCL+FN and

PCL+C constructs was found in the core. The perfused PCL+C constructs produced the greatest amount of mineral as well as the most uniformly distributed mineral throughout the construct core.

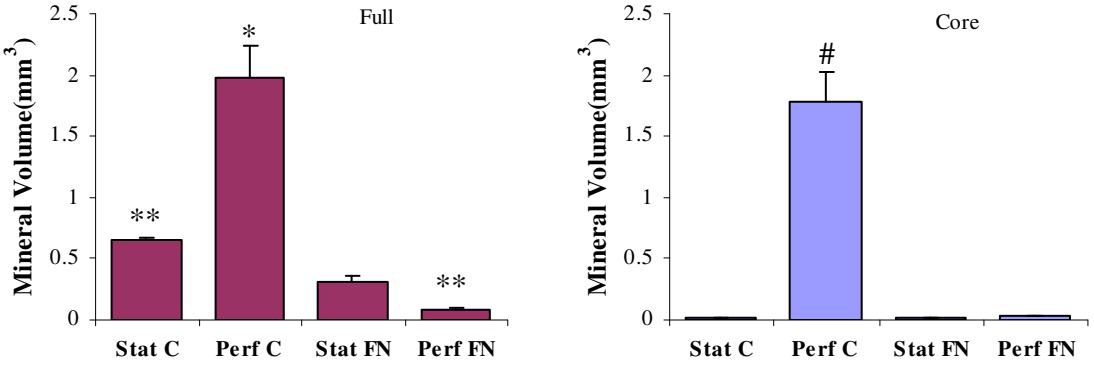

Figure 4-7. Micro-CT mineral volume quantification of perfused and static PCL+C and PCL+FN constructs (n=6). Both the entire construct and the core region were analyzed. General linear model ANOVA showed differences between culture groups ($p<0.0001$). Pairwise comparisons of data from the full construct indicated a statistical difference in the amount of mineral detected in the perfused PCL+C constructs compared with all other groups (*, $p<0.0001$), and a statistical difference between the mineral volume within static PCL+C constructs compared with the mineral volume within perfused PCL+FN constructs (** denotes different from **, $p<0.0316$). Analyzing the construct core revealed differences between the perfused PCL+C constructs and all other groups (#, $p<0.0001$).

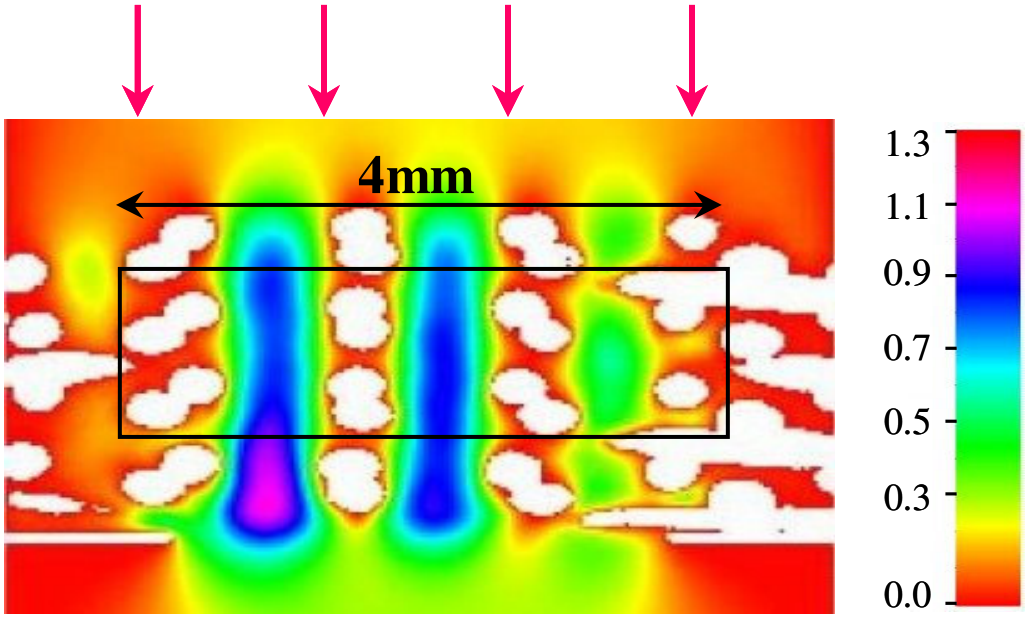

Figure 4-8. CFD modeling of media flow through a PCL scaffold. The black box corresponds to the region that was evaluated to determine the mineral volume in the core of the perfused and static constructs. Units of flow are mm/s.

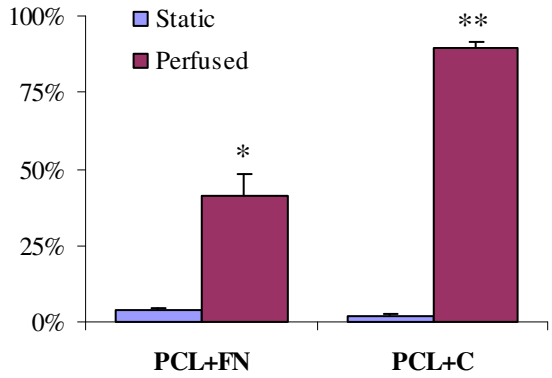

Figure 4-9. Mineralized matrix volume within the core of each construct (n=6). The amount of mineral within each construct core was divided by the total amount of mineral to calculate the percent of mineral volume that resided in the core. General linear model ANOVA indicated there were differences in each of the experimental groups ($p<0.0001$). Pairwise comparisons showed the percentage of mineral within the core of PCL+FN perfused constructs was different from all other groups (*, $p<0.0001$). Likewise perfused PCL+C perfused constructs (**, $p<0.0001$)

Discussion

The development of mineralized constructs comprised of biodegradable materials may be useful as bone graft substitutes for the treatment of bone defects *in vivo*. The goal of this study was to improve cell attachment and viability during perfusion by testing two different scaffold treatments in order to quantify mineralized matrix production on 3-D constructs. Perfusion bioreactors were successfully used for long term culture to produce biodegradable polymer constructs populated with cell mediated mineralized matrix throughout the full thickness of the scaffold. Confocal microscopy images showed viable cells present in the pore space of the PCL+C constructs at day 0 and at day 35, which demonstrated that cells were kept alive for the duration of the experiment. However, there were far fewer cells in the pore space of the PCL+FN constructs, which suggested that the cells that were initially adhered to the scaffold surface did not migrate or proliferate enough to bridge across the majority of the pores. Picrosirius Red staining viewed with confocal microscopy, as well as SEM images, showed that the lyophilized collagen formed a random mesh throughout the pores of the PCL. Collagen was present at 1, 3, and 7 days within acellular PCL+C scaffolds perfused at 0.2 ml/min. In addition to being a biologically active material, to which the cells adhere well,[112, 113] the collagen mesh may have acted as a net to trap cells during seeding and improve cell retention during perfusion. After 5 weeks of culture, macroporous PCL scaffolds seeded with rMSCs demonstrated significant differences in mineralized matrix deposition for static and perfusion culture conditions.

Perfusion Enhances Mineral Deposition Compared with Static Culture

High resolution (16 μm voxel resolution) micro-CT scanning and image analysis showed that perfusion specifically enhanced mineralization within the central core of PCL constructs compared with constructs grown in static culture. This effect was most pronounced when a microporous collagen Type I gel was lyophilized within macroporous PCL scaffolds compared with scaffolds that had been coated with FN prior to cell seeding. Van Den Dolder *et al.* perfused 0.8 mm thick, 86% porous, titanium mesh scaffolds seeded with rMSCs for 16 days. However, the deposited mineral formed a crust on the upstream portion of the scaffold and increased in thickness as the flow rate was increased.[10] Meinel *et al.* perfused both collagen and silk 1.5 mm thick human MSC seeded scaffolds (porosity not given) for 35 days, and, using micro-CT with low voxel resolution (35 x 250 μm), reported mineral localized to the periphery of the construct but did not quantify the mineral volume.[2] In contrast to those two studies, the perfused PCL+C constructs produced mineralized matrix deposits throughout the scaffold with multiple nucleation sites, which had grown into distinct nodules of various sizes.

Perfusion Increases Mineralization at the Construct Interior

Most of the mineral in the perfused constructs was located in the central core area, which correlated to the region that received maximum fluid flow as shown by the LB modeling in **Figure 4-8**. Fluid flow was directed through a 4 mm central annulus due to a lip (used to prevent the construct from moving in the bioreactor) on which the downstream face of the scaffold was resting. While there was active mass transport through the center of the construct, the CFD modeling indicated that minimal fluid flow

infiltrated the construct periphery and may have resulted in localized regions of stagnant media. In static culture, 98% of the mineral in the PCL+C constructs and 96% of the mineral in the PCL+FN constructs was located at the periphery. An inverse effect was observed in the perfused cultures, where 90% of the mineral produced in the PCL+C constructs and 41% of the mineral produced in the PCL+FN constructs was deposited at the interior of the scaffold. The relatively stationary media at the periphery of the scaffold may have limited mineral production, while the active fluid flow, increased mass transport, and applied shear stresses at the center may have upregulated mineral synthesis at the interior of the constructs. The bioreactor was initially designed to accommodate scaffolds with an irregular cylindrical shape, which required a large lip on the downstream face of the construct to prevent it from shifting and clogging downstream. Using a scaffold material such as PCL that can be sized to a defined cylindrical shape allows for the size of the lip to be reduced. Such a revision may enhance mineral deposition near the construct periphery by increasing the cross sectional area that is exposed to fluid flow, thereby improving mass transport throughout a larger percentage of the construct.

Lyophilized Collagen Improves Mineralization Compared with Fibronectin Coating

There was a significant difference in the amount of mineral produced in PCL+C constructs compared with PCL+FN constructs. Perfused PCL+C constructs produced 26 times the mineral volume as perfused PCL+FN constructs. Static PCL+C constructs produced twice the mineral volume as static PCL+FN constructs. Collectively, these results suggest that the interactions between the cells and the scaffold material they are

attached to are critical to determining the response to perfusion. Lan *et al*. reported that the number of MSCs that remained attached to tissue culture plastic doubled when the dish was coated with Type I collagen. Additionally, when those cells were subjected to fluid shear stresses on the order of 1.1 dynes/cm^2, almost all of the MSCs on the untreated tissue culture plastic were washed away, while 25% of the MSCs on collagen remained attached even with an applied shear stress of 1.3 dynes/cm^2.[112, 113] The collagen mesh may not only provide a favorable substrate the rMSCs adhere well to, but also act as a net to trap cells initially and improve cell adhesion, proliferation, and differentiation during perfusion. The heterogeneous shape of the mineral deposits within PCL+C constructs may be due to the random distribution of collagen within each pore as was shown by confocal and SEM imaging.

Conclusions

In summary, an axial perfusion bioreactor was successfully used for long-term culture to enhance the amount and distribution of mineralized matrix production within 3-D constructs in a scaffold dependent manner. PCL+C constructs produced significantly greater amounts of mineral than PCL+FN constructs. In addition, continuous perfusion significantly increased mineralized matrix deposition within PCL+C constructs compared with static cultures. The mineral was distributed throughout the entire thickness of 3 mm thick PCL+C constructs, however, possibly due to stagnant flow at the periphery, 90% of the mineral was localized to a central core, which excluded the outer 500 μm. Perfusion did not increase the total amount of mineral within PCL+FN constructs, but did increase the amount of mineral at the core of PCL+FN constructs. CFD analysis indicated that

mineralized matrix deposition coincided with regions of maximal fluid flow. To improve fluid flow throughout the scaffold, the lip on which the constructs sit in the bioreactor should be reduced in size.

CHAPTER 5 EFFECT OF SCAFFOLD THICKNESS ON PERFUSION-MEDIATED ENHANCEMENT OF MINERALIZED MATRIX FORMATION

Introduction

Researchers have recently demonstrated that perfusion increases mineralized matrix formation within thin (0.8-1.5 mm) constructs.[2, 9-11] We have successfully used perfusion culture to create constructs measuring 6.35 mm in diameter and 3 mm thick populated with cell-mediated mineral throughout the scaffold (Chapter 4). Unfortunately, constructs of this size would prove too small for most clinical applications. Even preclinical testing in a well-established small animal model would require an implant greater than 7mm in length. Therefore, we evaluated the effect of increasing scaffold thickness on perfusion-mediated enhancement of mineralized matrix formation. PCL-C scaffolds 3, 6 and 9mm in length were axially perfused at 0.2 ml/min for 35 days and mineralized matrix deposition was quantified with micro-CT. In addition to determining mineral volume, we developed a new image analysis procedure to calculate the size and number of mineral particles within the constructs. However, detection of radio-dense material is not sufficient to claim that cell-mediated mineral has been produced. Analysis by Fourier Transform Infrared Spectroscopy (FT-IR) has been used to characterize the chemical composition of bone produced *in vitro*.[114, 115] Therefore, we analyzed perfused constructs with FT-IR to determine if the mineral present in the scaffold possessed the appropriate chemical composition. It was hypothesized that increasing construct length would result in a proportional increase in mineralized matrix volume and would not affect the uniformity of spatial distribution or particle size.

Materials and Methods

Cell Source

Cells were harvested from 18 Sasco Sprague Dawley rats as described in Chapter 5. All cells were pooled and aliquoted into 20 cryovials before freezing. These cells were used in all subsequent perfusion experiments for this thesis. Monolayer control cultures were grown alongside each 3-D perfusion experiment. Von Kossa staining after 21 days confirmed that each thawed cell population produced similar amounts of mineralized matrix in 2-D culture.

Axial Perfusion Bioreactor Redesign

Given the results from Chapter 5, the inner cylindrical chamber of the axial perfusion bioreactor used in those studies was redesigned to reduce the size of the lip that the construct sits on. Previously, the circular lip was 1.27 mm deep, which formed a ring that covered 64% of the bottom surface of the construct. Reducing the lip to 0.64 mm in depth reduced the area of the ring. Subsequently, only 36% of the bottom face of the construct was covered.

Construct Seeding and Perfusion Culture

Fused deposition modeling was used to fabricate 3 mm thick PCL lattice sheets with the same geometry and architecture used in Chapter 5. After cleaning and sterilizing the PCL scaffolds, 75 μl type I collagen gels were cast in the scaffold pore space. Type I collagen was lyophilized as described in Chapter 5. Constructs were seeded with rMSCs

as described in Chapter 5 and then cultured in 6 ml of media (α-MEM plus 10% FBS and 1% a/a) without osteogenic supplements. After 1 week, constructs were stacked on top of each other in each bioreactor to create three experimental groups: 3, 6 and 9 mm thick constructs (n=6). Constructs were axially perfused for 5 weeks with 12 ml of media for each construct containing osteogenic supplements (50 μg/ml AA2-P, 3 mM β–GP, 10 nM Dex) at 0.2 ml/min. 8 ml of media was removed each week and replaced with a fresh 8 ml. The remaining 4 ml of conditioned media resided in the tubing and bioreactor during media changes.

Micro-CT Analysis

After 5 weeks of culture, constructs were carefully removed from each bioreactor in order to maintain continuity of the stacked constructs. Constructs of all three thicknesses were inserted into polycarbonate sleeves, which kept the 6 and 9 mm constructs aligned together for scanning purposes. The 3 mm thick constructs were also placed in the polycarbonate sleeves to ensure that x-ray attenuation in the micro-CT would not vary among construct lengths. *In vitro* mineralization on perfused constructs was quantified using a Micro-CT 40 (Scanco) at a voxel resolution of 16 μm. Samples were evaluated at a threshold of 72, a filter width of 1.2 and filter support of 2.0. X-ray attenuation was correlated to sample density using a standard curve generated by scanning hydroxyapatite phantoms with known mineral density. A threshold of 72 correlated to a linear attenuation of 1.15 cm^{-1} and a mineral density of 95 mg HA/cc.

Mineral volume and density were quantified throughout the entire construct as well as two concentric cylindrical subregions that excluded the outer 500 and 1000 μm of

the construct on the top and rounded sides. Mineral particle size and number were also quantified in this experiment. An Image Processing Language (IPL) script **(Appendix 4)**, which utilized Scanco software, was used to label each mineral particle, rank it by size and then save the data in a series of files, each containing 127 data points. Those files were combined in Excel; a macro grouped the particles together and then ranked them by size. Because the data did not follow a normal distribution, the data were transformed and graphed as a cumulative distribution plot. Only the largest particles in each construct that comprised 90% of the total mineral volume (LP90%) were analyzed. The percentage of cumulative particles was plotted as a function of particle size and graphed on a log scale.

Fourier Transform Infrared Spectroscopy Analysis

FT-IR spectroscopy was used to analyze the chemical composition of the mineralized matrix that was deposited by the rMSCs. Samples were prepared as described by Byers et al.[55] Briefly, cultures were fixed in 70% EtOH and dried in an oven at 40 °C to remove all aqueous components. A scalpel was used to scrape mineral deposits off of the PCL scaffold. The mineral was combined with Potassium Bromide (KBr) and compressed between two platens to form a thin film of mineral and KBr. KBr, an ionic salt that cannot be excited by the FT-IR beam, leaves no chemical signature to confound with the mineral. Spectra which showed peaks corresponding to chemical bonds, were comprised of 64 scans acquired at 4 cm^{-1} and were collected on a Nexus 470 FT-IR spectrometer (Thermo Nicolet, Madison, WI) under N_2 purge. These spectra were

displayed from 400 to 2000 cm^{-1}, which is the range that includes bands that are characteristic of bone's constituents.

Data Analysis

Data are reported as mean ± SEM and statistical analyses using Minitab12 were carried out using a general linear model (ANOVA) and Tukey's post-hoc test for pairwise comparisons with $p<0.05$ considered significant.

Results

Mineral volume and Density

Visual inspection of constructs after perfusion revealed significant extracellular matrix deposition, which entirely filled the majority of the pores. 3-D images of mineral content on PCL+C constructs displayed mineral deposition throughout the entire length of all constructs **(Figure 5-1)**. However, **Figure 5-2** illustrated that very little mineralized matrix was deposited at the interfaces between the stacked constructs. Mineralized matrix volume, mineral volume fraction (MVF), density, and radial spatial distribution were quantified throughout the entire construct as well as two concentric cylindrical subregions that excluded either the outer 500 μm on the top and rounded sides (500 core) or the outer 500 μm on the top and 1000 μm on the rounded sides (1000 core) of the construct. Mineral particle size and number were also quantified for the entire construct.

The total detected mineral volume increased 2.85-fold as the construct length was increased from 3 to 9 mm, while a 2.5-fold increase was detected in the 6 mm constructs

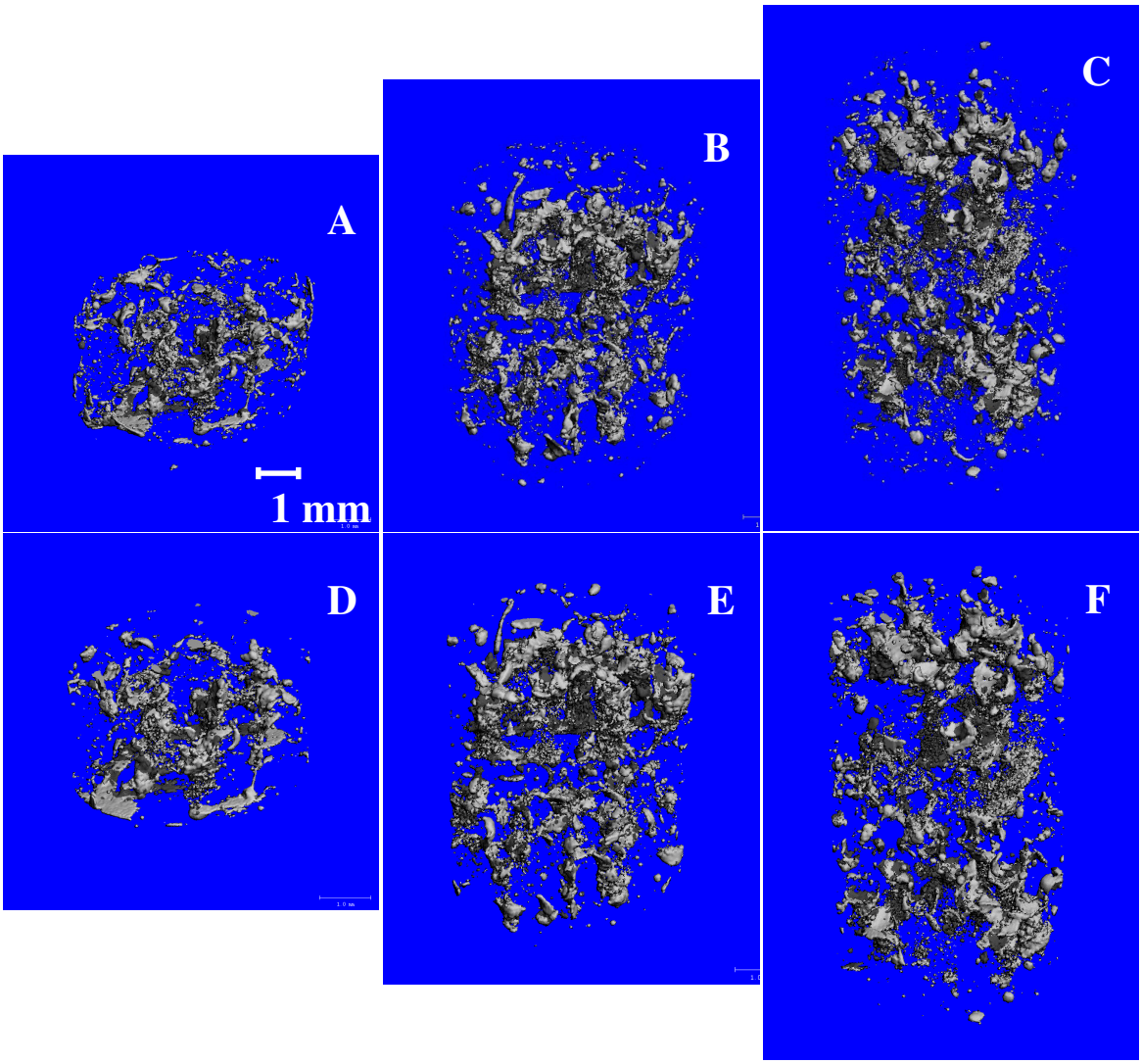

Figure 5-1. Representative isometric micro-CT images of mineralized matrix within perfused constructs, 3, 6 and 9mm in length. The top row (**A**, **B**, **C**) shows mineral within the entire construct. Images **D**, **E**, **F** show mineral throughout a cylindrical core (outer 500 μm excluded) within the construct.

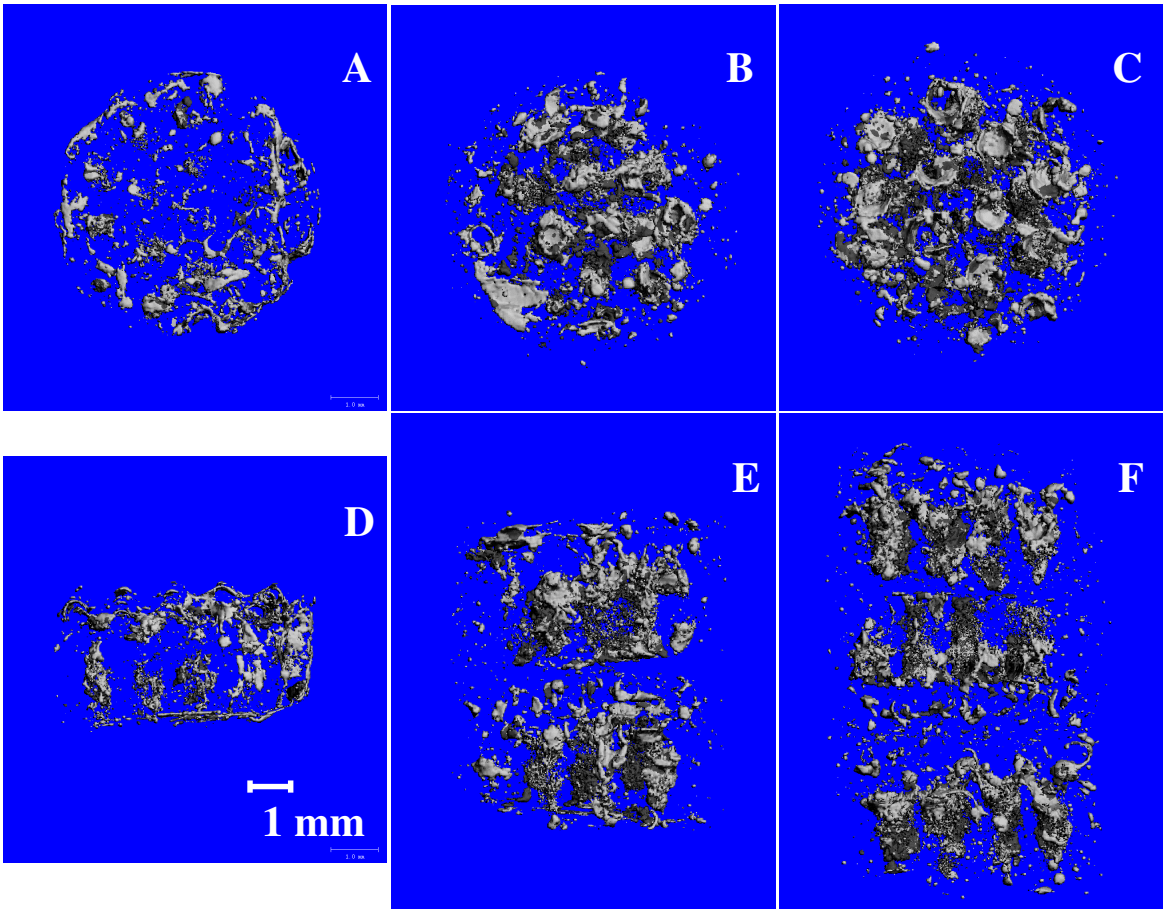

Figure 5-2. Representative micro-CT images of mineral deposits within stacked PCL+C scaffolds after 5 weeks of perfusion culture at 0.2 ml/min. Images in the top row (**A**, **B**, **C**) show the distribution of mineral looking at the constructs from the top. Images in the bottom row (**D**, **E**, **F**) depict mineral deposits throughout the full thickness of the constructs, which correlate to the images in the top row. The 6 and 9 mm constructs (**E**, **F**) show mineral localized within each individual 3 mm thick scaffold, but few mineral deposits at the interfaces between each scaffold.

compared with the 3 mm constructs (**Figure 5-3**). There was no statistical difference between the amount of mineral detected in the 6 and 9 mm constructs. The same increases in mineral volume were observed in the 500 core subregion. The differences in mineral volume were more pronounced in the 1000 core region where the total mineral volume increased 4-fold for both the 6 and 9 mm constructs compared with the 3 mm constructs. There were no statistical differences in the MVF across any of the construct sizes when analyzing the entire construct volume (**Figure 5-4**). There was an 84 % increase in the MVF within the 1000 core region of the 6 mm construct compared with the 3 mm construct. There was a non-significant, 52% increase in MVF from the 6 mm construct (500 core region) over the 3 mm (500 core region) of 52%. There was also a non-significant, 51% increase in MVF from the 6 mm construct (1000 core region) over the 9 mm construct (1000 core region).

Figure 5-5 displays the spatial distribution of mineralized matrix within perfused constructs of 3 different thicknesses. In the 3 mm thick constructs, a significantly smaller percentage of the total mineralized matrix (69%) was present in the 500 core region compared with 6 and 9 mm thick constructs (93% and 92% respectively). For the core analysis excluding the outer 1000 μm, there was again, a significantly smaller percentage of the total mineral mineralized matrix present in the 3 mm thick constructs (37%) compared with 6 and 9 mm thick constructs (62% and 52% respectively).

The mean value of mineral density within the entire construct and both subregions was determined for each construct size (**Figure 5-6**). When analyzing the entire scaffold, the mineral density detected in the 3 mm thick constructs was significantly higher (25%) than the density of the mineral in the 6 and 9 mm thick constructs. This percent increase

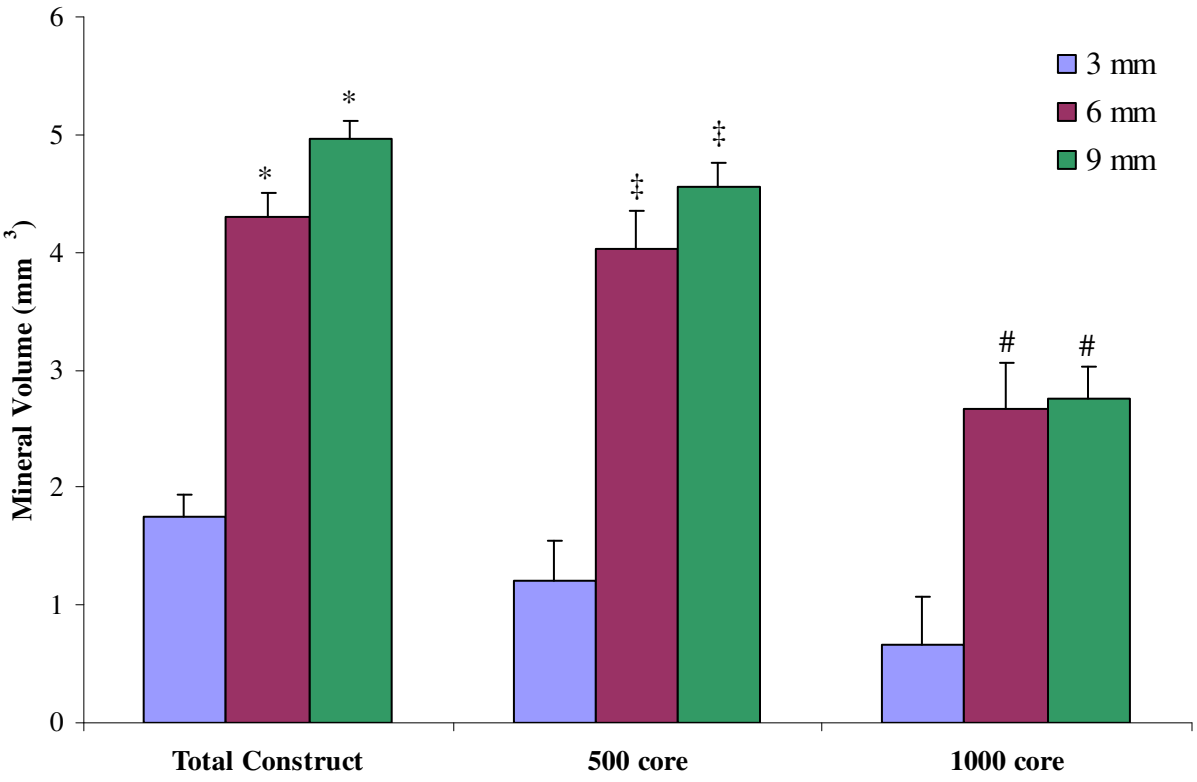

Figure 5-3. Mineralized matrix volume for perfused constructs of 3 different thicknesses (n=6) after 5 weeks of perfusion culture at 0.2 ml/min. Three different volumes of interest were analyzed for each construct: (1) Total construct, (2) a cylindrical subregion that excluded the outer 500 μm on the top and rounded surfaces (500 core), (3) a cylindrical subregion that excluded the outer 500 μm on the top surface and the outer 1000 μm on the rounded outer surface (1000 core). General Linear Model ANOVA analysis showed significant differences between mineral volumes detected in each construct size ($p<0.001$). Pairwise comparisons of the full construct (*) revealed a significant increase in mineralized matrix formation within the 6 and 9 mm constructs (4.308 and 4.967 mm^3) compared with the 3 mm thick constructs (1.743 mm^3) ($p<0.0002$). The same effect was shown in the 500 core (‡, $p<0.0001$) and 1000 core (#, $p<0.00009$) subregions as well. There was not a significant increase in mineral deposition when the length was further increased from 6 to 9 mm.

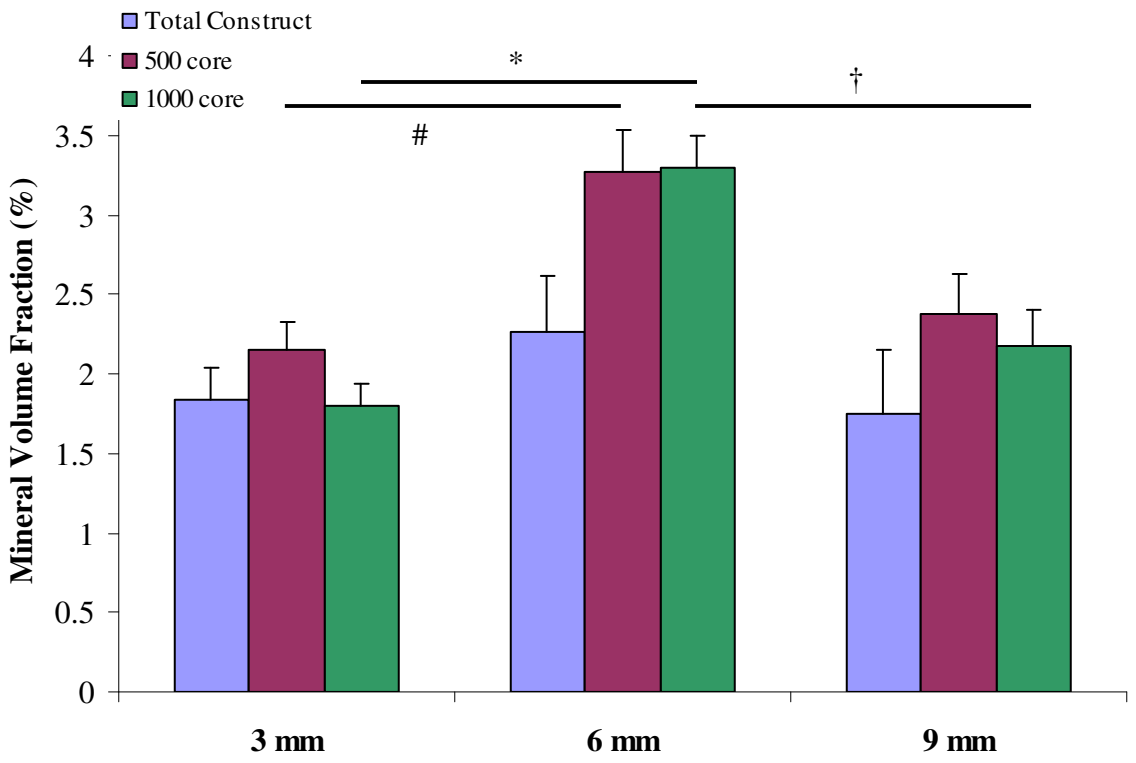

Figure 5-4. Mineralized matrix volume fraction (MVF) for perfused constructs of 3 different thicknesses (n=6) after 5 weeks of perfusion culture at 0.2 ml/min. Mineral volumes from Figure 6-3 were normalized by the volume of region being analyzed. General linear model ANOVA showed differences in groups ($p<0.0001$). Pairwise comparisons showed a significant increase in MVF from the 6 mm construct (1000 core region) over the 3 mm (1000 core region) (*, $p<0.0053$). There was a trend towards a significant increase in MVF from the 6 mm construct (500 core region) over the 3 mm (500 core region) (#, $p<0.0801$). There was also a trend towards a significant increase in MVF from the 6 mm construct (1000 core region) over the 9 mm (1000 core region) (†, $p<0.0867$).

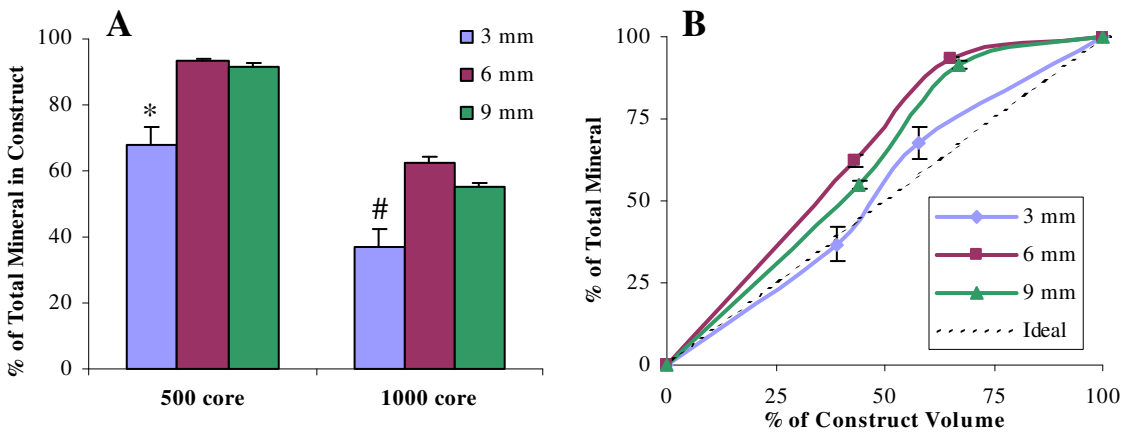

Figure 5-5. Mineral volume distribution within perfused constructs of 3 different thicknesses (n=6). (**A**) Each bar represents the percent of the total mineral in the construct that is found in each subregion (500 core or 1000 core) for a specific construct thickness (3, 6 or 9 mm). General Linear Model ANOVA analysis showed significant differences between mineralized matrix spatial distributions detected in each construct size ($p<0.001$). Pairwise comparisons showed a significantly smaller percentage of the total mineralized matrix in the 500 core region for 3 mm thick constructs compared with 6 and 9 mm thick constructs (*, $p<0.0003$). There was also a significantly smaller percentage of the total mineral mineralized matrix in the 1000 core region for 3mm thick constructs compared with 6 and 9 mm thick constructs (#, $p< 0.0081$). (**B**) Plot of the percentage of the total mineral detected in each evaluation subregion. An ideal construct with perfectly uniform mineral distribution throughout the scaffold would follow the dashed line.

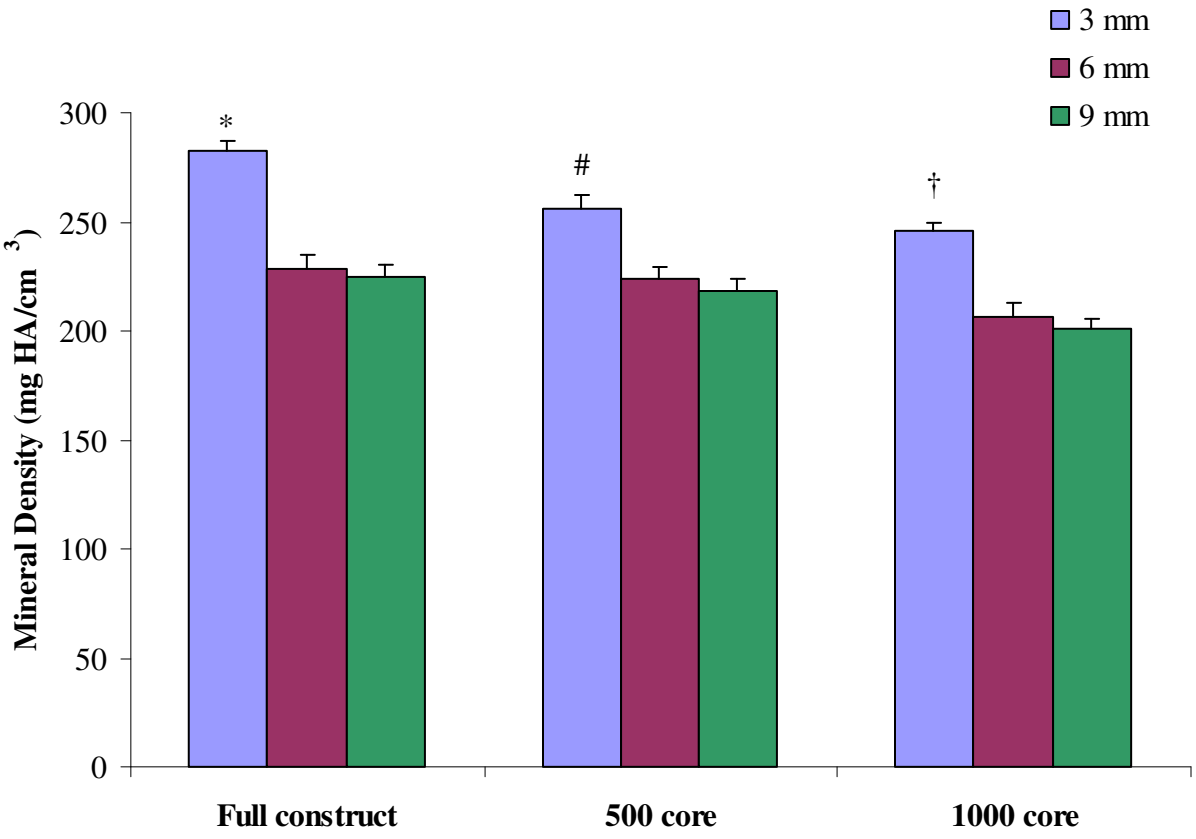

Figure 5-6. Mineralized matrix density measured by micro-CT for constructs of three different thicknesses (n=6) perfused at 0.2 ml/min. Mineral attenuation was correlated to a standard curve generated by scanning hydroxyapatite phantoms with known mineral density. General Linear Model ANOVA analysis showed significant differences between the densities of the mineralized matrix detected in each construct size ($p<0.001$). Pairwise comparisons showed that the mineral density detected in the 6 and 9 mm thick constructs was significantly lower than the density of the mineral in the 3mm thick constructs for all analysis regions. Full construct (*, $p< 0.0002$), 500 core (#, $p< 0.0001$), 1000 core (†, $p<0.0001$)

was consistent for both core subregions. There was no difference in the mineral density for the different analysis subregions.

Mineral Particle Size Distribution and Number

Scanco software (Scanco Medical, Switzerland) was used to determine the number and size of mineral particles within PCL+C constructs. A significant difference was observed in the total number of mineral particles detected within each construct as the thickness increased. There was a 74% increase in the number of particles detected in the 6 mm constructs compared with the 3 mm constructs, and a 78% increase in the number of particles detected in the 9 mm constructs compared with the 6 mm constructs (**Figure 5-7A**). For all constructs, regardless of thickness, over 90% of the total mineral volume was comprised of less than 5% of the total number of particles. There were 2.3 and 3.1-fold increases in the number of LP90% particles detected in the 9mm constructs compared with the 3 mm and 6 mm constructs, respectively (**Figure 5-7B**). Comparing the percentage of LP90% particles out of the total number of particles in each construct showed a 2.4-fold increase between the 3 and 6 mm constructs (**Figure 5-7C**). Regression analysis indicated there was a linear increase in the total number of mineral particles present in each construct as the construct length was increased (R^2 = 92.9%, **Figure 5-7D**). Cumulative distribution plots in **Figure 5-7E** illustrate size distributions for the LP90% particles within each size construct. There was a visual shift in the distribution of particle sizes in the 6 mm long constructs compared with the 3 and 9 mm long constructs.

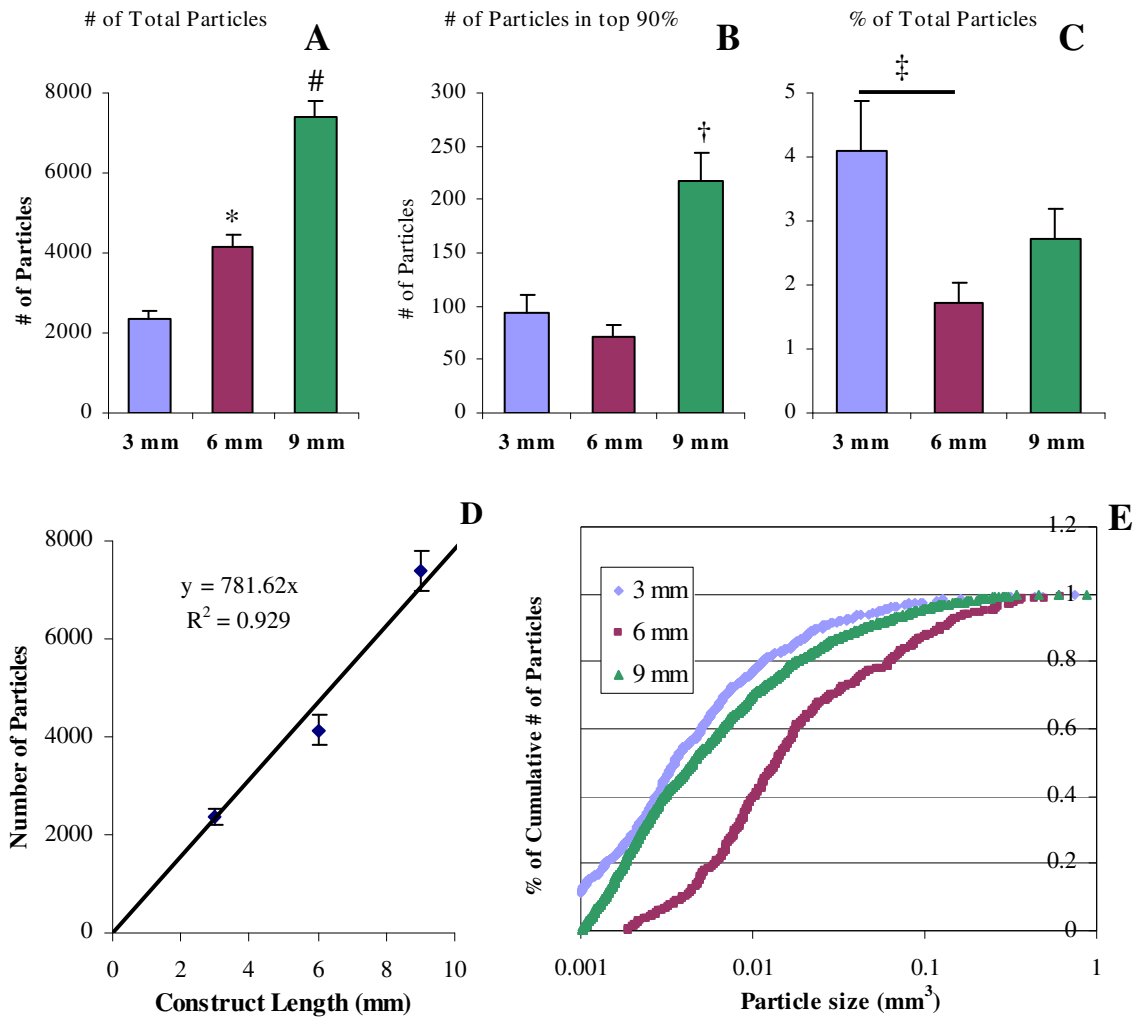

Figure 5-7. Mineral particle number and size distribution plots for each construct length (n=6). Plots of (**A**) the total number of mineral particles, (**B**) the number of mineral particles required to make up 90% (LP90%) of the total mineral, (**C**) the percentage of LP90 particles out of the entire number of particles, (**D**) linear regression of the number of mineral particles as a function of construct length, and (**E**) cumulative distribution plots to illustrate mineral particle size after 5 weeks in culture for each size construct. Pairwise comparisons indicated a statistically significant difference in the number of mineral particles detected for each different construct thickness (* denotes different from all, $p<0.0031$), (# denotes different from all, $p<0.0001$). There was a significant difference in the number of LP90 particles detected in the 9mm constructs compared with the 3 and 6 mm constructs († denotes different from all, $p<0.0001$). A significant difference in the percentage of LP90% particles out of the total number of particles in each construct was found between the 3 and 6 mm constructs (‡, $p<0.0198$). Regression analysis in Minitab indicated that the increase in the number of particles as a function of construct length followed a linear trend ($R^2 = 0.929$). Cumulative distribution plots showed a visual shift in average particle size within 6 mm constructs compared with 3 and 9 mm constructs.

Fourier Transform Infrared Spectroscopy

To confirm that mineral deposits on the perfused constructs were biological, FT-IR spectroscopy was used to characterize the chemical composition of the mineralized matrix that was deposited by rMSCs. The observed spectra in **Figure 5-8** displayed peaks that are representative of physiological bone composition.[114] Mineral from all three scaffold lengths exhibited the amide I and II peaks at 1650 and 1540 cm^{-1} which correlate to protein. The stretching (st) phosphate peaks near 1100 cm^{-1}, the stretching (st) carbonate peak at 870 cm^{-1}, as well as the phosphate bending (bd) doublet at 605 cm^{-1} and 560 cm^{-1} were also apparent in the mineral from all 3 lengths.

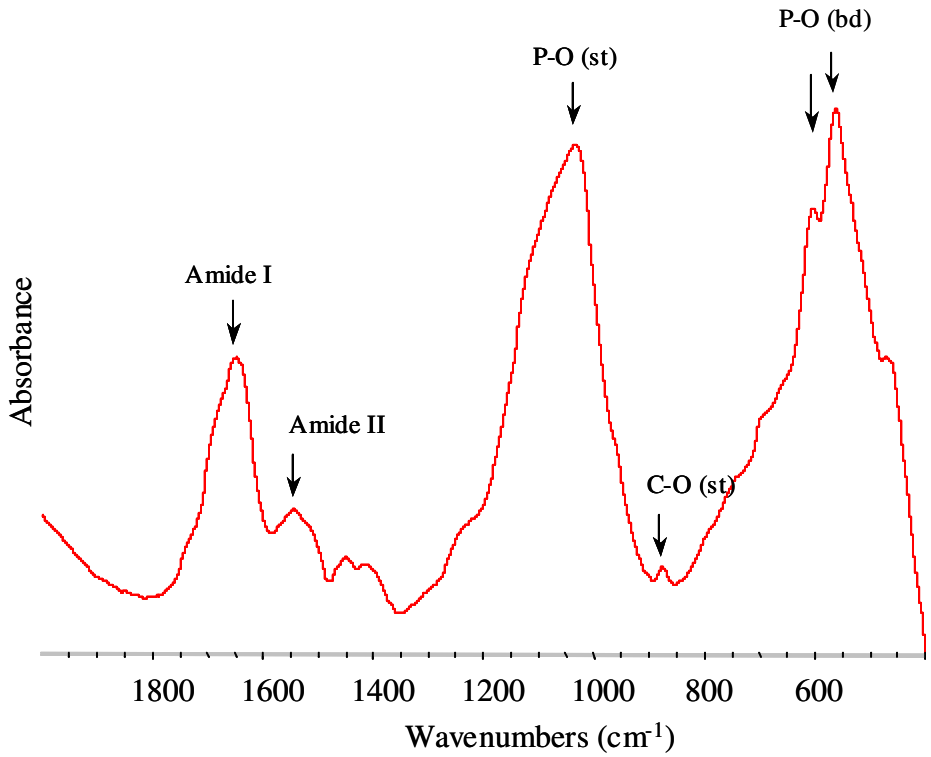

Figure 5-8. Representative FT-IR spectrum of mineral deposits removed from a 6mm stacked PCL+C construct. Mineral from all three scaffold lengths exhibited the amide I and II peaks which correlate to protein. The stretching (st) phosphate peaks near 1100 cm^{-1}, the stretching (st) carbonate peak at 870 cm^{-1} as well as the phosphate bending (bd) doublet at 605 cm^{-1} and 560 cm^{-1} were also apparent in the mineral from all 3 lengths. The above spectrum is characteristic of biological hydroxyapatite.

Discussion

Perfusion culture has been used, with varying levels of success, to produce mineral on thin (0.8-3.0 mm thick) titanium mesh, collagen sponge, and biodegradable polymer scaffolds.[2, 10-12] However, these scaffolds would be insufficient in size for use as a bone graft substitute in a pre-clinical, rat segmental defect model. Therefore we tested the effects of increasing scaffold length on the amount, distribution, and number of mineral particles that were deposited within perfused, cell seeded PCL+C scaffolds. Additionally, FT-IR analysis was used to characterize the mineral chemical composition within the constructs to ensure that the mineral was biological in nature.

General Observations

Mineral was detected throughout the entire length of the stacked scaffolds as shown in **Figure 5-1**, which indicates that the cells were able to produce mineral regardless on which stacked scaffold they were attached. Visual inspection of the constructs before scanning revealed extracellular matrix had accumulated between the scaffolds; however, this matrix was typically not mineralized and provided minimal structural support to bond the scaffold interfaces. This extracellular matrix occluded a majority of the pores on the top surface of the construct and may have hindered fluid flow through portions of the scaffold. Byers et *al*. reported that significant *in vitro* mineral formation at the periphery of PCL constructs seeded with control rMSCs inhibited mineral formation *in vivo*.[27] This result was attributed to the inability of blood vessels and native cells to infiltrate the implant due to the pre-existing matrix at the construct

exterior. Therefore, increasing scaffold pore size may be a beneficial method of preventing pores from becoming clogged during *in vitro* perfusion culture.

Micro-CT images in **Figure 5-2** show that little to no mineral had been deposited between the individual scaffolds in the 6 and 9 mm constructs. Scout views from the VivaCT, which show 2-D images of the constructs from the side, revealed small, angled gaps between the surfaces of the stacked constructs. The scaffolds were not perfect right circular cylinders, which caused the bottom of the scaffolds to sit at a slight angle when they were inserted into the bioreactor. This result, combined with the fact that the cut edges of the scaffolds were not completely smooth, resulted in gaps up to 500 μm in certain areas between the faces of stacked constructs.

Mineral Volume and Distribution Analysis

We hypothesized that the total mineral volume would increase proportionally as the construct length was increased. The total detected mineral volume effectively tripled as the construct length was increased from 3 to 9 mm (**Figure 5-3**). Additionally, the MVF was not statistically different for any of the construct sizes when the entire construct volume was compared (**Figure 5-4**). Both of these results supported our hypothesis that a proportional increase in mineral volume would accompany an increase in construct length. However, a 2.5-fold increase in mineral volume was detected as the scaffold length was doubled from 3 to 6 mm. Regression analysis in Minitab (data not shown, R^2 value = 0.70) suggested a weak linear relationship between construct length and mineral volume. It is possible that the porosity and the length of the 6 mm construct resulted in an optimal flow resistance and shear stress within the scaffold, which

stimulated the increased mineral growth. Using Darcy's Law, it would be possible to determine the energy loss within the 6 mm scaffold based on porosity and scaffold length. Replicating the same energy loss conditions in a 9 mm scaffold with greater porosity or a 3 mm scaffold with less porosity might be a way to increase mineral volume for scaffolds of those size.

The distribution of mineral throughout the construct was evaluated by analyzing three consecutively smaller cylinders of interest. The evaluation subregion sizes were selected based on previous studies, which reported mineral growth did not penetrate beyond 500 μm for statically cultured constructs.[6, 14] The percent of the total mineral detected in each subregion was plotted as a function of the percent of the total construct volume each subregion occupies (**Figure 5-5B**). The dotted (Ideal) line shows how a construct with mineral evenly distributed throughout the entire scaffold would be represented in such a plot. The percent of total mineral found in both subregions was shifted above the ideal line to a greater degree in both the 6 and 9 mm constructs than the 3 mm constructs. These results indicate that the mineral in the 3 mm construct was distributed more evenly throughout the entire construct, while the mineral in the larger constructs was more localized to the core region.

Mineral Particle Size and Density Analysis

On average, 25% of the total mineral particles detected in each construct were only one voxel in size and another 15% were only two voxels in size. These small particles contributed minimally to the overall mineral volume and produced a highly skewed particle size distribution. Because of their minimal contribution to the total

mineral volume, these small particles were neglected from the particle size distribution analysis. Even after selecting only the largest particles, which accounted for 90% of the total mineral (LP90%), the particle sizes did not follow a normal distribution. For analysis purposes, the mineral particle size data was transformed and displayed as a cumulative distribution.

We hypothesized that the number of mineral particles would increase proportionally as the construct length was increased. As seen in **Figure 5-7D**, there was a linear increase in the total number of mineral particles within each construct as the length was changed from 3 to 6 to 9 mm. Figure 5-7B shows that the number of LP90% particles within the 9 mm constructs was 2.3 times greater than the 3 mm constructs. The 9 mm constructs also contained almost 3 times the mineral as the 3 mm constructs, therefore, we would expect the particles in both of those constructs to be roughly the same size. The cumulative distribution plots which in **Figure 5-7E** support this conclusion. Two different mechanisms of increasing total mineral volume were observed in the 6 and 9 mm constructs. The 6 and 9 mm constructs contained roughly the same amount of total mineral, but the 9 mm constructs needed 3 times the number of LP90% particles to make up that mineral, therefore the 6 mm LP90% particles should be significantly greater in size. This conclusion is also borne out in the distribution plots. These large particles in the 6 mm constructs may have been several particles that grew together or if each one began as a single nucleation site. Scanning constructs at an earlier timepoint might help elucidate the mechanisms of increasing particle size.

Although no differences were detected in mineral density within the three different evaluation regions, there were significant differences in mineral density within

the constructs as the scaffolds increased in length. The mineral density data in **Figure 5-6** showed that the average mineral density of both the 6 and 9 mm long constructs was significantly less dense than the mineral in the 3 mm thick constructs. This may be an indication that the mineral was not as fully developed in the longer constructs. As mentioned previously, 40% of the mineral particles were two voxels or smaller. Considering that the number of mineral particles was increasing linearly in all the construct sizes (**Figures 5-7A and D**), there were significantly more of the particles of the smallest detectible size (the resolution of the micro-CT) within the 6 and 9 mm constructs compared with the 3 mm constructs. Smaller mineral particles are most likely, newly formed mineral deposits, which may therefore explain their lower mineral density. This large population of very small, possibly less developed, mineral particles may have contributed to reducing the overall mineral density detected by the micro-CT. Partial volume effects, which can overestimate sample volume in the micro-CT, may also have influenced the density measurement. Particles that are a fraction of a voxel may have been included when the threshold was set. These very small particles would then have been counted as a full voxel even if the associated mineral density was extremely low. Mineral density in 6 and 9 mm long constructs might increase if the time in culture was lengthened in order to facilitate an increase in mineral maturation of the smaller particles that have formed throughout the scaffold.

Conclusions

This study demonstrates that axial perfusion is a viable culture method for creating large mineralized constructs. As hypothesized, the number of mineral particles

within each scaffold increased proportionally as the scaffold length was increased. In addition, the mineral volume fraction remained constant as the construct length was increased from 3 to 9 mm. The mineral in the 3 mm construct was distributed more evenly throughout the entire construct, while the mineral in the larger constructs was more localized to the core region. Two complementary mechanisms of increasing total mineral volume were observed in the 6 and 9 mm constructs: increasing particle size, or increasing the number of mineral particles. A large number of pores on the top surface of each construct were filled with extracellullar matrix and completely occluded. This effect was also observed in previous perfusion experiments in Chapter 5 using PCL scaffolds with a porosity of 66%. In an attempt to mitigate this phenomenon, subsequent perfusion experiments will employ scaffolds with a larger pore diameter and greater porosity. Evaluating the effects of variable perfusion conditions to optimize mineralized matrix deposition and growth rate within large constructs would be a logical next step towards developing a bone graft substitute.

CHAPTER 6 EFFECTS OF TIME VARYING PERFUSION ON MINERALIZED MATRIX FORMATION WITHIN LARGE 3-D CONSTRUCTS IN VITRO

Introduction

Tissue engineered bone graft constructs, populated with cell-mediated mineralized matrix throughout the scaffold, may have enhanced osteoconduction and induction properties compared with non-mineralized implants. Before harvesting a tissue engineered bone graft substitute grown *in vitro* for surgical use, it would be advantageous to determine the amount of mineralized matrix that has developed on the construct. Several researchers have investigated the effects of increasing the rate of continuous perfusion through 3-D bone constructs on cell viability and function as well as matrix synthesis.[7, 8, 10, 64, 116] However, the effects of dynamic perfusion through 3-D constructs with respect to mineralized matrix growth and development has not been reported. Additionally, the onset of significant mineral deposition and growth rate in 3-D culture of large constructs has not been reported in the literature, possibly due to the non-trivial nature of collecting such data. Determining mineral growth rate requires multiple measurements of mineralized matrix volume on the same construct. Micro-CT offers a non-destructive way to perform repeat quantitative measurements on mineralized matrix formation within cell-seeded scaffolds grown *in vitro*. Previous experiments in our lab have shown that repeated micro-CT scanning did not significantly decrease mineral production of rMSCs seeded on demineralized bone matrix or polymeric scaffolds after 8 weeks in static culture.[14] This study also showed minimal mineralized matrix present after 4 weeks in culture. To determine whether repeat scans would inhibit cells from

synthesizing mineralized matrix during perfusion culture, rMSCs seeded on PCL+C scaffolds were scanned at 3 and 5 weeks in a Viva Micro-CT. Mineral deposition was compared with constructs scanned at only 5 weeks. The VivaCT was designed to accommodate anesthesia tubing through a port in the scanner to scan live animals. A bioreactor was inserted through that port and the flow loop tubing remained connected in order to preserve sterility during scanning. Repeat scanning was then used to evaluate the effects of different perfusion profiles on mineralized matrix deposition and growth rate on PCL+C scaffolds seeded with rMSCs during 5 weeks of culture.

Our results from Chapter 4 indicated that a continuous low flow rate (0.01 ml/min), for MC3T3-E1 cells seeded on trabecular bone, elevated cell proliferation and viability compared with static and higher flow rates (0.2 ml/min and above) after one week in culture. However, the higher continuous flow rates resulted in an upregulation of osteoblast specific genes Runx2, OCN and ALP (data not shown here).[64, 116] Experiments using parallel plate flow chambers, which applied pulsatile and oscillatory flow conditions to osteoblasts have shown increases in osteogenic gene expression, intracellular Ca^{2+} concentrations, and the production of nitric oxide and PGE_2 in comparison to static controls.[15, 16] These 2-D and 3-D flow results suggest that osteoblasts may be responsive to bouts of elevated flow rates superimposed on a low constant flow rate. To test the response of osteoblasts to dynamic flow conditions in a 3-D perfusion environment, rMSCs were seeded on 9 mm thick PCL+C scaffolds and perfused with three different flow regimes: low flow, high flow and low flow with intermittent high flow for one hour a day. Non-perfused control constructs were cultured simultaneously. All constructs were scanned at 3 and 5 weeks to quantify early mineral

formation, mineral growth rate changes, and changes in mineral particle size during culture. It was hypothesized that intermittent elevated flow would increase the amount of mineral at the early timepoint as well as the rate and amount of mineralized matrix synthesis compared with the continuous flow and control cultures. Additionally, it was hypothesized that mineral volume would increase due to an increase in mineral particle size.

Materials and Methods

In Vitro VivaCT Scanning - Bioreactor Design

The entire bioreactor chamber was inserted into the scanner without disconnecting the tubing so that the system remained closed and sterile. Therefore the bioreactor dimensions needed to mimic those of a standard VivaCT sample holder. The bioreactor base wall thickness was decreased to 0.76 mm to match the wall thickness of a standard micro-CT sample holder and create an x-ray "window" as shown in **Figure 6-1**. The thinner walls reduce x-ray attenuation and lower the background signal. Detailed drawings of the scanning bioreactor design can be found in **Appendix 5**.

Scaffold Preparation

Fused deposition modeling was used to fabricate 9 mm thick PCL lattice sheets comprised of 400 μm thick struts spaced 800 μm apart and layered in a 0/60/120 degree repeating pattern to produce a 75% porous structure. Scaffolds were cut using a 6 mm biopsy punch (Miltex) to create cylindrical scaffolds (6 mm ∅ x 9 mm long), which were then incubated in 5M NaOH for 4 hours at 37° C for cleaning purposes. 6 mm holes

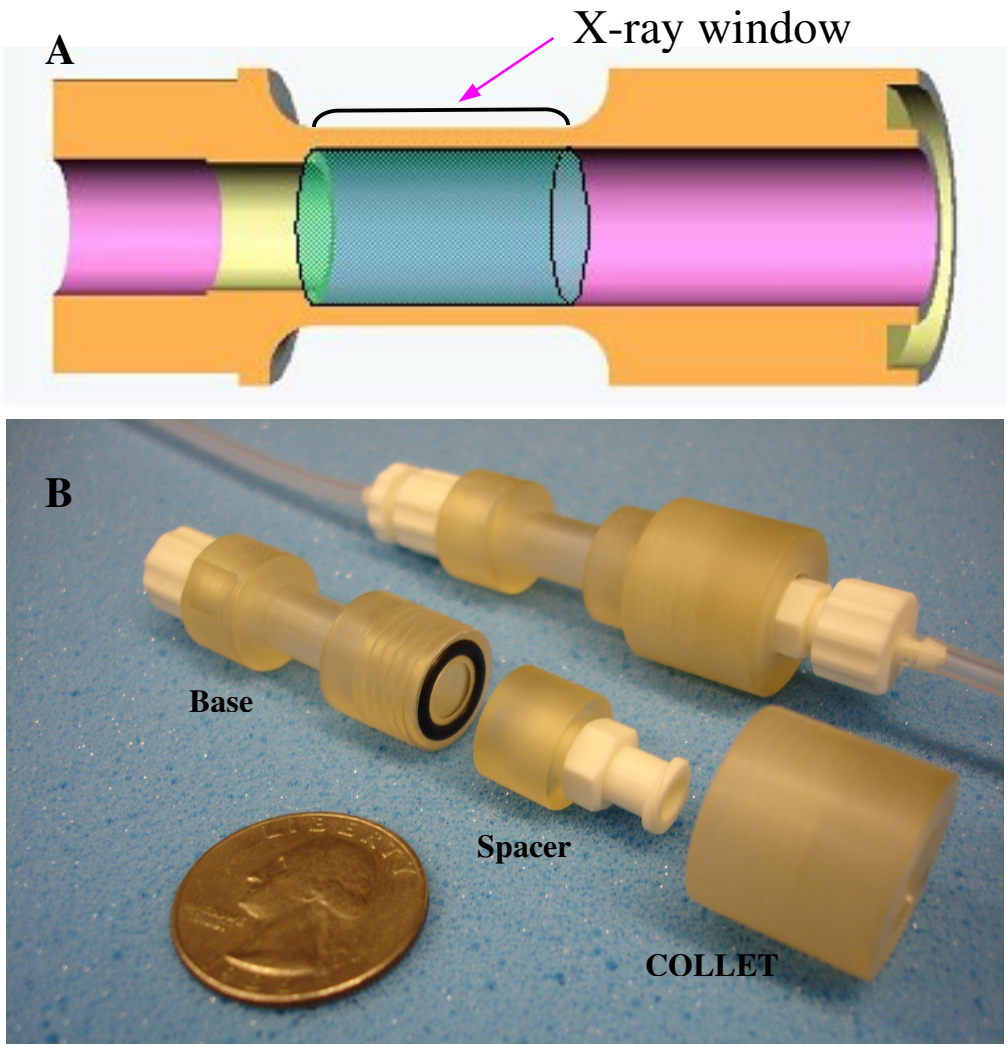

Figure 6-1. Bioreactor assembly capable of being scanned in the VivaCT. (**A**) Schematic of axial perfusion base. The construct sits on the yellow lip. The x-ray window is 10 mm in length. (**B**) Image of the perfusion bioreactor both assembled and unassembled. The black o-ring forms a water tight seal against the spacer when the collet is screwed onto the base. The white luer lock connections are sealed with Teflon tape to prevent leaks.

were milled out of a polycarbonate block to create a mold, which was used to cast collagen gels within the PCL scaffolds **(Appendix 6)**. 225 µl of the collagen/sodium bicarbonate solution was deposited in each of the holes. To prevent unpolymerized collagen from leaking out the bottom of the drilled holes, a thin piece of neoprene was compressed between the block and a polycarbonate sheet with five screws to seal the bottom **(Figure 6-2)**. Cut scaffolds were inserted into the sterile mold while the collagen solution was still liquid so that the fluid seeped up through the scaffold and infiltrated the entire pore space. After the molds were placed in sterile polycarbonate boxes, the scaffolds stood at room temperature for 30 min to allow the collagen to polymerize. The boxes were then transferred to a –80º C freezer for 90 minutes until frozen and finally placed in a lyophilizer (Labconco) overnight until dry.

Construct Seeding and Culture – Effect of Multiple X-ray Scans

rMSC cells were thawed, placed in 150mm tissue culture dishes, expanded for one passage, trypsinized, counted, and then seeded on scaffolds. PCL+C Scaffolds were placed in 6-well plates and six million cells, suspended in 120 µl of media (α-MEM with 10% FBS and 1% antibiotic/antimycotic), were deposited on each scaffold. The collagen mesh absorbed all of the media and constructs were subsequently placed in an incubator. After one hour, 9 ml of media without osteogenic supplements was added to each well to ensure that the entire construct was covered in media. After three days in culture, constructs were placed in the bioreactor and perfused at 0.2 ml/min with 18 ml of osteogenic media or placed in static culture with 18 ml of media. Ten ml of media with osteogenic supplements was changed once per week, which left 8 ml of conditioned

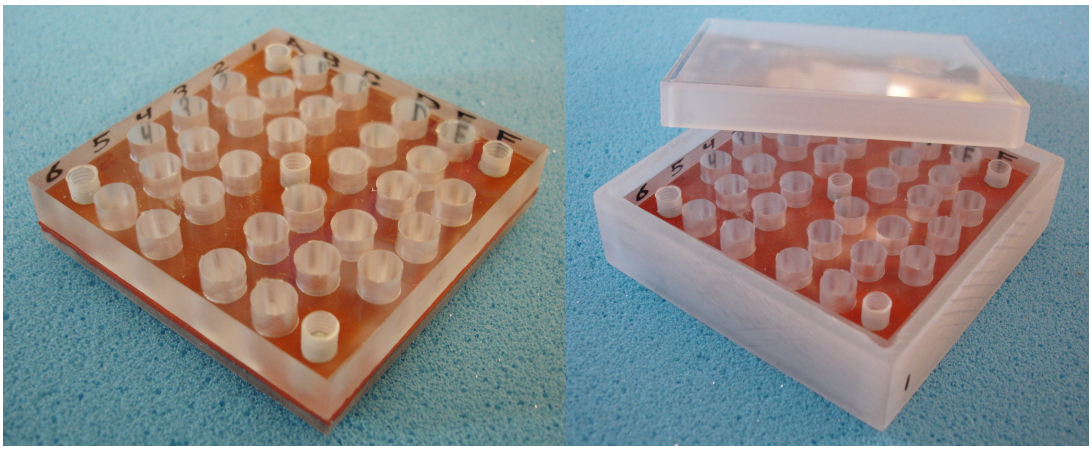

Figure 6-2. Mold used to cast collagen gels within PCL scaffolds. The red neoprene sheet seals the holes so that unpolymerized collagen does not seep out the bottom of the scaffold.

media in the tubing or the static wells at all times. The static constructs were cultured in custom designed 6 well plates (3.5 cm deep wells) to accommodate 18 ml of media. After three weeks, while still inside each bioreactor, half of the constructs (n=6) were scanned in the VivaCT at a voxel resolution of 21.5 μm and subsequently returned to perfusion culture. At 5 weeks, all scaffolds were scanned on the VivaCT at the same voxel resolution. Therefore, one group had been scanned once and one group had been scanned twice. This experiment was run in duplicate.

Construct Seeding and Culture - Time Varying Perfusion

Constructs were seeded in an identical manner as the Effect of Multiple X-ray Scan experiments. After 3 days in static culture, constructs were either placed in the perfusion bioreactor and axially perfused with one of three flow regimes (n=4): 0.2 ml/min continuous flow (0.2), 0.8 ml/min continuous flow (0.8), or 0.2 ml/min continuous flow for 23 hours/day plus one hour of culture with flow elevated to 0.8 ml/min (intermittent – INT), or they were placed in one of two control culture groups. The first control group consisted of constructs sitting in custom designed 6 well plates with 3.5 cm deep wells (Static). The second control group consisted of constructs in identical custom 6 well plates that were placed on an orbital rocker plate (RP). The RP constructs were agitated at a frequency of 0.5 Hz. Constructs in both control groups received 18 ml of media with osteogenic supplements. Ten ml of media with osteogenic supplements was changed once per week leaving 8 ml of conditioned media in the bioreactor and tubing or the control wells at all times. All constructs were scanned at 3 and 5 weeks. This experiment was run in triplicate.

Confocal Scanning Microscopy

After 3 days in static culture, two PCL+C constructs were stained with calcein and ethidium homodimer, then viewed with confocal microscopy to visualize the distribution of live and dead cells prior to receiving osteogenic media and beginning perfusion culture. Constructs were cut in half down the long axis and imaged on the top, bottom, rounded outer surface, and the top, middle and bottom sections of the cut face. Constructs from each experiment group were also stained after 35 days in culture to examine cell distribution and viability at the end of the experiment.

VivaCT Scanning and Analysis

In vitro mineralization on perfused constructs was quantified using a VivaCT (Scanco Medical, Switzerland) at a voxel resolution of 21.5 μm. After 3 weeks of culture, each set of bioreactors, which contained one experimental group of constructs, was removed from the incubator and transported to the VivaCT. Each individual bioreactor was fed through the VivaCT anesthesia port system and clamped in place for scanning purposes. The scanning region was isolated to the x-ray window **(Figure 6-1)** in the bioreactor. After scanning all constructs, the bioreactors were then returned to the incubator and perfusion was restarted. Under sterile flow hood conditions, static and rocker plate control constructs were aseptically removed from 6 well plates and inserted into a sterile VivaCT sample holder (**Figure 6-3**). After scanning, constructs were returned to the 6 well plates and culture was resumed. Both the bioreactor window and the sample holder from **Figure 6-3** were machined to the same wall thickness to ensure uniform x-ray attenuation for each set of scans.

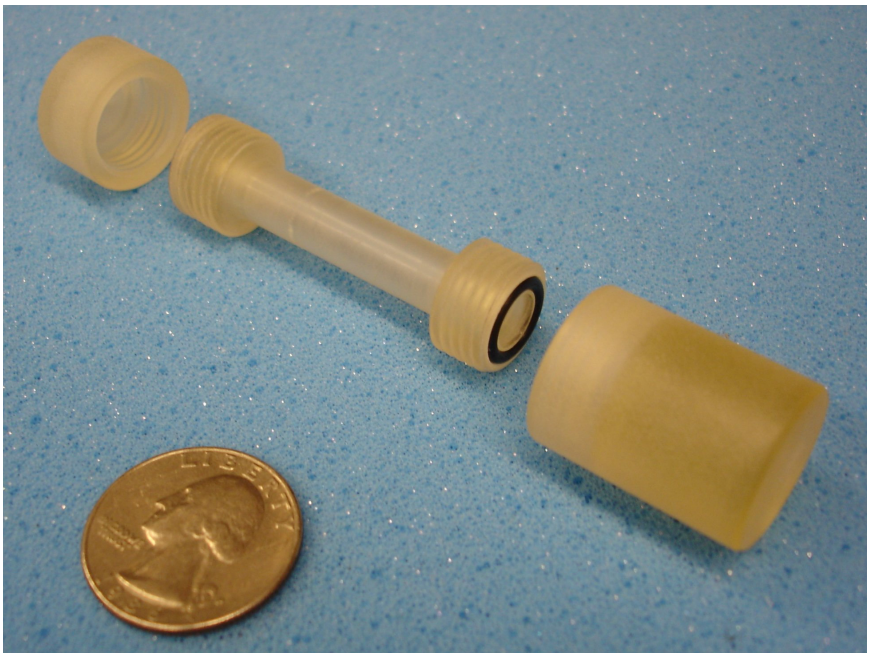

Figure 6-3. VivaCT sample holder for static and rocker control constructs. O-ring seals on either end prevent media leaks and maintain sterility in the VivaCT. Three constructs can be placed in the holder at one time to minimize overall scan time.

Samples were evaluated at a threshold of 92, a filter width of 1.2 and filter support of 2.0. X-ray attenuation was correlated to sample density using a calibration curve generated by scanning hydroxyapatite standards, each with a known mineral density. A threshold of 92 correlated to a linear attenuation of 1.15 cm^{-1} and a mineral density of 95 mg HA/cc. Mineral volume and density were quantified throughout the entire construct as well as the two concentric cylindrical subregions that were used for analysis in Chapter 5. Mineral particle size and number were also quantified in this experiment using the same method as Chapter 5. The largest particles, which comprised 90% of the total mineral volume (LP90%) in each construct, were analyzed to compare mineral particle size differences among experimental groups as well as between weeks 3 and 5. The mineral particle sizes were not normally distributed; therefore, the LP90% particles from all of the constructs within each of the 5 groups were combined together to generate a continuous distribution of particle sizes for each experimental group. The percentage of cumulative LP90% particles was plotted as a function of particle size on a log scale.

Fourier Transform Infrared Spectroscopy Analysis

FT-IR spectroscopy was used to analyze the chemical composition of the mineralized matrix that was deposited by the rMSCs. Samples were prepared as described in Chapter 5. Spectra which showed peaks corresponding to chemical bonds, were comprised of 64 scans acquired at 4 cm^{-1} and were collected on a Nexus 470 FT-IR spectrometer (Thermo Nicolet, Madison, WI) under N_2 purge. These spectra were

displayed from 400 to 2000 cm^{-1}, which is the range that includes bands that are characteristic of bone's constituents.

Data Analysis

Data are reported as mean ± SEM and statistical analyses using Minitab12 were carried out using a general linear model (ANOVA) and Tukey's post-hoc test for pairwise comparisons with $p<0.05$ considered significant.

Results

General Observations – Effect of Multiple X-Ray Scans

Confocal microscopy showed both live and dead cells distributed throughout the entire construct for both experimental groups **(Figure 6-4)**. Consistent with our previous experiments, there appeared to be a greater number of live cells, as well as a smaller number of dead cells, within the perfused constructs compared with the static constructs. There was no discernable difference in viability between the constructs that had been scanned twice compared with the constructs that had been scanned once.

Visual inspection of 3-D images of mineral deposition on PCL+C constructs revealed mineral deposition throughout the entire length of all constructs at all thicknesses **(Figure 6-5)**. Only trace amounts of mineral were present in the static constructs at both 3 and 5 weeks. There was no visible difference in the mineral particle shape and distribution found on constructs that had been scanned twice compared with those that had been scanned once. Mineralized matrix volume and density were quantified throughout the entire construct.

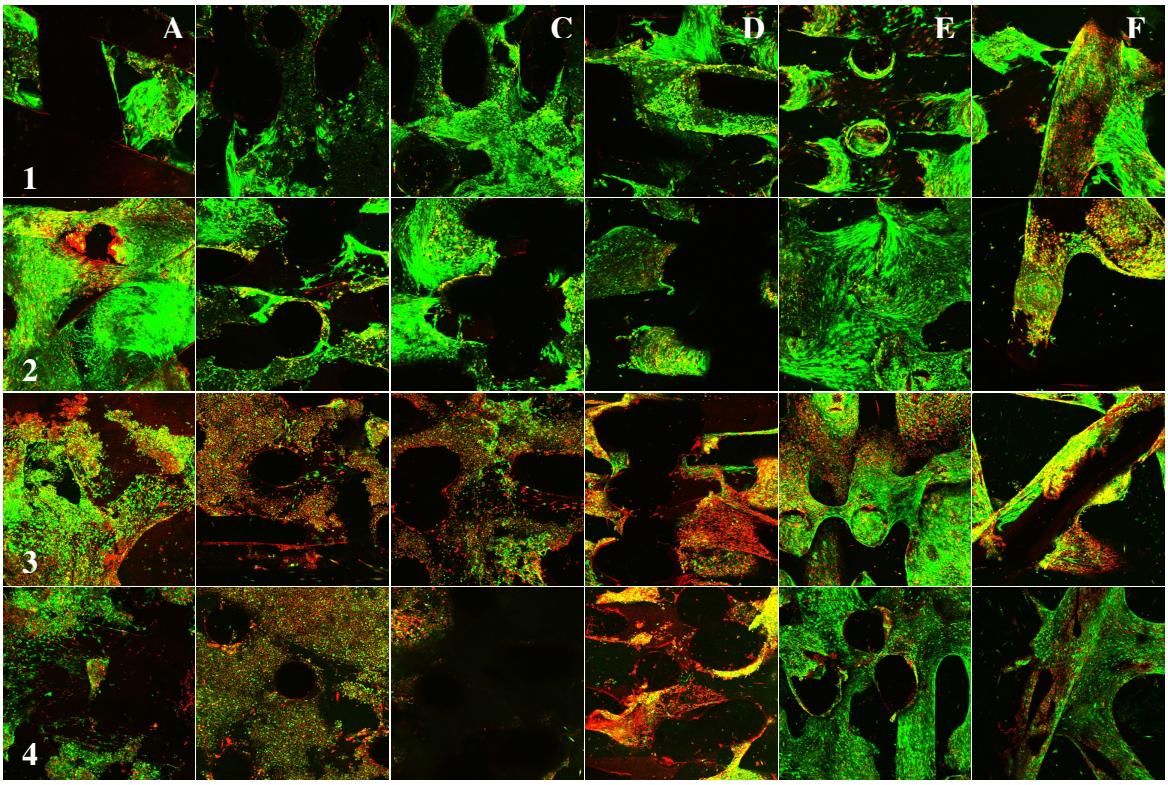

Figure 6-4. Confocal microscopy images of 9mm long constructs stained with calcein and ethidium homodimer to visualize live (green) and dead (red) cells. Images were taken using a 5X objective. Row 1 shows representative images of constructs perfused at 0.2 ml/min and scanned once. Row 2 shows representative images of constructs perfused at 0.2 ml/min and scanned twice. Row 3 shows representative images of static constructs scanned once. Row 4 shows representative images of static constructs scanned twice. All constructs were cut in half down the long axis and each face was imaged. Columns A-F designate the region of the construct that the image was taken from. A – bottom face, B – the bottom region of the cut face, C – middle region of the cut face, D – top region of the cut face, E – rounded outer surface, F – top face.

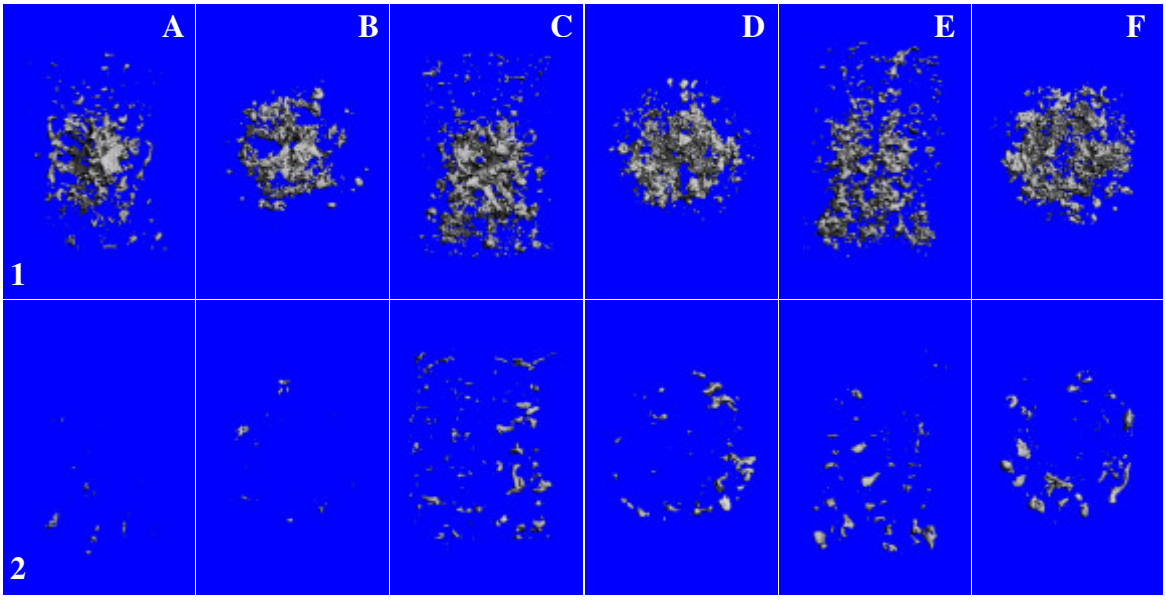

Figure 6-5. Representative VivaCT images of perfused (row 1) and statically (row 2) cultured PCL+C scaffolds seeded with rMSCs. Column A shows a side view of a construct at 3 weeks. Column B shows the same construct from the top view. Column C shows a side view of the same construct in column A, this time at 5 weeks. Column D shows the top view of the construct in column C. Column E shows the side view of a construct that has only been scanned at 5 weeks. Column F shows the same construct from the top view.

Mineral Volume and Density

No significant differences were detected in mineralized matrix volume within constructs that had been scanned twice compared with those that had been scanned once (**Figure 6-6**). There was no significant difference in mineralized matrix volume detected between experiment replicates at any timepoint. Additionally, there were no significant differences in mineral density for scaffolds that had been scanned twice compared with those that had been scanned once. However, there was a statistical difference in mineral density between experimental replicates.

General Observations – Effect of Time Varying Perfusion

Confocal microscopy showed both live and dead cells distributed throughout the entire construct for all experimental groups after 5 weeks of culture **(Figure 6-7)**. The 0.2 ml/min and intermittent flow groups exhibited a qualitative increase in viable cells throughout the construct compared with the other culture conditions. There was no visual discernable difference in the distribution of live and dead cells among the remaining groups.

Visual inspection of scaffolds after perfusion revealed minimal pore occlusion after 5 weeks of culture. Visual inspection of micro-CT images of PCL+C constructs showed that mineral was distributed throughout the full length of the scaffold for all groups except for the Static culture constructs. The mineral was localized to the periphery as well as a scattered ring of mineral at the bottom of the Static constructs. Comparing the week 5 images to the week 3 images, the mineral particles increased in size, but the general shape, location, and distribution of mineral particles was very similar between repeat scans **(Figure 6-8, 6-9)**. Examining the tubing in the perfusion culture

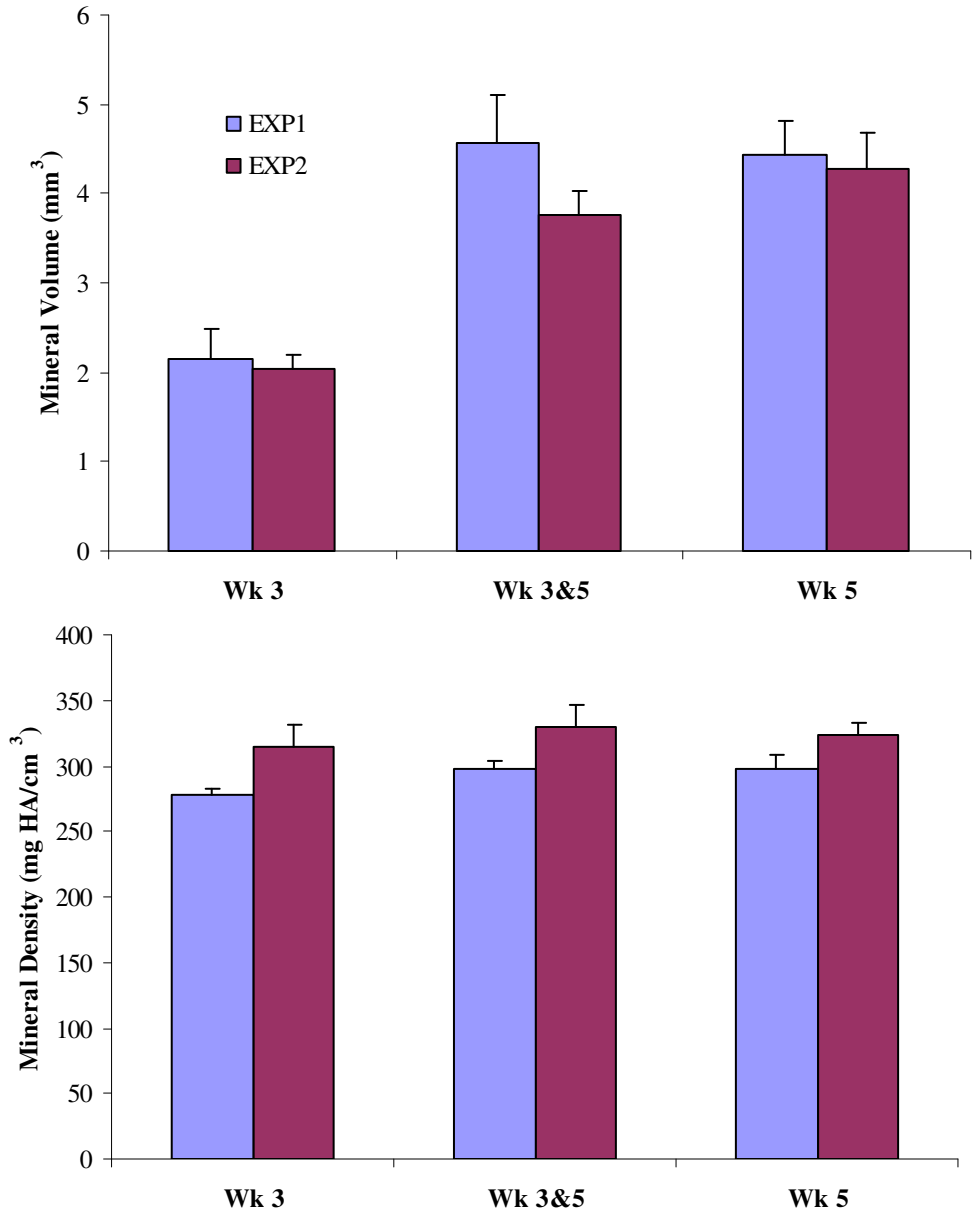

Figure 6-6. Mineralized matrix volume and density within 9 mm thick 75% porous PCL+C constructs (n=6) detected by micro-CT scanning at a voxel resolution of 21.5 μm. One group of constructs was scanned at 3 and 5 weeks while the second group was scanned only at 5 weeks. General Linear Model ANOVA showed no significant differences in mineralized matrix volume within constructs that had been scanned twice compared with those that had been scanned once ($p=0.8606$). There was no significant difference in mineralized matrix volume detected between Experiment 1 and 2 at any timepoint ($p=0.2411$). General Linear Model ANOVA performed on density measurements showed no significant effect of multiple scanning. However, there was a significant difference in mineral density between Experiment 1 and Experiment 2 ($p<0.02$).

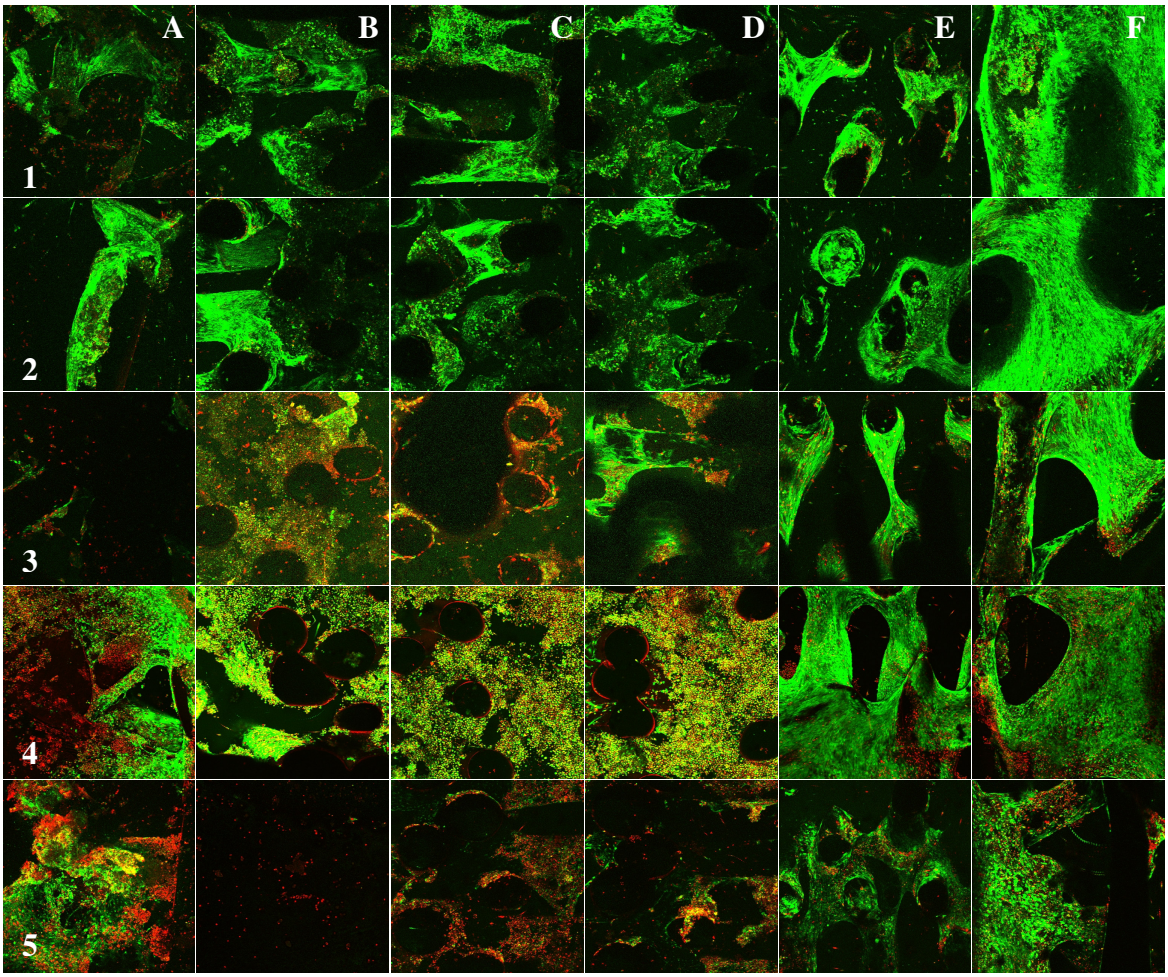

Figure 6-7. Representative confocal microscopy live/dead images from each experimental group: 1 – 0.2 ml/min, 2 – 0.2→0.8 ml/min, 3 – 0.8 ml/min, 4 – static, 5 – rocker after 5 weeks of culture. Live cells are green, red cells are dead. Columns A-F designate the region of the construct that the image was taken from. (A) bottom face, (B) the bottom region of the cut face, (C) middle region of the cut face, (D)– top region of the cut face, (E) rounded outer surface, (F) top face.

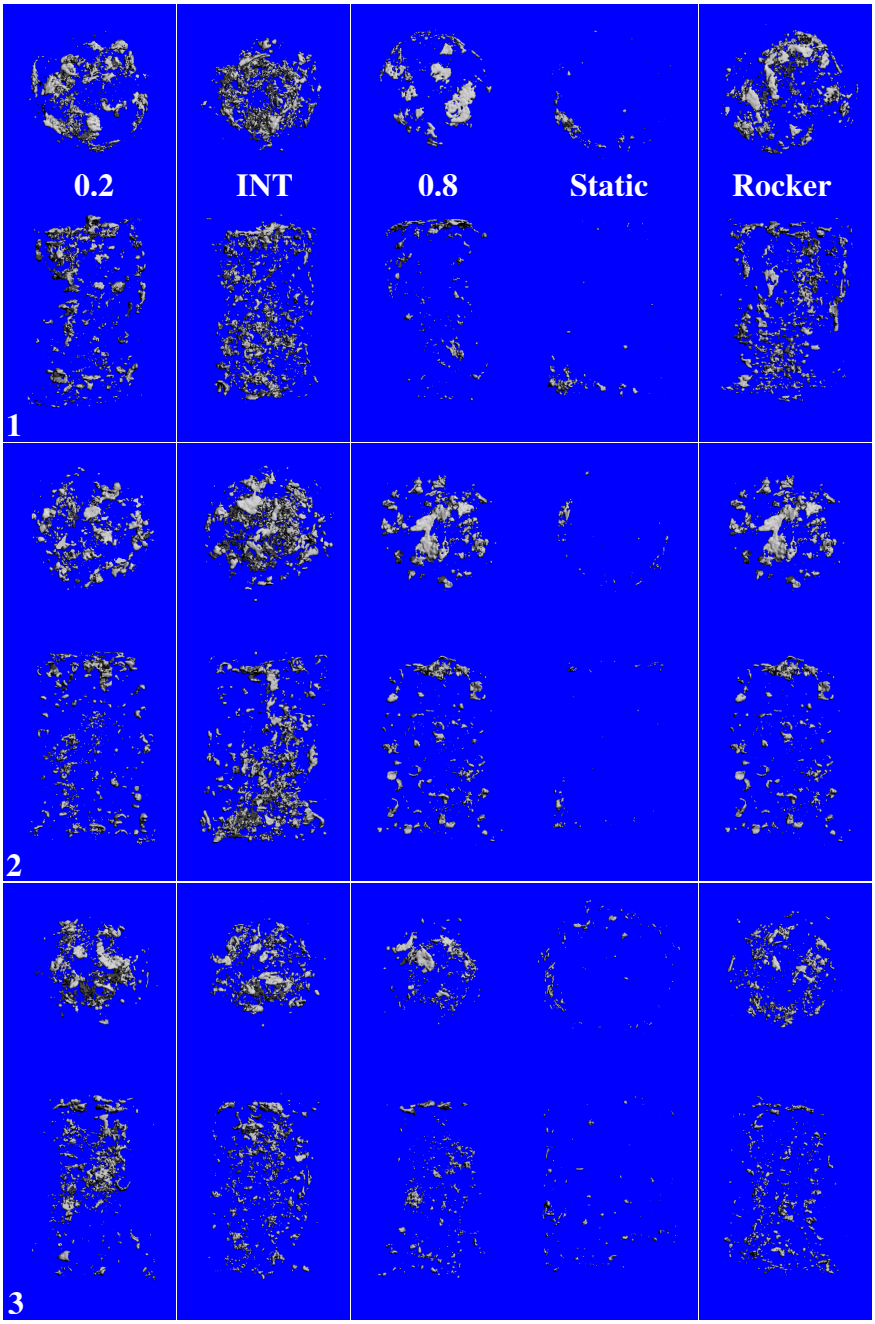

Figure 6-8. Representative VivaCT images of constructs (top and side view) from each experimental group and from each repeated experiment after 3 weeks of culture. Columns designate which experimental group each image was generated from. Rows labeled 1-3 designate which experimental replicate each image was generated from.

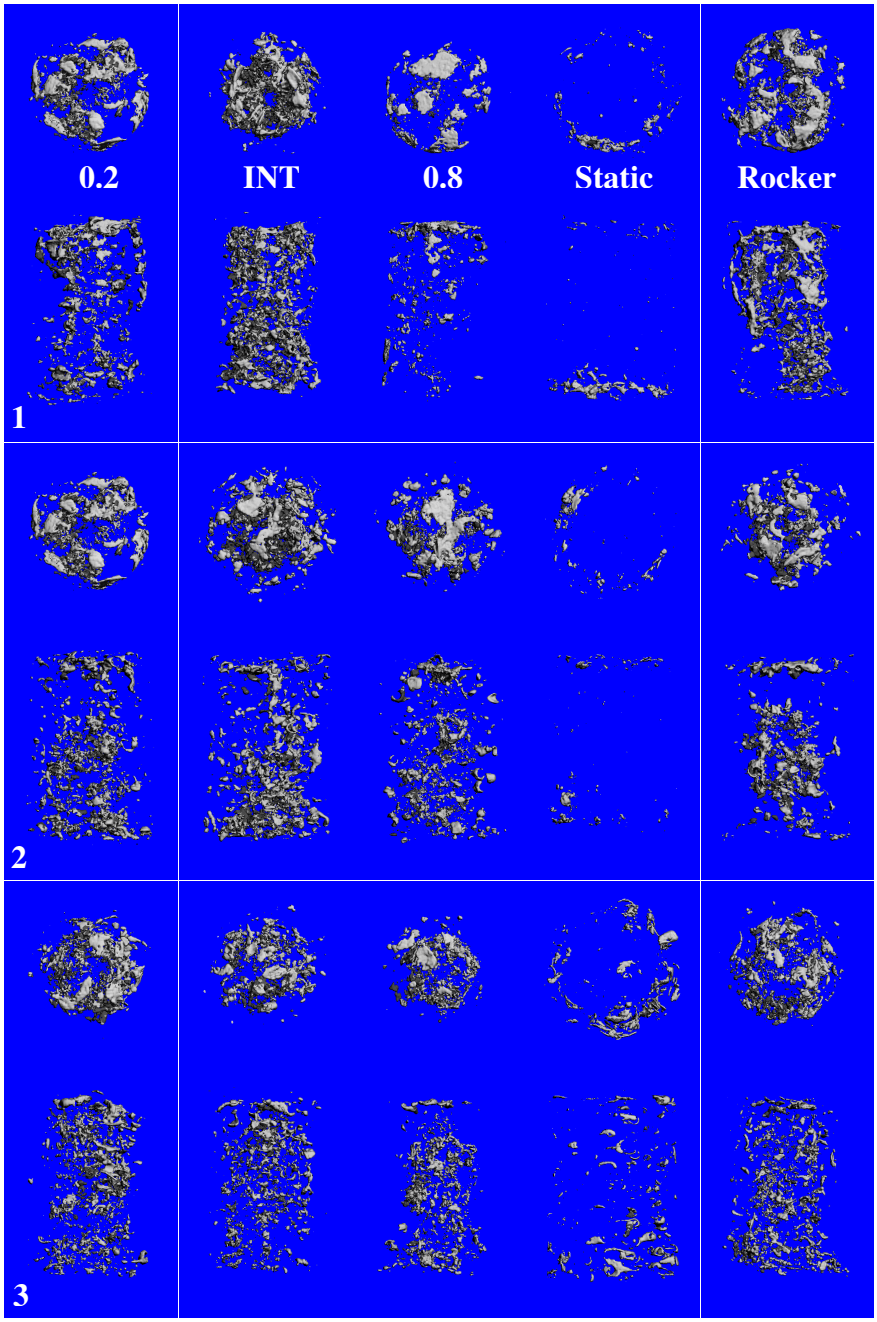

Figure 6-9. Representative VivaCT images of constructs (top and side view) from each experimental group and from each repeated experiment after 5 weeks of culture. Columns designate which experimental group each image was generated from. Rows labeled 1-3 designate which experimental replicate each image was generated from.

revealed particles of matrix downstream from the constructs in all flow groups. The amount of debris was not quantified, but there appeared to be more material in the tubing of the 0.8 ml/min flow group compared with the tubing for the INT constructs. Minimal debris was observed in the tubing for the 0.2 ml/min constructs. There was also substantial mineral deposited within the RP control constructs.

Mineral Volume and Density Quantification

There were significant differences in mineralized matrix volume within constructs in different culture conditions at both 3 and 5 weeks (**Figure 6-10**). After 3 weeks in culture, 0.2 ml/min constructs had produced twice as much mineral as 0.8 ml/min constructs and 18 times as much mineral as static constructs. INT flow scaffolds produced 2.8 and 23.5 times as much mineral as 0.8ml/min and Static constructs, respectively. RP constructs produced twice the mineral as 0.8 ml/min constructs and 17 times as much mineral as static constructs. Eight times as much mineral was detected in 0.8 ml/min constructs compared with Static, but the overall amounts were so low that they were not statistically significant. There were no statistical differences in the amount of mineralized matrix produced among the 0.2 ml/min, INT flow, and RP cultures. These trends were mimicked after 5 weeks of culture, but the percent differences in mineral volume among construct groups were not as pronounced. Constructs from the 0.2 ml/min, INT and RP showed 2.0, 2.5 and 2.1-fold increases in mineral volume compared with 0.8 ml/min constructs. Those same three groups had mineral volume increases of 6.2, 7.7, and 6.4-fold (much lower than at 3 weeks), compared with Static constructs. At 5 weeks there were still no differences in mineral volume among the 0.2, INT and RP

constructs. When comparing week 3 mineral volume to week 5, the following increases were seen: 2.4, 2.3, 2.6, 7.0, and 2.6-fold for 0.2 ml/min, INT, 0.8 ml/min, Static, and RP constructs. The rate of mineral deposition followed the same trends as the total amount of mineral that was deposited (**Figure 6-11**).

There were no statistical differences in mineral density for any of the construct groups at any timepoint, regardless of what volume of interest was analyzed (**Figure 6-12**). Mineral density values for Static constructs were not included in the statistical analysis because the amount of mineral was insufficient for the VivaCT to calculate a density measurement for several of the samples.

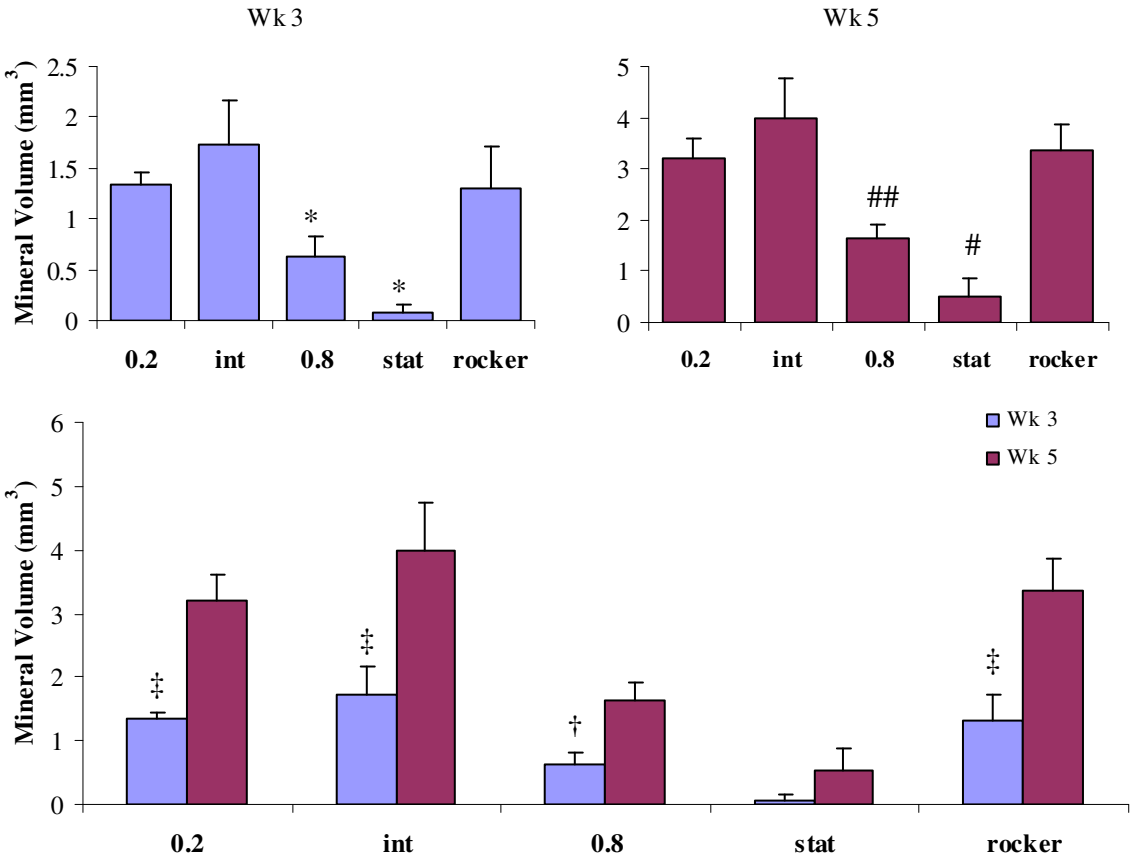

Figure 6-10. Mineralized matrix volume within the entire volume of 9 mm thick 75% porous PCL+C constructs detected by micro-CT scanning at weeks 3 and 5 for all experimental groups (n=4, 3 replicates). General Linear Model ANOVA revealed significant differences in mineralized matrix volume within constructs in different culture conditions at both timepoints. Pairwise comparisons showed that at week 3, * denotes statistically different from non-* groups ($p<0.013$). At 5 weeks, ## denotes different from all groups ($p<0.050$), # denotes different from all groups ($p<0.001$). Comparing mineral volume at 3 weeks to mineral volume at 5 weeks, † denotes ($p<0.044$), while ‡ denotes ($p<0.001$)

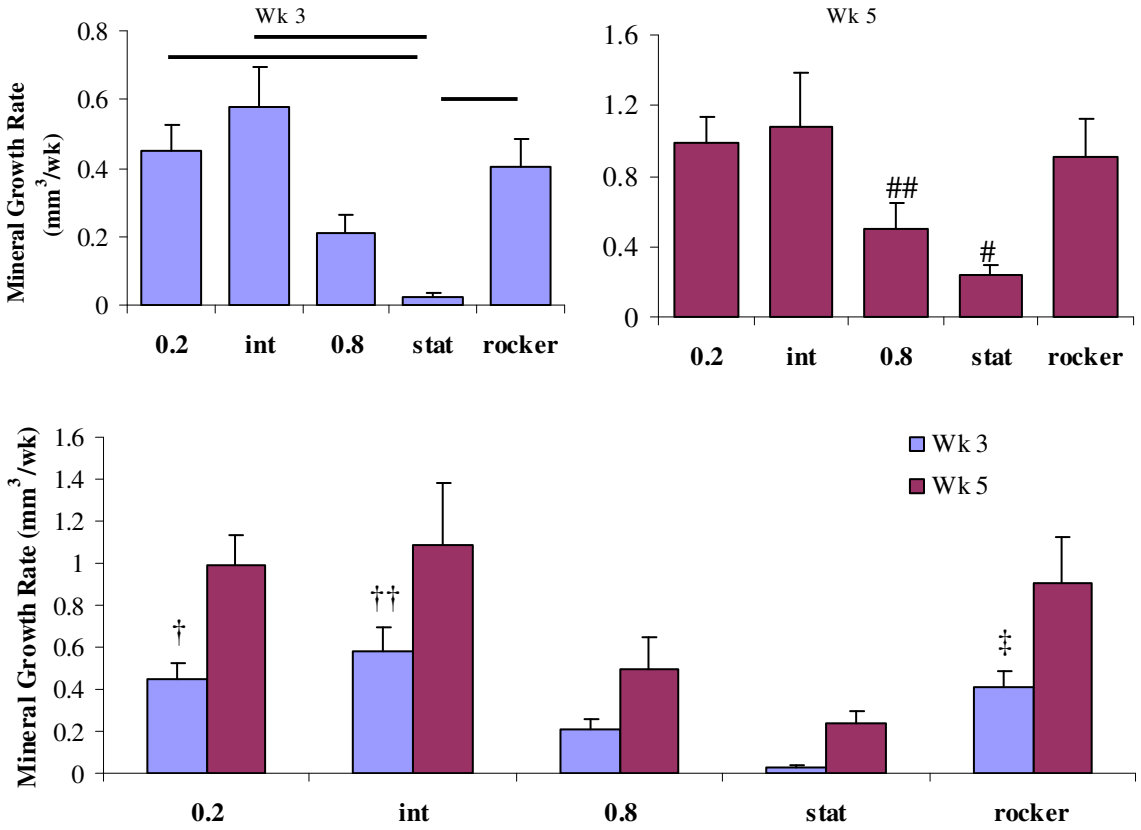

Figure 6-11. Mineral deposition rate within the entire volume of PCL+C constructs measured at 3 and 5 weeks for each culture condition (n=4, 3 replicates). General Linear Model ANOVA revealed significant differences in mineralized matrix deposition rate within constructs in different culture conditions at both timepoints. Pairwise comparisons showed that at week 3, 0.2 was different from stat ($p<0.028$), int was different from stat ($p<0.0006$) and rocker was different from stat ($p<0.0005$). At 5 weeks, ## denotes different from all unmarked groups ($p<0.003$), # denotes different from all unmarked groups ($p<0.0001$). Comparing mineral deposition rate at 3 weeks to mineral volume at 5 weeks, † denotes ($p<0.0011$), †† denotes ($p<0.0051$), while ‡ denotes ($p<0.0005$).

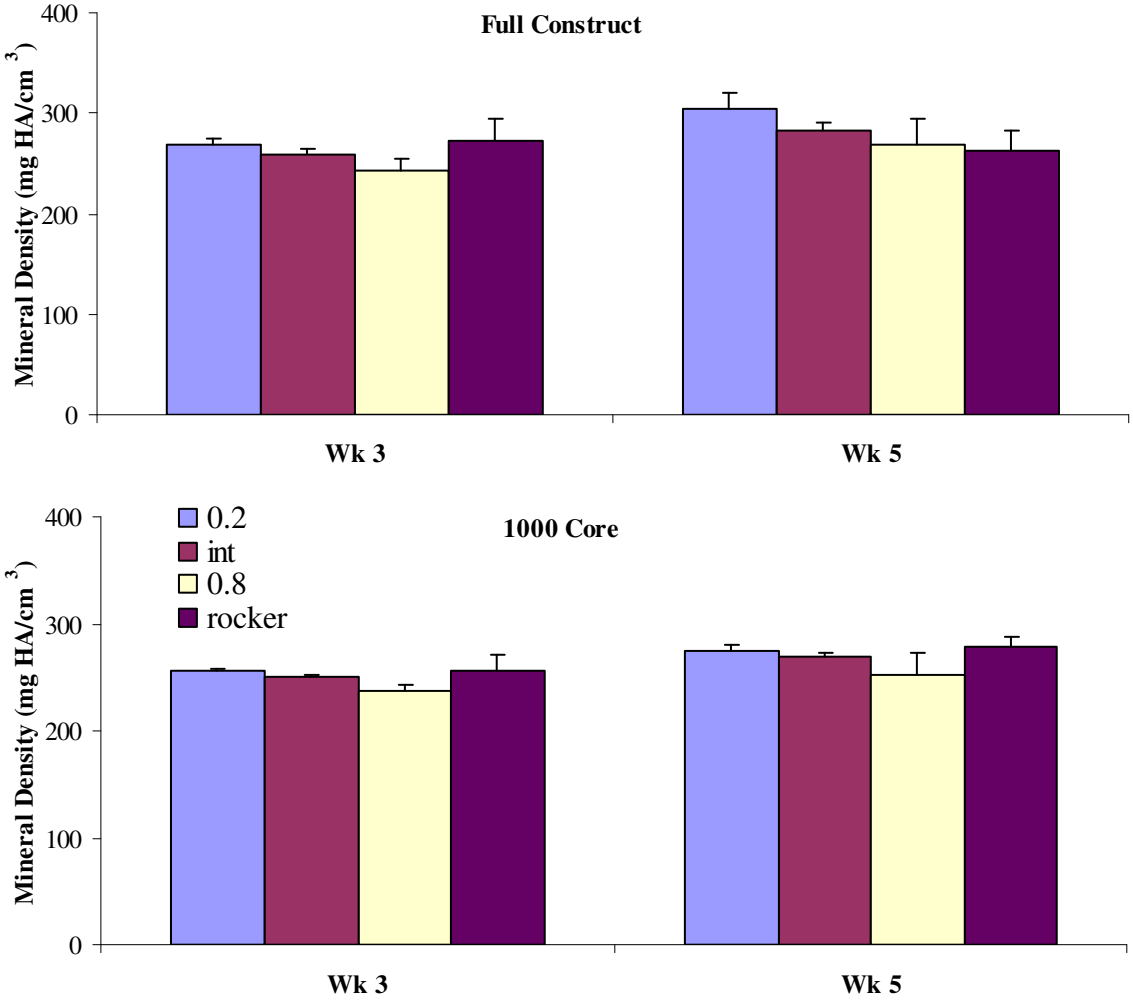

Figure 6-12. Mineralized matrix density detected by micro-CT scanning within 9 mm thick 75% porous PCL+C constructs at weeks 3 and 5 for all experimental groups (n=4, 3 replicates). General Linear Model ANOVA showed no significant differences in mineralized matrix density within constructs in different culture conditions at either timepoint. Mineral density values from static cultures were excluded here because density measurements were below the detection limit of the micro-CT due to the small amount of mineral within static constructs.

Mineral Spatial Distribution

These same trends and relative increases in mineral volume that were seen in the full construct volume, both among groups and between weeks, were observed in the 500 core and 1000 core subregions, as well (1000 core shown in **Figure 6-13**). After 3 weeks of culture, over 80% of the mineral was located in the 500 core and over 60% was detected within the 1000 core subregion, for all experimental groups except the Static case. For Static constructs, only 30% of the detected mineral was located within the 500core and just 10% was present in the 1000 core subregion **(Figure 6-14)**. After 5 weeks of culture, over 90% of the total mineral volume was detected within the 500 core and over 70% was within the 1000 core. The distribution of mineral within Static constructs remained the same as at 3 weeks. The small amount of mineral at the 1000 core in the Static culture constructs, resulted in increases in mineral volume greater than 100-fold for the 0.2 ml/min, INT and RP constructs, and greater than 50-fold for the 0.8 ml/min constructs compared with Static constructs.

Mineral Particle Size Distribution and Number

Scanco software was used to determine the number of mineral particles as well as the mineral particle size within PCL+C constructs. The total number of particles within each construct is shown in **Figure 6-15**. At 3 weeks, there was a 1.8-fold increase in the number of mineral particles for both the 0.2 ml/min and INT constructs compared with the 0.8 ml/min constructs. RP constructs contained a comparable number of mineral particles to the 0.2 ml/min and INT constructs, but not statistically more than the 0.8 ml/min constructs. There were significantly fewer mineral particles in the Static

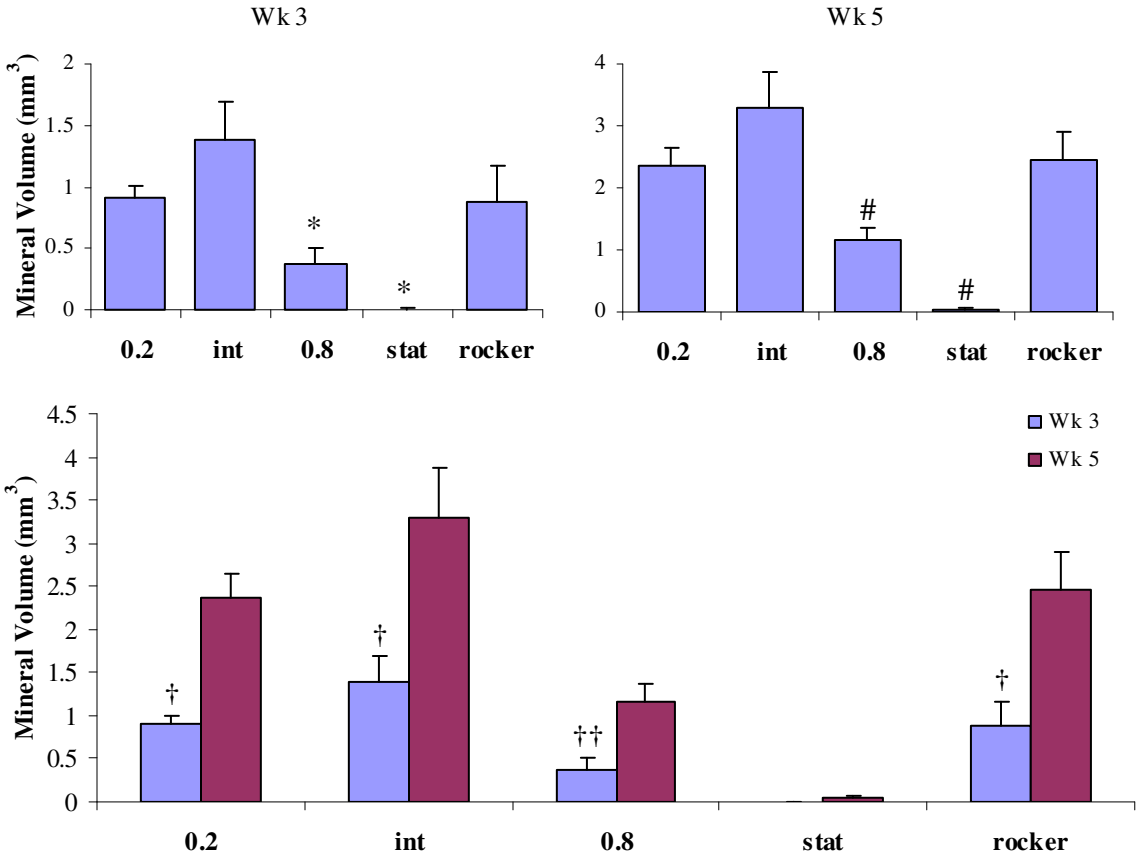

Figure 6-13. Mineralized matrix volume within the 1000 core region of 9 mm thick 75% porous PCL+C constructs detected by micro-CT scanning at weeks 3 and 5 for all experimental groups (n=4, 3 replicates). The core region excluded the outer 1000 radial microns from the rounded sides and 500 microns from the top surface of the construct. General Linear Model ANOVA revealed significant differences in mineralized matrix volume within constructs in different culture conditions at both timepoints. Pairwise comparisons showed that at week 3, * denotes statistically different from non-* groups ($p<0.0211$). At 5 weeks, # denotes different from all groups ($p<0.01$), # denotes different from all groups ($p<0.01$). Comparing mineral volume at 3 weeks to mineral volume at 5 weeks, † denotes ($p<0.0001$), while ‡ denotes ($p<0.001$).

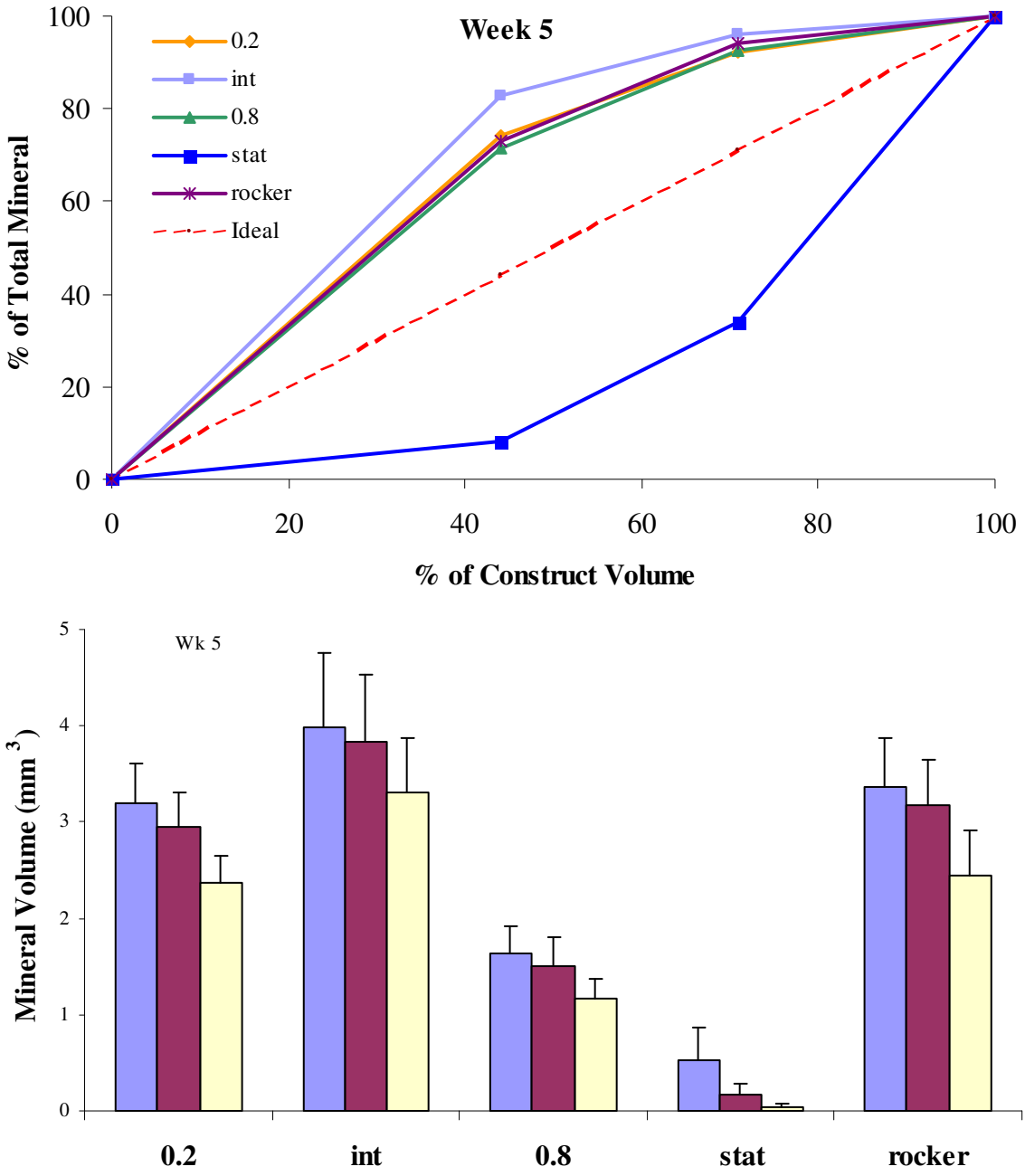

Figure 6-14. Plots of mineral volume for each culture group after analyzing the entire construct and 2 subsequent smaller subregions (n=4, 3 replicates). Mineralized matrix volume was quantified throughout the full construct as well as two concentric cylindrical subregions that excluded the outer 500 (500core) and 1000 μm (1000core) of the construct on the top and rounded sides. The dotted red line represents a construct with mineral distributed perfectly evenly throughout. For all groups except for the static case, after 5 weeks of culture that number had increased to 75% of the total mineral volume was located within the smallest core region.

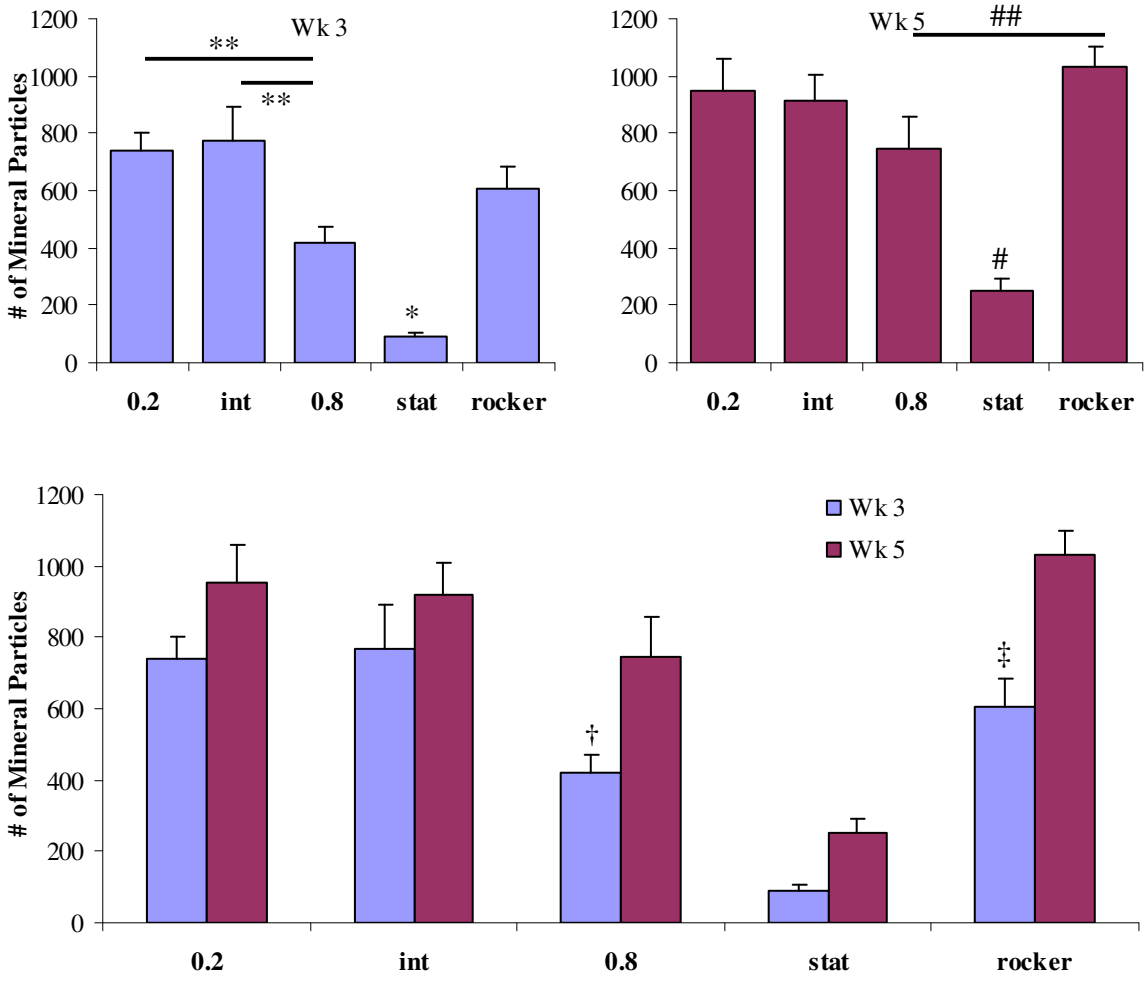

Figure 6-15. Plots of the number of particles in the entire construct at 3 and 5 weeks (n=4, 3 replicates). General Linear Model ANOVA revealed significant differences in the number of mineral particles within constructs in different culture conditions at both timepoints. Pairwise comparisons showed that at week 3, static was different from all groups * ($p<0.002$), and 0.8 ml/min was different from 0.2 and intermittent flow (**, $p<0.0007$). At 5 weeks, # denotes different from all groups ($p<0.0001$). Additionally, 0.8 ml/min was different from rocker (##, $p<0.0189$). Mineral particle number was compared within experimental groups at 3 and 5 weeks, † denotes ($p<0.038$), ‡ denotes ($p<0.002$).

constructs compared with all other groups at week 3. The increases in the number of mineral particles in each of the groups compared with the Static constructs were 8.5, 8.9, 4.8, and 7.0-fold for the 0.2 ml/min, INT, 0.8 ml/min and RP constructs, respectively. These relative increases were diminished in every group at 5 weeks.

The number of mineral particles present in the 0.2 ml/min and INT flow constructs increased only 28 and 19%, respectively, from week 3 to 5, and the increases were not statistically significant. The only significant increases in mineral particle number from week 3 to 5 were for the 0.8 ml/min and RP groups. The number of particles in the 0.8 ml/min constructs increased 77% and 70%, respectively. Additionally, at 5 weeks, the RP constructs contained 38% more particles than the 0.8 ml/min constructs. The number of mineral particles in Static constructs increased 187% from week 3 to 5, but the increase was not statistically significant.

As in Chapter 5, the smallest particles contributed minimally to the overall mineral volume and forced each data set to have a skewed distribution of particle size; therefore they were not included in the particle size distribution analysis. Cumulative distribution plots in **Figure 6-16** illustrate mineral particle size distributions for particles within constructs for each experimental group. A visible shift in the particle sizes was observed for specific experimental groups at certain timepoints. In general, the Static constructs exhibited smaller particles than any of the other constructs at both 3 and 5 weeks. At 3 weeks there was no observable difference in the particle size distribution between any of the perfused constructs or the RP case. However, at 5 weeks, the distributions of the non Static groups were not as tightly packed together. There appeared to be an increase in the particle size for the INT constructs compared with other

culture conditions. More definitive increases in particle size were exhibited between week 3 and 5 in **Figure 6-17**. Except for the 0.2 ml/min case, there was a trend, which indicated that a smaller percentage of the total number of particles was required in week 5 compared with week 3 to account for 90% of the mineral.

Fourier Transform Infrared Spectroscopy

To confirm that mineral deposits on the perfused constructs were biological in nature FT-IR spectroscopy was used to characterize the chemical composition of the mineralized matrix that was deposited by rMSCs subjected to five different culture conditions. Spectra were displayed on a relative absorbance scale. The observed spectra (**Figure 6-18**) displayed peaks that are representative of physiological bone composition. Mineral from all five experimental groups exhibited the amide I and II peaks at 1650 and 1540 cm^{-1} which correlate to protein. The stretching (st) phosphate peaks near 1100 cm^{-1}, the stretching (st) carbonate peak at 870 cm^{-1} as well as the phosphate bending (bd) doublet at 605 cm^{-1} and 560 cm^{-1} were also apparent for all groups.

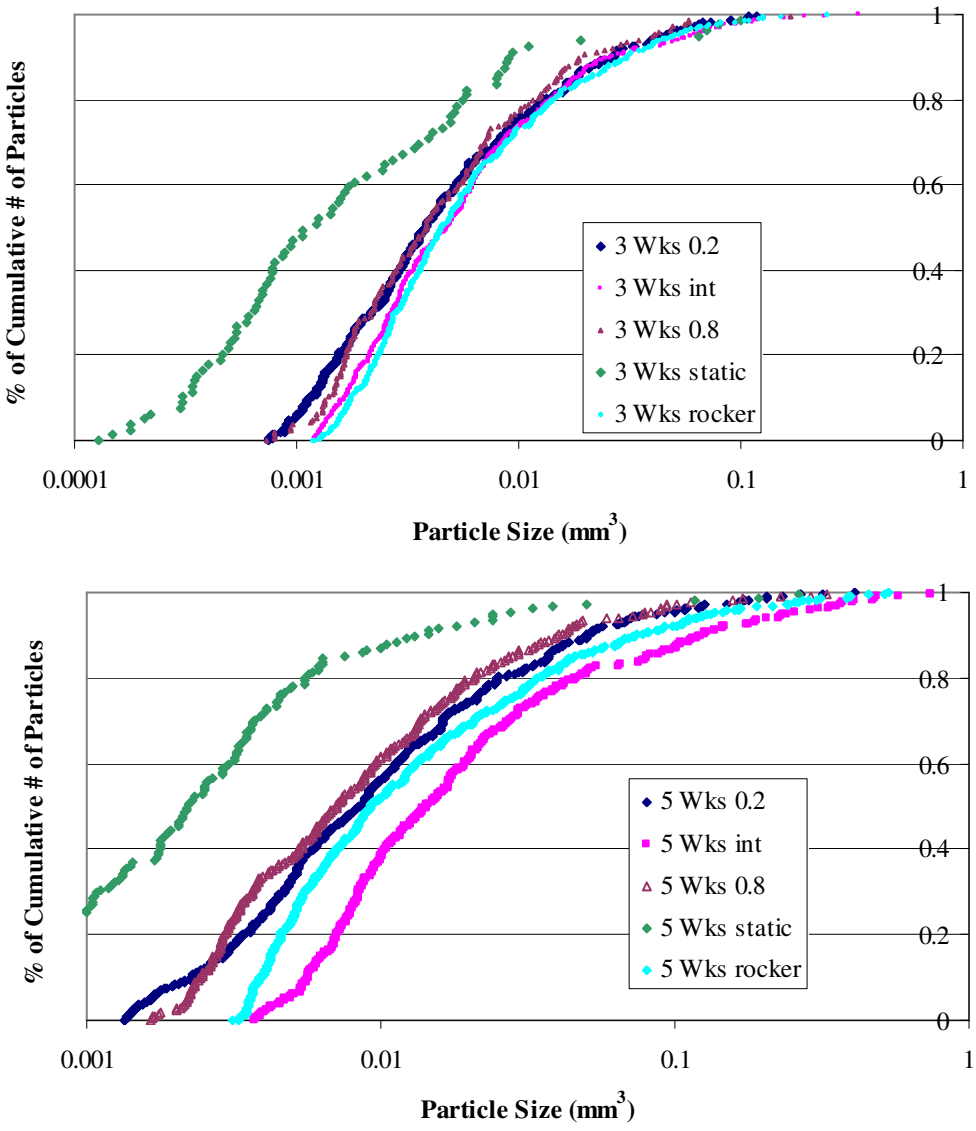

Figure 6-16. Cumulative plot of the size distribution of the largest mineral particles, which comprise 90% of the total mineral volume at weeks 3 and 5, within PCL+C constructs. At both timepoints, the particle size distributions followed a similar trend for all culture conditions except for the static case. However, the data were not normally distributed, therefore mean particle sizes were not compared statistically.

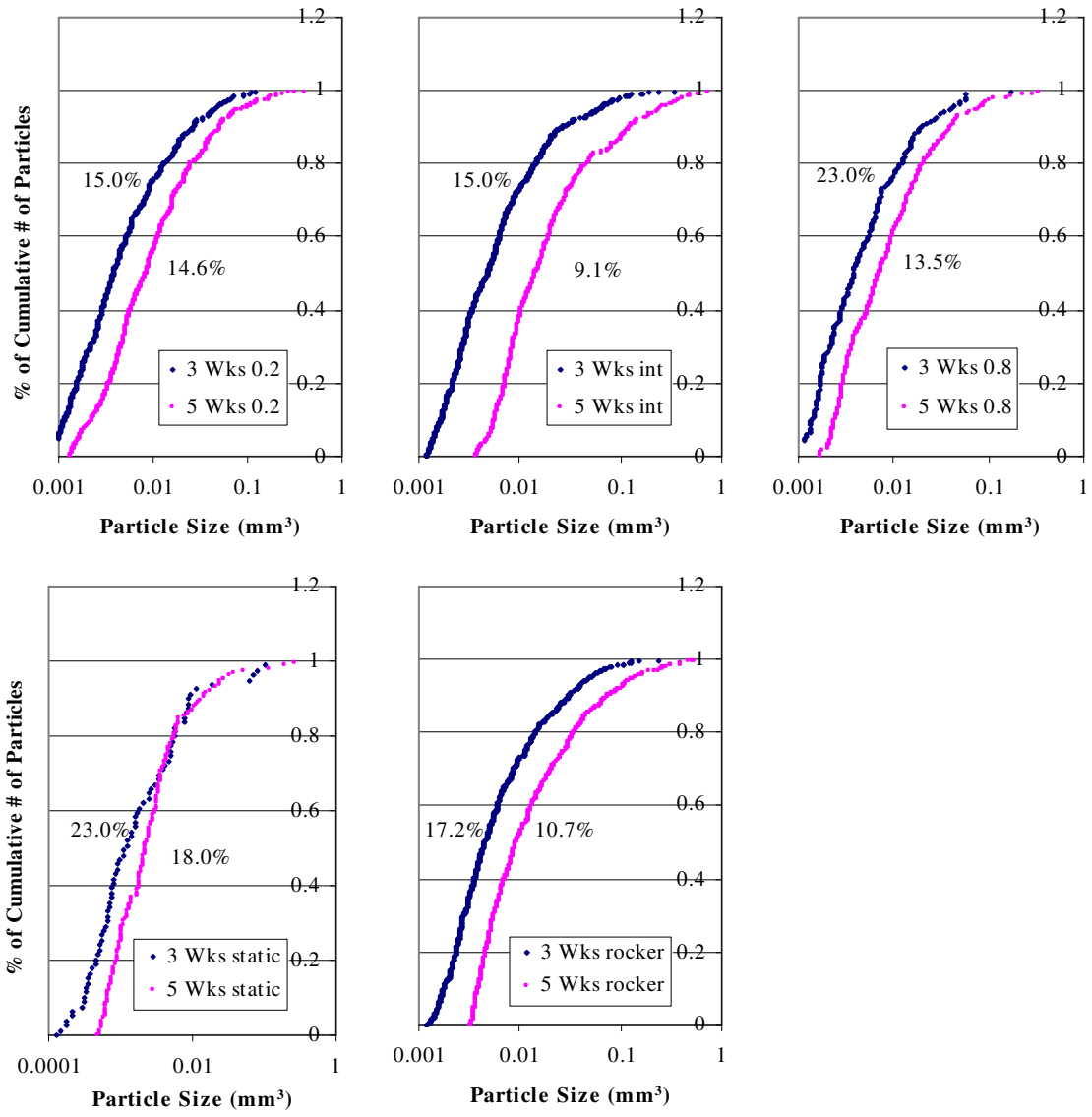

Figure 6-17. Cumulative plots comparing mineral particle sizes for the largest particles in each construct that made up 90% of the total mineral volume at weeks 3 and 5 for each culture group. The percentages shown in each plot tell what percent of the total number of particles made up 90% of the mineral volume. There was an observable shift in the distribution of particle sizes from week 3 to week 5 for all culture conditions except the static case. These data were not normally distributed, therefore mean particle sizes were not compared statistically.

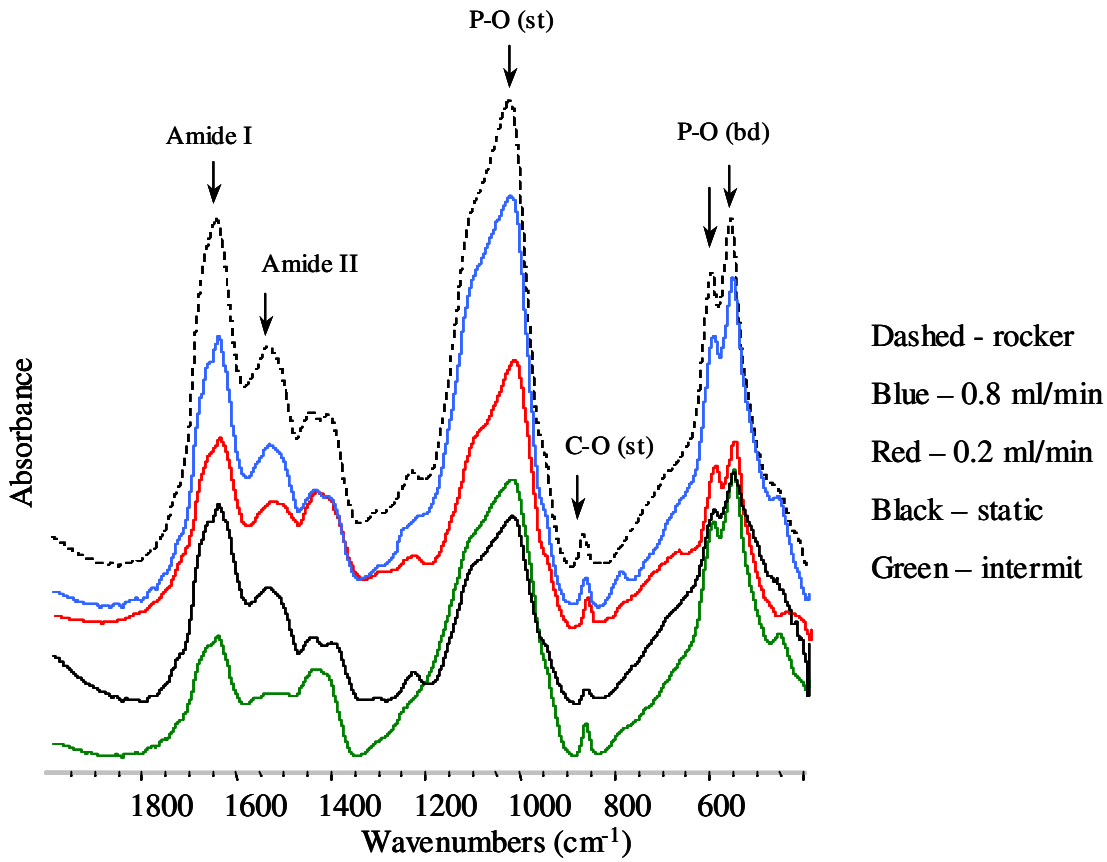

Figure 6-18. Representative FT-IR Spectra of mineral deposits removed from PCL+C constructs which had been either been perfused at 0.2 ml/min, 0.8 ml/min, intermittent elevated flow, or cultured as controls in static or orbital rocker plate conditions. Spectra are displayed on a relative absorbance scale. Mineral from all culture conditions exhibited the amide I and II peaks which correlate to protein. The stretching (st) phosphate peaks near 1100 cm^{-1}, the stretching (st) carbonate peak at 870 cm^{-1} as well as the phosphate bending (bd) doublet at 605 cm^{-1} and 560 cm^{-1} were also apparent in the mineral from all 5 culture conditions. The above spectrum is characteristic of biological hydroxyapatite.

Discussion

To efficiently determine if a graft is suitable for implantation during the development phase of engineering a bone graft substitue, it would be advantageous to monitor the growth of the construct during the time that it is in culture. Janssen et al. recently measured oxgen consumption in a perfusion bioreactor to estimate cell proliferation as a method for monitoring graft development.[117] Significant measureable observations of interest when culturing a bone graft substitute include the amount and distribution of mineral volume as well as the number and size of mineral particles within the potential graft. An imaging method using micro-CT scanning and a transportable perfusion bioreactor system was developed to aseptically quantify and analyze mineral formation over time in culture within cell seeded scaffolds.

It was determined that repeated x-ray scans of the same construct did not inhibit mineralized matrix formation or mineral density. This method was then used to evaluate the effects of time varying perfusion on the amount, distribution, and rate of mineralized matrix formation within 9 mm long, 75% porous, rMSC seeded PCL+C scaffolds at two different timepoints during culture. Three different perfusion cell culture conditions for creating large bone tissue engineering constructs *in vitro* were tested: 0.2 ml/min continuous flow, 0.8 ml/min continuous flow, or 0.2 ml/min continuous flow for 23 hours/day plus one hour of culture with flow elevated to 0.8 ml/min. The 0.8 ml/min group was selected as the high flow rate condition because it was within the range of high flow rates that had shown increased mineral deposition by Bancroft et al. on perfused rMSC seeded titanium mesh scaffolds.[9] Two control cultures were also maintained. The first control group consisted of constructs sitting in custom designed 6 well plates with

extra deep wells. The second control group consisted of constructs in 6 well plates that were placed on an orbital rocker plate. The rocker plate constructs were agitated at a frequency of 0.5 Hz in order to facilitate movement of media around the constructs and prevent waste products from building up at the periphery of the construct.

Culture Method Development

Changes were made to the culture protocol in three areas for this Aim: scaffold porosity was increased, scaffold cleaning time was reduced, and the collagen lyophilization procedure was altered. A more porous scaffold was used in these experiments compared with the scaffolds used in Chapters 5 and 6 for three reasons. First, as discussed in Chapter 6, scaffolds with a porosity of 66% resulted in occluded pores. Increasing the porosity to 75% resulted in less, but did not eliminate, pore occlusion in perfused constructs compared with 66% porous scaffolds. Second, increasing the porosity and the pore size may improve diffusion through all culture groups, both static and perfused, thus enhancing cell viability. This provided a more rigorous test of the benefits of perfusion compared with static culture in creating mineralized matrix throughout a construct. Confocal microscopy indicated that viable cells were detected throughout static constructs. Therefore, the minimal matrix observed in Static constructs could not be attributed to the absence of viable cells within the scaffold. Finally, previous experiments in our lab using PCL scaffolds with a porosity of 66% that were implanted in a rat segmental defect model proved to be excessively rigid. The ends did not easily deform, which made implantation into the defect site a difficult procedure. Increasing the porosity of the scaffold to 75% should allow for more

deformation at either end of the scaffold so that it fits more easily into the rat segmental defect model.

The cleaning time in 5M NaOH for these scaffolds was reduced compared with previous scaffolds because the increased porosity resulted in fewer connections between each layer of the scaffold at the strut interfaces. Incubation in NaOH for the standard 12 hours resulted in fragile scaffolds with reduced resistance to either tension or shear. Initial gel casting attempts using the methods from Chapter 5 and 6 in which the collagen solution was deposited on the top surface of the scaffold resulted in a heterogeneous distribution of lyophilized collagen localized to the top half of the scaffold. Filling the polycarbonate mold with the collagen solution first, and then inserting the scaffold into the mold ensured that the collagen infiltrated the entire length of the scaffold and did not sit on top of the scaffold due to surface tension and the low viscosity of the collagen solution.

General Observations – Confocal and VivaCT Images

Qualitative confocal microscopy images indicated that multiple x-ray scans did not appear to negatively affect cell viability or distribution within both static and perfused constructs. No differences were observed in the amount or density of mineralized matrix deposited on the scaffolds between constructs that had been scanned once and constructs that had been scanned twice. Dudziak et *al*. previously studied the effect of ionizing radiation on osteoblast cells. They reported increases in ALP activity, but decreases in TGFβ-2 and –3 as well as cell proliferation in a radiation dose-dependent manner.[118] The radiation doses used in the experiments of Dudziak et *al*. were slightly higher than

the local doses that the VivaCT applies to samples. The VivaCT effective dose may actually be 1000 times lower than the local dose depending on the x-ray intensity, energy and sample type.[119] Therefore, it was not unexpected that sequential x-ray scans on the same sample would not significantly diminish mineralized matrix production and density. These results indicate that repeated x-ray scanning did not significantly affect cell viability, distribution and mineral production during subsequent experiments.

Confocal microscopy qualitatively indicated that cell viability was similar between 0.2 ml/min and INT perfusion groups. Both of these groups appeared to contain a greater percentage of viable cells at the interior of the construct compared with 0.8 ml/min, Static and RP constructs. Additionally, the outer surfaces of the Static and RP constructs were populated with a proportion of viable cells comparable to the perfused constructs, which suggests that mass transport of nutrient and waste products was adequate to sustain viable cells at the construct periphery. These viability results are similar to Chapter 4 where low flow groups coincided with significantly higher cell viability at the center of trabecular bone constructs than higher flow and static cultures. The continuous elevated flow rate may have applied detrimental shear stresses that damaged a portion of the cells, which led to increased cell death. The lack of convective flow through static and RP constructs may have caused a buildup of waste products within the construct, which led to an elevated level of cell death compared with the 0.2 ml/min and INT constructs. Therefore, confocal microscopy images suggest that low continuous flow or intermittent high flow superimposed on low flow through 75% porous PCL+C constructs supplied a beneficial culture environment at the construct interior for

cell viability and possibly cell function compared with a consistent high flow rate or control cultures.

Visual inspection of micro-CT images showed that mineral was distributed throughout the full length of the scaffold for all construct groups except for the Static culture constructs where the mineral was localized to the periphery and a scattered ring of mineral at the bottom of the construct. The Static mineral pattern is similar to the mineralized matrix distribution detected in perfused 1.5 mm thick collagen sponge constructs reported by Meniel et *al*.[2] Comparing the week 5 images to the week 3 images, the mineral particles have increased in size, but the general shape and distribution of mineral particles was very similar between repeat scans. This suggests that a possible mechanism of mineral volume increase may have been due to increasing particle size rather than an increase in the total number of mineral particles.

Effect of Culture Conditions on Mineralized Matrix Volume

Comparing the mineral volumes within the constructs from different groups showed that improved mass transport enhanced mineralized matrix production. The 0.2 ml/min, INT, and RP culture conditions were superior to the 0.8 ml/min flow and the Static cultures for retaining mineral within perfused constructs. The relative amounts of debris found in the downstream portion of the tubing suggest that mineralized extracellular matrix may have been washed out of the scaffolds in the 0.8 and INT perfusion groups, with the effect most obvious in the 0.8 ml/min construct tubing. It is possible that the 0.8 ml/min flow rate resulted in mineralized matrix production at a comparable or even increased level to the 0.2 ml/min and INT conditions; however, a

significant portion of the mineral particles that had been deposited may have been washed away. Collecting the debris deposited in the tubing in future perfusion studies might more accurately quantify both the total amount of mineral that was synthesized by the cells as well as determine the loss of mineral from the construct due to excessive perfusion. Regardless, since there was debris downstream of all the perfused constructs, developing better methods to retain mineral that has been synthesized on a construct would be worthwhile.

Although both the Static and RP constructs exhibited viable cells throughout the entire scaffold, albeit at a reduced level compared with the 0.2 and INT constructs, only the RP constructs produced a significant amount of mineral. The amount and distribution of mineral in the RP case was most similar to the INT scaffolds. The movement of the rocker plate, in addition to removing the diffusion layer of media around the constructs, may have also resulted in active fluid convection through the scaffold. Therefore, active mass transport as well as shear stresses from cyclic convective fluid flow may have existed at various depths inside the RP constructs. Determining the fluid flow patterns and estimating the associated shear stresses within the RP constructs would require sophisticated modeling approaches applied previously for other bioreactor designs.[120] However, to understand the mechanism of mineral deposition within RP constructs, future work to model the flow field throughout the scaffold would be advantageous. Additionally, culturing constructs on a series of rocker plates at multiple frequencies may help elucidate a threshold frequency, above which, compared with static culture, significant mineral synthesis occurs. The relative absence of mineralized matrix, in

conjunction with the presence of viable cells within Static constructs suggest that culture conditions which may sustain cell life are not sufficient to promote mineralization.

Effect of Culture Conditions on Mineral Spatial Distribution

The results in **Figure 6-14** showed that after 3 and 5 weeks of culture, over 80, and then 90% of the total mineral volume was detected within the 1000 core region for all but the Static constructs. The 1000 core region comprises only 45% of the total construct volume, which indicates that a disproportionate amount of mineral was localized to the center of the scaffold in the perfused and RP constructs. This region corresponds to the volume receiving maximum fluid flow velocity in the perfused constructs, based on the CFD modeling done in Chapter 4, and consequently the highest shear stresses. Sikavitsas et al. reported that mineral deposition on perfused titanium mesh constructs was significantly enhanced as fluid viscosity, and correspondingly, shear stress was increased.[11] A slightly different mechanism may be at work within the RP constructs. The orbital motion of the rocker plate may have produced a rotating current in the construct wells, which created a fluid flow gradient directed towards the center of the scaffold. Finally, the scaffold geometry may be partially responsible for the mineral location. The spaces between the PCL struts result in large, incomplete pores on the cut edges of the scaffold. There is not as much surface area for the collagen to attach to at the scaffold periphery. As a result, the collagen may not bridge the outer pores as well as the inner pores. With less collagen present, the cells are less likely to attach and deposit matrix at the construct exterior.

Effect of Culture Conditions on Mineral Particle Size and Number

Comparing to results from Chapter 5, between the 66% and 75% porous scaffolds there was a significant reduction in the number of detected mineral particles. The individual CT systems that were used for each experiment play a large role in producing this effect. The micro-CT was used at a resolution of 16 μm, while the VivaCT was scanning at a 21.5 μm voxel resolution, which means the micro-CT can detect more, smaller particles than the Viva. Resolution does not scale linearly with voxel size. Additionally, in situations where the micro-CT40 detects two particles that are 16 μm apart, the Viva will combine those particles into one. Both of these phenomena result in the VivaCT detecting significantly fewer particles than the micro-CT. However, the difference in overall mineral detected would be minimal for two reasons. First, when the VivaCT combines two smaller particles into one larger one, the volume of both particles is preserved and counted. Second, the size of the particles that would not be detected is so small, that even missing 10,000 particles would only account for a volume that was 0.08 mm^3.

Increases in the total mineral volume within 3-D bone constructs grown *in vitro* are due to a combination of two mechanisms: an increase in either the (1) number or (2) size of mineral particles. Therefore, the number of mineral particles, as well as the mineral particle size within each construct, was quantified with the VivaCT and analyzed to elucidate the mechanisms of mineral growth across the various culture conditions. Because the mineral particle sizes were not normally distributed, even after selecting the LP90% particles, it was not valid to divide the amount of mineral by the number of particles and calculate an average particle size for each construct. Therefore, cumulative

distribution plots were generated to observe general trends in the particle size distributions of each experimental group.

The cumulative distribution plots, along with the data from **Figure 6-15**, suggest that increasing mineral particle size and number contribute in varying degrees to increasing total mineral volume within constructs in each of the culture groups. Each construct group experienced different relative increases in mineral volume between week 3 and 5, therefore the contributions of each mechanism must be evaluated in relative terms. **Figure 6-16** illustrates how at 3 weeks, the distribution of the LP90% mineral particles within Static constructs is shifted relative to the particles detected in all other constructs. Additionally, the shape and location of the LP90% mineral particle size distributions are similar for all the non-Static constructs. At 5 weeks, the particles within the static constructs were still the smallest of any of the groups, however, the distributions of the remaining groups were more separated from one another than at 3 weeks.

Increasing Particle Size Drives INT and 0.2 ml/min Mineral Volume Increases

Analyzing the distribution of each of the groups revealed that the INT flow condition stimulated the greatest visible shift to the right in particle size distribution when compared with the particle size distributions of other groups at 5 weeks and to the INT particle size distribution at 3 weeks. **Table 6-1** shows that there were 35 more particles greater than 0.1 mm^3 and 3 particles greater than 0.5 mm^3 within all the INT constructs at 5 weeks than there were at 3 weeks. These observations, in combination with the results in **Figure 6-15**, which documents the minimal increase in the number of mineral particles

between week 3 and 5, dictates that the mechanism of mineral growth for the INT constructs was primarily an increase in mineral particle size, especially the largest particles.

The 0.2 ml/min constructs also showed a relatively small percent increase in the number of mineral particles from week 3 to week 5 compared with the 0.8 ml/min, Static and RP constructs. The shift in the particle size distribution was not as pronounced as the INT culture group, there was also almost no decrease in the percentage of LP90% particles, and there were only 18 particles greater than 0.1 mm^3 , but an increase of 119 in the number of particles detected within the 0.2 ml/min constructs, at week 5 than at week 3. This suggests that in order for the mineral volume to double from week 3 to 5, there was a large increase in the medium size particles between 0.1 and 0.01 mm^3. and a smaller shift in the mineral particle distribution plot comparing week 3 to week 5. Those results imply that increases in mineral volume for 0.2 ml/min constructs, in comparison to INT constructs, were more a result of a large increase in medium sized particles rather than increasing the size of the biggest particles.

Table 6-1. Particle size increases. This table shows the increase in the number of particles of a certain size between weeks 3 and 5 for each experimental group.

Group	Particle Size (mm^3)		
	0.5 (extra large)	0.1 (large)	0.01 (medium)
0.2 ml/min	0	18	119
INT	3	35	84
0.8 ml/min	0	6	65
Static	0	2	33
RP	2	30	107

Increased Number of Particles Responsible for 0.8 ml/min and Static Mineral Volume Increases

Of the perfused constructs, the 0.8 ml/min group showed the smallest shift in particle size distribution and the greatest percent increase in the number of particles. Additionally, there were almost no large particles created between weeks 3 and 5, and less than half as many medium particles compared with the 0.2 ml/min constructs. Therefore, increases in mineral volume for 0.8 ml/min constructs, compared with the other flow groups, were predominantly due to increasing the number of small to medium sized mineral particles within the construct. The Static constructs showed no definitive shift in mineral particle size between 3 and 5 weeks, however the number of mineral particles increased by 187%, by far the largest percentage of any of the experimental groups. Static culture was the condition most dependent upon synthesizing new mineral particles to increase mineral volume.

RP Constructs rely on Both Mechanisms to Increase Mineral Volume

The RP constructs appeared to be an amalgam of both phenomena. They displayed an almost identical percent increase in mineral particles to the 0.8 ml/min constructs, but also a distribution shift very similar in magnitude to the 0.2 ml/min constructs. It appears that out of all the groups, the RP conditions may have had the most balance between increasing mineral particle number as well as size in order to enhance mineral volume. These conclusions suggest that individual mineral particle growth may be closely related to dynamic culture conditions, specifically flow mediated shear stress. Cumulative distribution plots in **Figure 6-17** support this theory where the effect seems

to be most pronounced for the INT constructs. The periodic increasing flow rate may have provided a shear stimulus which upregulated matrix synthesis in the cells. Although the cells within 0.8 ml/min constructs may have been receiving similar shear stresses to encourage matrix synthesis, the continual high flow rate would be more likely to dislodge larger particles than smaller particles. Because the INT constructs experienced a low flow rate over 95% of the time they were in culture, there was much less time for the intermittent high flow rate to dislodge large mineral particles.

Conclusions

Constructs from all perfusion groups as well as dynamic RP controls contained significantly more mineral at both 3 and 5 weeks compared with static controls. In addition, INT constructs contained consistently greater amounts of mineralized matrix as well as elevated rates of mineral production at both timepoints compared with all other experimental groups, however these values were statistically different from only the static and 0.8 culture groups. Both INT and 0.2 ml/min constructs displayed better cell viability than all other groups. While a minimum level of perfusion improves mineral deposition compared with static culture, flow rates above a certain level are deleterious to matrix deposition and retention. Mineral particle analysis indicated that increases in mineral volume within INT and 0.2 ml/min perfused constructs were predominantly due to mineral particle growth. For Static and 0.8 ml/min constructs, steady increases in the number of mineral particles were largely responsible for increases in total mineral volume. Finally, RP culture conditions combined both mechanisms to double mineralized matrix deposition from week 3 to 5. While the RP condition produced

constructs with amounts and distributions of mineralized matrix similar to the INT and 0.2 ml/min groups, it is unclear if this culture method would perform as well with larger or less porous constructs. There may be a limiting scaffold size that any or all of these culture methods are effective at producing mineralized matrix. Finally, other than the Static case, each of these culture conditions offers a viable method for producing mineralized matrix on a bone tissue-engineering construct. Determining what type of mineral deposition is appropriate for greatest efficacy *in vivo* as well as how quickly an *in vitro* graft would be ready for implantation are two important questions that this system and the recently developed analysis techniques will able to evaluate.

CHAPTER 7

FUTURE CONSIDERATIONS

Together, these studies help lay a foundation for evaluating various in vitro bone tissue-engineering strategies, developing a viable bone graft substitute, and further identifying mechanisms by which mineral growth and development occurs *in vitro*. This controlled perfusion system is well suited to investigating *in vitro* mineral formation mechanisms as well as assisting and optimizing *in vivo* graft development.

The controlled nature of the perfusion system lends itself to parametric analysis. Constructs of specific porosity generate an associated resistance and pressure drop depending on the fluid flow rate. We have seen a flow rate dependence on mineralized matrix deposition and maybe more importantly, retention. As the flow rate was increased from 0.2 to 0.8 ml/min, there was a definite visual increase in the amount of construct debris that was washed off the scaffold. Perfusing multiple scaffold porosities at different flow rates would allow us to plot favorable vs. unfavorable, flow and porosity conditions. Using Darcy's law, we could calculate, based on permeability and flow rate, what combinations of porosity and flow result in beneficial shear stresses for mineral synthesis and retention. Therefore, if the porosity of the scaffold was changed, we could predict what flow rate should be employed for optimal mineral deposition.

As was described in Chapter 5 and 6, there were varying amounts of extracellular matrix within each scaffold, which occluded a portion of the pores. These occlusions effectively changed the scaffold geometry and consequently the flow within the scaffold. The VivaCT can distinguish unmineralized matrix from fluid, therefore it would be

possible to set the evaluation threshold lower and determine a new scaffold geometry at various times throughout the course of an experiment. Combining the change in permeability due to change in construct architecture with the Darcy's law analysis, we could reduce or increase the flow rate to maintain an optimal shear stress throughout the construct.

Extending perfusion time beyond 5 weeks might show whether mineral density would increase over time. There may also be a limit to the amount of mineral that a scaffold or the culture volume of the perfusion system can support. The repeated scanning technique allows for an indefinite culture time in order to see if the rate of mineral deposition were to decrease or increase over time.

The next logical step for this cell culture method is to evaluate how proficient perfused constructs are at generating bone *in vivo*. Initially, an ectopic model such as the rat subcutaneous model could be used to evaluate the retention of cell viability within the interior of perfused constructs after *in vivo* implantation. If the perfused constructs are demineralized prior to implantation, this model could also be used to directly test whether matrix produced within perfusion bioreactors possesses osteoinductive properties. Therefore, to test the osteoinductive capabilities of these constructs, an ectopic site, such as the back of a rat, should be chosen as an implantation site. If the construct was successful in producing bone, there are several interesting permutations of this experiment, including the following: The construct could be devitalized prior to implantation in order to determine if cells are necessary for generating bone growth. If just the deposited mineral is sufficient for osteoinduction, the issue of transplanting non-autologous viable cells into a patient's body could be avoided.

We have also shown that collagen significantly increases construct function when lyophilized. Freeze-dried constructs would be much easier to store and ship for future use than constructs containing viable tissue. Because off-the-shelf availability is sought after for a commercially available product, it would be worth testing the effects of lyophilizing an entire construct after the *in vitro* culture time to determine if it was still effective at enhancing bone formation *in vivo*.

We saw a difference in the amount of mineral deposited (data not shown) between 66% and 75% porous scaffolds. Porosity may have an even larger effect on mineral formation *in vivo* due to possible physical barriers to vascular and cellular infiltration of the graft. Implanting scaffolds of various porosities after different amounts of time in vitro (to modulate the amount of extracellular matrix is present within the scaffold) may alter bone formation. Additionally, we have shown that different culture conditions (0.2, INT, RP) resulted in similar total mineral volumes, but different mineral particle sizes. Mineral particle size may affect the in vivo healing response with respect to cell and vascular invasion as well as mineral remodeling. Using different culture methods to generate mineral particles of various sizes may aid in selecting which culture methods to pursue for future study and improvement. While the INT protocol is more involved due to the variable flow characteristics, if larger particles result in faster healing times, then it would be worth the effort.

After establishing that perfused constructs will make bone at an ectopic site, implanting these constructs into a load bearing, critical sized, segmental defect would be a stringent test of the efficacy of such a bone graft substitute. Our lab has developed a robust, rat, femoral defect model that requires an implant 7 mm in length. We have

shown the ability to produce 9 mm long by 6 mm diameter constructs populated with mineral throughout the core of the scaffold. To ensure that significant amounts of mineral had filled the entire implant, it would be reasonable to culture a construct that was larger in diameter than was necessary and then size the scaffold to a smaller diameter for implantation purposes.

We have shown that deposited mineral within perfused scaffolds was localized to the core region of the constructs. Using this result it may be possible to direct mineral deposition within a construct by changing scaffold porosity or localizing where lyophilized collagen is present. In this way, we might be able to deposit mineral in physiologically relevant shapes by constructing scaffolds with geometries like the tubular shape of a femur. The well-controlled environment of this perfusion system and the associated quantitative analysis techniques make it a valuable tool for multiple bone tissue engineering applications.

APPENDICES

Appendix 1. Lattice Boltzmann code theory and shear stress estimation

The code used for this study employs the "re-interpreted bounce-back condition" at solid-fluid boundaries.[121] In this method, a no-slip condition is implicitly imposed on solid-fluid interfaces, via inversion of mass distribution on solid nodes during the collision step.[122] This condition places the zero velocity flow position approximately 1/2 lattice into the fluid, from the nodes in the solid wall, as shown in **Figure A-1**. Black circles denote the "nodes" of the automaton. A solid at node (x,y) is considered a square "block" extending from x-0.5 to x+0.5, and from y-0.5 to y+0.5; solids are represented in the figure as gray blocks. This interpretation assigns a constant volume to each solid block, and thus makes it very convenient to account for volume changes, and allows a 1:1 map from voxel volume to LB volume. When this interpretation of the solid-fluid interface is used, some of the LB fluid is resident on the solid nodes. The fluid resident on the nodes must be considered in an account of applied body force, or dispersion of tracers. The effect of the fluid at the interface decreases as the system is scaled to use more nodes to represent the same solid.

The 3-D velocity field at any point in the experiment, $u_e(x,y,z)$, can be determined from the corresponding $u_{LB}(x,y,z)$ in LB calculation according to:

$$u_e(x,y,z) = u_{LB}(x,y,z)\cdot(U_e/U_{LB}) \quad (1)$$

U_e = average flow speed in experimental setup (mm/sec)

U_{LB} = average flow speed in the LB model (lattice units/timestep)

Since both the experiment and LB calculations were done in the Darcy realm, the ratio of body force to average flow speed was nearly constant. For the range $0.15 < Re < 0.9$, which encompass all the LB simulations and the experiment, the U_{LB}/(body force) ratio varied by less than 0.7%. Hence it was not necessary to obtain an exact match between the experimental and LB Reynolds numbers.

Shear Stress Estimation

Assuming that the media was a Newtonian fluid, shear stresses, τ, were estimated by multiplying the symmetric part of the gradient of the velocity field by the dynamic viscosity, of the cell culture media:

$$\tau = \nu\left(\frac{1}{2}\right)(\nabla U + \nabla U^T) \tag{2}$$

τ = shear stress tensor

ν = experimental dynamic viscosity

U = 3-D velocity vector

The derivatives of the velocity field were calculated using a finite differences formula for the nine partial derivatives for each fluid voxel in the model.

$$\frac{dU_x}{dx}(i,j,k) = \frac{U_x(i+lu,j,k) - U_x(i-lu,j,k)}{2*lu} \tag{3}$$

$$\frac{dU_x}{dy}(i,j,k) = \frac{U_x(i,j+lu,k) - U_x(i,j-lu,k)}{2*lu}$$

$$\frac{dU_x}{dz}(i,j,k) = \frac{U_x(i,j,k+lu) - U_x(i,j,k-lu)}{2*lu}$$

lu = one lattice unit, the length of one side of an element in the LB model (μm)

This same calculation was used to determine the partials of U_y and U_z. Next, the 3x3 partials matrix for each point in the field was added to its own transpose to produce a symmetric strain matrix. After the eigenvalues of the symmetric matrix were found using the Jacobi method, the largest absolute-value eigenvalue (largest component of the tensor) was selected for each fluid voxel. Statistics were calculated for these largest absolute-value eigenvalues for every fluid voxel bordering on the scaffold surfaces to determine the mean and maximum fluid speed gradient. A Cannon-Fenske routine glass viscometer (Fisher Scientific) submerged in a water bath at 37 °C was used to measure the viscosity of the cell culture media (α-MEM, Gibco). Multiplying the mean and maximum fluid speed gradient by the dynamic viscosity produced shear stress estimates over the scaffold surface.

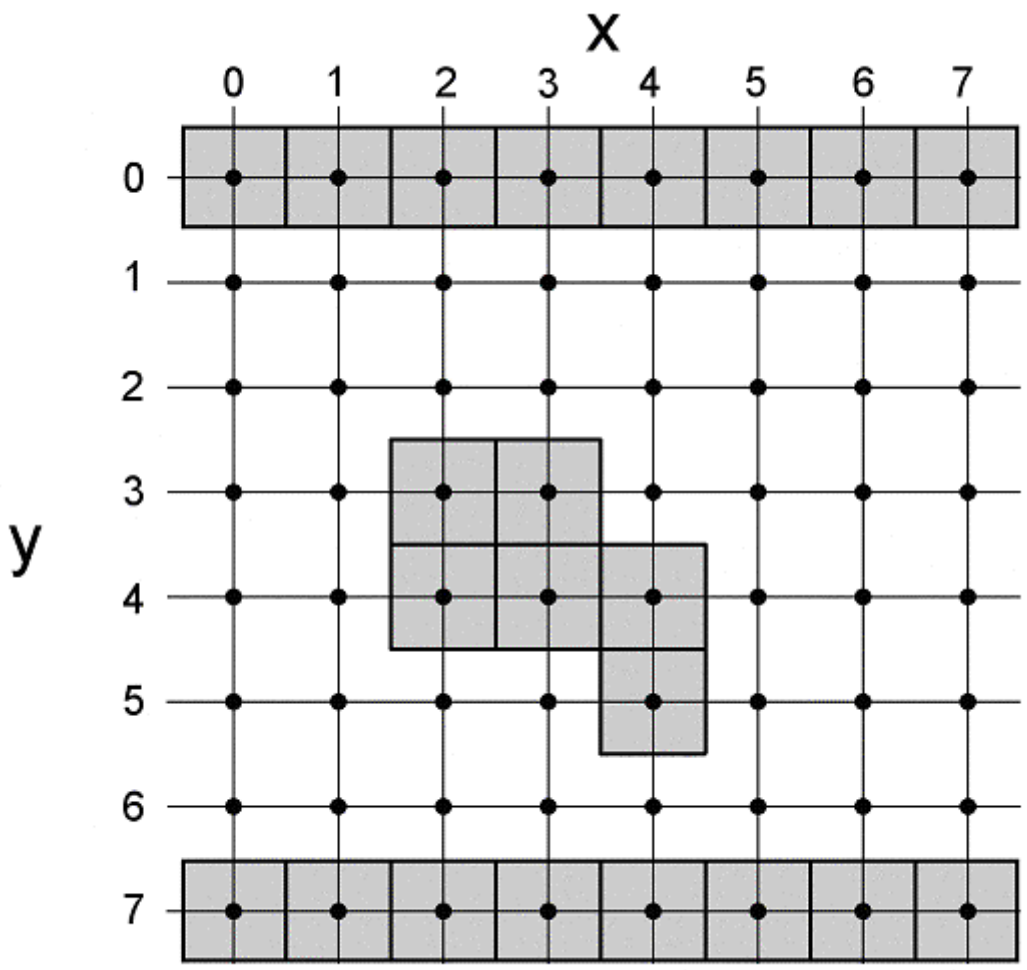

Figure A-1. Re-interpreted bounce back boundaries. The gray boxes show the boundary of solid nodes with the re-interpreted bounce-back condition. The solid-fluid interface is placed halfway between a solid node (e.g. 3,3) and the adjacent fluid node (e.g. 4,3).

Appendix 2. Effect of AA2-P on Mineralized Matrix Synthesis on 3-D Constructs and the Effect of Media Change Frequency on Mineral Nodule Formation in Monolayer.

Methods

rMSC cells were seeded on PLDL scaffolds (5 mm , 3 mm thick) and cultured for 56 days under static conditions. Media was changed once per week for constructs receiving AA2-P. Media was changed every 2 days for constructs receiving media with ascorbic acid.

To test the effect of media change frequency, osteogenic media containing AA2-P was changed every 2, 3, 4 or 6 days for 21 days. Plates were stained with Von Kossa to determine the percentage of the dish that was covered in mineral.

Results

Micro-CT analysis showed a 56% increase in mineral deposition on constructs receiving AA2-P over the constructs receiving AA ($p<0.0003$). Therefore using AA2-P and changing media once per week did not negatively affect mineral synthesis on rMSC seeded polymer scaffolds. Changing media every 6 days did not inhibit nodule formation compared with changing media more frequently.

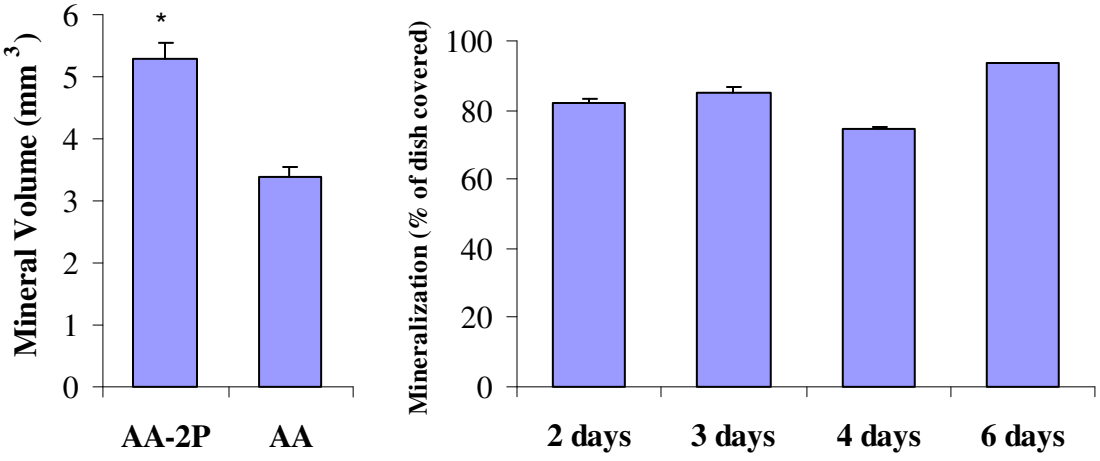

Appendix 3. Axial perfusion bioreactor drawings. Bioreactor base.

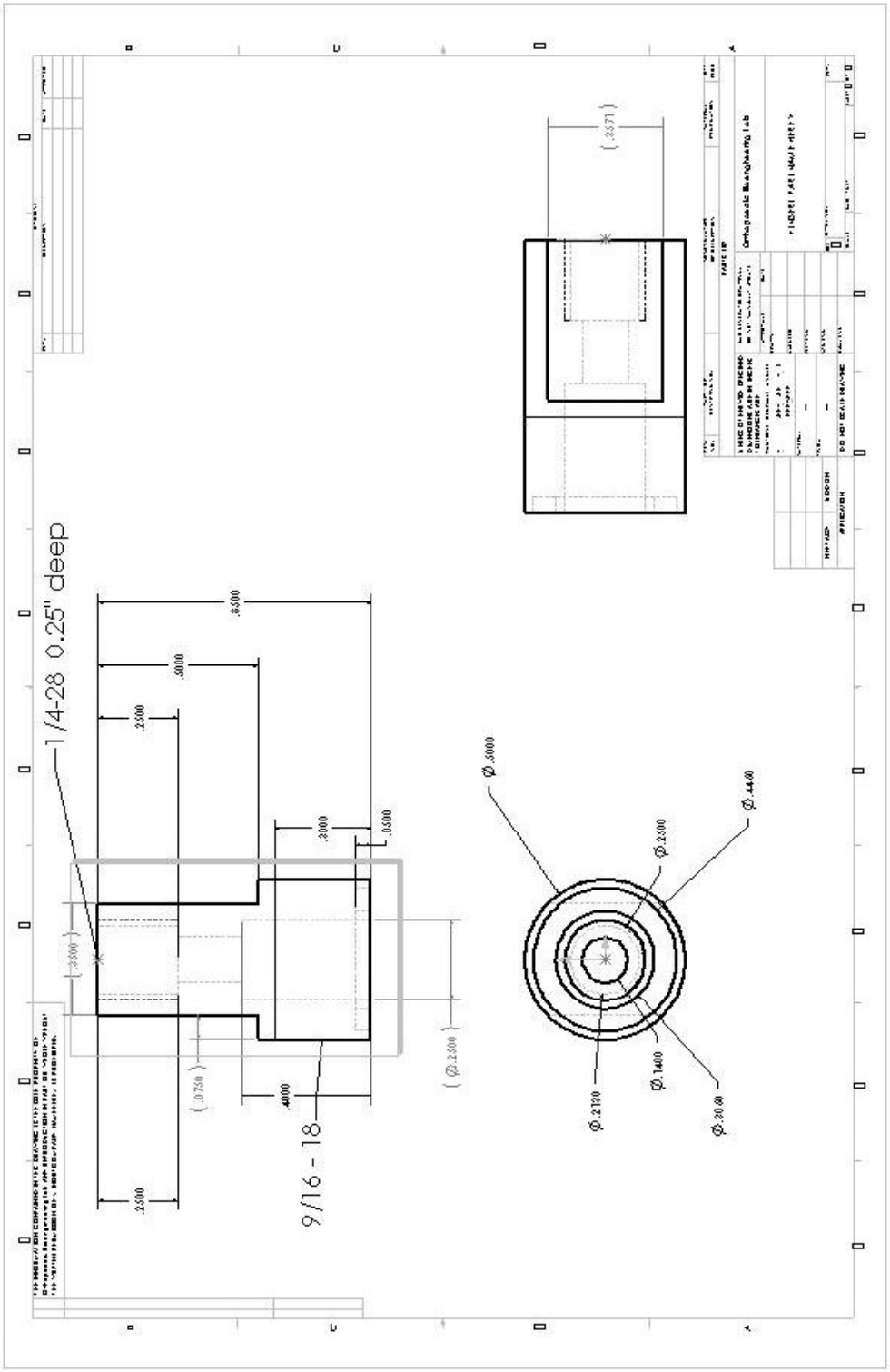

Bioreactor Collet.

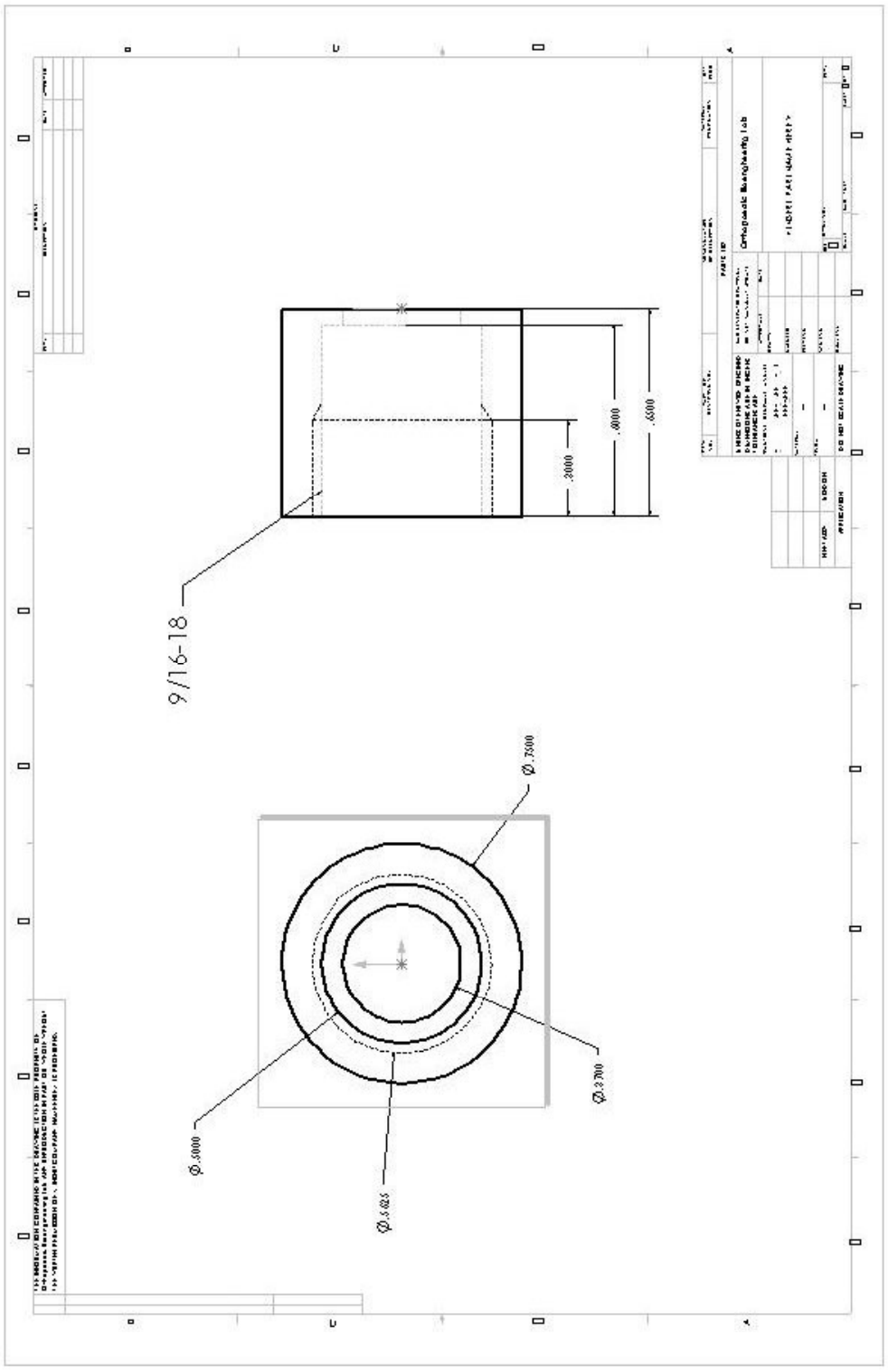

Bioreactor Spacer, compressed between collet and base to seal o-ring groove.

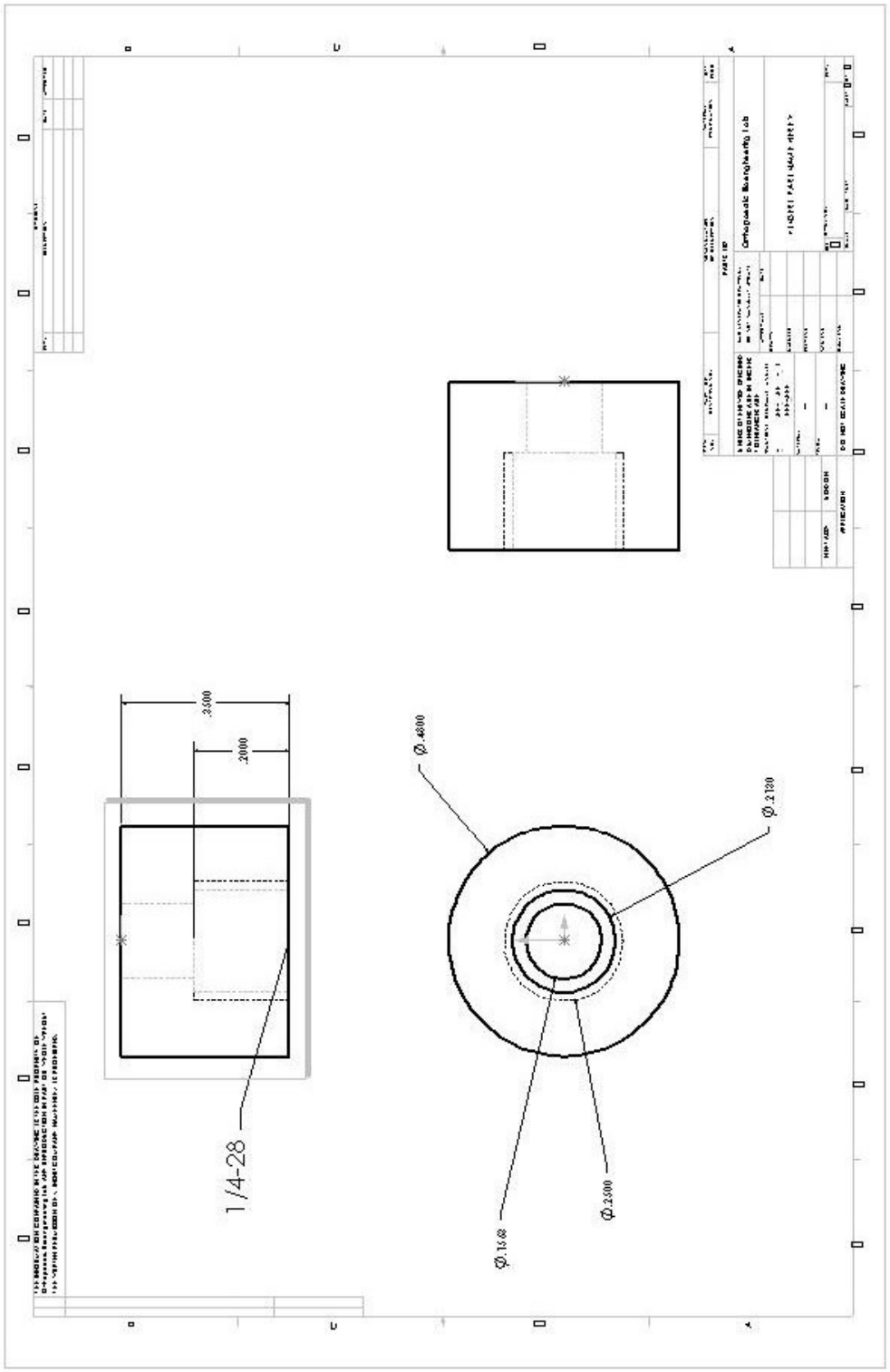

Reservoir – Side.

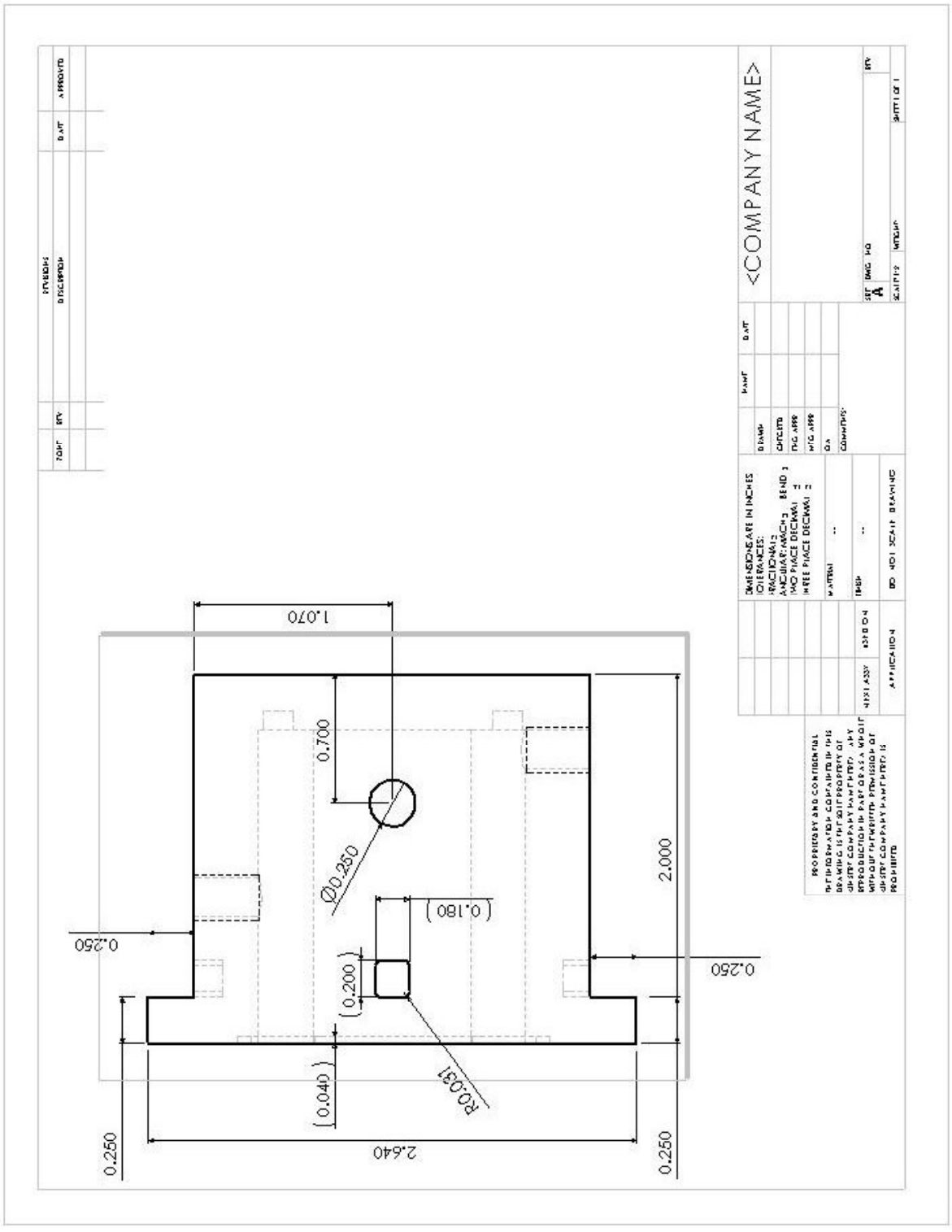

Reservoir – Front .

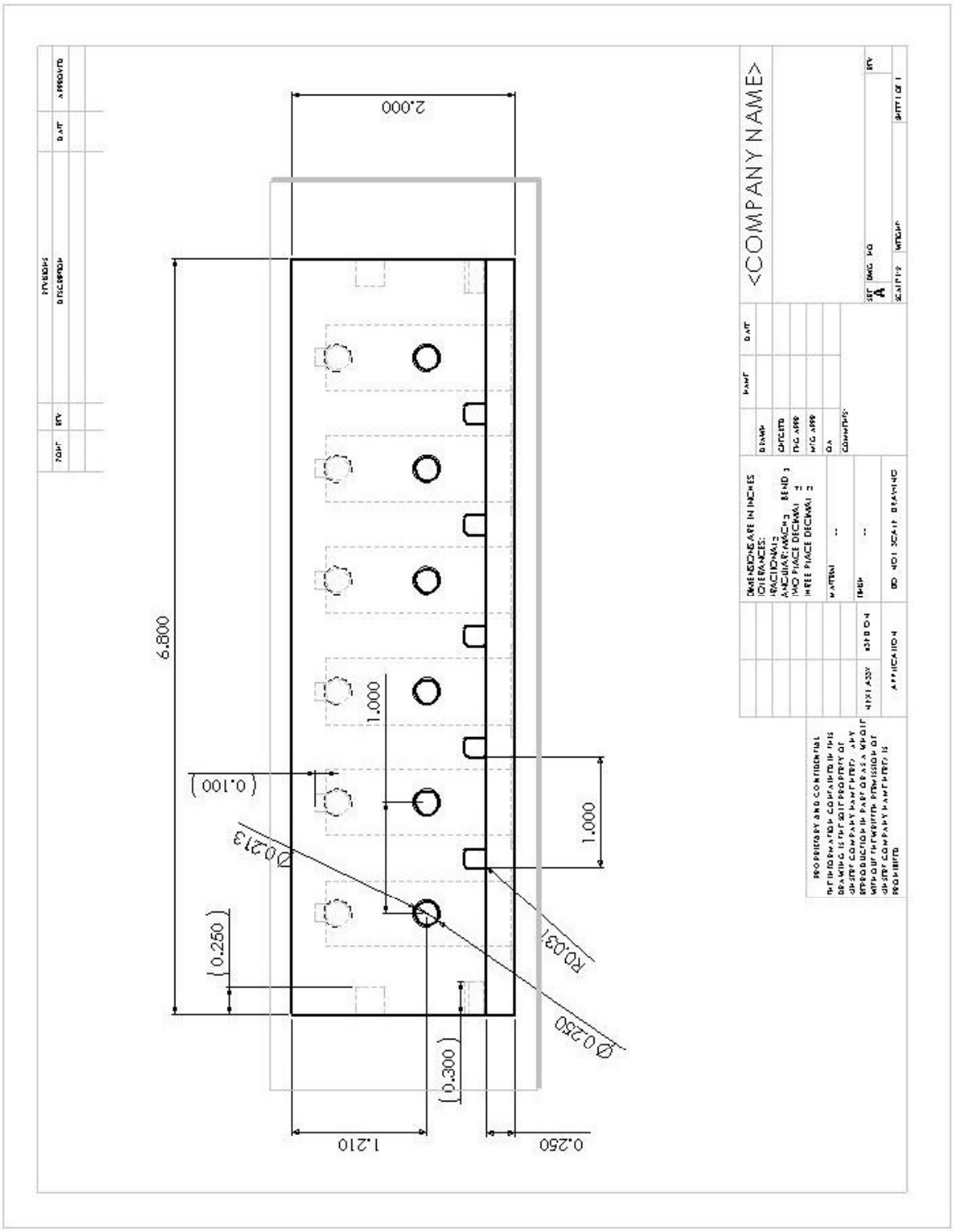

Reservoir – Top.

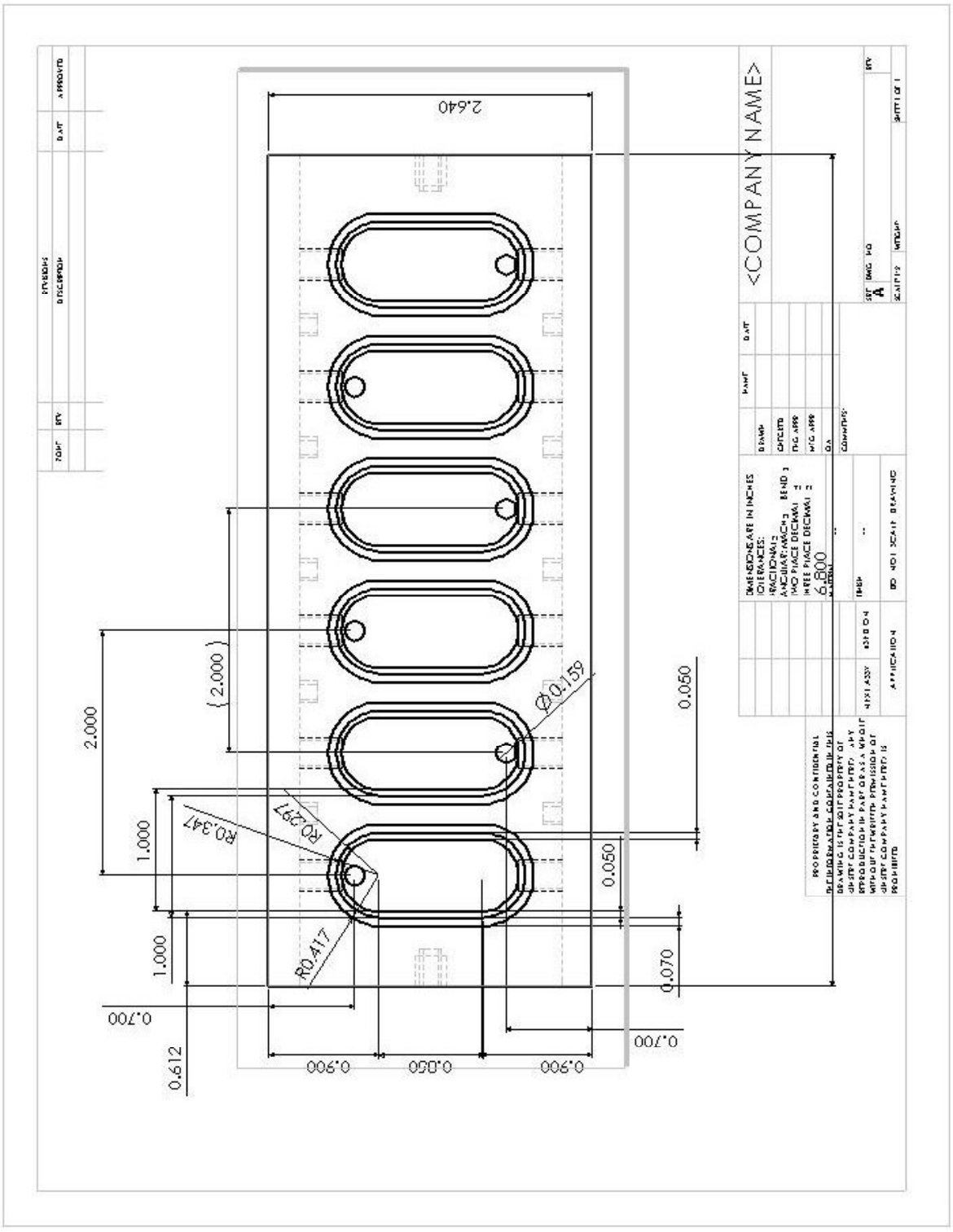

Reservoir Lid.

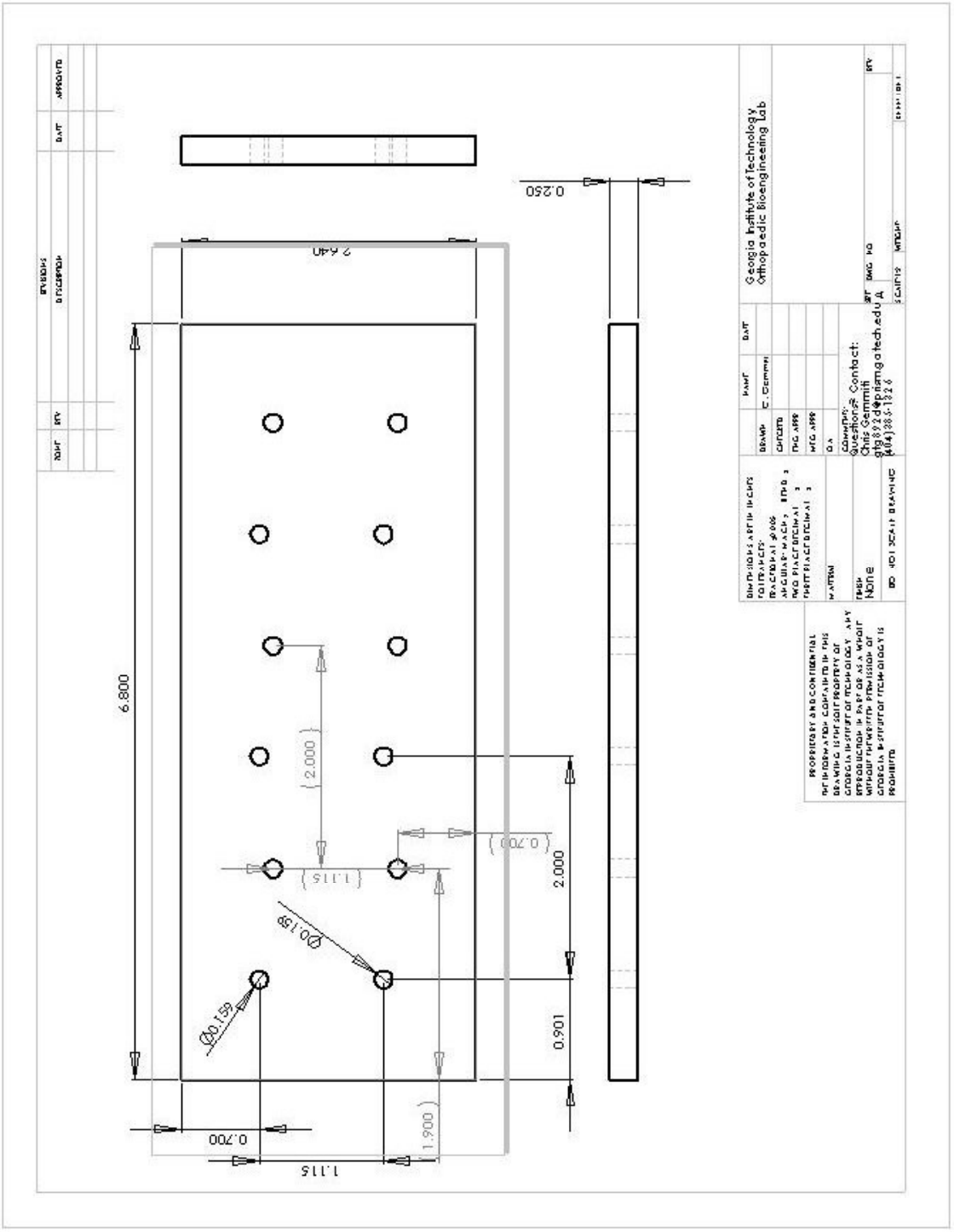

Reservoir Base Plate – Front.

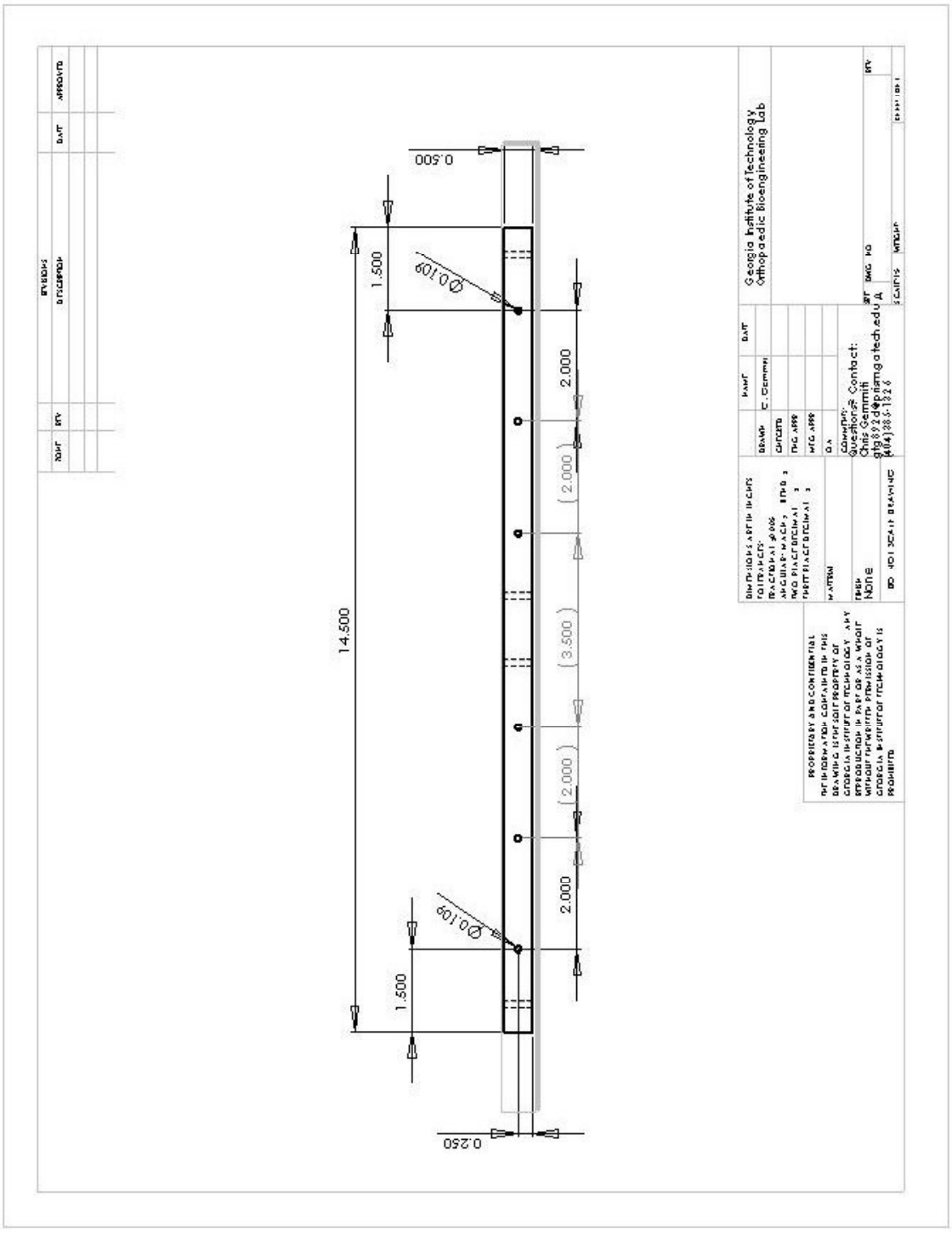

Reservoir Base Plate – Top.

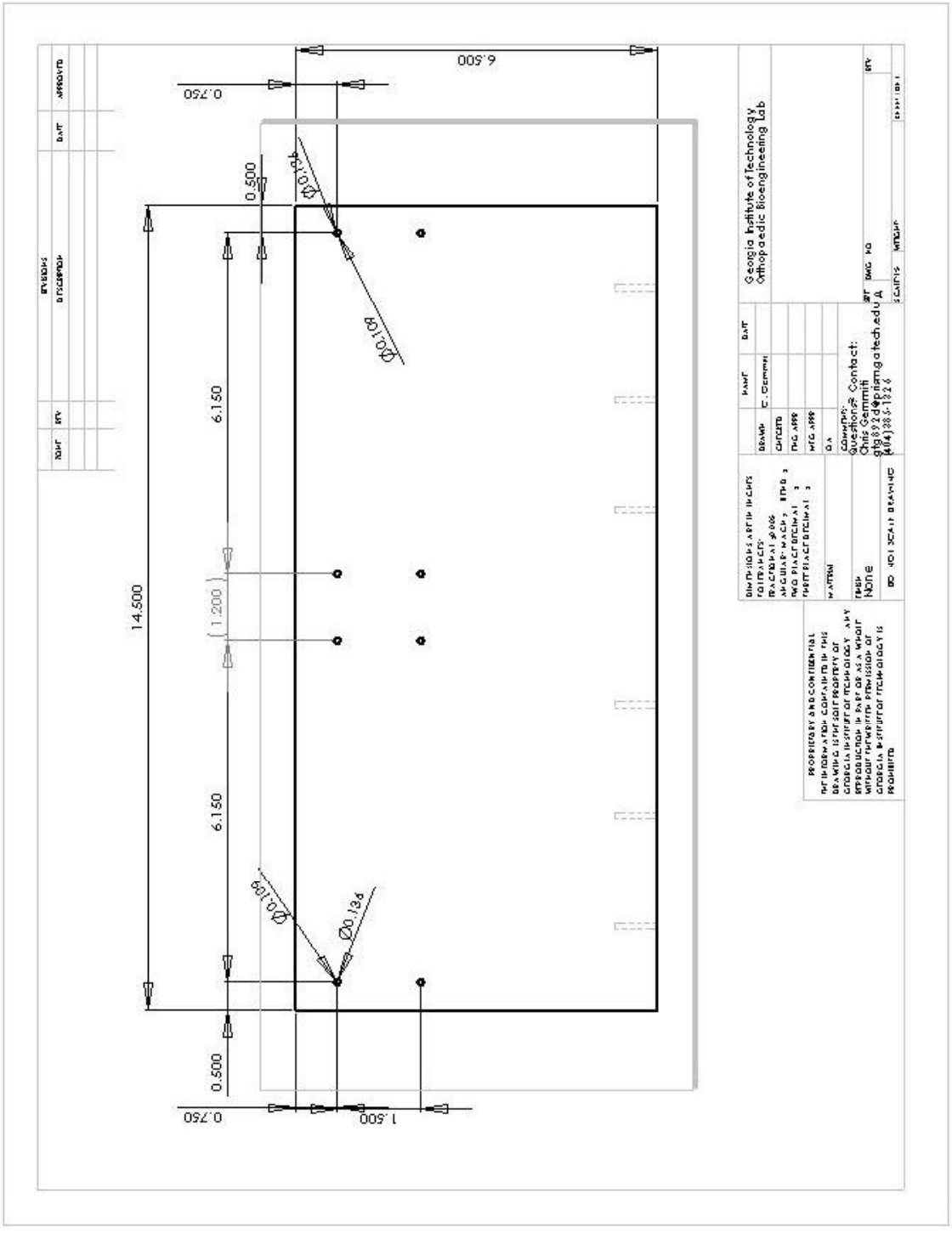

Reservoir Holder.

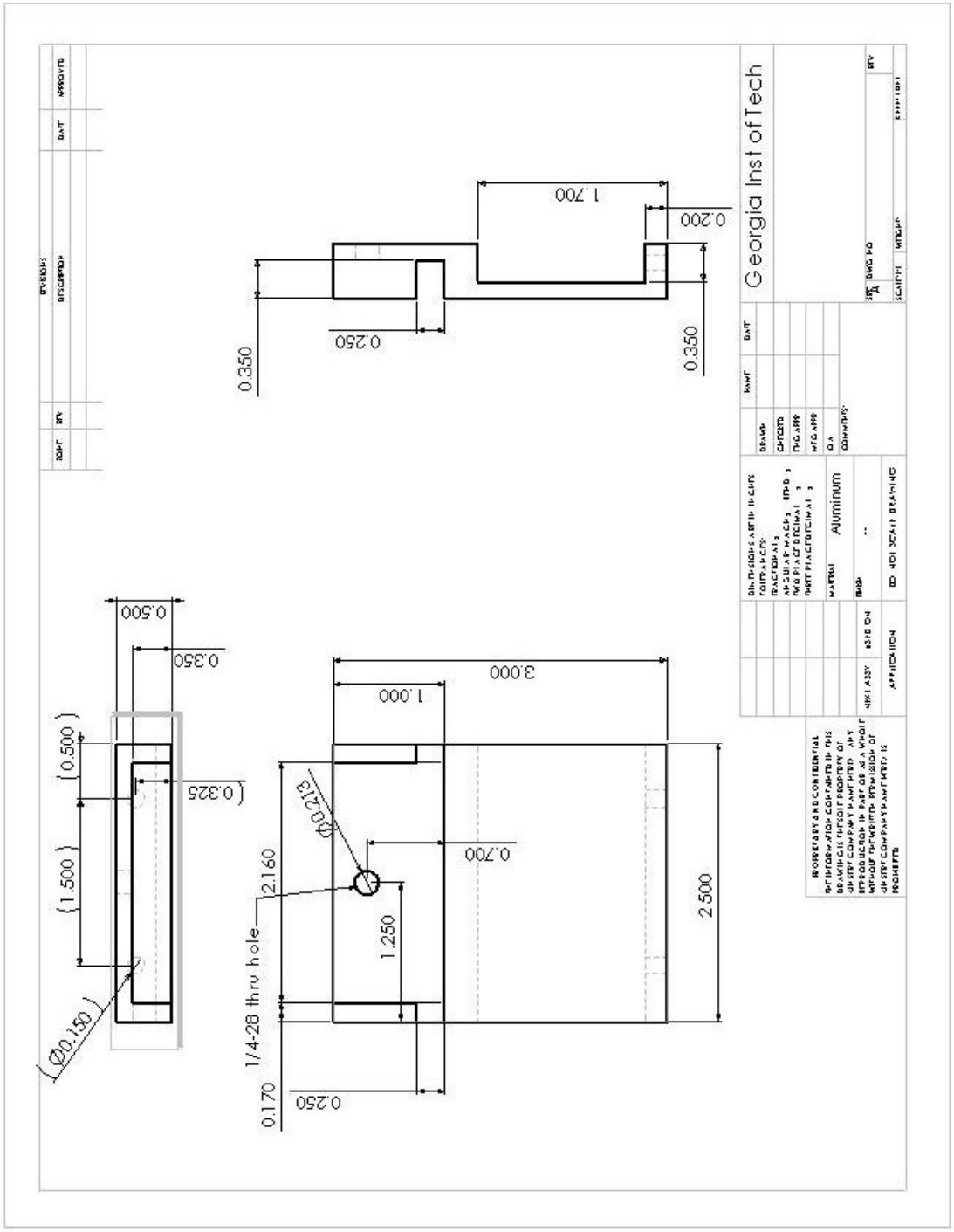

Bioreactor Holder – Side.

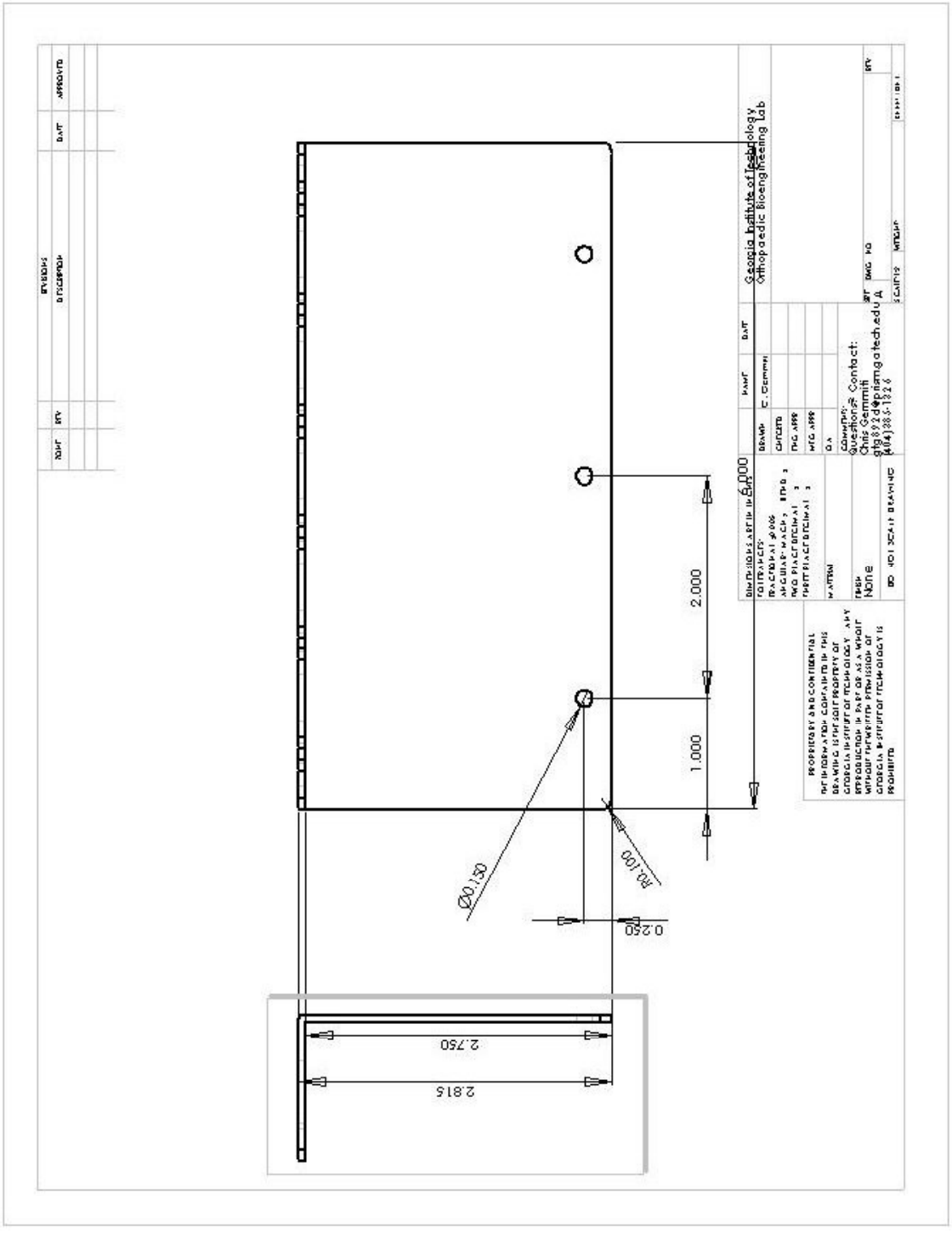

Bioreactor Holder – Top.

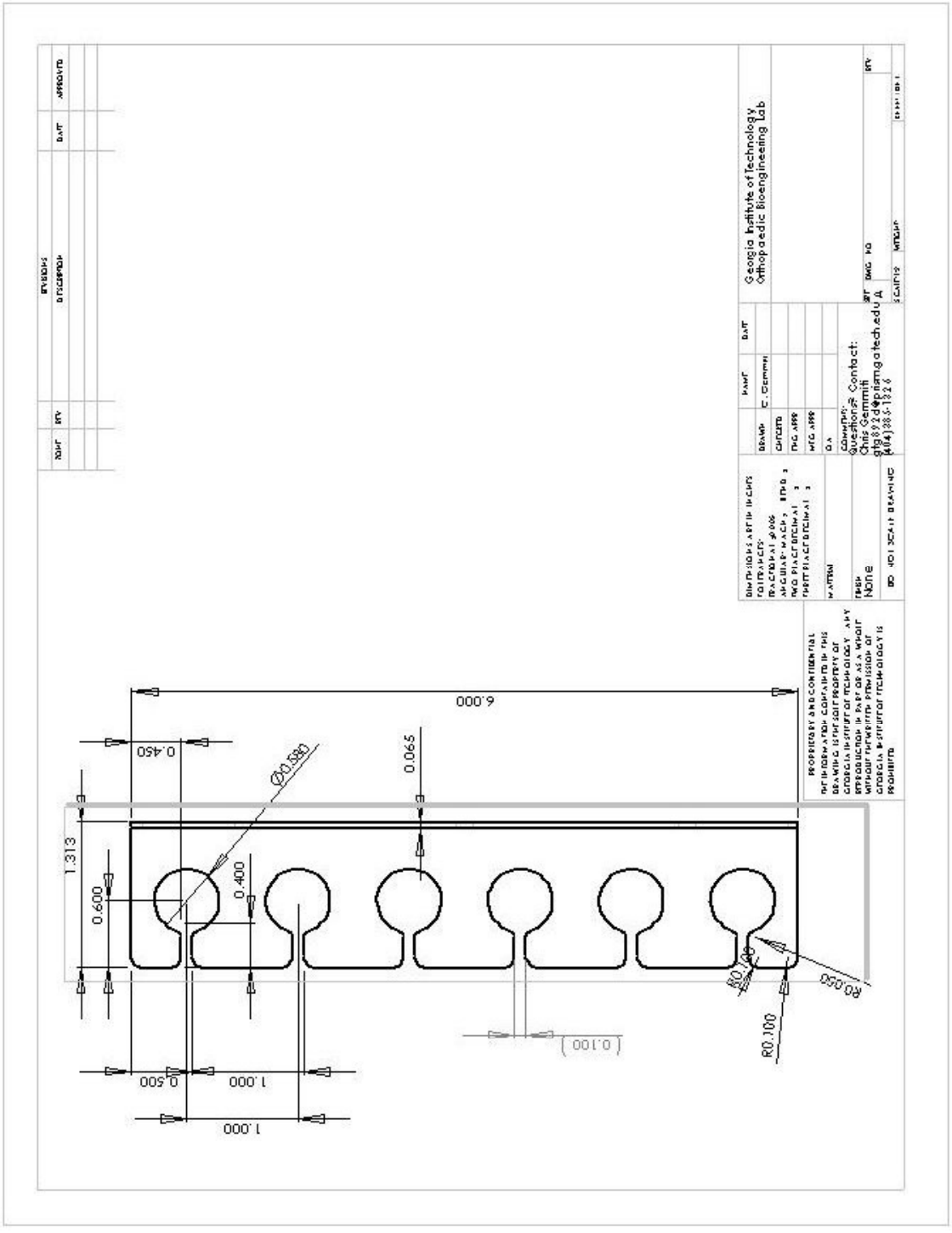

Appendix 4. IPL script to count mineral particle size and number.

```
$!         _/_/_/  _/_/_/    _/
$!          _/    _/    _/  _/           Image Processing Language
$!         _/    _/_/_/    _/
$!        _/    _/        _/             (c)  Andres Laib, Scanco Medical AG
$!     _/_/_/  _/        _/_/_/_/
$!
$!
$!  IPL Batch Scanco
$!
$   if p1 .EQS. ""
$       THEN
$       write sys$output "Give C0001234.aim ! Exit"
$       exit
$   endif
$
$   define   org_file    'p1'
$   histo_file_1 = p1 - F$PARSE(p1,,,"VERSION") - ".AIM" + "_all_points1.txt"
$   histo_file_2 = p1 - F$PARSE(p1,,,"VERSION") - ".AIM" + "_all_points2.txt"

$
$   show log org_file
$!
$   ipl_scanco_prog := $um:ipl_scanco_m.exe
$!
$   ipl_scanco_prog


/read in "org_file

/cl_image in cl

/histo
   -input                      cl
   -fileout_or_screentab       "histo_file_1
   -from_val                           -1
   -to_val                     -1
   -nr_bins_in_tab             -1
   -dt_type                            auto
   -count_zeros                        false

/cl
   -input_output       in
   -first_rank         127
   -last_rank          10000

/cl_image in cl

/histo
   -input                      cl
   -fileout_or_screentab       "histo_file_2
   -from_val                           -1
   -to_val                     -1
   -nr_bins_in_tab             -1
   -dt_type                            auto
   -count_zeros                        false

/cl
   -input_output       in
   -first_rank         127
   -last_rank          10000

..
$ exit
```

Appendix 5. VivaCT Scanning Bioreactor Base.

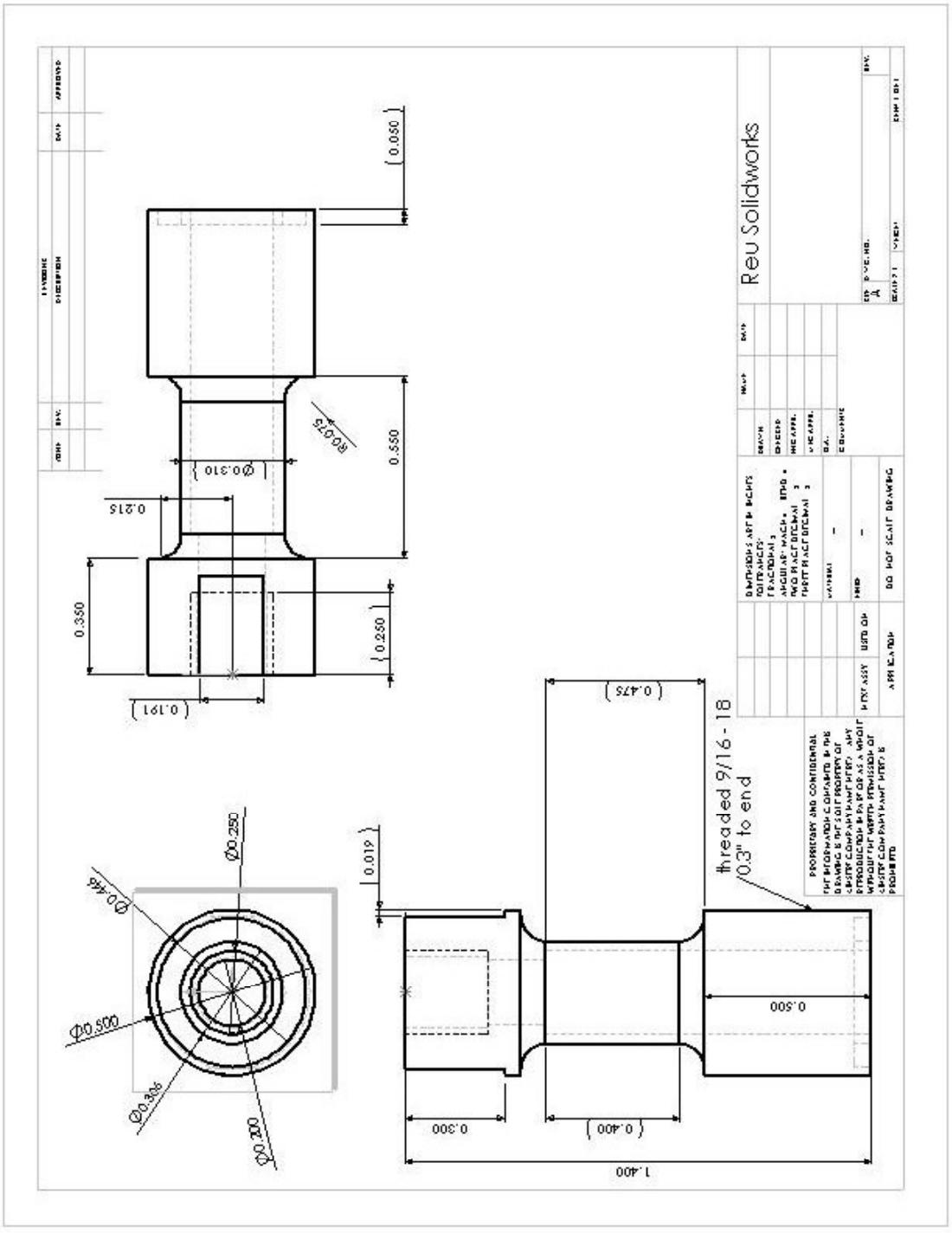

VivaCT Scanning Bioreactor Spacer.

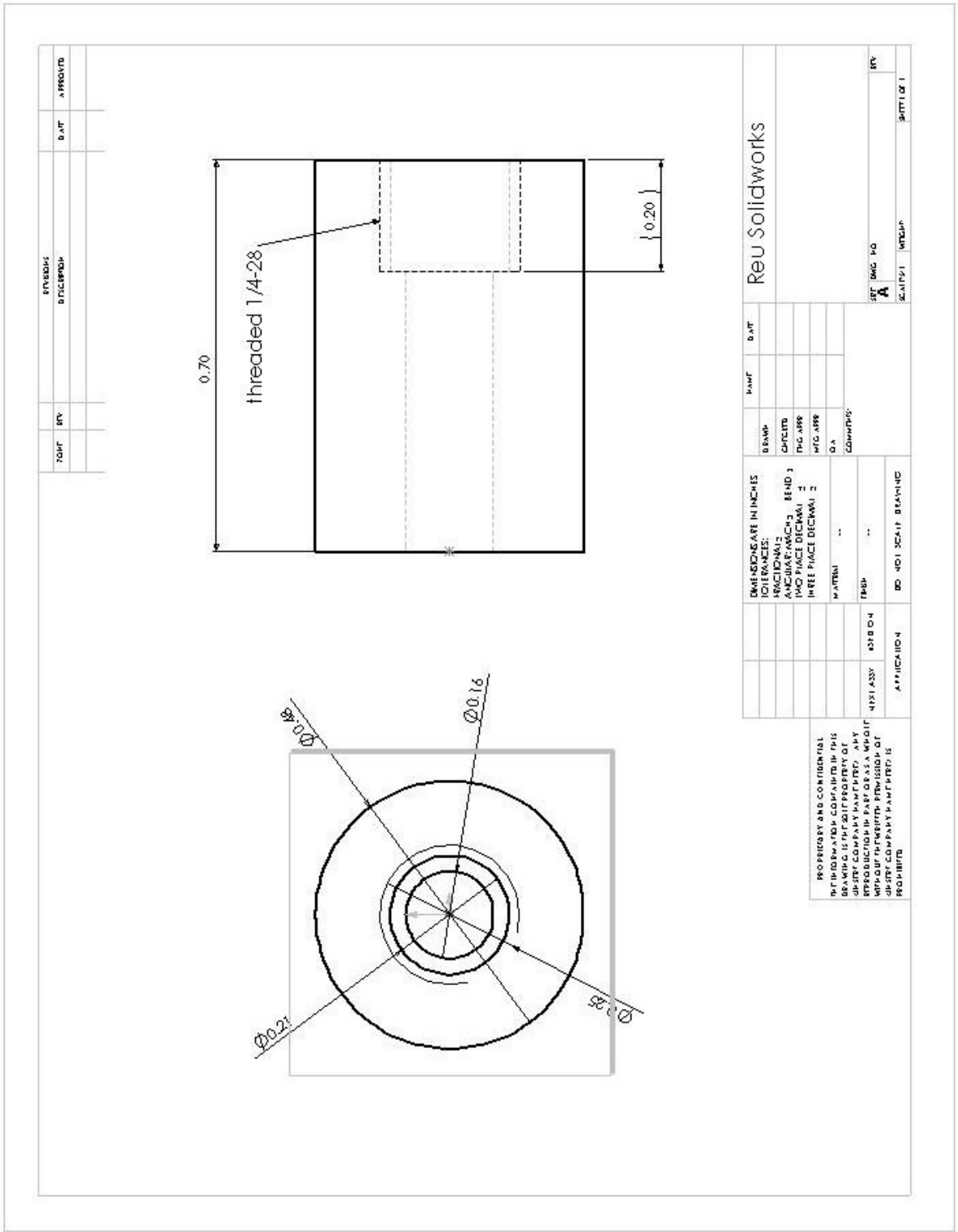

VivaCT Scanning Bioreactor Collet.

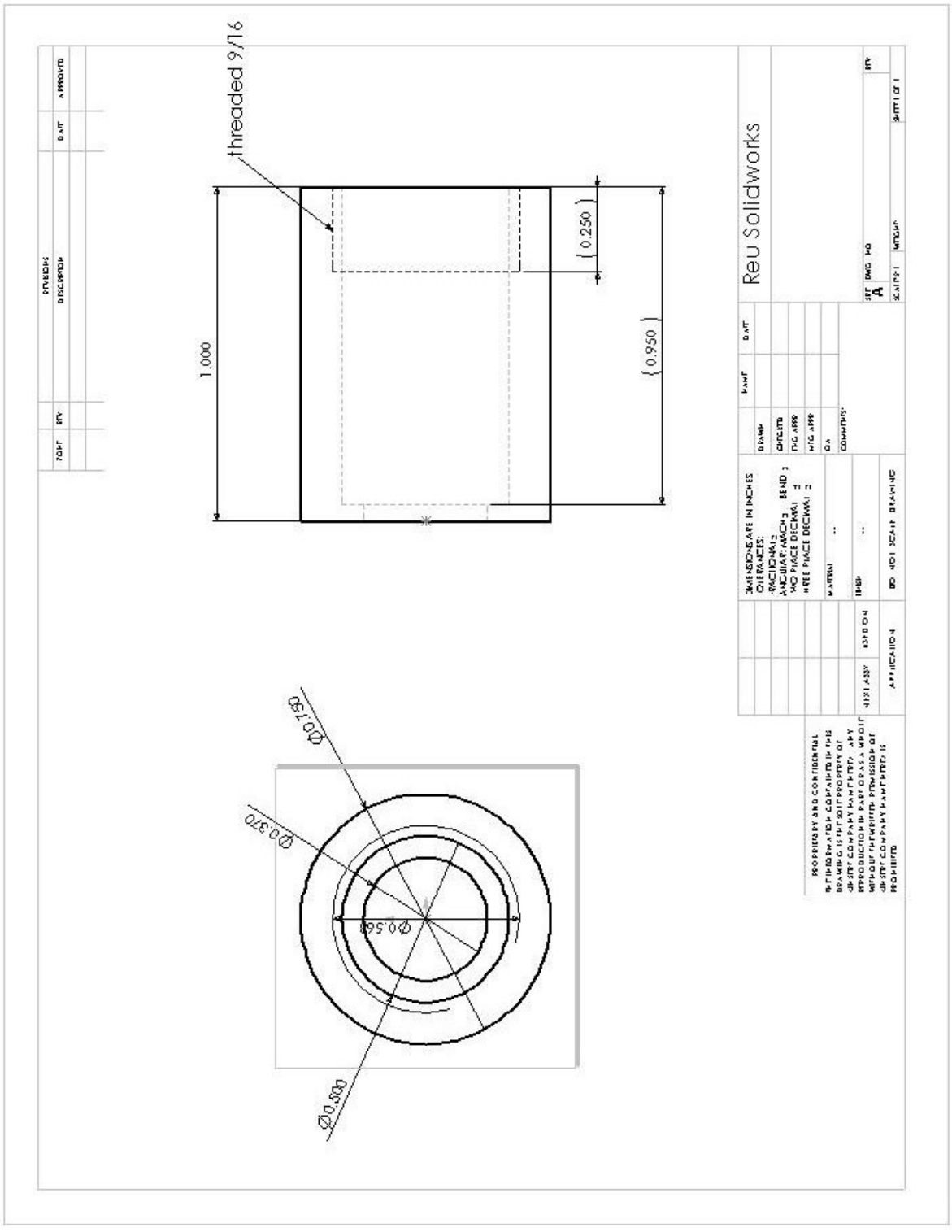

Appendix 6. Collagen Lyophilzation Mold Drawings. Polycarbonate mold.

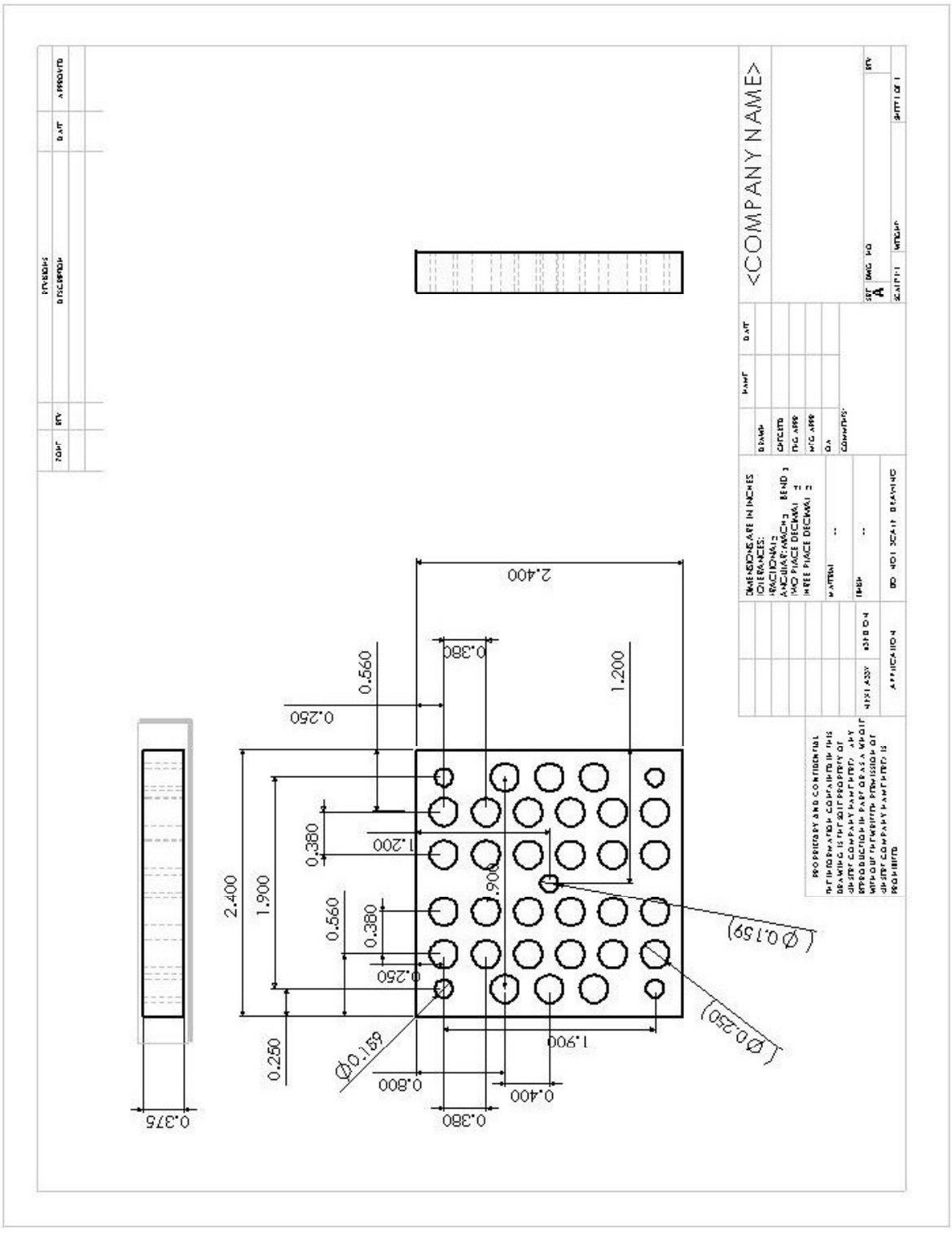

Collagen Base Plate.

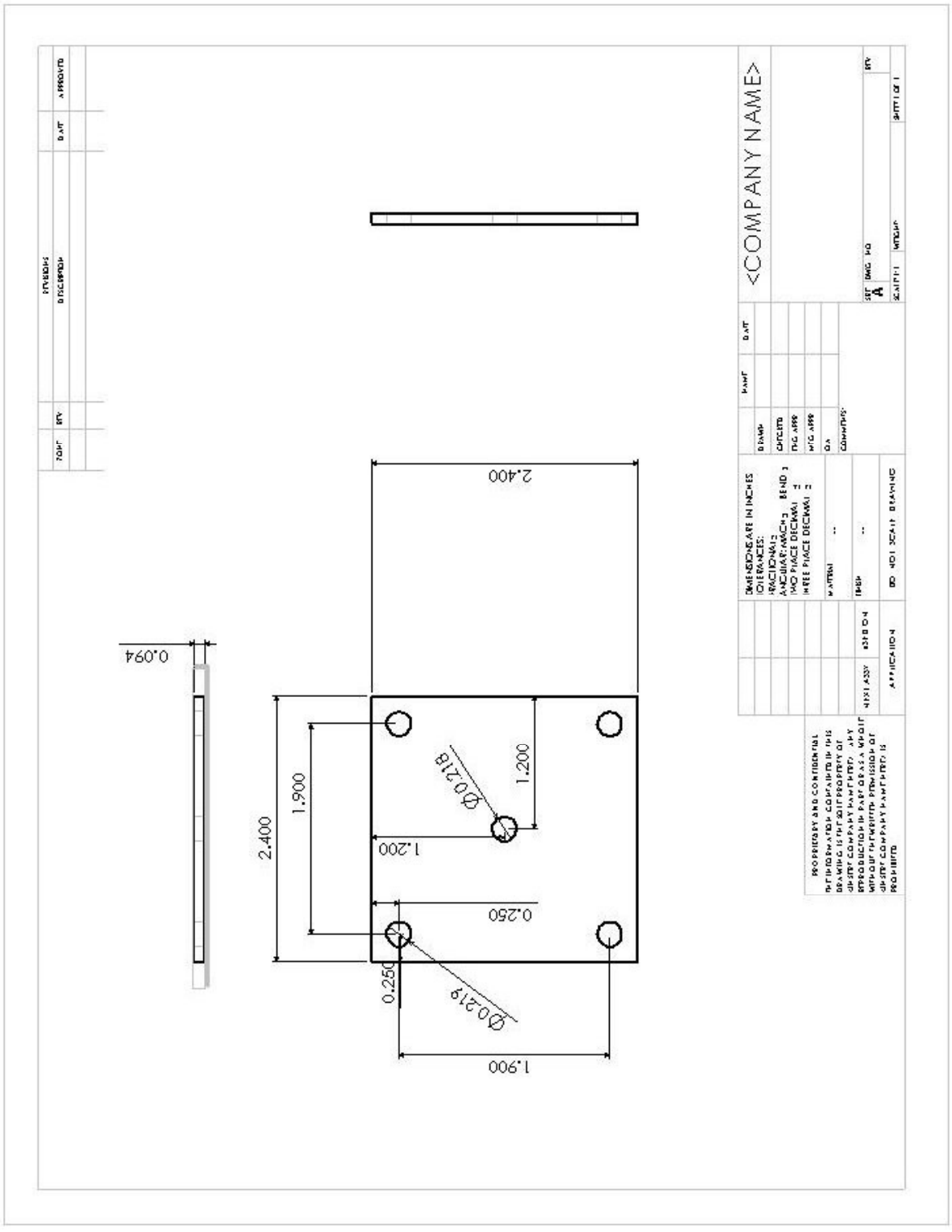

Mold Box.

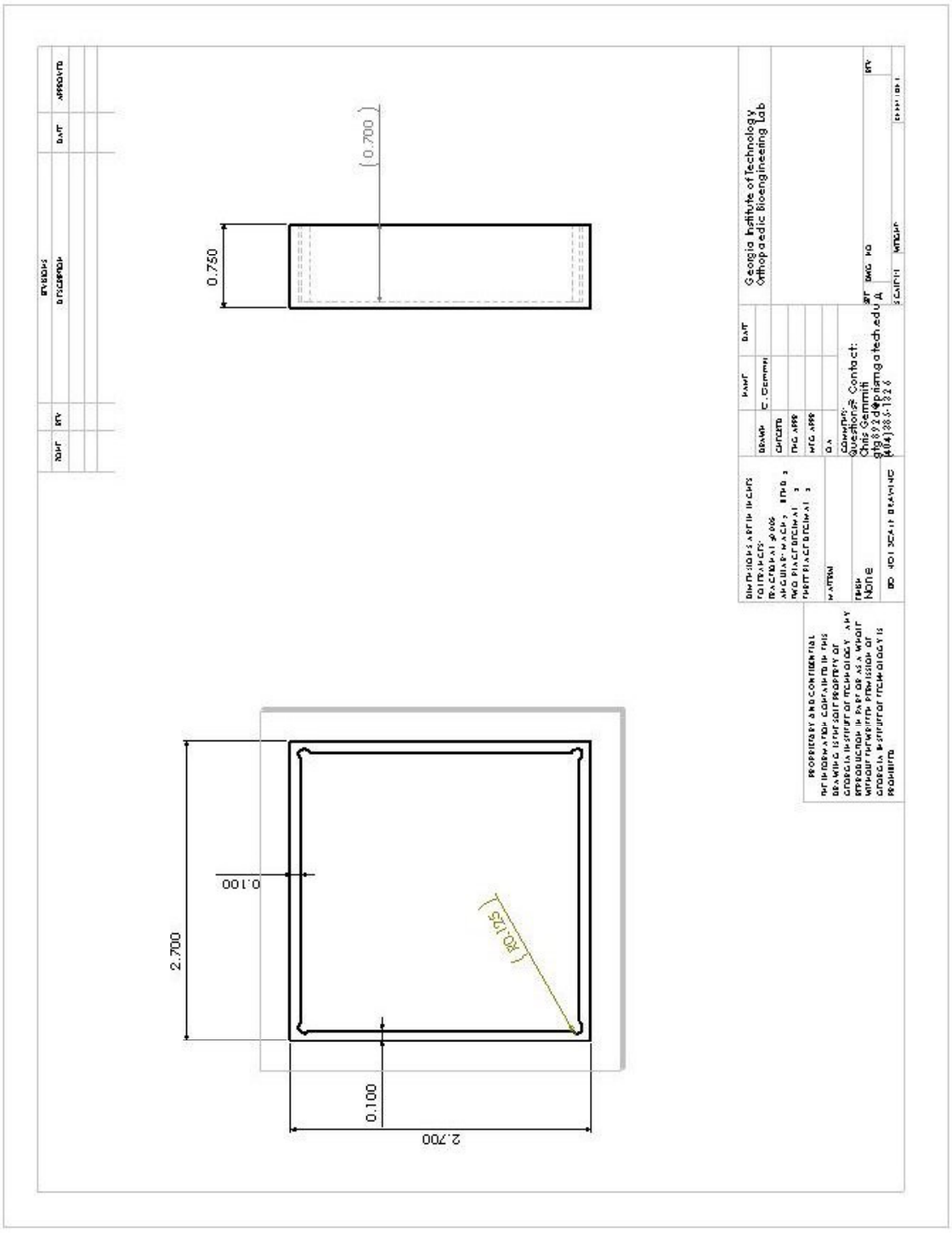
0.700
0.750
2.700
0.100
2.700
0.100
R0.705
Georgia Institute of Technology
Orthopaedic Bioengineering Lab
Chris Gemmiti
gtg592d@gatech.edu
(404)385-1826
None

Mold Box Lid.

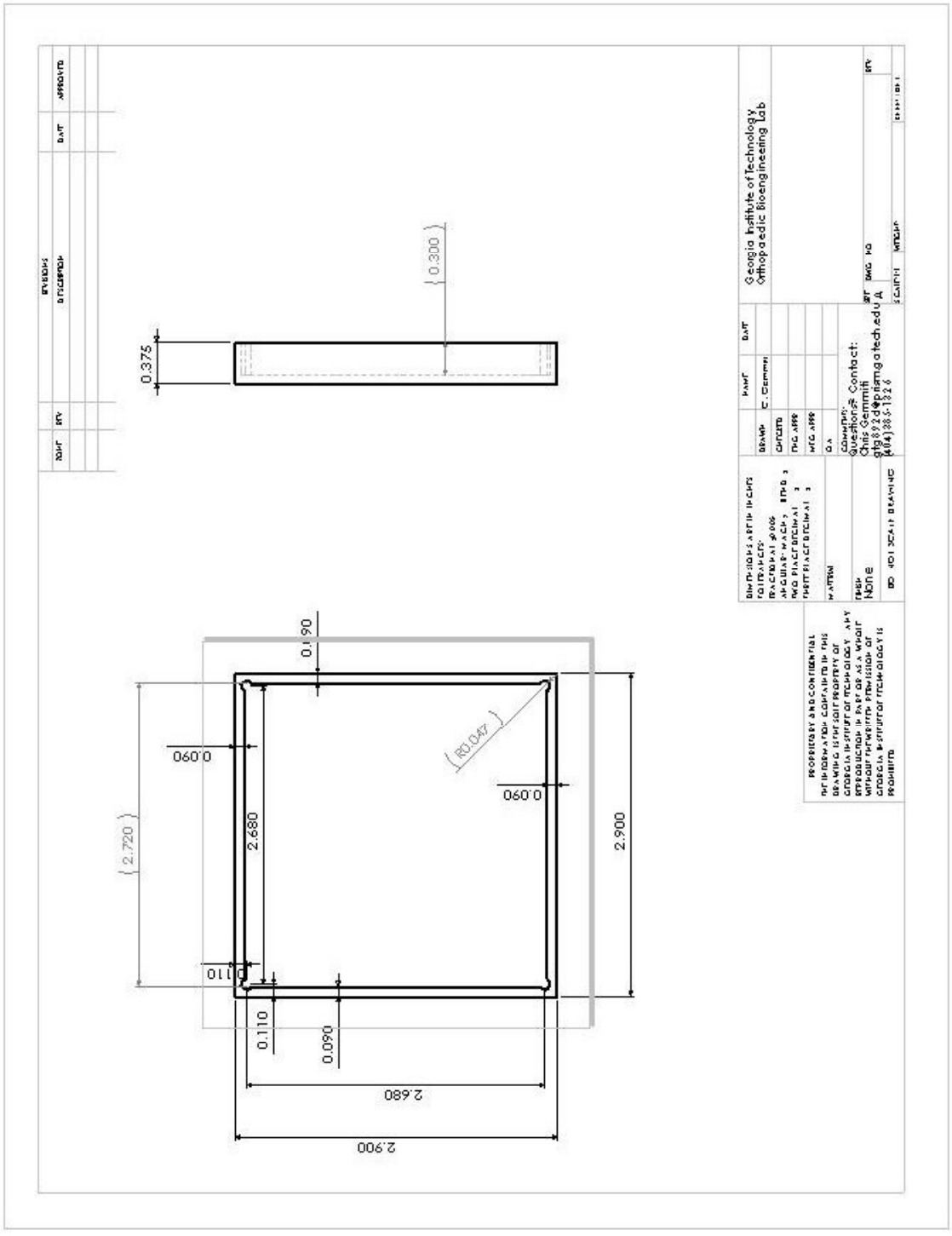
0.375
0.300
0.190
R0.047
0.090
0.090
2.720
2.680
2.900
0.110
0.110
0.090
2.680
2.900
Georgia Institute of Technology
Orthopaedic Bioengineering Lab
Contact:
Chris Gemmiti
cgemmiti@omega.tech.edu

REFERENCES

1. Porter, B., R. Zauel, H. Stockman, R. Guldberg, and D. Fyhrie, *3-D computational modeling of media flow through scaffolds in a perfusion bioreactor.* J Biomech, 2005. 38(3): p. 543-9.

2. Meinel, L., V. Karageorgiou, R. Fajardo, B. Snyder, V. Shinde-Patil, L. Zichner, D. Kaplan, R. Langer, and G. Vunjak-Novakovic, *Bone tissue engineering using human mesenchymal stem cells: effects of scaffold material and medium flow.* Ann Biomed Eng, 2004. 32(1): p. 112-22.

3. Einhorn, T.A., *Clinically applied models of bone regeneration in tissue engineering research.* Clin Orthop, 1999(367 Suppl): p. S59-67.

4. Schantz, J.T., D.W. Hutmacher, C.X. Lam, M. Brinkmann, K.M. Wong, T.C. Lim, N. Chou, R.E. Guldberg, and S.H. Teoh, *Repair of calvarial defects with customised tissue-engineered bone grafts II. Evaluation of cellular efficiency and efficacy in vivo.* Tissue Eng, 2003. 9 Suppl 1: p. S127-39.

5. Sikavitsas, V.I., J. van den Dolder, G.N. Bancroft, J.A. Jansen, and A.G. Mikos, *Influence of the in vitro culture period on the in vivo performance of cell/titanium bone tissue-engineered constructs using a rat cranial critical size defect model.* J Biomed Mater Res A, 2003. 67(3): p. 944-51.

6. Ishaug-Riley, S.L., G.M. Crane-Kruger, M.J. Yaszemski, and A.G. Mikos, *Three-dimensional culture of rat calvarial osteoblasts in porous biodegradable polymers.* Biomaterials, 1998. 19(15): p. 1405-12.

7. Glowacki, J., S. Mizuno, and J.S. Greenberger, *Perfusion enhances functions of bone marrow stromal cells in three- dimensional culture.* Cell Transplant, 1998. 7(3): p. 319-26.

8. Goldstein, A.S., T.M. Juarez, C.D. Helmke, M.C. Gustin, and A.G. Mikos, *Effect of convection on osteoblastic cell growth and function in biodegradable polymer foam scaffolds.* Biomaterials, 2001. 22(11): p. 1279-88.

9. Bancroft, G.N., V.I. Sikavitsas, J. van den Dolder, T.L. Sheffield, C.G. Ambrose, J.A. Jansen, and A.G. Mikos, *Fluid flow increases mineralized matrix deposition in 3D perfusion culture of marrow stromal osteoblasts in a dose-dependent manner.* Proc Natl Acad Sci U S A, 2002. 99(20): p. 12600-5.

10. Van Den Dolder, J., G.N. Bancroft, V.I. Sikavitsas, P.H. Spauwen, J.A. Jansen, and A.G. Mikos, *Flow perfusion culture of marrow stromal osteoblasts in titanium fiber mesh.* J Biomed Mater Res, 2003. 64A(2): p. 235-241.

11. Sikavitsas, V.I., G.N. Bancroft, H.L. Holtorf, J.A. Jansen, and A.G. Mikos, *Mineralized matrix deposition by marrow stromal osteoblasts in 3D perfusion*

culture increases with increasing fluid shear forces. Proc Natl Acad Sci U S A, 2003. 100(25): p. 14683-8.

12. Porter, B.D., R. Zauel, D. Hutmacher, D. Fyhrie, and R.E. Guldberg. *Perfusion Significantly Increases Mineralized Matrix Production at the Interior of 3-D PCL Composite Scaffolds*. in *Transactions of the 51st Annual Orthopaedic Research Society Meeting*. 2005. Washington, D.C.

13. Oest, M.E., K.M. Dupont, and R. Guldberg, *Quantification of Mineralization and Vascularization During Segmental Done Defect Repair.* Journal of Orthopaedic Research. Submitted 2005.

14. Cartmell, S., K. Huynh, A. Lin, S. Nagaraja, and R. Guldberg, *Quantitative microcomputed tomography analysis of mineralization within three-dimensional scaffolds in vitro.* J Biomed Mater Res, 2004. 69A(1): p. 97-104.

15. Klein-Nulend, J., E.H. Burger, C.M. Semeins, L.G. Raisz, and C.C. Pilbeam, *Pulsating fluid flow stimulates prostaglandin release and inducible prostaglandin G/H synthase mRNA expression in primary mouse bone cells.* J Bone Miner Res, 1997. 12(1): p. 45-51.

16. Bakker, A.D., K. Soejima, J. Klein-Nulend, and E.H. Burger, *The production of nitric oxide and prostaglandin E(2) by primary bone cells is shear stress dependent.* J Biomech, 2001. 34(5): p. 671-7.

17. Marieb, E.N., *Human Anatomy and Physiology*. Third ed, ed. R. Heyden. 1995, Redwood City, CA: The Benjamin/Cummings Publishing Company, Inc. 1040.

18. Yaszemski, M.J., R.G. Payne, W.C. Hayes, R. Langer, and A.G. Mikos, *Evolution of bone transplantation: molecular, cellular and tissue strategies to engineer human bone.* Biomaterials, 1996. 17(2): p. 175-85.

19. Cowin, S.C., *Bone Mechanics*, in *Bone Mechanics*, S.C. Cowin, Editor. 1989, CRC Press: Boca Raton. p. 97-127.

20. Cowin, S.C., *Bone Mechanics*, in *Bone Mechanics*, S.C. Cowin, Editor. 1989, CRC Press: Boca Raton. p. 129-157.

21. Hayes, W.C., *Basic Orthopaedic Biomechanics*, V.C. Mow and W.C. Hayes, Editors. 1991, Raven Press: New York. p. 93-142.

22. Majeska, R.J., *Cell Biology of Bone*. Bone Mechanics. 2001.

23. Senn, N., *On the healing of aseptic cavities by implantation of antiseptic decalcified bone.* Am J Med Sci, 1889. 98: p. 219-243.

24. Moore, W.R., S.E. Graves, and G.I. Bain, *Synthetic bone graft substitutes.* ANZ J Surg, 2001. 71(6): p. 354-61.

25. Lane, J.M., E. Tomin, and M.P. Bostrom, *Biosynthetic bone grafting.* Clin Orthop Relat Res, 1999(367 Suppl): p. S107-17.

26. Bruder, S.P. and B.S. Fox, *Tissue engineering of bone. Cell based strategies.* Clin Orthop Relat Res, 1999(367 Suppl): p. S68-83.

27. Byers, B.A., R.E. Guldberg, and A.J. Garcia, *Synergy between genetic and tissue engineering: Runx2 overexpression and in vitro construct development enhance in vivo mineralization.* Tissue Eng, 2004. 10(11-12): p. 1757-66.

28. Vacanti, C.A., W. Kim, J. Upton, M.P. Vacanti, D. Mooney, B. Schloo, and J.P. Vacanti, *Tissue-engineered growth of bone and cartilage.* Transplant Proc, 1993. 25(1 Pt 2): p. 1019-21.

29. Lin, A.S., T.H. Barrows, S.H. Cartmell, and R.E. Guldberg, *Microarchitectural and mechanical characterization of oriented porous polymer scaffolds.* Biomaterials, 2003. 24(3): p. 481-9.

30. Hutmacher, D.W., T. Schantz, I. Zein, K.W. Ng, S.H. Teoh, and K.C. Tan, *Mechanical properties and cell cultural response of polycaprolactone scaffolds designed and fabricated via fused deposition modeling.* J Biomed Mater Res, 2001. 55(2): p. 203-16.

31. Trantolo, D.J., S.T. Sonis, B.M. Thompson, D.L. Wise, K.U. Lewandrowski, and D.D. Hile, *Evaluation of a porous, biodegradable biopolymer scaffold for mandibular reconstruction.* Int J Oral Maxillofac Implants, 2003. 18(2): p. 182-8.

32. Whitaker-Brothers, K. and K. Uhrich, *Poly(anhydride-ester) fibers: role of copolymer composition on hydrolytic degradation and mechanical properties.* J Biomed Mater Res A, 2004. 70(2): p. 309-18.

33. Hedberg, E.L., H.C. Kroese-Deutman, C.K. Shih, R.S. Crowther, D.H. Carney, A.G. Mikos, and J.A. Jansen, *In vivo degradation of porous poly(propylene fumarate)/poly(DL-lactic-co-glycolic acid) composite scaffolds.* Biomaterials, 2005. 26(22): p. 4616-23.

34. Leiggener, C.S., R. Curtis, A.A. Muller, D. Pfluger, S. Gogolewski, and B.A. Rahn, *Influence of copolymer composition of polylactide implants on cranial bone regeneration.* Biomaterials, 2006. 27(2): p. 202-7.

35. Liu, X., Y. Won, and P.X. Ma, *Surface modification of interconnected porous scaffolds.* J Biomed Mater Res A, 2005. 74(1): p. 84-91.

36. Wan, Y., Y. Wang, Z. Liu, X. Qu, B. Han, J. Bei, and S. Wang, *Adhesion and proliferation of OCT-1 osteoblast-like cells on micro- and nano-scale topography structured poly(L-lactide).* Biomaterials, 2005. 26(21): p. 4453-9.

37. Price, R.L., K. Ellison, K.M. Haberstroh, and T.J. Webster, *Nanometer surface roughness increases select osteoblast adhesion on carbon nanofiber compacts.* J Biomed Mater Res A, 2004. 70(1): p. 129-38.

38. Rizzi, S.C., D.J. Heath, A.G. Coombes, N. Bock, M. Textor, and S. Downes, *Biodegradable polymer/hydroxyapatite composites: surface analysis and initial attachment of human osteoblasts.* J Biomed Mater Res, 2001. 55(4): p. 475-86.

39. Rea, S.M., R.A. Brooks, S.M. Best, T. Kokubo, and W. Bonfield, *Proliferation and differentiation of osteoblast-like cells on apatite-wollastonite/polyethylene composites.* Biomaterials, 2004. 25(18): p. 4503-12.

40. Claase, M.B., M.B. Olde Riekerink, J.D. de Bruijn, D.W. Grijpma, G.H. Engbers, and J. Feijen, *Enhanced bone marrow stromal cell adhesion and growth on segmented poly(ether ester)s based on poly(ethylene oxide) and poly(butylene terephthalate).* Biomacromolecules, 2003. 4(1): p. 57-63.

41. Toworfe, G.K., R.J. Composto, C.S. Adams, I.M. Shapiro, and P. Ducheyne, *Fibronectin adsorption on surface-activated poly(dimethylsiloxane) and its effect on cellular function.* J Biomed Mater Res A, 2004. 71(3): p. 449-61.

42. Klee, D., Z. Ademovic, A. Bosserhoff, H. Hoecker, G. Maziolis, and H.J. Erli, *Surface modification of poly(vinylidenefluoride) to improve the osteoblast adhesion.* Biomaterials, 2003. 24(21): p. 3663-70.

43. Williams, D., *The golden anniversary of titanium biomaterials.* Med Device Technol, 2001. 12(7): p. 8-11.

44. Wiskott, H.W. and U.C. Belser, *Lack of integration of smooth titanium surfaces: a working hypothesis based on strains generated in the surrounding bone.* Clin Oral Implants Res, 1999. 10(6): p. 429-44.

45. Levy, R.A., T.M. Chu, J.W. Halloran, S.E. Feinberg, and S. Hollister, *CT-generated porous hydroxyapatite orbital floor prosthesis as a prototype bioimplant.* AJNR Am J Neuroradiol, 1997. 18(8): p. 1522-5.

46. Hollister, S.J., R.D. Maddox, and J.M. Taboas, *Optimal design and fabrication of scaffolds to mimic tissue properties and satisfy biological constraints.* Biomaterials, 2002. 23(20): p. 4095-103.

47. Taboas, J.M., R.D. Maddox, P.H. Krebsbach, and S.J. Hollister, *Indirect solid free form fabrication of local and global porous, biomimetic and composite 3D polymer-ceramic scaffolds.* Biomaterials, 2003. 24(1): p. 181-94.

48. Sakaguchi, Y., I. Sekiya, K. Yagishita, and T. Muneta, *Comparison of human stem cells derived from various mesenchymal tissues: superiority of synovium as a cell source.* Arthritis Rheum, 2005. 52(8): p. 2521-9.

49. Aubin, J.E., *Osteoprogenitor cell frequency in rat bone marrow stromal populations: role for heterotypic cell-cell interactions in osteoblast differentiation.* J Cell Biochem, 1999. 72(3): p. 396-410.

50. Pittenger, M.F., A.M. Mackay, S.C. Beck, R.K. Jaiswal, R. Douglas, J.D. Mosca, M.A. Moorman, D.W. Simonetti, S. Craig, and D.R. Marshak, *Multilineage potential of adult human mesenchymal stem cells.* Science, 1999. 284(5411): p. 143-7.

51. Ishaug, S.L., G.M. Crane, M.J. Miller, A.W. Yasko, M.J. Yaszemski, and A.G. Mikos, *Bone formation by three-dimensional stromal osteoblast culture in biodegradable polymer scaffolds.* J Biomed Mater Res, 1997. 36(1): p. 17-28.

52. Okumura, M., H. Ohgushi, Y. Dohi, T. Katuda, S. Tamai, H.K. Koerten, and S. Tabata, *Osteoblastic phenotype expression on the surface of hydroxyapatite ceramics.* J Biomed Mater Res, 1997. 37(1): p. 122-9.

53. Yoshikawa, T., H. Ohgushi, and S. Tamai, *Immediate bone forming capability of prefabricated osteogenic hydroxyapatite.* J Biomed Mater Res, 1996. 32(3): p. 481-92.

54. Breitbart, A.S., D.A. Grande, R. Kessler, J.T. Ryaby, R.J. Fitzsimmons, and R.T. Grant, *Tissue engineered bone repair of calvarial defects using cultured periosteal cells.* Plast Reconstr Surg, 1998. 101(3): p. 567-74; discussion 575-6.

55. Byers, B.A. and A.J. Garcia, *Exogenous Runx2 expression enhances in vitro osteoblastic differentiation and mineralization in primary bone marrow stromal cells.* Tissue Eng, 2004. 10(11-12): p. 1623-32.

56. Gersbach, C.A., B.A. Byers, G.K. Pavlath, and A.J. Garcia, *Runx2/Cbfa1 stimulates transdifferentiation of primary skeletal myoblasts into a mineralizing osteoblastic phenotype.* Exp Cell Res, 2004. 300(2): p. 406-17.

57. Gersbach, C.A., B.A. Byers, G.K. Pavlath, R.E. Guldberg, and A.J. Garcia, *Runx2/Cbfa1-genetically engineered skeletal myoblasts mineralize collagen scaffolds in vitro.* Biotechnol Bioeng, 2004. 88(3): p. 369-78.

58. Iyoda, K., T. Miura, and H. Nogami, *Repair of bone defect with cultured chondrocytes bound to hydroxyapatite.* Clin Orthop Relat Res, 1993(288): p. 287-93.

59. Lane, J.M., A.W. Yasko, E. Tomin, B.J. Cole, S. Waller, M. Browne, T. Turek, and J. Gross, *Bone marrow and recombinant human bone morphogenetic protein-2 in osseous repair.* Clin Orthop Relat Res, 1999(361): p. 216-27.

60. Freed, L.E., J.C. Marquis, A. Nohria, J. Emmanual, A.G. Mikos, and R. Langer, *Neocartilage formation in vitro and in vivo using cells cultured on synthetic biodegradable polymers.* J Biomed Mater Res, 1993. 27(1): p. 11-23.

61. Griffith, C.K., C. Miller, R.C. Sainson, J.W. Calvert, N.L. Jeon, C.C. Hughes, and S.C. George, *Diffusion limits of an in vitro thick prevascularized tissue.* Tissue Eng, 2005. 11(1-2): p. 257-66.

62. Goldstein, A.S., G. Zhu, G.E. Morris, R.K. Meszlenyi, and A.G. Mikos, *Effect of osteoblastic culture conditions on the structure of poly(DL- lactic-co-glycolic acid) foam scaffolds.* Tissue Eng, 1999. 5(5): p. 421-34.

63. Bujia, J., M. Sittinger, W.W. Minuth, C. Hammer, G. Burmester, and E. Kastenbauer, *Engineering of cartilage tissue using bioresorbable polymer fleeces and perfusion culture.* Acta Otolaryngol, 1995. 115(2): p. 307-10.

64. Cartmell, S.H., B.D. Porter, A.J. Garcia, and R.E. Guldberg, *Effects of medium perfusion rate on cell-seeded three-dimensional bone constructs in vitro.* Tissue Eng, 2003. 9(6): p. 1197-203.

65. Bilgen, B., I.M. Chang-Mateu, and G.A. Barabino, *Characterization of mixing in a novel wavy-walled bioreactor for tissue engineering.* Biotechnol Bioeng, 2005.

66. Sikavitsas, V.I., G.N. Bancroft, and A.G. Mikos, *Formation of three-dimensional cell/polymer constructs for bone tissue engineering in a spinner flask and a rotating wall vessel bioreactor.* J Biomed Mater Res, 2002. 62(1): p. 136-48.

67. Bueno, E.M., B. Bilgen, R.L. Carrier, and G.A. Barabino, *Increased rate of chondrocyte aggregation in a wavy-walled bioreactor.* Biotechnol Bioeng, 2004. 88(6): p. 767-77.

68. Duray, P.H., S.J. Hatfill, and N.R. Pellis, *Tissue culture in microgravity.* Sci Med (Phila), 1997. 4(3): p. 46-55.

69. Botchwey, E.A., S.R. Pollack, E.M. Levine, and C.T. Laurencin, *Bone tissue engineering in a rotating bioreactor using a microcarrier matrix system.* J Biomed Mater Res, 2001. 55(2): p. 242-53.

70. Freed, L.E., A.P. Hollander, I. Martin, J.R. Barry, R. Langer, and G. Vunjak-Novakovic, *Chondrogenesis in a cell-polymer-bioreactor system.* Exp Cell Res, 1998. 240(1): p. 58-65.

71. Qiu, Q., P. Ducheyne, H. Gao, and P. Ayyaswamy, *Formation and differentiation of three-dimensional rat marrow stromal cell culture on microcarriers in a rotating-wall vessel.* Tissue Eng, 1998. 4(1): p. 19-34.

72. Saini, S. and T.M. Wick, *Concentric cylinder bioreactor for production of tissue engineered cartilage: effect of seeding density and hydrodynamic loading on construct development.* Biotechnol Prog, 2003. 19(2): p. 510-21.

73. Williams, K.A., S. Saini, and T.M. Wick, *Computational fluid dynamics modeling of steady-state momentum and mass transport in a bioreactor for cartilage tissue engineering.* Biotechnol Prog, 2002. 18(5): p. 951-63.

74. Yu, X., E.A. Botchwey, E.M. Levine, S.R. Pollack, and C.T. Laurencin, *Bioreactor-based bone tissue engineering: the influence of dynamic flow on osteoblast phenotypic expression and matrix mineralization.* Proc Natl Acad Sci U S A, 2004. 101(31): p. 11203-8.

75. Porter, B.D., R. Zauel, D. Hutmacher, R.E. Guldberg, and D. Fyhrie. *Perfusion Significantly Increases Mineral Production Inside 3-D PCL Composite Scaffolds*. in *Proceedings of the American Society for Mechanical Engineering Summer Bioengineering Meeting,*. 2005. Vail, CO.

76. Johnson, D.L., T.N. McAllister, and J.A. Frangos, *Fluid flow stimulates rapid and continuous release of nitric oxide in osteoblasts.* Am J Physiol, 1996. 271(1 Pt 1): p. E205-8.

77. McAllister, T.N., T. Du, and J.A. Frangos, *Fluid shear stress stimulates prostaglandin and nitric oxide release in bone marrow-derived preosteoclast-like cells.* Biochem Biophys Res Commun, 2000. 270(2): p. 643-8.

78. McAllister, T.N. and J.A. Frangos, *Steady and transient fluid shear stress stimulate NO release in osteoblasts through distinct biochemical pathways.* J Bone Miner Res, 1999. 14(6): p. 930-6.

79. Ogata, T., *Fluid flow-induced tyrosine phosphorylation and participation of growth factor signaling pathway in osteoblast-like cells.* J Cell Biochem, 2000. 76(4): p. 529-38.

80. Owan, I., D.B. Burr, C.H. Turner, J. Qiu, Y. Tu, J.E. Onyia, and R.L. Duncan, *Mechanotransduction in bone: osteoblasts are more responsive to fluid forces than mechanical strain.* Am J Physiol, 1997. 273(3 Pt 1): p. C810-5.

81. Reich, K.M. and J.A. Frangos, *Effect of flow on prostaglandin E2 and inositol trisphosphate levels in osteoblasts.* Am J Physiol, 1991. 261(3 Pt 1): p. C428-32.

82. Jiang, G.L., C.R. White, H.Y. Stevens, and J.A. Frangos, *Temporal gradients in shear stimulate osteoblastic proliferation via ERK1/2 and retinoblastoma protein.* Am J Physiol Endocrinol Metab, 2002. 283(2): p. E383-9.

83. Hillsley, M.V. and J.A. Frangos, *Alkaline phosphatase in osteoblasts is down-regulated by pulsatile fluid flow.* Calcif Tissue Int, 1997. 60(1): p. 48-53.

84. Smalt, R., F.T. Mitchell, R.L. Howard, and T.J. Chambers, *Mechanotransduction in bone cells: induction of nitric oxide and prostaglandin synthesis by fluid shear stress, but not by mechanical strain.* Adv Exp Med Biol, 1997. 433: p. 311-4.

85. Klein-Nulend, J., M.H. Helfrich, J.G. Sterck, H. MacPherson, M. Joldersma, S.H. Ralston, C.M. Semeins, and E.H. Burger, *Nitric oxide response to shear stress by human bone cell cultures is endothelial nitric oxide synthase dependent.* Biochem Biophys Res Commun, 1998. 250(1): p. 108-14.

86. Jacobs, C.R., C.E. Yellowley, B.R. Davis, Z. Zhou, J.M. Cimbala, and H.J. Donahue, *Differential effect of steady versus oscillating flow on bone cells.* J Biomech, 1998. 31(11): p. 969-76.

87. Edlich, M., C.E. Yellowley, C.R. Jacobs, and H.J. Donahue, *Oscillating fluid flow regulates cytosolic calcium concentration in bovine articular chondrocytes.* J Biomech, 2001. 34(1): p. 59-65.

88. Freed, L.E., G. Vunjak-Novakovic, and R. Langer, *Cultivation of cell-polymer cartilage implants in bioreactors.* J Cell Biochem, 1993. 51(3): p. 257-64.

89. Holy, C.E., M.S. Shoichet, and J.E. Davies, *Engineering three-dimensional bone tissue in vitro using biodegradable scaffolds: investigating initial cell-seeding density and culture period.* J Biomed Mater Res, 2000. 51(3): p. 376-82.

90. Kim, S.S., H. Utsunomiya, J.A. Koski, B.M. Wu, M.J. Cima, J. Sohn, K. Mukai, L.G. Griffith, and J.P. Vacanti, *Survival and function of hepatocytes on a novel three-dimensional synthetic biodegradable polymer scaffold with an intrinsic network of channels.* Ann Surg, 1998. 228(1): p. 8-13.

91. Vacanti, J.P., R. Langer, J. Upton, and J.J. Marler, *Transplantation of cells in matrices for tissue regeneration.* Adv Drug Deliv Rev, 1998. 33(1-2): p. 165-182.

92. Vandenburgh, H., M. Del Tatto, J. Shansky, J. Lemaire, A. Chang, F. Payumo, P. Lee, A. Goodyear, and L. Raven, *Tissue-engineered skeletal muscle organoids for reversible gene therapy.* Hum Gene Ther, 1996. 7(17): p. 2195-200.

93. Rothenburger, M., P. Vischer, W. Volker, B. Glasmacher, E. Berendes, H.H. Scheld, and M. Deiwick, *In vitro modelling of tissue using isolated vascular cells on a synthetic collagen matrix as a substitute for heart valves.* Thorac Cardiovasc Surg, 2001. 49(4): p. 204-9.

94. Seliktar, D., R.A. Black, R.P. Vito, and R.M. Nerem, *Dynamic mechanical conditioning of collagen-gel blood vessel constructs induces remodeling in vitro.* Ann Biomed Eng, 2000. 28(4): p. 351-62.

95. Ziegler, T. and R.M. Nerem, *Tissue engineering a blood vessel: regulation of vascular biology by mechanical stresses.* J Cell Biochem, 1994. 56(2): p. 204-9.

96. Takezawa, T., M. Inoue, S. Aoki, M. Sekiguchi, K. Wada, H. Anazawa, and N. Hanai, *Concept for organ engineering: a reconstruction method of rat liver for in vitro culture.* Tissue Eng, 2000. 6(6): p. 641-50.

97. Freed, L.E. and G. Vunjak-Novakovic, *Microgravity tissue engineering.* In Vitro Cell Dev Biol Anim, 1997. 33(5): p. 381-5.

98. Botchwey, E.A., S.R. Pollack, S. El-Amin, E.M. Levine, R.S. Tuan, and C.T. Laurencin, *Human osteoblast-like cells in three-dimensional culture with fluid flow.* Biorheology, 2003. 40(1-3): p. 299-306.

99. Raimondi, M.T., F. Boschetti, L. Falcone, G.B. Fiore, A. Remuzzi, E. Marinoni, M. Marazzi, and R. Pietrabissa, *Mechanobiology of engineered cartilage cultured under a quantified fluid-dynamic environment.* Biomech Model Mechanobiol, 2002. 1(1): p. 69-82.

100. Martys, N.C., H., *Simulation of multicomponent fluids in comples three-dimensional geometries by the Lattice Boltzmann method.* Physics Review E, 1996. 53: p. 743-750.

101. Stockman, H.W., *A 3D Lattice Boltzmann Code for Modeling Flow and Multicomponent Dispersion*. 1999, SAND99-0162, Sandia National Laboratories: Albuquerque, NM.

102. Stockman, H.W., C. Li, and J.L. Wilson, *A lattice-gas and lattice Boltzmann study of mixing at continuous fracture junctions: importance of boundary conditions.* Geophysics Research Letters, 1997. 24(12): p. 1515-1518.

103. Sudo, H., H.A. Kodama, Y. Amagai, S. Yamamoto, and S. Kasai, *In vitro differentiation and calcification in a new clonal osteogenic cell line derived from newborn mouse calvaria.* J Cell Biol, 1983. 96(1): p. 191-8.

104. Feldkamp, L.A., S.A. Goldstein, A.M. Parfitt, G. Jesion, and M. Kleerekoper, *The direct examination of three-dimensional bone architecture in vitro by computed tomography.* J Bone Miner Res, 1989. 4(1): p. 3-11.

105. Smalt, R., F.T. Mitchell, R.L. Howard, and T.J. Chambers, *Induction of NO and prostaglandin E2 in osteoblasts by wall-shear stress but not mechanical strain.* Am J Physiol, 1997. 273(4 Pt 1): p. E751-8.

106. Chung, C.Y., A. Iida-Klein, L.E. Wyatt, G.H. Rudkin, K. Ishida, D.T. Yamaguchi, and T.A. Miller, *Serial passage of MC3T3-E1 cells alters osteoblastic function and responsiveness to transforming growth factor-beta1 and bone morphogenetic protein-2.* Biochem Biophys Res Commun, 1999. 265(1): p. 246-51.

107. Holtorf, H.L., J.A. Jansen, and A.G. Mikos, *Flow perfusion culture induces the osteoblastic differentiation of marrow stroma cell-scaffold constructs in the absence of dexamethasone.* J Biomed Mater Res A, 2005. 72(3): p. 326-34.

108. Mueller, S.M., S. Mizuno, L.C. Gerstenfeld, and J. Glowacki, *Medium perfusion enhances osteogenesis by murine osteosarcoma cells in three-dimensional collagen sponges.* J Bone Miner Res, 1999. 14(12): p. 2118-26.

109. Donahue, S.W., H.J. Donahue, and C.R. Jacobs, *Osteoblastic cells have refractory periods for fluid-flow-induced intracellular calcium oscillations for short bouts of flow and display multiple low-magnitude oscillations during long-term flow.* J Biomech, 2003. 36(1): p. 35-43.

110. Hata, R. and H. Senoo, *L-ascorbic acid 2-phosphate stimulates collagen accumulation, cell proliferation, and formation of a three-dimensional tissuelike substance by skin fibroblasts.* J Cell Physiol, 1989. 138(1): p. 8-16.

111. Zein, I., D.W. Hutmacher, K.C. Tan, and S.H. Teoh, *Fused deposition modeling of novel scaffold architectures for tissue engineering applications.* Biomaterials, 2002. 23(4): p. 1169-85.

112. Lan, C.W., F.F. Wang, and Y.J. Wang, *Osteogenic enrichment of bone-marrow stromal cells with the use of flow chamber and type I collagen-coated surface.* J Biomed Mater Res A, 2003. 66(1): p. 38-46.

113. Lan, C.W. and Y.J. Wang, *Collagen as an immobilization vehicle for bone marrow stromal cells enriched with osteogenic potential.* Artif Cells Blood Substit Immobil Biotechnol, 2003. 31(1): p. 59-68.

114. Bonewald, L.F., S.E. Harris, J. Rosser, M.R. Dallas, S.L. Dallas, N.P. Camacho, B. Boyan, and A. Boskey, *von Kossa staining alone is not sufficient to confirm that mineralization in vitro represents bone formation.* Calcif Tissue Int, 2003. 72(5): p. 537-47.

115. Boskey, A.L., N.P. Camacho, R. Mendelsohn, S.B. Doty, and I. Binderman, *FT-IR microscopic mappings of early mineralization in chick limb bud mesenchymal cell cultures.* Calcif Tissue Int, 1992. 51(6): p. 443-8.

116. Cartmell, S.H.P., B.D.; Garcia, A. J.; Guldberg, R.E., *Effects of Media Perfusion Rate on Cell Seeded 3D Bone Constructs In Vitro.* Tissue Eng, 2003. In Press(Oct).

117. Janssen, F.W., J. Oostra, A. Oorschot, and C.A. van Blitterswijk, *A perfusion bioreactor system capable of producing clinically relevant volumes of tissue-engineered bone: In vivo bone formation showing proof of concept.* Biomaterials, 2006. 27(3): p. 315-23.

118. Dudziak, M.E., P.B. Saadeh, B.J. Mehrara, D.S. Steinbrech, J.A. Greenwald, G.K. Gittes, and M.T. Longaker, *The effects of ionizing radiation on osteoblast-like cells in vitro.* Plast Reconstr Surg, 2000. 106(5): p. 1049-61.

119. Koller, B., *vivaCT questions*, M. Oest, Editor. 2003, Scanco Medical.

120. Sucosky, P., D.F. Osorio, J.B. Brown, and G.P. Neitzel, *Fluid mechanics of a spinner-flask bioreactor.* Biotechnol Bioeng, 2004. 85(1): p. 34-46.

121. Cournubert, R.d.H., D; Levermore, D, *A Knudsen layer theory for lattice gasses.* Physica D, 1991. 47: p. 241-259.

122. Chen, S.J., ; Martinez, D., Mei, R., *On Boundary conditions in Lattice Boltzmann methods.* Physics Fluids, 1996. 8: p. 2527-2535.

VITA

Blaise Damian Porter (all 7 lbs. 7 oz. of him) was brought into this world in Houston, TX at 7:17pm on October 2, 1975. He was the first of the Porter brood and according to his mother, the event was so arduous, he was almost the last. Sitting at 4 months, walking by 6, when his first word was "ball," it was a foregone conclusion this little dude would be mopping the courts or gridiron with athletic prowess and panache. If his parents had only known, you can't teach 5'6". During those early years, his parents feared he might be orally challenged when he had not improved his vocabulary by the age of 2. They needn't have been concerned. Shortly after acquiring a little brother, he regaled his parents with stories of ways to show "affection" for his younger sibling.

After 3 years on a dairy farm and an Army base, he returned to the city of his birth where he learned the joys of organized sports (and really cool team uniforms). Between trips to Des Moines and Vegas, he gained an appreciation for having family across the country. Although he didn't know it at the time, between the ages of 6 and 7 he observed racism and family dysfunction in the outside world, which he will never forget. In 1982, a second younger brother who was treated much better than the first arrived on the scene. Shortly after, Blaise embarked on his second great adventure when he tagged along with the rest of his family on a journey to Saudi Arabia for 6 weeks and learned that beheadings and hand removal are excellent deterrents to theft and murder.

His return to the US coincided with a move to the land he now claims as home, the great state of Minnesota. Initially made fun of because of his southern drawl, he quickly made lifelong friends with Gatz, Muellner, Ernie, EA and Miller. A slight hiccup occurred in 1988 (the year after Notre Dame won the national championship) when Blaise was diagnosed with a non-malignant brain tumor. Upon successful stereotactic surgery and recovery, his career path in engineering medical advances was chosen.

A third brother showed up right before high school, which was a time to interact with luminous individuals such as Bob Gardner and others who more eccentric if not as wide thinking. Cross Country and Basketball gave way to Football and Baseball over the years with a the crowning achievement of leading the Lourdes High School baseball team to its first state tournament. Along the way, it became obvious that Physics and Math were intriguing disciplines and the P Bandits were not to be trifled with. A wonderful relationship with a girl turned into heartache during his sophomore year at St. Olaf where fortunately he made lifelong friends with the members of St. John's house. More at home in the Science Center (he had a key) than his own room, he was subsequently smitten with his current sporting love, Ultimate Frisbee. After graduating with honors and distinction, he matriculated to the south in hopes of becoming a Helluva Engineer.

Graduate school encompassed more than he expected in every way and he was lucky enough to travel halfway around the world and throughout North America to share his work with the scientific community (and solidify his spot on the All Conference team). Combining an affinity for 100-mile bike rides and 26.2-mile runs with his willingness to take on any ingestion challenge, dominance as the Whopper King was almost preordained. The amplitude of the vicissitudes he encountered during those 7.339 years stretched him as a person and prepared him to be ready for his life in the real world, but more importantly, his life with Jenny.